INTERNATIONAL TECHNOLOGY CORPORATION

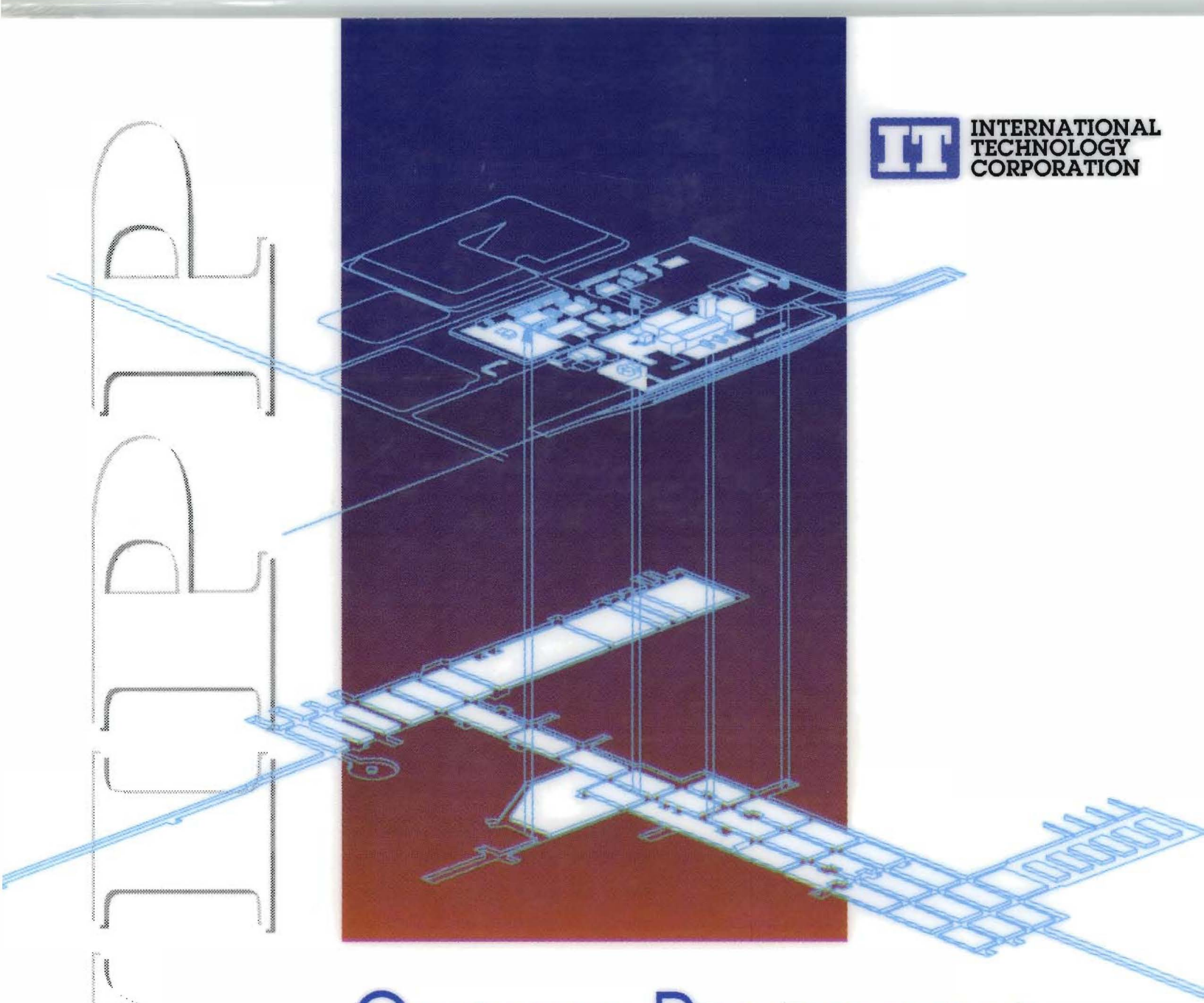

GROUND-PENETRATING RADAR SURVEYS AT THE WIPP SITE

JANUARY 1991 TO FEBRUARY 1992

GROUND-PENETRATING RADAR SURVEYS AT THE WIPP SITE

JANUARY 1991 TO FEBRUARY 1992

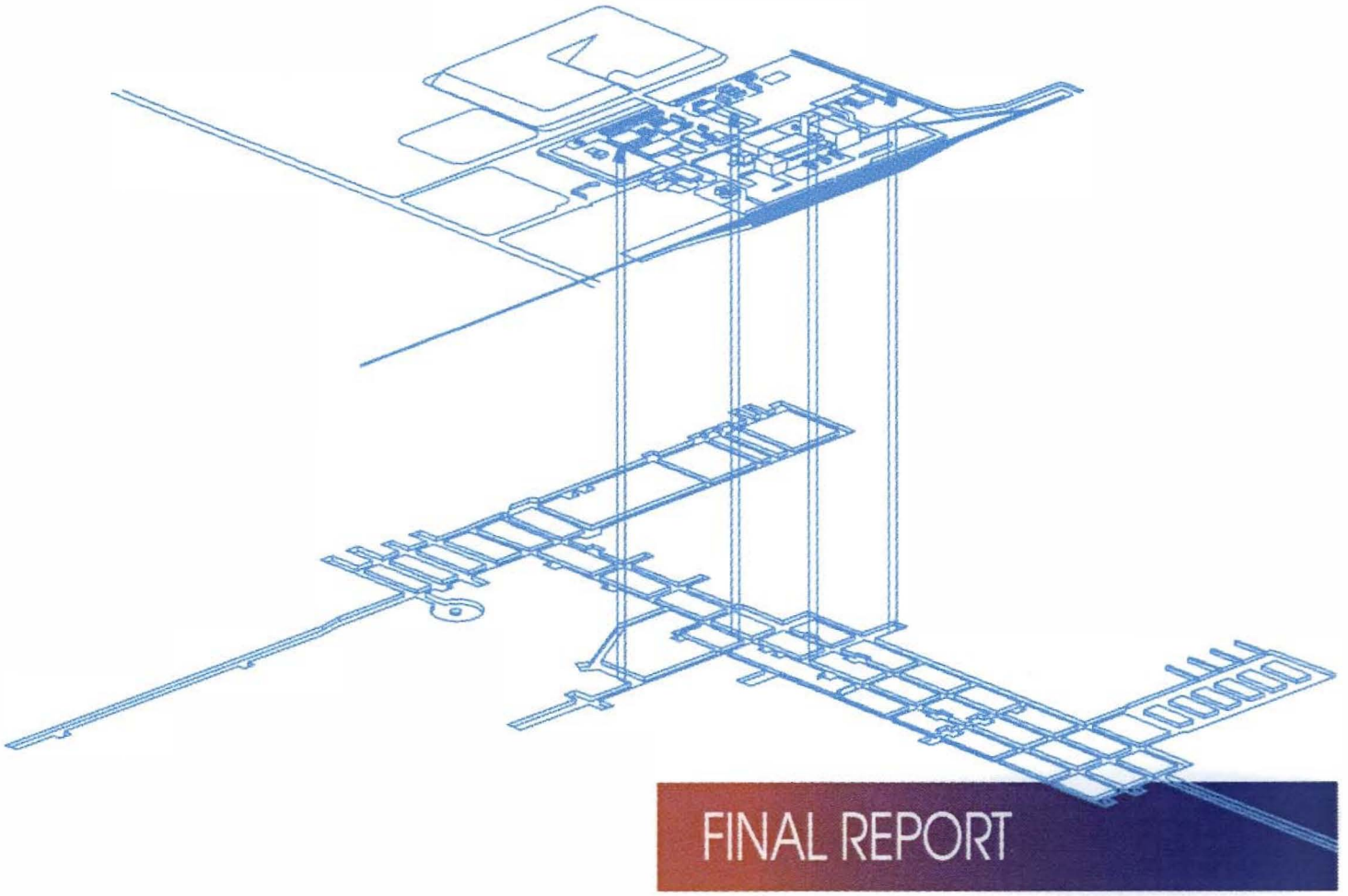

FINAL REPORT

Table of Contents

List of Tables iv

List of Figures v

List of Abbreviations/Acronyms viii

1.0 Introduction 1-1

1.1 Instrumentation and Digital Processing 1-2

1.2 Description of the GPR Profiles 1-4

1.3 Velocity of the 500-MHz Wave in the Repository Salt 1-4

1.4 Resolution and Reflectivity 1-8

2.0 GPR Surveys in the Vicinity of the Overcast at E-0, N-150 2-1

2.1 Introduction 2-1

2.2 E-0, N-150 Intersection, Roof Surveys 2-1

2.3 Comparisons 1991 and 1992 Roof Surveys 2-2

2.4 Results of the GPR Surveys Near the E-0, N-150 Intersection, March 1991 2-2

2.5 Results of the GPR Surveys Near the E-0, N-150 Intersection, February 1992 2-3

2.6 Results of Comparisons Between 1991 and 1992 Radar Profiles 2-4

2.7 Summary 2-4

3.0 GPR Surveys in Room 1, Panel 1 3-1

3.1 Introduction 3-1

3.2 Room 1, Panel 1, Floor Surveys 3-1

3.2.1 Results of GPR Floor Surveys in Room 1, 1991 3-1

3.2.2 Results of GPR Floor Surveys in Room 1, 1992 3-2

3.3 Results of Comparisons Between 1991 and 1992 GPR Floor Surveys 3-3

3.4 Discussion of Room 1, Floor Results 3-3

3.5 Room 1, Panel 1, Roof Surveys 3-4

3.6 Discussion of Room 1 Roof Results 3-5

3.7 Summary of Room 1 GPR Survey Results 3-6

4.0 GPR Surveys in Room 6, Panel 1 4-1

4.1 Introduction 4-1

4.2 Room 6, Panel 1, Floor Surveys 4-1

4.3 Discussion of Room 6 Floor Results 4-2

4.4 Room 6, Panel 1, Roof Surveys 4-3

Table of Contents *(Continued)*

4.5 Discussion of Room 6 Roof Results 4-4
4.6 Summary of Room 6 Results 4-5
5.0 GPR Surveys of the S-1950 Drift Roof 5-6
5.1 Introduction 5-6
5.2 S-1950 Drift Surveys 5-6
5.3 S-1950 Drift Results 5-7
5.4 Discussion and Summary of the S-1950 Drift Results 5-8
6.0 N-1420 Drift Roof; Room B to Room D 6-1
6.1 Introduction 6-1
6.2 Results of GPR Surveys in the N-1420 Drift 6-2
6.3 Summary of N-1420 GPR Survey Results 6-4
7.0 GPR Surveys in Room Q and Room Q Access Drift 7-1
7.1 Introduction 7-1
7.2 Results of Room Q Surveys 7-1
7.2.1 Circumferential Survey at 77 Ft from Collar 7-2
7.2.2 Circumferential Survey at 65 Ft From Collar 7-3
7.2.3 Circumferential Survey at 43 Ft from Collar 7-4
7.3 Results of Room Q Axial Surveys 7-5
7.4 Discussion of Room Q Radar Survey Results 7-5
7.5 Room Q Access Results 7-6
7.6 Discussion of Room Q Access Results 7-7
7.7 Summary 7-7
8.0 References 8-1

Appendix A—Instrumentation Settings, Processing Sequences, and Radar Profiles: E-0, N-150 Overcast

Appendix B—Instrumentation Settings, Processing Sequences, and Radar Profiles: Room 1, Panel 1

Appendix C—Instrumentation Settings, Processing Sequences, and Radar Profiles: Room 6, Panel 1

Appendix D—Instrumentation Settings, Processing Sequences, and Radar Profiles: S-1950 Drift Roof

Table of Contents *(Continued)*

Appendix E—Instrumentation Settings, Processing Sequences, and Radar Profiles: N-1420 Drift Roof

Appendix F—Instrumentation Settings, Processing Sequences, and Radar Profiles: Room Q and Room Q Access Drift

List of Tables

Table	Title
1-1	Calculated Wave Velocities

List of Figures

Figure	Title
1-1	Surface and Underground Layout of the WIPP Facility As of December 31, 1991
1-2	Locations of GPR Surveys Performed in 1991 and 1992 (WIPP Underground Excavations As of December 31, 1991)
1-3	Diagrammatic Cross Section of a Typical Waste Storage Room at the WIPP
1-4	Frequency Histogram of the Velocity Data
2-1	Locations of GPR Traverses Conducted on the Roof of E-0 near the E-0, N-150 Overcast, March 1991
2-2	Locations of GPR Traverses Conducted on the Roof of E-0 near the E-0, N-150 Overcast, February 1991
2-3	View Looking East, Diagrammatic Cross Section of E-0, N-150 Overcast
2-4	View Looking East; Traverses 7 and 8; E-0, N-150 Overcast: March 1991
2-5	Diagrammatic Representation of the Location of North and South Rib Surveys; E-0, N-150 Overcast: March 1991
2-6	North and South Rib; E-0, N-150 Overcast: March 1991
2-7	View Looking East; Traverses B and I; E-0, N-150 Overcast: February 1992
3-1	Locations of GPR Floor and Roof Traverses and Roof Boreholes in Room 1, Panel 1
3-2	S-1862 Traverse, Room 1, Panel 1 Floor: June 1991
3-3	S-1822 Traverse, Room 1, Panel 1 Floor: June 1991
3-4	S-1862 Traverse, Room 1, Panel 1 Floor: January 1992
3-5	Diagrammatic Cross Section of Room 1, Panel 1
3-6	S-1742 Traverse, Room 1, Panel 1 Roof: June 1991

List of Figures *(Continued)*

Figure	Title
4-1	Locations of GPR Floor Traverse in Room 6, Panel 1
4-2	S-1667 Traverse, Room 6, Panel 1 Floor: January 1992
4-3	S-1674 Traverse, Room 6, Panel 1 Floor: January 1992
4-4	S-1811 Traverse, Room 6, Panel 1 Floor: January 1992
4-5	Locations of GPR Roof Traverses and Roof Boreholes in Room 6, Panel 1
4-6	S-1736 Traverse, Room 6, Panel 1 Roof: January 1992
4-7	S-1798 Traverse, Room 6, Panel 1 Roof: January 1992
4-8	S-1807 Traverse, Room 6, Panel 1 Roof: January 1992
5-1	Locations of GPR Roof Traverses and Roof Boreholes in the S-1950 Drift, Panel 1
5-2	E-0606 Traverse, S-1950 Drift Roof: February 1992
5-3	E-0920 Traverse, S-1950 Drift Roof: February 1992
5-4	Traverse E, E-0920 to E-1060, S-1950 Drift Roof: February 1992 (Vertical Exaggeration 3.5x)
6-1	Locations at GPR Surveys on Roof of N-1420 Drift and EEP Arrays #31, 32, and 33
6-2	E-1480 Traverse, N-1420 Drift Roof: June 1991
6-3	E-1560 Traverse, N-1420 Drift Roof: June 1991
6-4	E-1620 Traverse, N-1420 Drift Roof: June 1991
6-5	E-1120 Traverse, N-1420 Drift Roof: June 1991
6-6	Traverse D, E-1470 to E-1580, N-1420 Drift Roof: June 1991 (Vertical Exaggeration 4x)

List of Figures *(Continued)*

Figure	Title
7-1	Plan View, Room Q Showing Locations of GPR Surveys
7-2	Room Q, GRP Surveys Cross-Sectional View, Looking West (not to scale)
7-3	Isometric View of the Pore Pressure Test Boreholes Relative to the Instrumentation Area and Collar
7-4	Cross-Sectional View of Room Q and the Borehole Array at 75 Feet from the Collar
7-5	Survey 4, Room Q, Circumferential Survey, 77 Feet from the Collar: March 1991
7-6	Survey 6, Room Q, Circumferential Survey, 65 Feet from the Collar: March 1991
7-7	Survey 8, Room Q, Circumferential Survey, 43 Feet from the Collar: March 1991
7-8	Survey 9, Room Q, Axial Survey: March 1991 (Vertical Exaggeration 1.5x)
7-9	Survey 10, Room Q, Axial Survey: March 1991 (Vertical Exaggeration 1.5x)
7-10	Locations of GPR Traverses in Room Q (S-90 Drift)
7-11	Traverse 5, Room Q Access: March 1991

List of Abbreviations/Acronyms

DOE	U.S. Department of Energy
EEP	Excavation Effects Program
ft	foot/feet
GPR	ground-penetrating radar
GSSI	Geophysical Survey Systems Inc.
IT	IT Corporation
m	meter(s)
MHz	megahertz
ns	nanoseconds
SIR-3	Subsurface Interface Radar System-3
SNL/NM	Sandia National Laboratories/New Mexico
SPDV	Site Preliminary Design Validation
WIPP	Waste Isolation Pilot Plant

1.0 Introduction

The Waste Isolation Pilot Plant (WIPP), a U.S. Department of Energy (DOE) research facility, was established to demonstrate the safe disposal of defense-generated transuranic radioactive waste in the United States. The WIPP facility is 26 miles (42 kilometers) east of Carlsbad, New Mexico. The underground workings of the WIPP are approximately 2,150 feet (ft) (655 meters [m]) below the surface (Figure 1-1) in the Salado Formation. The Salado Formation and underlying Castile Formation make up an evaporite sequence over 3,280 ft (1,000 m) thick. The Salado Formation is predominantly bedded halite with minor amounts of argillaceous halite, polyhalitic halite, anhydrite, and clay.

Ground-penetrating radar (GPR) surveys were conducted at the WIPP site in 1991 and 1992 in various areas of the underground workings. The areas surveyed are shown in Figure 1-2 and include the following: (1) The E-0, N-150 overcast area (surveyed in March 1991 and February 1992); (2) Room 1 Panel 1 (surveyed in June 1991 and February 1992); (3) Room 6, Panel 1 (surveyed in January 1991); (4) S-1950 Access Drift (surveyed in February 1992); (5) N-1420 Drift (surveyed in June 1991); and (6) Room Q and Room Q Access Drift (surveyed in March 1991). This report includes data and interpretations derived from these surveys.

GPR is an electromagnetic reflection technique that is sensitive to variations in the dielectrical properties of rock or soil. Interfaces with differing dielectrical properties cause some of the transmitted electromagnetic wave energy to be reflected back to the surface, where it is detected by a coupled antenna/receiver. GPR surveys produce a continuous record of the subsurface conditions in real time as the antenna is moved over the ground surface. The radar reflection technique is analogous to seismic reflection methods, and many of the GPR data-processing schemes incorporate the same algorithms that seismic data processors use.

GPR has been used to map bedrock depth and soil stratigraphy and to detect voids and identify karst features in various rock and soil types (Davis and Annan, 1989). In the underground at the WIPP site, reflections from either air-filled or brine-filled voids, fractures, and stratigraphic contacts are generated by contrasts between the relative dielectric constants of these features and the enclosing halite or anhydrite. Thus, GPR is useful for examining the effects of creep closure on waste storage rooms, access drifts, and experimental rooms.

Creep closure occurs at a rate of a few inches per year in the WIPP excavations (DOE, 1991a). The closure process induces plastic deformation of the halite, as well as fracturing of the halite within the disturbed rock zone. Fracturing occurs because of the contrast in mechanical properties of halite, clay, and anhydrite rock units. Two units in particular, Marker Bed 139 (MB139) and anhydrite "b," appear to have a significant effect on the fracturing observed near the underground excavations. MB139 is an anhydrite unit varying between 2.5 and 3.0 ft in thickness. The top is about 5.0 ft (1.5 m) below the floor of a typical waste room excavation, whereas anhydrite "b" is about 7.0 ft (2.1 m) above the roof of a waste room excavation. Both anhydrite units are underlain by thin clay seams. MB139 is underlain by clay E, and anhydrite "b" is underlain by clay G. The location of the anhydrite units, clay layers, and associated fracturing around a typical waste storage room excavation are shown in Figure 1-3. Using GPR, these units, as well as the fracturing near the excavations, can be identified and observed over time.

GPR surveys conducted in 1991 and 1992 were performed prior to the development of formal procedures for conducting GPR surveys in the underground excavations. The methods used to conduct the surveys were adapted from the operations manual of the radar system (GSSI, 1987) and were similar to those outlined in WIPP procedure #07-318 (DOE, 1990a). A detailed description of WIPP GPR survey practices is also contained in Francke (1990) and in Kannenberg (1991).

1.1 Instrumentation and Digital Processing

A Geophysical Survey Systems, Inc. (GSSI), Subsurface Interface Radar System-3 (SIR-3) was used to conduct the radar surveys. A 500-megahertz (MHz) (1 MHz = 1 x 10^6 cycles/ second) antenna was used both to transmit and receive electromagnetic waves. The antenna was modified prior to the 1991 surveys to include a dual-transmit power and a dual-receiver gain function. The four possible settings for the 500-MHz antenna are included in Appendix A. The instrument settings used to conduct the surveys are included in Appendices A through F.

Using the SIR-3, data was recorded to an analog tape deck and printed on a chart recorder. Analog data on magnetic tape was subsequently digitized and processed using RADAN I processing software (GSSI, 1989). Digital processing of the data includes horizontal scaling, stacking, horizontal high-pass filtering, deconvolution, vertical bandpass filtering, and

horizontal low-pass filtering. All processing sequences used on the radar data are included in the appendices.

Digital processing of the radar data was done to remove multiple reflections and enhance the radar images by increasing the signal-to-noise ratio of the data. Processing schemes were adapted from the guidelines suggested in the RADAN processing software manual (GSSI, 1989) and from the personal experience of IT geophysicists. A minimal amount of data processing was performed on the data to avoid excess filtering, which can change or remove information. The processing sequences vary slightly between different surveyed areas due to small differences in data quality. A brief description of the type of data processing performed follows.

Horizontal scale normalization was performed first on the data, because variations in the walking speed of the person towing the GPR antenna distorts the horizontal scale. Using the RADAN software, it is possible to normalize the horizontal scale by removing scans or interpolating between scans to arrive at a specific number of scans per linear meter.

After horizontal scale normalization, the data was stacked. Stacking is a data reduction technique that averages a given number of scans, then outputs the average. Stacking increases the signal-to-noise ratio and reduces the size of data files for greater ease in further data manipulations. The amount of stacking depends upon the amount of data collected. Usually, the more data that was collected in a particular survey, the greater the amount of stacking. Care was taken not to overstack data, which can change the appearance of relevant geological features.

Next, a horizontal high-pass filter was applied to the data. Radar images collected at the WIPP site using the SIR-3 generally tend to have a band of low frequency noise that extends across the entire radar profile. This low frequency noise was generated by the SIR-3 radar unit, and a horizontal high-pass filter removes this system noise.

After horizontal high-pass filtering, predictive deconvolution of the data was performed to remove multiple reflections that occur in the data. Often, reflections from air-filled or brine-filled voids or fractures cause multiple reflections or "ringing" in the data set. To remove these multiple reflections, deconvolution is used. Since deconvolution adds considerable output noise to the data, additional frequency filtering is required after deconvolving the data.

Vertical band-pass filtering of the data was performed to remove noise generated by deconvolution. In addition, a horizontal low-pass filter was also applied to the data. Thus, the data is both vertically and horizontally band-pass-filtered. Band-pass filters remove noise at frequencies higher and lower than the specified high and low cut-off frequencies. Care was taken to avoid changing or removing any important information when applying these filters.

1.2 Description of the GPR Profiles

The radar profiles produced from each GPR traverse are cross sections showing travel time to the reflectors versus antenna position. The x-axis of the radar profiles represents the lateral distance of the traverse along the surface, and the y-axis represents the two-way travel time of the reflections; i.e., the time required for the reflected wave to travel from the antenna to the reflecting interface and back to the antenna. A GPR traverse that is completed along the roof or floor a particular drift produces a plane of radar data which extends from the excavation surface into the roof or floor along the line that the antenna is towed. Positive radar amplitude values are displayed as white, whereas negative amplitude values are displayed as black.

Along the right side of the radar profiles is a two-way travel time scale, with units of nanoseconds (ns) (10^{-9} seconds). The excavated surface of either the roof or floor of the surveyed areas is at 0 ns on the radar profiles. Reflections between 0 and 60 ns in the floor radar profiles are from voids, fractures, and stratigraphic contacts located beneath the floor; and reflections between 0 and 60 ns in the roof radar profiles are from voids, fractures, and stratigraphic contacts located above the roof. The depth or height to any relevant geologic feature in a GPR profile is usually expressed as a two-way travel time followed by the distance in ft.

1.3 Velocity of the 500-MHz Wave in the Repository Salt

The wave velocity of the 500-MHz antenna must be obtained to determine the depth below the floor or height above the roof of a particular feature in a GPR traverse. The wave velocity will vary with location in the underground, because the velocity is a function of several parameters, including porosity of the salt, fluid content of the pores (i.e., air or brine), and mineralogical variations in the Salado Formation. Because of porosity changes induced by creep closure of the excavations, the wave velocity can also change with time, even in a specific location. Wherever possible, the wave velocity was calculated from direct correlation

with borehole observations (or known distance) to GPR-detected stratigraphic contacts. The results are compiled in Table 1-1.

The database of radar velocities for halite in Table 1-1 consists of 40 velocity measurements that have been determined from the radar data in this report. (Two-way travel time is rounded to the nearest ns, and velocity is rounded to the nearest one-hundredth of a ft per ns in Table 1-1.) The database in Table 1-1 does not include velocity data from previous radar studies of the WIPP site, which were biased toward higher velocity values due to difficulties in determining the correct position of the floor/roof surface from the radar profiles.

The velocity values from Table 1-1 have been calculated from radar data collected from the roof at various locations in the repository. No velocity data from the floor have been included in this database. It is not known at this time whether or not the average wave velocity for the floor will be the same as the average wave velocity from the roof. However, since the wave velocity in air is approximately 1.0 ft/ns, any increase in the air-filled porosity will likely also increase the wave velocity. Because the floor of a typical waste storage room generally tends to have more fracturing of the halite than the roof, the wave velocity may be greater for the floor. Nevertheless, due to the lack of accurate velocity measurements from the floor of the repository, it is presently assumed that the radar wave velocity for halite in the floor is the same as the wave velocity of halite in the roof.

To calculate an average wave velocity for WIPP halite, the distribution of the velocity data was determined. Figure 1-4 is a frequency histogram of the velocity data from Table 1-1. The shape of the frequency histogram indicates that the data is log-normally distributed. Therefore, the average velocity value can be determined by taking the geometric mean of the velocity data. The geometric mean calculated from the data in Table 1-1 is 0.37 ft/ns.

The mean wave velocity of 0.37 ft/ns was used to convert two-way travel times in ns to distance to reflectors in ft. This conversion is accomplished by dividing the two-way travel time by two to determine the one-way travel time and then multiplying by the mean velocity of 0.37 ft/ns to calculate the distance in ft to the feature of interest. Because of small variations in the wave velocity of the halite, distance measurements to a particular feature calculated using an average wave velocity may not be strictly accurate. However, these measurements are a good approximation of the actual depth of the feature.

Table 1-1
Calculated Wave Velocities

Room/Drift Location	Location of GPR Traverse (Survey Date)	Borehole Number	Reflector	Distance to Reflector (ft)[a]	Two-Way Travel Time (ns)[b]	Velocity (ft/ns)[c]
Room 1 Panel 1 Roof	S-1862 (6/20/91)	01017	Clay G	6.55	36	0.37
Room 1 Panel 1 Roof	S-1862 (6/20/91)	OH83	Clay G	6.70	37	0.36
Room 1 Panel 1 Roof	S-1862 (6/20/91)	OH84	Clay G	6.70	37	0.37
Room 1 Panel 1 Roof	S-1862 (6/20/91)	OH85	Clay G	6.80	37	0.37
Room 1 Panel 1 Roof	S-1862 (6/20/91)	OH86	Clay G	6.70	37	0.36
Room 1 Panel 1 Roof	S-1782 (6/20/91)	01018	Clay G	7.00	39	0.36
Room 1 Panel 1 Roof	S-1782 (6/20/91)	OH87	Clay G	7.00	37	0.37
Room 1 Panel 1 Roof	S-1782 (6/20/91)	OH88	Clay G	7.20	37	0.39
Room 1 Panel 1 Roof	S-1782 (6/20/91)	OH89	Clay G	7.30	41	0.36
Room 1 Panel 1 Roof	S-1782 (6/20/91)	OH90	Clay G	6.20	34	0.36
Room 1 Panel 1 Roof	S-1702 (6/20/91)	01019	Clay G	6.52	36	0.36
Room 1 Panel 1 Roof	S-1702 (6/20/91)	OH82	Clay G	6.75	36	0.38
Room 1 Panel 1 Roof	S-1702 (6/20/91)	OH91	Clay G	6.70	38	0.35
Room 1 Panel 1 Roof	S-1702 (6/20/91)	OH92	Clay G	6.50	36	0.36
Room 1 Panel 1 Roof	S-1702 (6/20/91)	OH94	Clay G	6.60	35	0.38
Room 6 Panel 1 Roof	S-1798 (1/31/92)	BPC1	Clay G	6.70	35	0.39
Room 6 Panel 1 Roof	S-1807 (1/31/92)	BPC1	Clay G	6.70	34	0.40
Room 6 Panel 1 Roof	S-1807 (1/31/92)	BPC2	Clay G	5.85	33	0.36
Room 6 Panel 1 Roof	S-1807 (1/31/92)	BPC3	Clay G	6.10	33	0.37
Room 6 Panel 1 Roof	S-1811 (1/31/92)	BPC2	Clay G	5.85	29	0.40
Room 6 Panel 1 Roof	S-1811 (1/31/92)	BPC3	Clay G	6.10	29	0.43

Table 1-1 *(Continued)*
Calculated Wave Velocities

Room/Drift Location	Location of GPR Traverse (Survey Date)	Borehole Number	Reflector	Distance to Reflector (ft)[a]	Two-Way Travel Time (ns)[b]	Velocity (ft/ns)[c]
S-1950 Drift Roof	E-0660 (2/6/92)	OH95	Clay G	6.40	34	0.38
S-1950 Drift Roof	E-0854 (2/6/92)	OH96	Clay G	6.90	37	0.37
S-1950 Drift Roof	E-1060 (2/6/92)	OH97	Clay G	6.00	34	0.35
S-1950 Drift Roof	E-1062 (2/6/92)	OH97	Clay G	6.00	33	0.36
S-1950 Drift Roof	Traverse I (2/6/92)	DHP401	Clay G	8.30	38	0.44
S-1950 Drift Roof	Traverse G (2/6/92)	DHP401	Clay G	8.30	37	0.45
N-1420 Drift Roof	E-1100 (6/19/91)	EEP Array #33-E	Clay I	5.10	28	0.37
N-1420 Drift Roof	E-1100 (6/19/91)	EEP Array #33-A	Clay I	5.20	30	0.35
N-1420 Drift Roof	E-1100 (6/19/91)	EEP Array #33-C	Clay I	5.30	30	0.36
N-1420 Drift Roof	E-1120 (6/19/91)	EEP Array #33-E	Clay I	5.10	28	0.37
N-1420 Drift Roof	E-1120 (6/19/91)	EEP Array #33-A	Clay I	5.20	29	0.36
N-1420 Drift Roof	E-1120 (6/19/91)	EEP Array #33-C	Clay I	5.30	30	0.36
N-1420 Drift Roof	E-1380 (6/19/91)	EEP Array #31-E	Clay I	4.60	24	0.39
N-1420 Drift Roof	E-1380 (6/19/91)	EEP Array #31-A	Clay I	4.50	23	0.39
N-1420 Drift Roof	E-1380 (6/19/91)	EEP Array #31-C	Clay I	4.10	24	0.35
N-1420 Drift Roof	E-1480 (6/19/91)	EEP Array #32-E	Clay I	4.75	24	0.39
N-1420 Drift Roof	E-1480 (6/19/91)	EEP Array #32-A	Clay I	5.00	26	0.39
N-1420 Drift Roof	E-1480 (6/19/91)	EEP Array #32-C	Clay I	5.00	26	0.38

[a]ft = feet
[b]ns = nanoseconds
[c]ft/ns = feet per nanosecond

1.4 Resolution and Reflectivity

Resolution is the measure of a technique's ability to distinguish between the top and bottom of a particular reflector. Resolution is strongly dependent on the frequency of the transmitted signal; short wavelengths can resolve more closely spaced interfaces than can long wavelengths. However, short wavelengths cannot penetrate as deeply into the subsurface as longer wavelengths, because rock and soil tend to filter out high-frequency electromagnetic energy (i.e., the earth is a low-pass filter).

An estimate of the resolution of the radar system is simply the velocity times the period of the transmitted wave (Annan and others, 1988). Using the experimentally determined average wave velocity of 0.37 ft/ns, the resolution of the 500-MHz wave in the repository salt is calculated to be about 0.75 ft (0.23 m). Therefore, the 500-MHz antenna system can detect separate reflections from interfaces about 0.75 ft (0.23 m) apart. Even if a feature is too thin for the radar to resolve its top and bottom clearly, it can still yield a strong reflection (Annan and others, 1988).

For layers that are thin compared to the radar wavelength (i.e., less than 0.75 ft (0.23 m)), the response amplitude (i.e., the reflectivity) is proportional to the layer thickness (Annan and others, 1988). For the thin-layer case, the response amplitude increases with increasing layer thickness up to the resolution of the system. For example, two air-filled fractures, one with an aperture of 2 inches (0.8 cm) and one with an aperture of 3 inches (1.2 cm), would both be below the resolution of the 500-MHz radar system, although not below the detection limit. The reflected amplitude of the 3-inch (1.2 cm) aperture fracture would be greater than the reflected amplitude of the 2-inch (0.8 cm) aperture fracture, assuming the two fractures were located in salt with identical values of relative dielectric constants. The response amplitude may also be a function of fracture brine content. An interface of dry salt and brine-saturated material has a larger dielectric constant contrast than an interface of dry salt and air. Hence, an interface of dry salt and brine will return much larger amplitude reflections than dry salt and air. Therefore, variations in response amplitudes on the same GPR traverse from year to year may be caused by either an increase or decrease in the fracture aperture width or an increase or decrease in brine content of the fracture.

To compare the reflectivity of any GPR traverse from year to year, the conditions of the radar experiment must be identical. The data must be collected with the same radar instruments, and the same instrument settings must be used. Additionally, to compare the response

amplitudes of a particular feature, the data must be processed in the same fashion from year to year. Radar data collected from the WIPP site in 1991 were recorded in analog form on an audio cassette deck, and the input gains on the cassette deck were noted. Unfortunately, the original cassette deck was damaged and then replaced with a different cassette deck. Because different analog cassette decks measure the input gains differently, the exact conditions of the experiment could not be reproduced in the GPR data collected in 1992. Therefore, quantitative comparisons between data collected in 1991 and data collected in 1992 could not be achieved using the SIR-3. However, qualitative comparisons can still be made. Using a digital data acquisition system such as the Subsurface Interface Radar System-10 on future radar surveys could enable quantitative comparisons to be made.

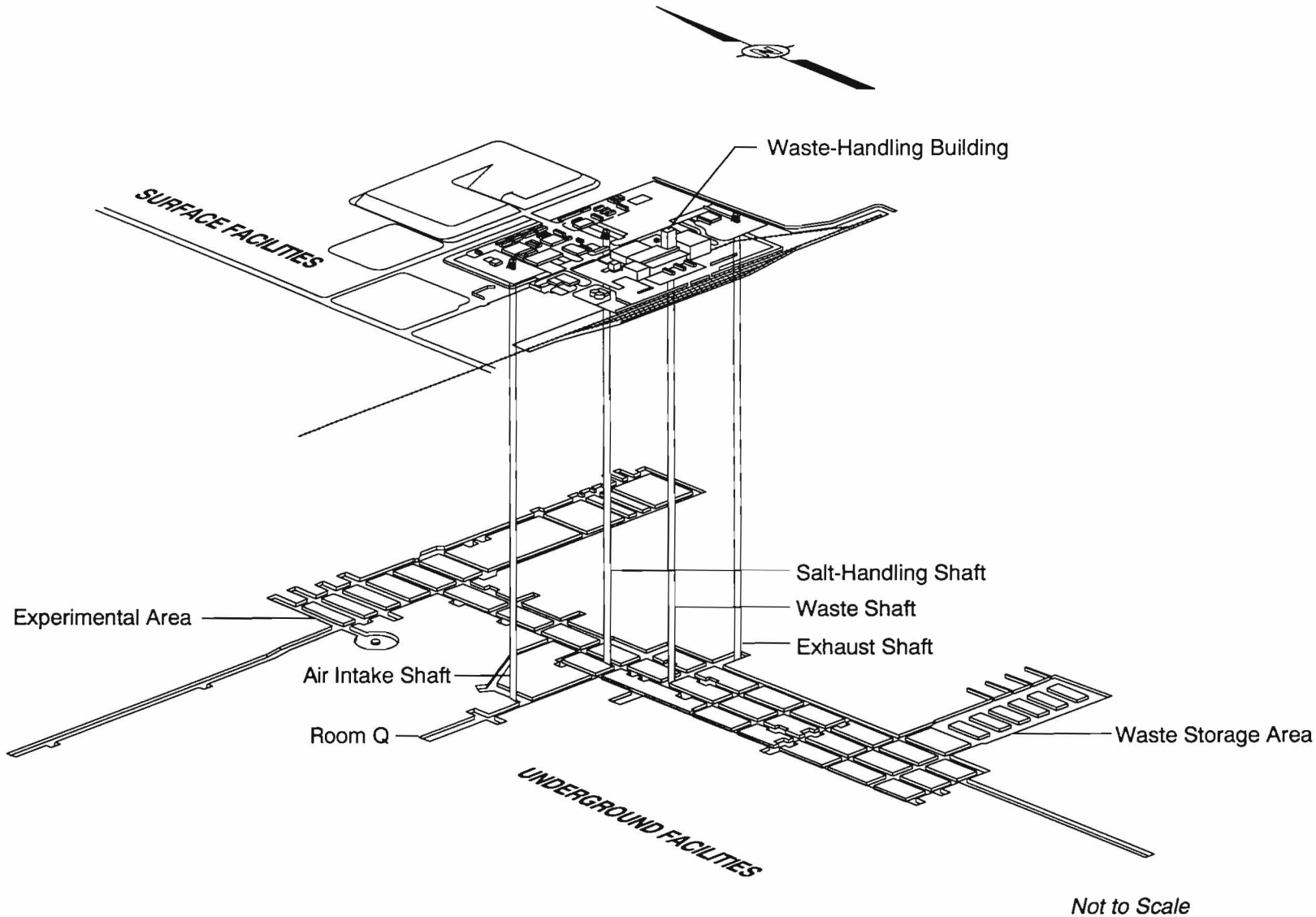

Figure 1-1
Surface and Underground Layout of the WIPP Facility
As of December 31, 1991

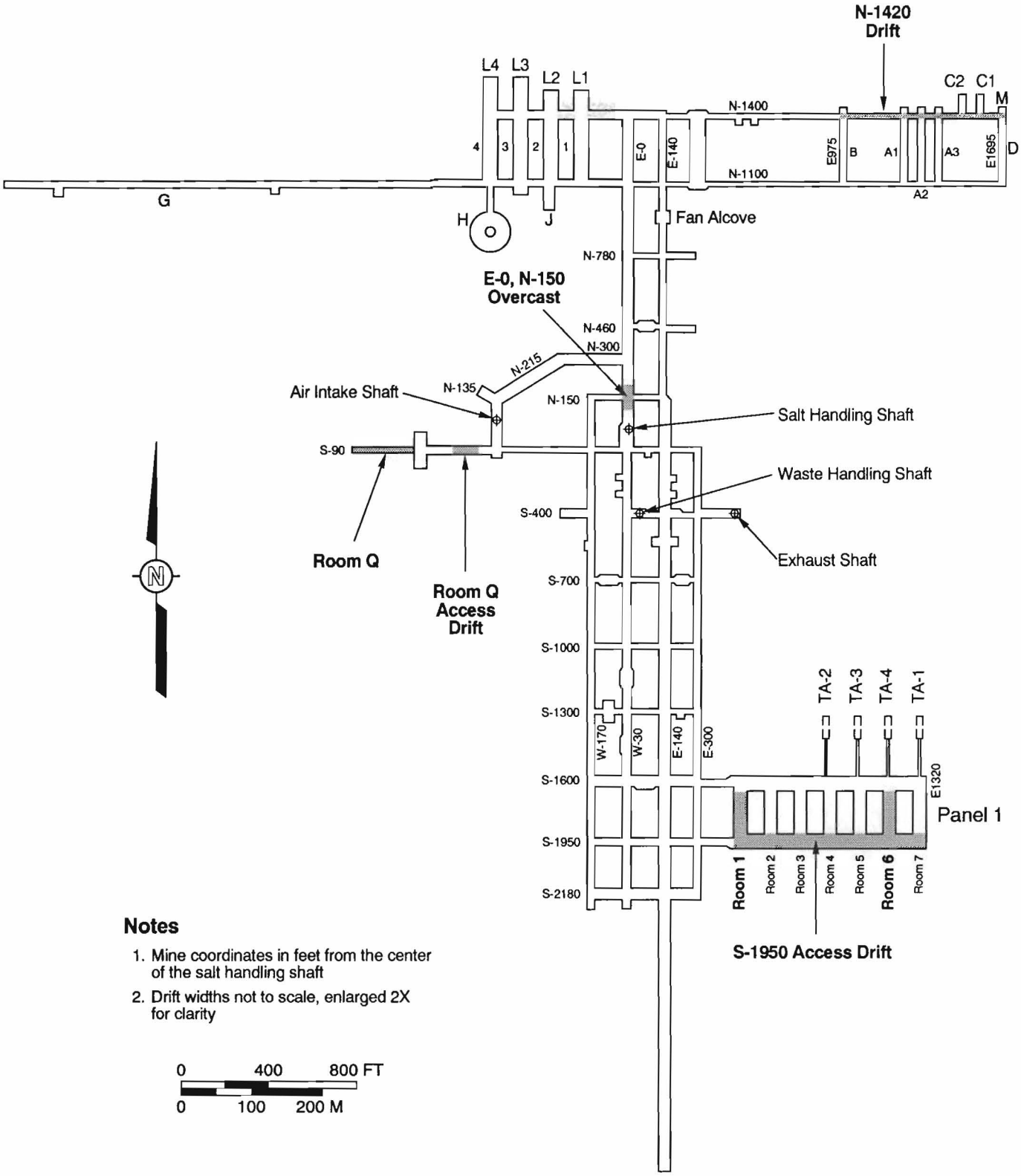

Figure 1-2
Locations of GPR Surveys Performed in 1991 and 1992
(WIPP Underground Excavations As of December 31, 1991)

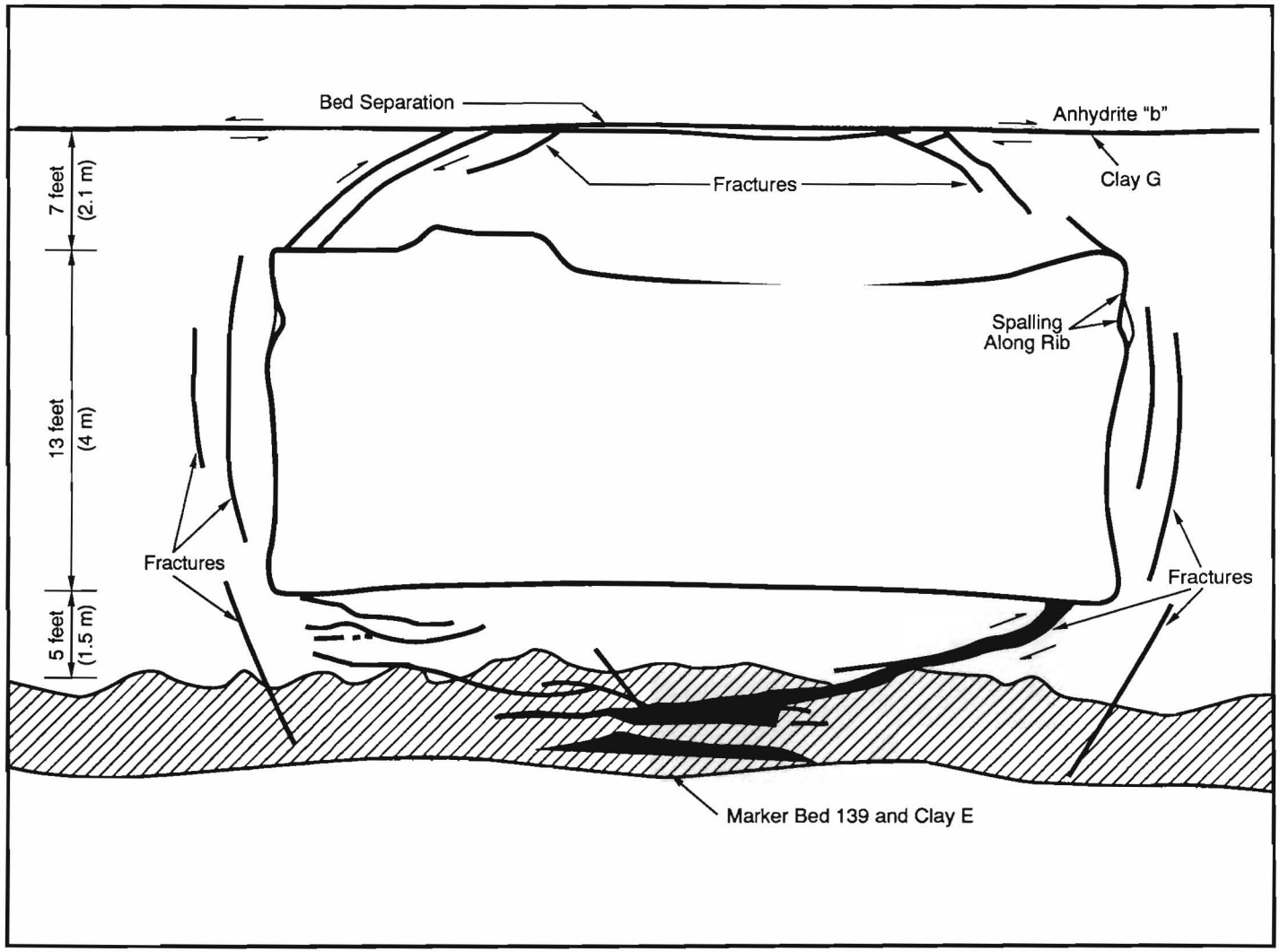

Figure 1-3
Diagrammatic Cross Section of a Typical Waste Storage Room at the WIPP

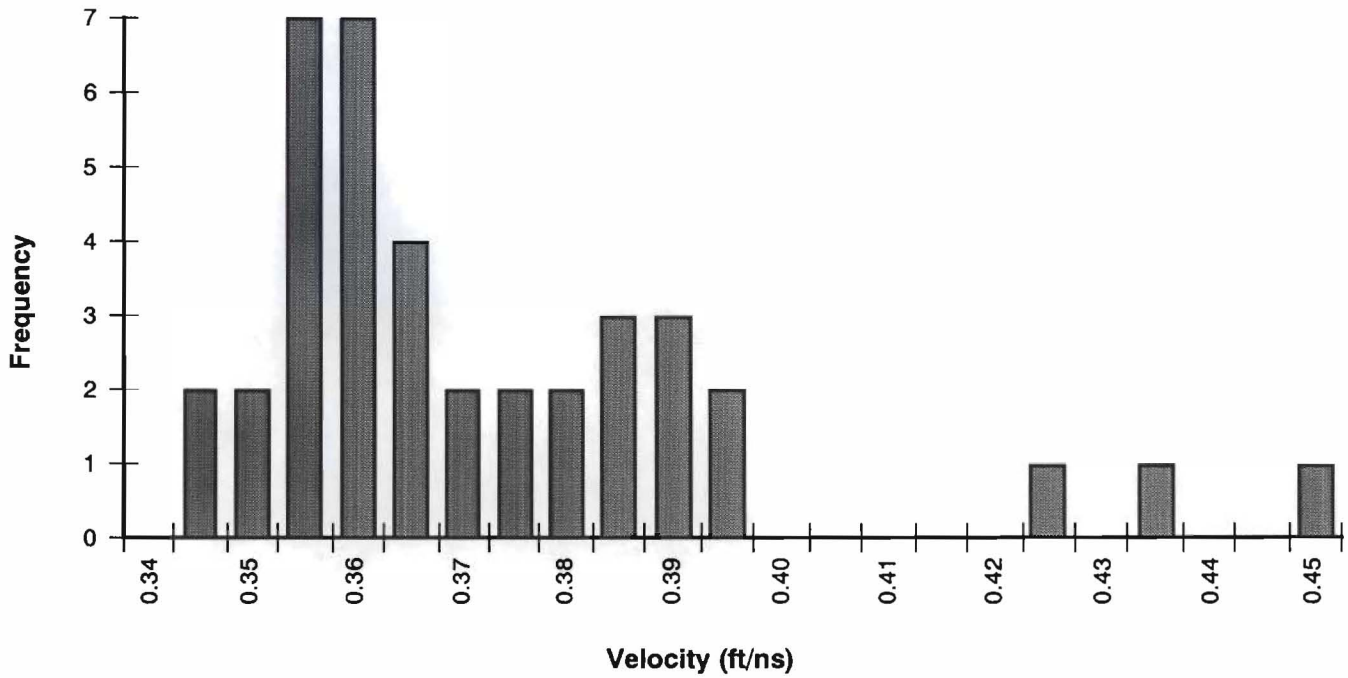

Figure 1-4
Frequency Histogram of the Velocity Data

2.0 GPR Surveys in the Vicinity of the Overcast at E-0, N-150

2.1 Introduction

GPR surveys were conducted on the roof of the E-0 Drift in the vicinity of the overcast at the E-0, N-150 intersection in March 1991 and February 1992. (See Figure 1-2 for the location of the E-0, N-150 intersection.) Radar surveys were performed to determine the extent of fracturing in the vicinity of the E-0, N-150 overcast. Radar surveys collected in successive years are compared qualitatively to determine if changes in fracturing have occurred.

The E-0, N-150 overcast was constructed so that the exhaust airflow that moves through the N-150 Drift would not mix with the intake airflow, which moves through the E-0 Drift. At the intersection of the E-0 and the N-150 Drift, the exhaust air from the N-150 Drift is forced up over the E-0 Drift through the overcast. Since the collection of radar data in February 1992, the geometry of the E-0, N-150 overcast has undergone engineering modification. Only the original geometry of the overcast as of February 1992 is discussed in this report.

2.2 E-0, N-150 Intersection, Roof Surveys

The locations of the eight original E-0 roof traverses collected on March 14, 1991, are shown in Figure 2-1. Also shown in Figure 2-1 are the locations of the brow north of the intersection and the bulkhead immediately south of the intersection. Two GPR traverses were also conducted above the intersection within the overcast—one on the north rib and one on the south rib in March 1991. The locations of 14 radar traverses collected in February 1992 are shown in Figure 2-2. Radar profiles from the E-0, N-150 overcast area that are not discussed in the body of this report are included in Appendix A, along with the instrumentation settings used to conduct the radar traverses and the processing sequences used to analyze the data.

A diagrammatic cross section of the overcast area is shown in Figure 2-3. This figure illustrates the geometry of the overcast area as of February 1992. The view of the figure is looking east and shows the north brow, the south bulkhead, and anhydrite "b." Anhydrite "b" is located about 7.5 ft above the roof of the E-0 Drift. The location of the antenna for GPR surveys collected within the overcast is also shown. Additionally, the locations of the vertical planes of GPR data from surveys conducted along the roof of the E-0 Drift are shown. This

data is collected when the antenna is moved along the roof surface. The antenna position for these surveys is not shown.

Reflections that occur in GPR traverses from the roof of the E-0 Drift are discussed below. The average radar wave velocity of 0.37 ft/ns was used to convert the two-way travel times of the reflections in ns to distances to the reflectors in ft (see Section 1.3). Thus, dividing the two-way travel time of the reflection by 5.35 ns/ft gives the distance to the reflections (5.35 is two times the reciprocal of 0.37 ft/ns).

2.3 Comparisons 1991 and 1992 Roof Surveys

Because radar data collected in March 1991 was collected with different instrumentation settings than radar data collected in February 1992, it was necessary to use different processing sequences when analyzing this data. Processing was accomplished so that radar profiles from March 1991 and February 1992 were similar in appearance to facilitate qualitative comparisons between 1991 and 1992 data.

Evidence of additional deformation due to continued creep closure of the E-0, N-150 intersection opening includes an increase in a previously detected fracture's lateral and vertical extent and the development of additional fractures in the deforming salt. Increased response amplitudes (i.e., reflectivity) of fractures could also indicate a change in the aperture and/or brine content of the fracture. Since data collection and processing sequences are different from the 1991 and the 1992 surveys, this interpretation is highly subjective (Figures 2-4 and 2-7 and Appendix A).

2.4 Results of the GPR Surveys Near the E-0, N-150 Intersection, March 1991

Figure 2-4 shows traverse 7 and traverse 8 from the roof of the E-0 Drift. Traverse 8 was conducted along the center of the E-0 Drift from the north brow to the north edge of the overcast (Figures 2-4 and 2-1), while traverse 7 was conducted from the south edge of the overcast to the bulkhead south of the intersection again along the center of the E-0 Drift (Figures 2-4 and 2-1).

Traverse 8 (Figure 2-4) shows many reflections due to fracturing in the roof of the E-0 Drift north of the overcast area. The fractures begin and extend downward from between about 20 ns (3.7 ft) to about 35 ns (6.5 ft) into the roof (Figure 2-4). The fractures angle downward until they terminate against the north rib of the overcast at 10 ns (1.9 ft), 20 ns (3.7 ft), and

25 ns (4.7 ft). Additionally, one fracture starts at about 45 ns (8.4 ft) into the roof, angles downward, towards anhydrite "b"/clay G zone at about 34 ns (6.4 ft).

Fractures displaying similar geometries were detected in traverse 7 conducted from the south edge of the overcast to the bulkhead south of the E-0, N-150 intersection (Figures 2-4 and 2-1). Reflections interpreted to be due to fractures intersect the south rib of the overcast at 10 ns (1.9 ft), 18 ns (3.4 ft), and 34 ns (6.4 ft) (Figure 2-4). These fractures extend downward from distances between 17 and 43 ns (3.2 and 8.0 ft) into the roof.

GPR surveys were also conducted within the overcast along the north and south ribs of the overcast. Figure 2-5 is a diagrammatic representation of the E-0, N-150 intersection and overcast area. Also shown are the locations of the cross-sectional planes of radar data collected by the two GPR surveys performed within the overcast. The radar data for the two traverses are presented in Figure 2-6, which shows the radar profile from a traverse conducted along the north and south rib above the intersection and within the overcast. The length of the traverses are 10 ft (3.05 m) and begin from the estimated position of the west rib of the E-0 Drift. The largest amplitude reflections for the radar survey completed along the north rib occur at about 28 ns (5.2 ft) into the north rib (Figure 2-6). Large amplitude reflections also occur in the radar survey completed along the south rib. These reflections occur at about 43 ns (8.0 ft) on the west and decrease in time to about 35 ns (6.6 ft) near the center of the radar profile. These large amplitude reflections, which occur in the north and south ribs of the overcast, are believed to be due to vertical east-west striking tensile fractures. These fractures have been mapped and have an aperture width of about 3/16 inch (4.8 millimeters) (Terril, 1991).

2.5 Results of the GPR Surveys Near the E-0, N-150 Intersection, February 1992

Sixteen additional radar surveys were collected approximately one year later (February 10, 1992) from the roof of the E-0 Drift. The locations of GPR traverses collected in February 1992 are shown in Figure 2-2. Traverse B and traverse I were performed in the same locations as traverses 7 and 8 (Figure 2-3) surveyed in March 1991. Figure 2-7 shows the radar profiles for traverses B and I. Traverse B was conducted along the center of the E-0 Drift from the north brow to the north edge of the overcast (Figures 2-7 and 2-2). Traverse I was conducted from the south edge of the overcast to the bulkhead south of the N-150 intersection (Figures 2-7 and 2-2).

Traverse B shows many reflections caused by fracturing in the roof of the E-0 Drift (Figure 2-7). The fractures start between 20 ns (3.7 ft) and 50 ns (9.4 ft) into the roof and angle downward until they terminate against the north rib of the overcast at 10 ns (1.9 ft), 15 ns (2.8 ft), and 25 ns (4.7 ft). Two fractures start between 45 and 50 ns (8.4 and 9.4 ft) into the roof and angle downward towards the anhydrite "b"/clay G zone at about 34 ns (6.4 ft).

Traverse I also shows many reflections caused by fractures in the roof of the E-0 Drift immediately south of the overcast area. Fractures start between 25 and 50 ns (4.7 and 9.4 ft) into the roof and extend downward until they intersect the south rib of the overcast at 15 ns (2.8 ft), 27 ns (5.1 ft), 35 ns (6.5 ft), and 41 ns (7.3 ft) into the roof.

2.6 Results of Comparisons Between 1991 and 1992 Radar Profiles

Comparison of radar surveys collected in February 1992 from the roof of the E-0 Drift (Figure 2-7) with radar surveys collected in March 1991 (Figure 2-4) indicates that some important changes occurred between successive radar surveys.

Radar surveys from 1992 indicate that creep closure of the E-0, N-150 has continued to cause brittle deformation of the overcast area. Evidence of continued brittle deformation is indicated by the increase in length of some fractures in the 1992 surveys as compared to the 1991 surveys. Additionally, the number of fractures detected by GPR in 1992 increased from the number of fractures detected in 1991 (Figures 2-4 and 2-7). The reflectivity also may have increased in the GPR traverses conducted 1992, but this result cannot be quantified. If the reflectivity has truly increased, this would suggest that either fracture aperture widths may have increased and/or fractures may have a higher brine content. The increase in the abundance and length of fractures indicates that brittle deformation has to occur in the roof of the E-0 Drift near the overcast.

2.7 Summary

The general orientation of reflections interpreted to be due to fractures are shown in a diagrammatic cross section of the E-0, N-150 overcast (Figure 2-3). Fractures appear to begin near and above anhydrite "b" and 3 to 4 ft (0.9 to 1.2 m) below anhydrite "b." These fractures extend down to intersect or nearly intersect the north and south ribs of the overcast. Fracturing was verified by physical observation of the overcast. Cracks in both the north and south ribs of the overcast were identified. These cracks had aperture widths that were usually

1/8 inch (3 millimeters) or less. Cracks were generally horizontal and developed parallel to the E-0 roof surface. It is believed that these cracks represent the intersection of at least some of the fractures shown in Figures 2-4 and 2-7.

Physical observations from the roof of the E-0 Drift immediately north and south of the E-0, N-150 intersection detected vertical fractures in the roof that strike east-west (Terril, 1991). Reflections that occur in the GPR profiles from within the overcast along the north and south ribs (Figure 2-5) are believed to be due to vertical fractures located about 5 to 8 ft (1.5 to 2.4 m) into the north and south ribs of the overcast. It is not known how far up into the roof the vertical tensile fractures extended.

If the vertical fractures extended far enough into the roof to intersect the inclined fractures that extend downward from near anhydrite "b" and intersect the ribs of the overcast, conditions are favorable for a partially detached block to form. GPR, along with detailed physical observations, detected and monitored fracturing occurring in the roof of the E-0 Drift. Since the 1992 radar surveys of this area, the overcast geometry has undergone engineering modificaiton to prevent detached blocks from forming.

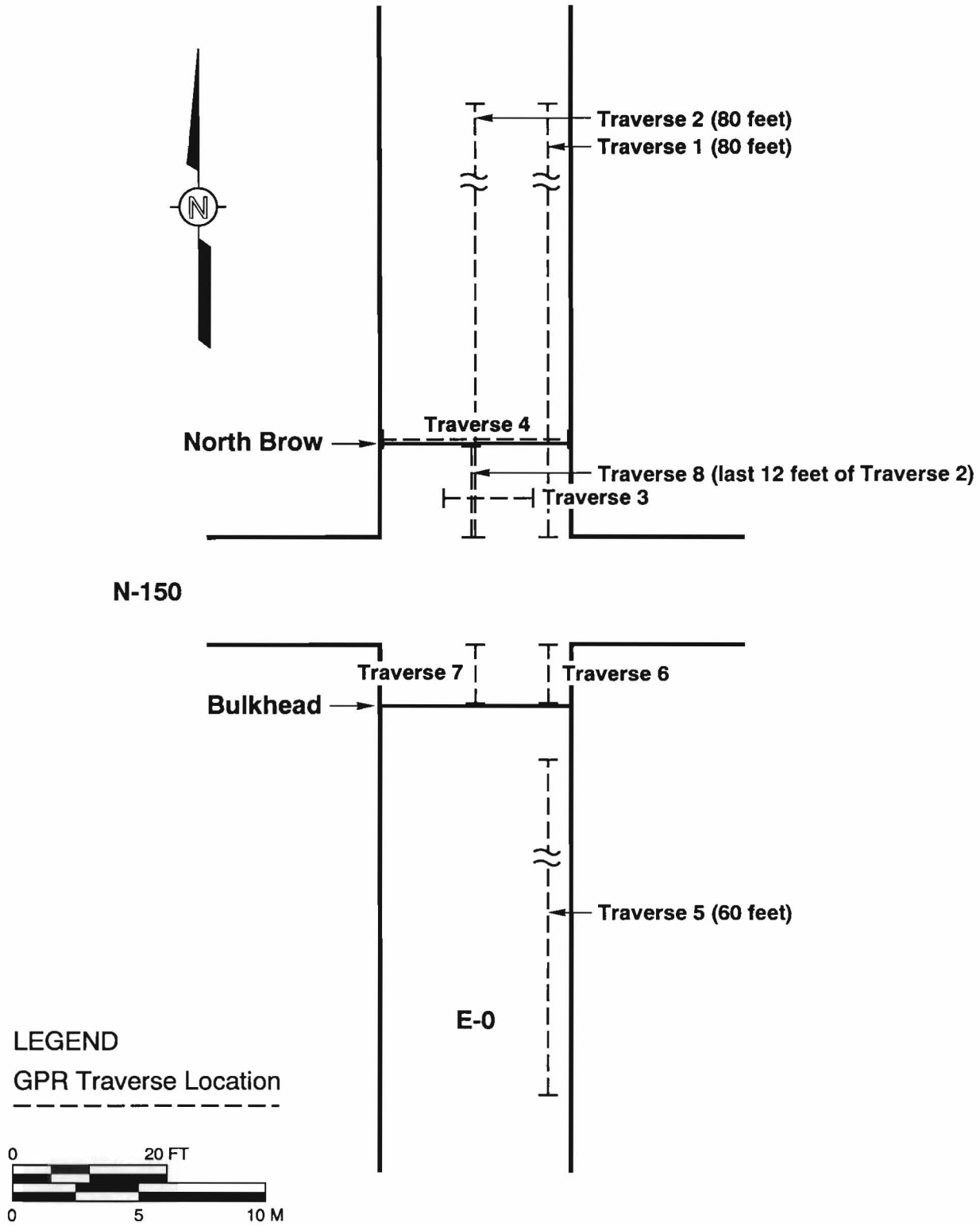

Figure 2-1
Locations of GPR Traverses
Conducted on the Roof of E-0, Near the E-0, N-150 Overcast,
March 1991

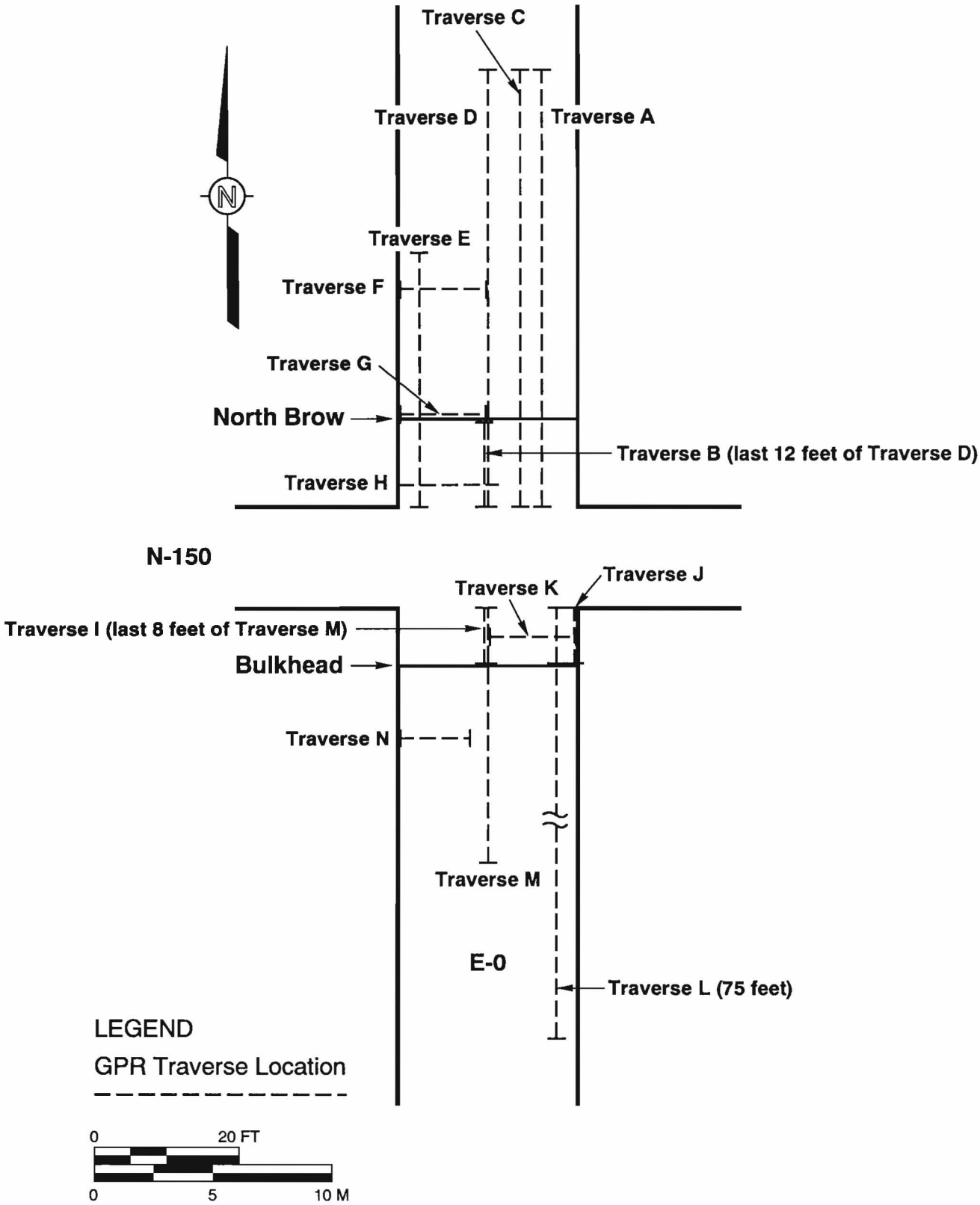

Figure 2-2
Location of GPR Traverses
Conducted on the Roof of E-0, Near the E-0, N-150 Overcast,
February 1992

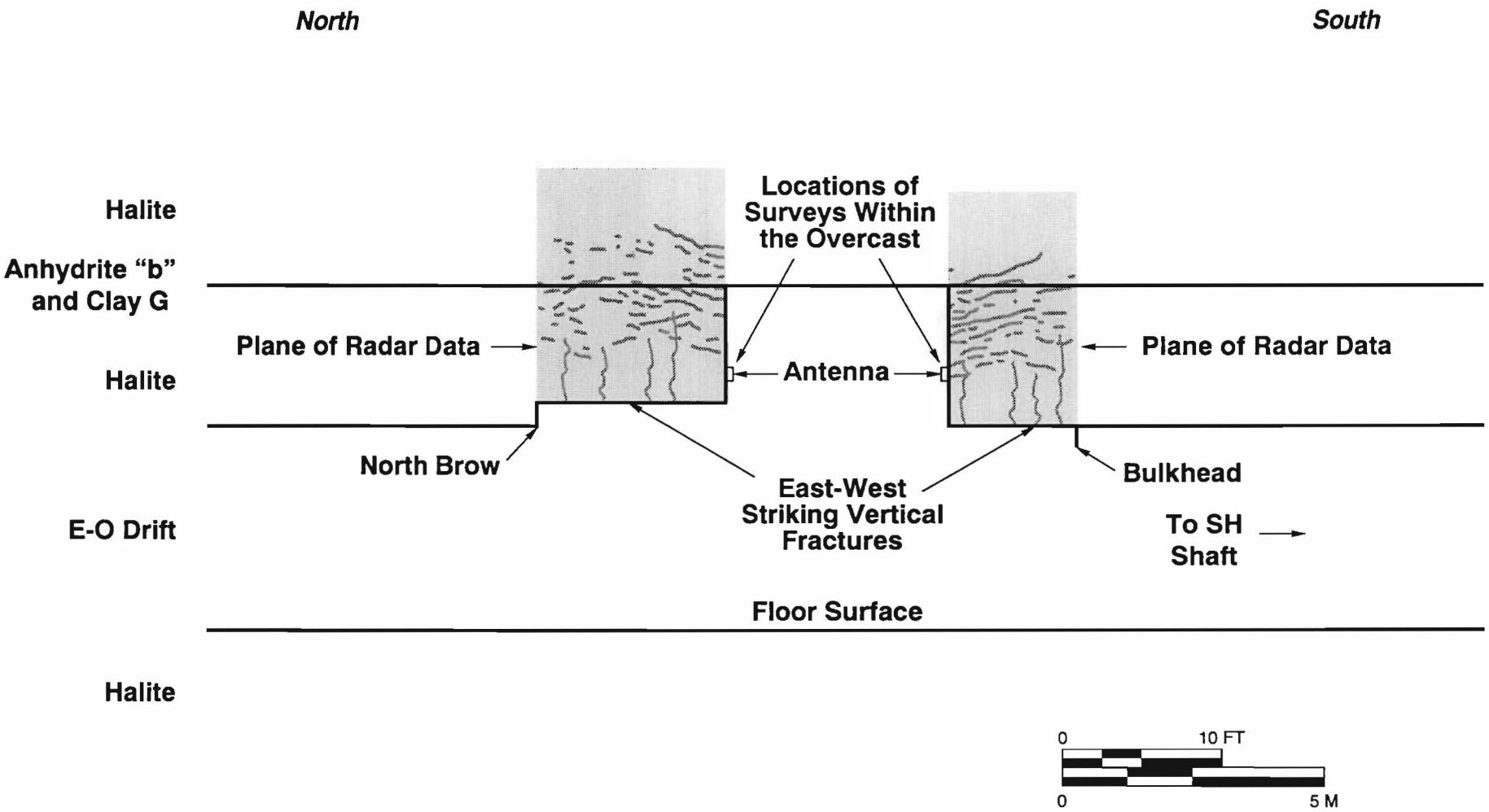

Figure 2-3
View Looking East, Diagrammatic Cross Section of E-0, N-150 Overcast

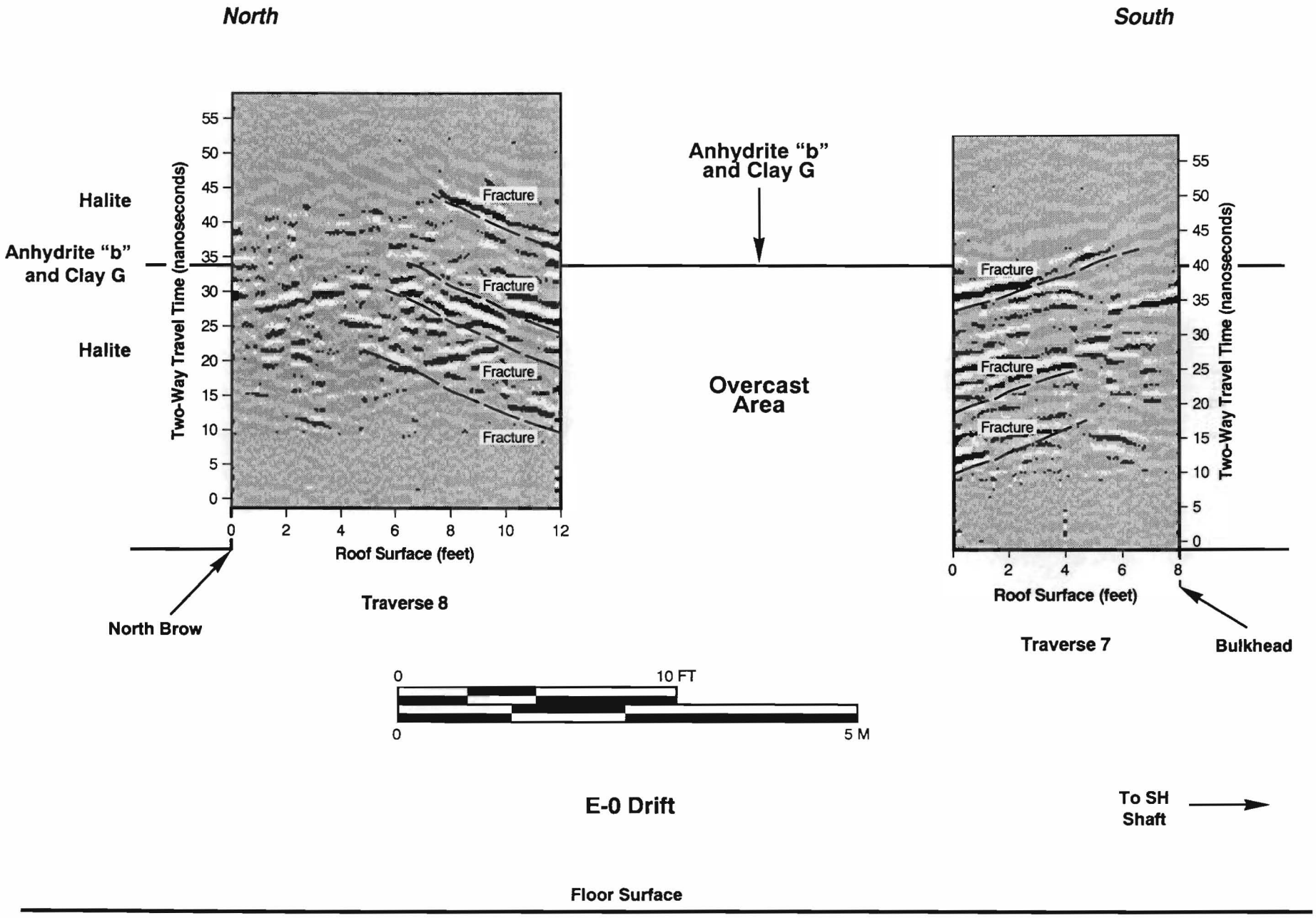

Figure 2-4
View Looking East; Traverses 7 and 8; E-0, N-150 Overcast: March 1991

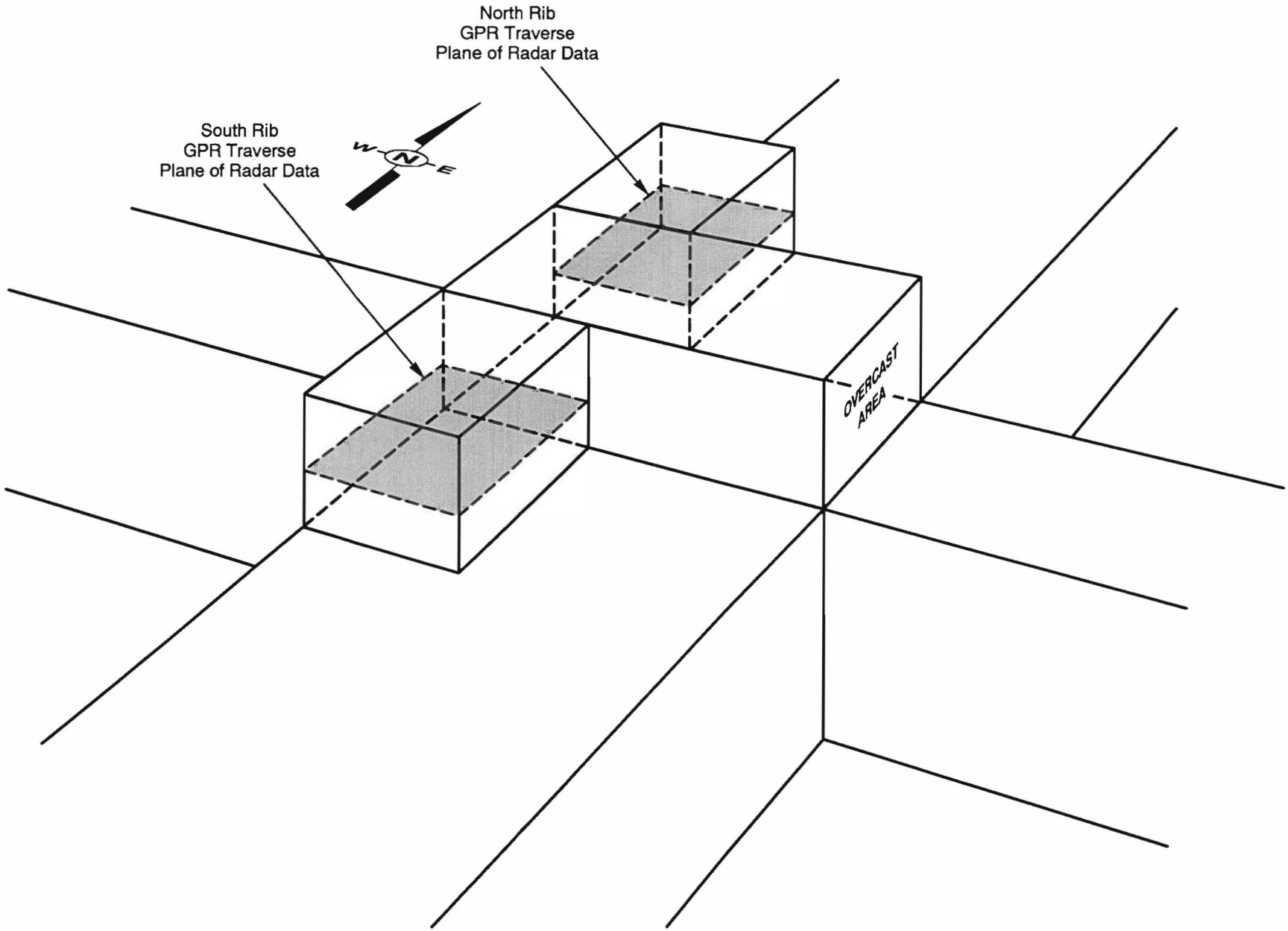

Figure 2-5
Diagrammatic Representation of the Location of North and South Rib Surveys; E-0, N-150 Overcast: March 1991

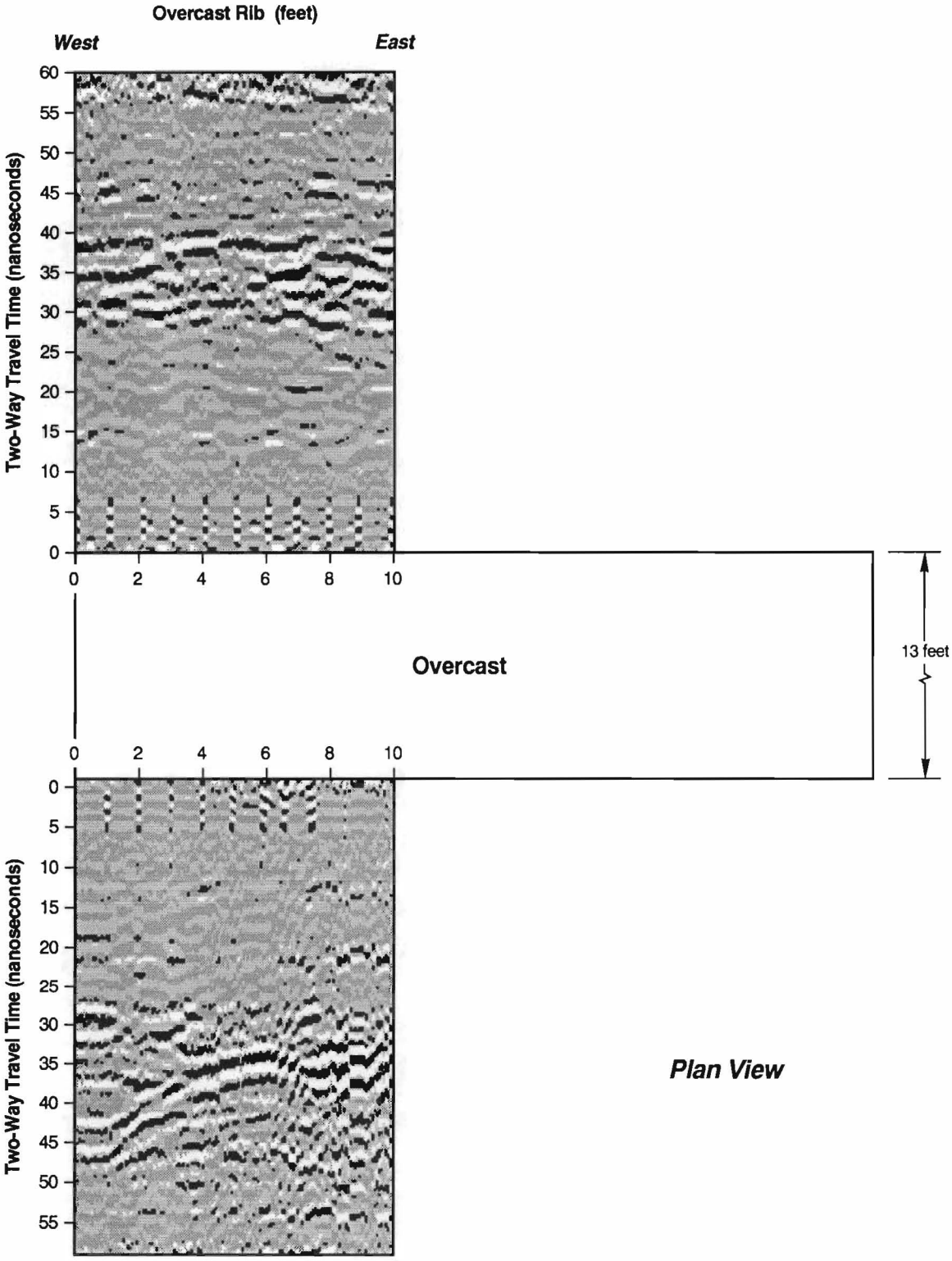

Figure 2-6
North and South Rib; E-0, N-150 Overcast: March 1991

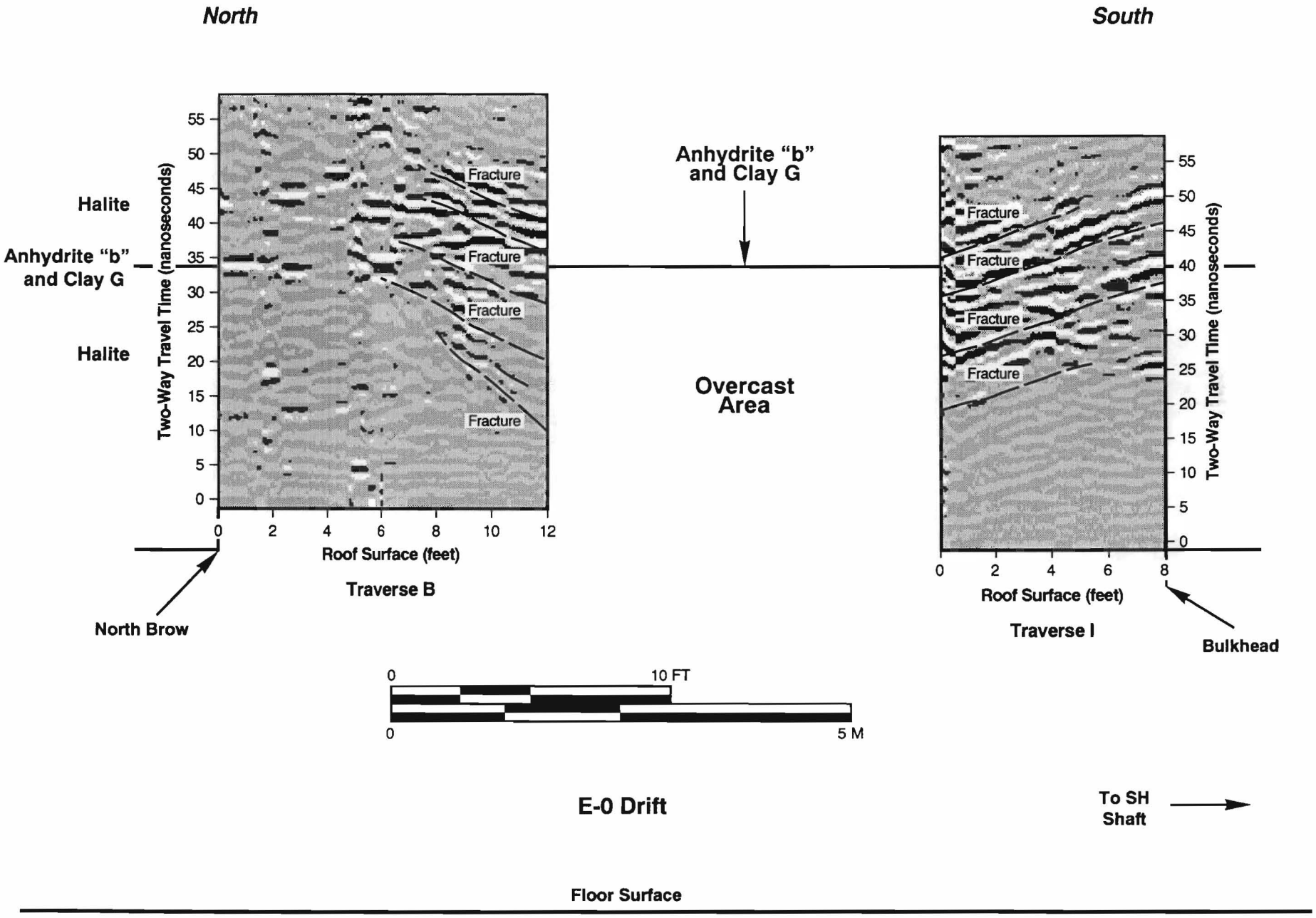

Figure 2-7
View Looking East; Traverses B and I; E-0, N-150 Overcast: February 1992

3.0 GPR Surveys in Room 1, Panel 1

3.1 Introduction

Twenty-two GPR surveys were conducted in Room 1, Panel 1, on June 19 and June 20, 1991 (see Figure 1-2 for the location of Room 1, Panel 1). Eleven of these surveys were performed on the floor, and eleven surveys were performed on the roof of Room 1. Eleven additional floor surveys were collected on February 10, 1992. The locations of the floor and roof GPR surveys in Room 1 are shown in Figure 3-1. The GPR traverses were conducted from west to east perpendicular to the long axis of Room 1, Panel 1. GPR surveys completed in June 1991 and February 1992 were conducted at the same locations as GPR surveys conducted in March 1991. A complete analysis of previously collected radar data from Room 1, Panel 1, for March 1990 to March 1991 is given in DOE, 1991b.

3.2 Room 1, Panel 1, Floor Surveys

The GPR traverses along which the 1991 and 1992 surveys were conducted are shown in Figure 3-1. These traverses are labeled using the WIPP descriptive mine coordinates. The origin of the mine coordinate system is the salt-handling shaft. Since the radar profiles from the GPR traverses conducted on the floor of Room 1 in 1991 and 1992 are similar in appearance, only three different profiles are included and discussed in the body of this report. The remaining radar profiles are included in Appendix B, along with the instrumentation settings used to conduct the traverses and the processing sequences used to produce the radar profiles.

Since there are no boreholes in the floor of Room 1, Panel 1, with which to correlate the GPR results, the average wave velocity of 0.37 ft/ns was used to convert two-way travel times to the reflectors in ns into distance to the reflectors in ft. The two-way travel time to the reflector can be divided by 5.35 ns/ft to give the distance to the reflector in ft.

3.2.1 Results of GPR Floor Surveys in Room 1, 1991

Figure 3-2 is the radar profile from the S-1862 traverse (see Figure 3-1 for the location of radar surveys). An inclined fracture that intersects or nearly intersects the floor surface extends from near the west rib and angles deeper into the floor. The fracture terminates at about 26 ns (4.9 ft). At the inclined fracture's terminus, undulatory reflections extend across the room. The undulatory reflections occur at about 26 ns (4.9 ft). It is believed that the undulatory reflections are at the upper contact of MB139, and the inclined fracture's terminus

is at the fracture's intersection with the top of MB139. Discontinuous reflections at 40 ns (7.5 ft) occur near the west rib, near the center of the room, and near the east rib. These reflections are believed to be due to clay E at the base of MB139. The area between 26 ns and 40 ns (4.9 ft and 7.5 ft) is relatively free of reflections, except near the west rib. This area is interpreted to be MB139, and the reflections in this area, near the west rib, are fractures developed within MB139.

Figure 3-3 is the radar profile from the S-1822 traverse (locations shown in Figure 3-1). An inclined fracture, developed from about 9 ns (1.7 ft) to about 23 ns (4.3 ft) into the floor, extends from near the east rib and angles deeper into the floor. The fracture terminates at the presumed upper contact of MB139. Fractures are also developed above the top of MB139 and extend across the width of the room at about 10 to 26 ns (1.9 to 4.9 ft) into the floor. Large amplitude reflections also occur at about 40 to 45 ns (7.5 to 8.4 ft) into the floor on the west side of the room and near the east rib. These reflections are believed to be due to clay E.

3.2.2 Results of GPR Floor Surveys in Room 1, 1992

Figure 3-4 is the radar profile from the S-1862 traverse from January 1992. This is the same floor traverse that is presented in Figure 3-2 from June 1991. The locations of major fractures and the location of MB139 remain unchanged. However, additional fracturing is noted in the radar data from 1992. Reflections that occur at 5 to 8 ns (0.9 to 1.5 ft) near the east rib are interpreted to be due to subhorizontal fractures near the floor surface. These reflections are not apparent in the data collected in June 1991. In addition, the reflectivity at the lower contact of MB139 has increased.

Curved, concave-down reflections extend from bed separations located at the lower contact of MB139, and intersect at about 47 ns, beneath the center of the floor. These are interpreted to be artifacts generated by reflections from the bed separations. The bed separations are apparently extremely reflective. Stormont (1990) discussed inclinometer measurements conducted in vertically down boreholes near the ribs of two 33-ft-span rooms. These measurements indicated shear offsets along the bottom of MB139 that develop at the rate of about 0.4 inches/year (1.6 mm/year). The excavation of Room 1 was completed in 1986 (DOE, 1991c); therefore, shear offsets with apertures on the order of 2 inches (0.8 cm) (5 years x 0.4 inch/yr) could be developed below clay E in the floor of Room 1, assuming a constant rate of offset. Although 2 inches (0.8 cm) is below the resolution of the 500-MHz

radar system, it is detectable. It is possible that the offsets or bed separations are filled with brine and that the brine greatly increases the reflectivity of the separations.

Figure 3-5 is a schematic diagram showing the location of these bed separations, which may be brine filled. During creep closure of the room, these bed separations could develop between clay E and the underlying salt. Separations may provide an opening in which brine could accumulate. If the geometry of the bed separation or the halite beneath MB139 is curved concave-upward, and the reflections from this feature have a curvature greater than that of approaching wavefronts, then reflection ray paths cross one another on their way to and from the surface. This results in what is knows as the "bow-tie" effect (Dobrin, 1976), which can be observed in the radar profile (Figure 3-4) and other profiles from the floor of Room 1. These reflections are artifacts caused by concave-upward bed separations below MB139.

3.3 Results of Comparisons Between 1991 and 1992 GPR Floor Surveys

Comparison of radar surveys collected in June 1991 and January 1992 show increased amounts of fracturing in surveys collected in January 1992. Subhorizontal fracturing observed near the east rib about 0.9 to 1.5 ft (0.3 to 0.5 m) into the floor of the 1992 data (Figure 3-4) is not observed in GPR data from June 1991 (Figure 3-2). Additionally, increased reflectivity combined with perhaps a greater concave-upward curvature to the interpreted bed separations below MB139 has created a well-defined "bow-tie" effect in the radar data from 1992 (Figure 3-4), which is not present in the data from 1991. This data suggest that increased fracturing and deformation of the halite in the floor of Room 1 occurred between June 1991 and January 1992.

3.4 Discussion of Room 1, Floor Results

There are several types of fractures interpreted to occur in the floor of Room 1. They include the following:

- Inclined fractures near the ribs, which extend from near either rib and angle deeper into the floor, occur in many of the radar traverses from Room 1.

- Subhorizontal fractures that are present across the width of Room 1. These fractures occur between about 10 ns (1.9 ft) to 25 ns (4.7 ft) into the floor. The subhorizontal fractures that occur at about 5 ft often extend from the terminus of fractures, which are developed diagonally from near the ribs.

- Bed separations along clay E. These displacements are caused by bed separations or debonding of the halite below clay E. These separations often occur near the ribs at about 7 to 8 ft into the floor.

There is a zone between the interpreted subhorizontal fractures that occur at about 25 ns (4.7 ft) and clay E at about 35 to 40 ns (6.6 to 7.5 ft) that is relatively free of reflections. This is the estimated location of MB139. Based on this estimated location of MB139, reflections interpreted to be due to fractures occur mainly in the halite above the anhydrite and near clay E below the anhydrite. This general pattern is consistent in all of the radar profiles of the floor of Room 1 and suggests that fracture development is influenced by the presence of MB139.

3.5 Room 1, Panel 1, Roof Surveys

GPR traverses completed on the roof of Room 1 were conducted along the same locations as floor traverses. Roof traverses were completed in June 1991. Lights, cables, and pipes associated with the proposed bin experiments were suspended from the roof of the room at the time of the surveys. These metallic objects presented obstacles that required successively lowering and raising the GPR antenna. Reflections from both the objects and from the roof when the antenna was being lowered or raised caused multiple reflections to be reverberated throughout the 60-ns time range at these particular locations. Therefore, the radar profiles from the Room 1 roof contain a considerable amount of noise. In order to avoid closely spaced pipes and cables near the ribs, the radar traverses were conducted beginning 6 ft from the west rib and concluding 5 ft from the east rib. The total length represented by the horizontal axis of the radar profile from the Room 1 roof is 22 ft, not the full 33-ft width of the room.

The GPR surveys conducted at S-1702, S-1782, and S-1862, (Figure 3-1) were used in part to determine the 500-MHz wave velocity in the halite (see section 1-3). The distances to clay G/anhydrite "b" from the roof surface were taken from the logs of the roof boreholes. The one-way travel time of the reflections from clay G were determined from the radar profiles taken from the traverses located nearest the boreholes, and velocities were calculated (see Section 1-3). The average wave velocity calculated above (0.37 ft/ns) was used to convert two-way travel times to the reflectors in ns to distance to the reflectors in ft. The two-way travel time to the reflector can be divided by 5.35 ns/ft to give the distance to the reflector in ft.

In order to understand how fractures are developing in Room 1, it is useful to know how fracturing has proceeded in the older Site Preliminary Design Validation (SPDV) Test Rooms. Previous GPR surveys from the roof of SPDV Test Room 3 show fractures extending from near each rib and angling deeper into the roof, presumably intersecting with bed separations near clay G (DOE, 1991d). In a later stage of the room's deformation, these fractures could presumably create a triangular- or wedge-shaped salt mass that is nearly decoupled from the surrounding salt. Fractures displaying this geometry could presumably have been developed to a sufficient degree to generate the rock fall in SPDV Test Room 1 (see DOE, 1990b and 1991c). Therefore, it is of interest to determine if fracture development in the roof of Room 1 and other waste storage rooms will proceed in a manner similar to those observed in the SPDV Test Rooms.

The radar profiles of the Room 1 roof only show the middle 22 ft of the room. Therefore, inclined fractures extending from near the roof surface, from each rib, and angling deeper into the roof (i.e., similar to fractures observed in SPDV Test Room 3) would not be readily apparent in this data. Figure 3-6 is the radar profile from the S-1742 traverse (see Figure 3-1 for traverse location). At the left edge of the radar profile, reflections interpreted to be due to a fracture occur at 24 ns (4.5 ft). This fracture is located 6 ft east of the west rib. It is unknown whether or not this fracture extends down to the west rib. The fracture is obscured by the noise generated by reflections from a pipe suspended from the roof and continues angling upward deeper into the roof east of the pipe. The fracture extends to about 32 ns (6.0 ft) into the roof. Clay G is located about 35 ns (6.5 ft) into the roof. Numerous bed separations can be seen just below clay G between 25 and 32 ns (4.7 to 6.0 ft). Near the center of the room, reflections interpreted to be due to another inclined fracture occur from about 25 to 32 ns (4.7 to 6.0 ft) into the roof. Even though this fracture does not extend to the east rib, it is possible that this fracture could be developing into an inclined fracture that will eventually intersect the rib, similar to those observed in SPDV Test Room 3. The S-1742 traverse (Figure 3-6) was the only traverse where these inclined fractures were observed in the Room 1 roof.

3.6 Discussion of Room 1 Roof Results

Other radar traverses collected in the Room 1 roof are similar in appearance to the traverse from S-1742 described above, except for development of the inclined fractures. Appendix B contains radar profiles from the Room 1 roof, that are not discussed above. Except for noise from cables and pipes, the first approximately 25 ns (4.7 ft) of these roof radar profiles are

relatively free from reflections. Thus, little brittle deformation has occurred in the roof in about the first 5 ft. From between about 25 to 38 ns (4.7 to 7.1 ft), numerous reflections interpreted to be bed separations below clay G extend across the roof in Room 1. These bed separations presumably develop due to the opposing directions of lateral movement of salt and the overlying clay G and anhydrite "b," which is usually located about 35 to 38 ns (6.5 to 7.1 ft) into the roof. Above clay G/anhydrite "b" there are few reflections, except areas where noise has been generated from pipes and cables.

3.7 Summary of Room 1 GPR Survey Results

In Room 1, fractures develop diagonally in the floor from near the ribs, extend deeper into the floor, and generally flatten as they intersect MB139. Relatively large amplitude reflections extending from the ribs are believed to be due either to bed separations that occur at the clay E/salt interface or to clay E itself. Subhorizontal reflections also occur at about 1 to 2 ft (0.3 to 0.6 m) into the floor, generally extend partially across the opening, and are present in many of the radar traverses. These reflections are interpreted to be due to fractures or separations developed horizontally within the salt.

Most of the fractures in the Room 1 roof are interpreted to occur below clay G and anhydrite "b." These fractures or bed separations occur between about 5 to 6.5 ft (1.5 to 2.0 m) into the roof. The area between the roof surface and these fracture or bed separations is relatively free from reflections. Reflections near clay G, which are interpreted to be due to bed separations developed between clay G and the underlying salt, probably formed due to the opposing directions of lateral movement of the salt and the overlying clay G and anhydrite "b." Thus, clay G/anhydrite "b" has a pronounced effect on brittle deformation in the roof of Room 1. Inclined fractures that extend up from near the ribs were detected in traverse S-1742 (Figure 3-6). It is not known whether or not the fracture near the west end of this traverse intersects the roof surface near the west rib. The other inclined fracture in this traverse (Figure 3-6) extends down from 32 ns near the center of the drift to about 25 ns. This fracture may be developing into an inclined fracture that could eventually intersect the rib, similar to those observed in SPDV Test Room 3. Additional radar surveys in this area could be used to monitor fracture development in the roof of Room 1.

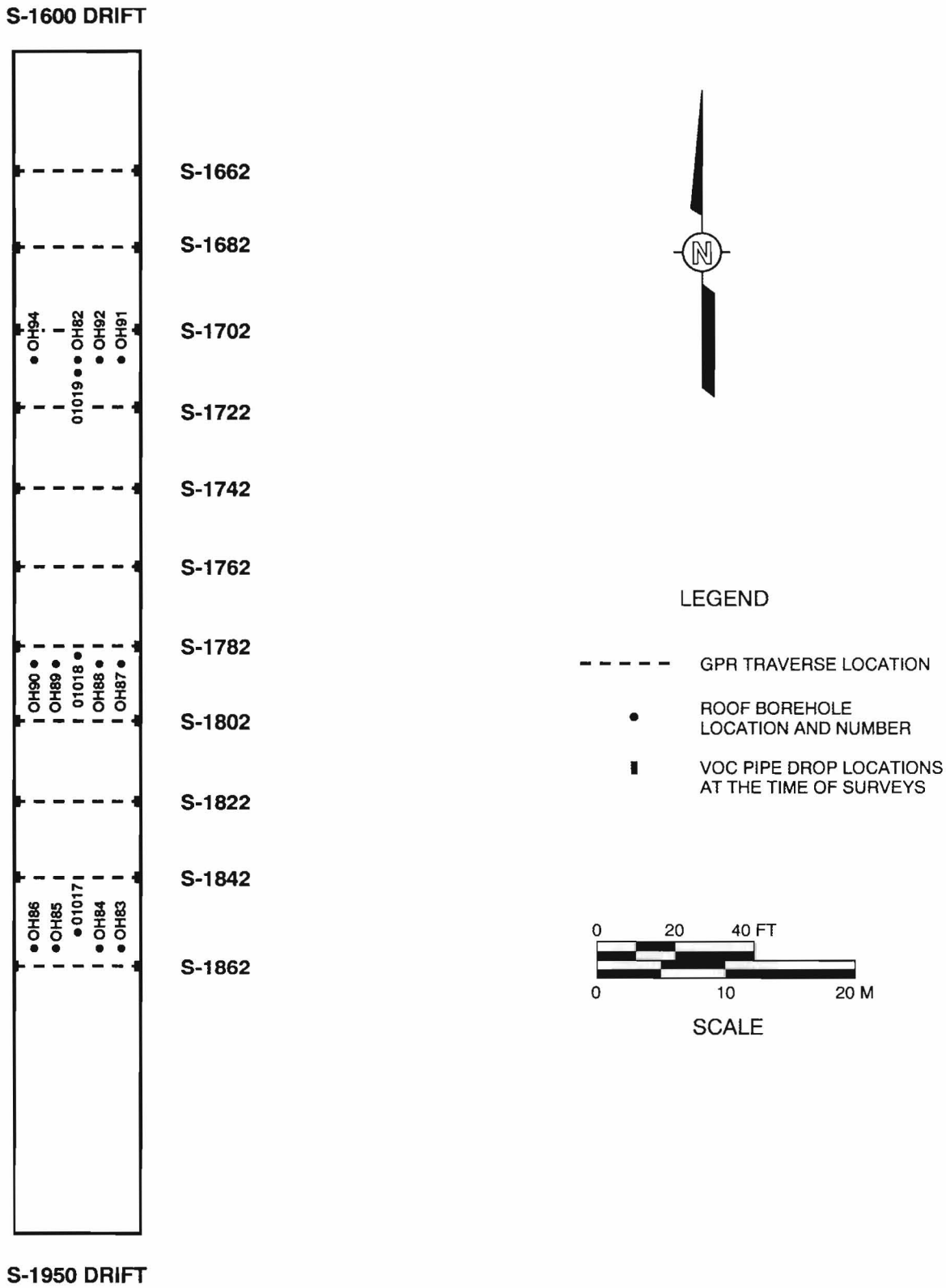

Figure 3-1
Locations of GPR Floor and Roof Traverses and Roof Boreholes in Room 1, Panel 1

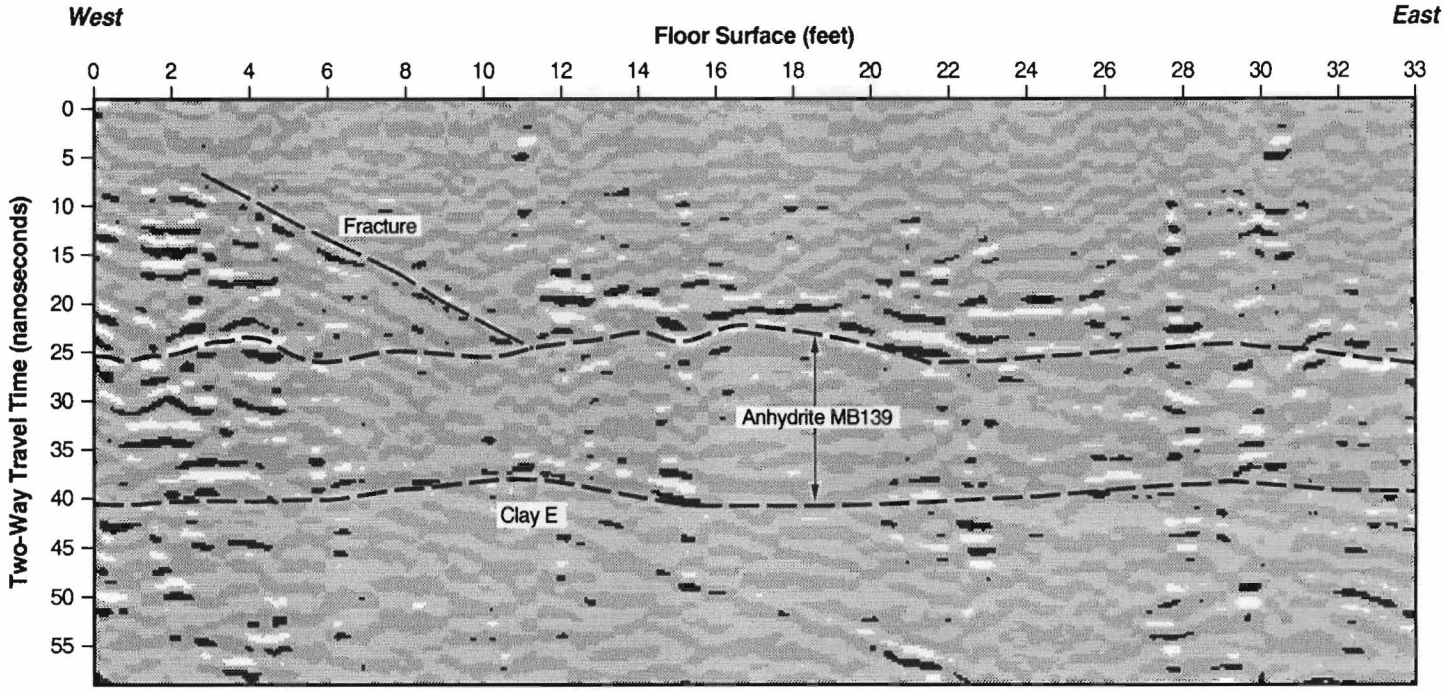

Figure 3-2
S-1862 Traverse, Room 1, Panel 1 Floor: June 1991

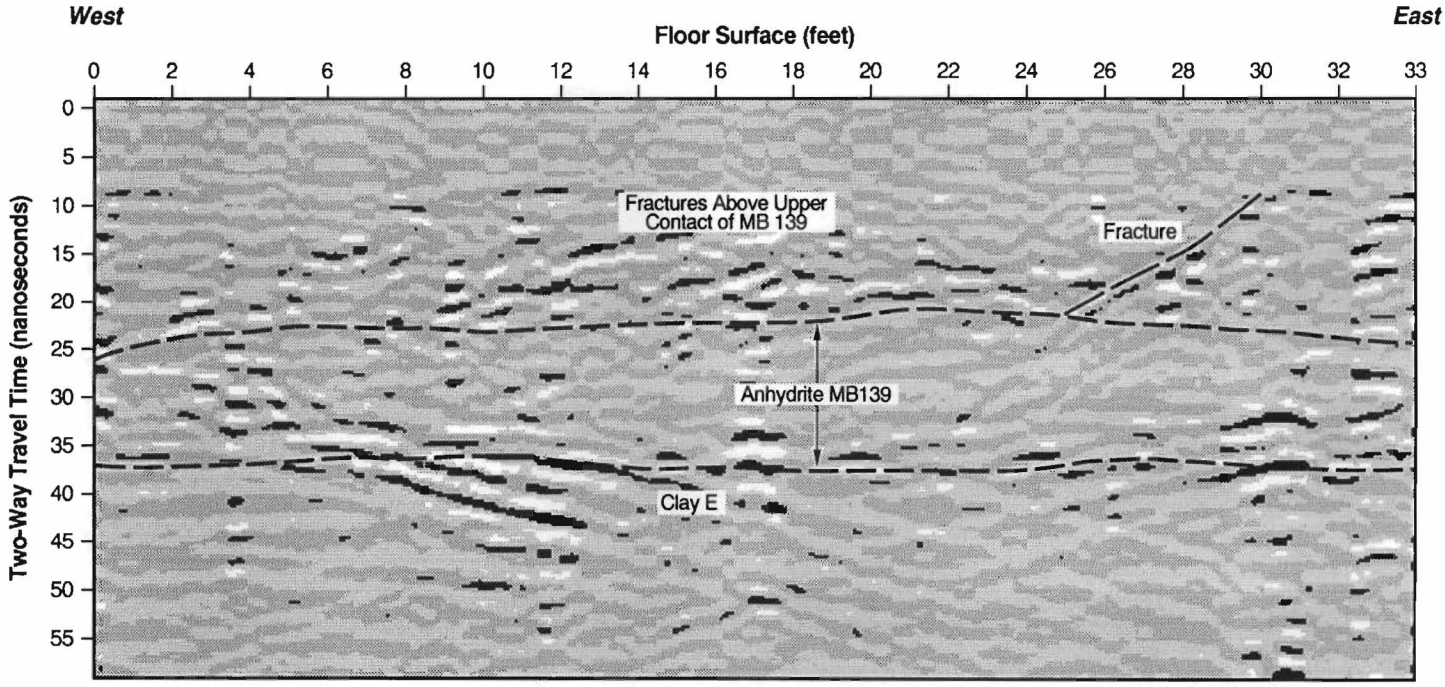

Figure 3-3
S-1822 Traverse, Room 1, Panel 1 Floor: June 1991

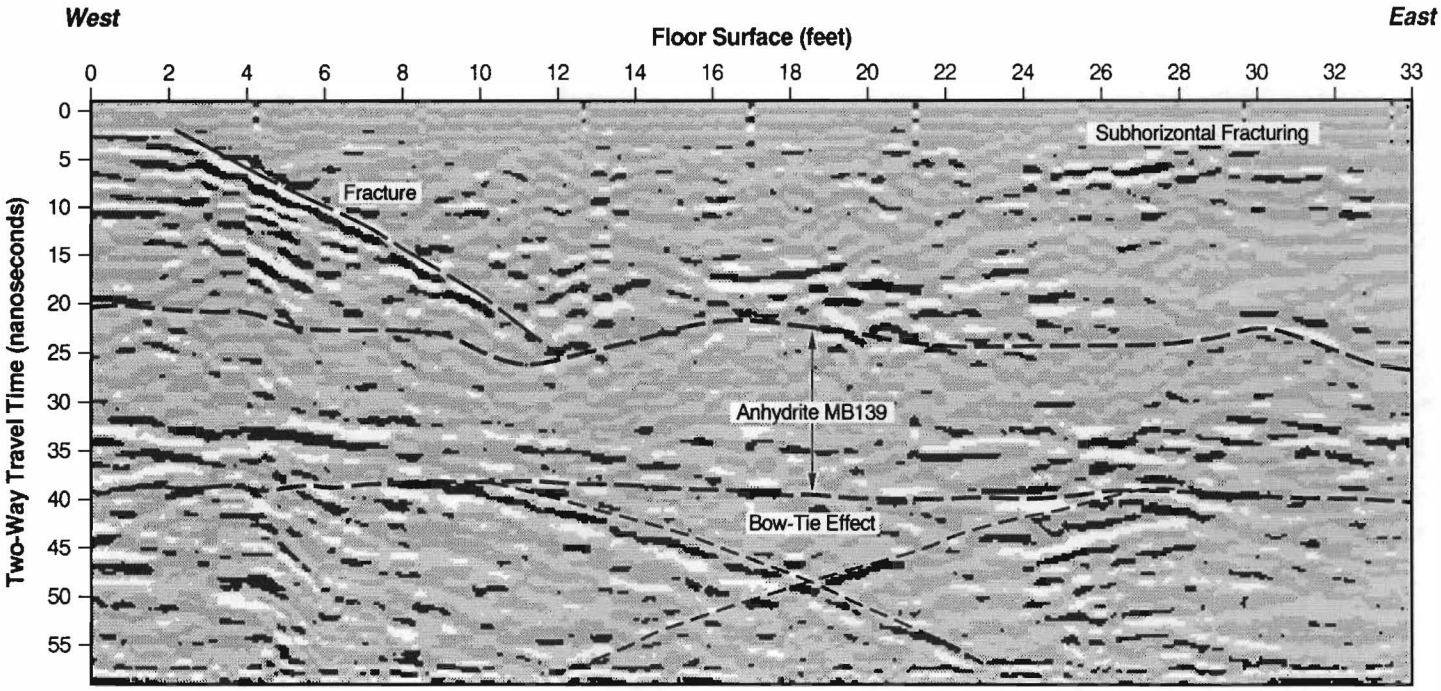

Figure 3-4
S-1862 Traverse, Room 1, Panel 1 Floor: January 1992

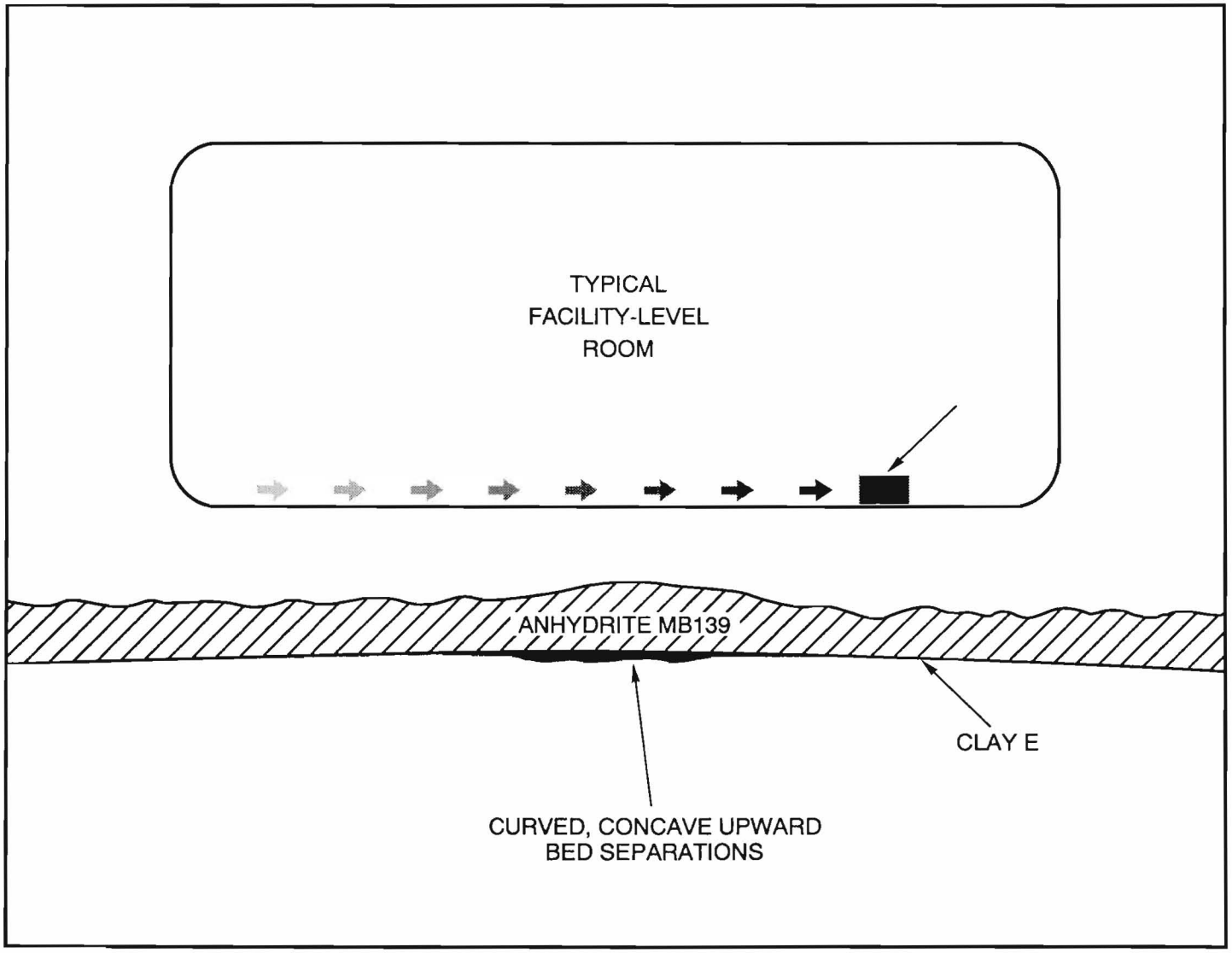

Figure 3-5
Diagrammatic Cross Section of Room 1, Panel 1

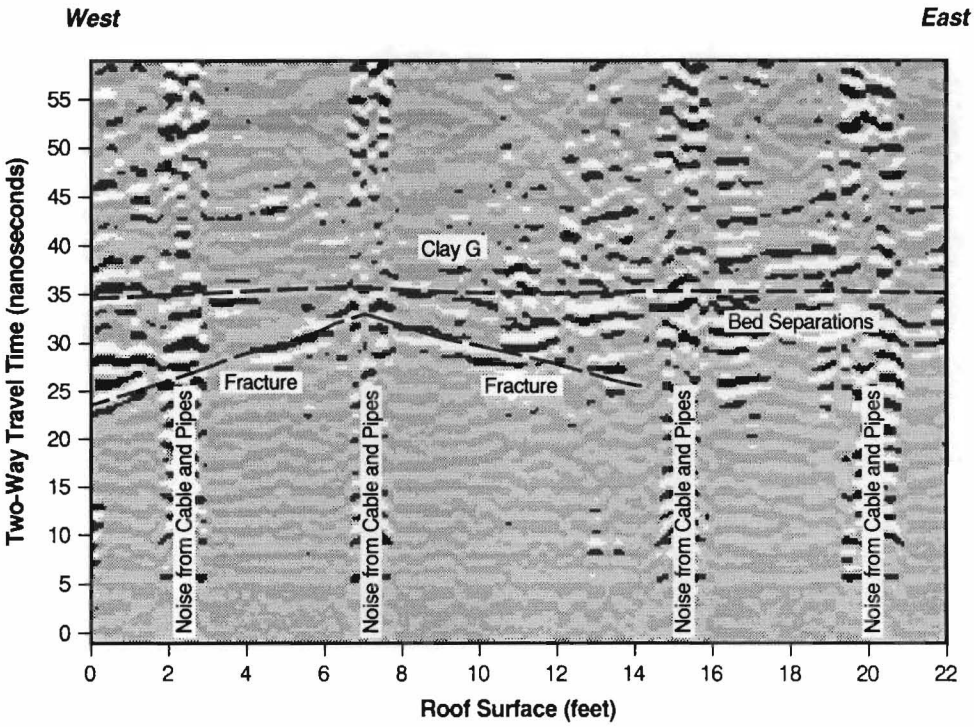

Figure 3-6
S-1742 Traverse, Room 1, Panel 1 Roof: June 1991

4.0 GPR Surveys in Room 6, Panel 1

4.1 Introduction

GPR traverses were conducted on the floor and roof of Room 6, Panel 1, on January 29, January 30, and January 31, 1992. (See Figure 1-2 for the location of Room 6, Panel 1.) All traverses were conducted from west to east perpendicular to the long axis of Room 6, with the exception of two axial profiles. One 138-ft (42 m) long axial profile was conducted on the floor, and another 158-ft (48 m) long axial profile was conducted along the roof. GPR surveys were completed at the same locations as previous GPR surveys conducted in March 1990 and March 1991. A complete analysis of previously collected radar data from Room 6, Panel 1, for March 1990 and March 1991 is given in DOE, 1991b.

4.2 Room 6, Panel 1, Floor Surveys

The location of GPR floor traverses conducted in January 1992 are shown in Figure 4-1. These traverses are labeled using the WIPP descriptive mine coordinates with the origin located at the salt-handling shaft. Three radar profiles from the Room 6 floor are discussed below. The remaining radar profiles not discussed in the following sections are included in Appendix C. These radar profiles are all similar in appearance. Processing sequences used to process the data from Room 6 are also included in Appendix C. No boreholes were located in the Room 6 floor at the time of these surveys with which to calculate a wave velocity. Two-way travel times of reflections from the Room 6 floor were converted to distances using the average wave velocity of 0.37 ft/ns calculated above (see Section 1-3). The two-way travel time in ns may be divided by 5.35 ns/ft to give the distance to the reflector in ft.

Figure 4-2 is the radar profile from the S-1667 traverse located in the northern part of Room 6 (see Figure 4-1 for the location). Undulatory reflections occur at about 25 ns (4.7 ft) across the width of the excavation. It is believed that these undulatory reflections are the upper contact of MB139. An inclined fracture that intersects the floor surface extends from the west rib and angles deeper into the floor. The fracture terminates at about 33 ns (6.2 ft). This is below the upper contact of MB139; thus, MB139 is also fractured at this location. Reflections near the west and east ribs at about 40 ns (7.5 ft) into the floor are due to clay E at the lower contact of MB139. Subhorizontal fracturing is present between 0 and 20 ns (0 and 3.7 ft) into the floor. Some subhorizontal fracturing of MB139 can also be seen. The greatest amount of subhorizontal fracturing, however, is located between 3 and 15 ns (0.6 and 2.8 ft) into the floor.

Seven ft south of the S-1667 traverse is another traverse S-1674 with many of the same features as the S-1667 traverse described above. The S-1674 traverse is shown in Figure 4-3 (see Figure 4-1 for locations of radar surveys). Continuous undulatory reflections across the room are present at about 25 ns (4.7 ft) in this traverse. This is the presumed location of the upper contact of MB139. Reflections that occur at about 40 ns (7.5 ft) into the floor are also present across the entire profile. These are interpreted to be caused by clay E below MB139; thus, the upper and lower contacts of MB139 are at about 25 and 40 ns (4.7 and 7.5 ft), respectively. An inclined fracture that nearly intersects the floor surface extends down from the west rib and angles deeper into the floor continuing to the lower contact of MB139 at about 35 ns (6.5 ft). This fracture extends deeper into the floor of Room 6 than the inclined fracture noted above in the S-1667 traverse (Figure 4-2). Numerous subhorizontal fractures are present between 3 and 20 ns (0.6 and 3.7 ft) in the S-1674 traverse. Additionally, numerous subhorizontal fractures are also present within MB139.

Figure 4-4 is the radar profile from the S-1811 traverse near the center of Room 6 (Figure 4-1). Undulatory reflections are developed at about 25 ns (4.7 ft). Reflections are also developed near the west rib at about 40 ns (7.5 ft). These reflections are assumed to be the upper and lower contacts of MB139. Inclined fractures that extend down from the ribs do not exist in traverse S-1811; however, there is a well-developed fracture that cuts across MB139 near the center of the room. Well-developed subhorizontal fractures are also present at about 10 ns (1.9 ft) into the floor.

4.3 Discussion of Room 6 Floor Results

The types of fractures interpreted to occur in the Room 6 floor include (1) fairly flat, shallow fractures from about 0.6 to 3.7 ft into the floor that occur nearly throughout the room; (2) fractures that either extend from shallow depths (i.e., 0 to 2.0 ft) near the west rib and angle deeper into the floor into MB139 or extend from MB139 and angle up towards the floor surface; and (3) fractures within MB139 which are either developed subhorizontally or which cut across the anhydrite.

In general, transects from the floor in the northern 100 ft of the room show the most deformation, with well-developed fractures that extend from shallow depths near the west rib and angle deeper into the floor. This could indicate that the rate of brittle deformation in the floor is greater in this area than in the southern 200 ft of the room. Fracture development in the floor of Room 6 appears to be influenced by the presence of MB139. Although many

fractures do occur within the estimated location of MB139, the majority of interpreted fractures occur in the salt above the anhydrite, along the upper contact of the anhydrite, and at the clay E/salt interface below the anhydrite.

4.4 Room 6, Panel 1, Roof Surveys

The location of GPR surveys completed on the Room 6 roof are shown in Figure 4-5, along with the locations of three boreholes in the roof. These boreholes and radar surveys from transects S-1798, S-1807, and S-1811 were used in part to determine to a 500-MHz wave velocity in the halite (Section 1-3). The average wave velocity (0.37 ft/ns) was used to convert two-way travel times to the reflectors in ns to distance to the reflectors in ft (see Section 1-3). The two-way travel time to a reflector may be divided by 5.35 ns/ft to give the distance to the reflector in ft.

Noise was introduced into the radar profiles from lights, cables, and pipes suspended from the roof of the room at the time of the surveys. Reflections from the metallic objects and from the roof when the antenna was lowered and raised around these objects caused multiple reflections to be reverberated throughout the 60-ns time range at these locations. To avoid closely spaced pipes and cables near the ribs of the room, the traverses were conducted from the west rib and concluded 5 ft (1.5 m) from the east rib. The total length represented by the horizontal axis of the radar profile from the Room 6 roof is 28 ft (8.5 m), not the full 33-ft (10.0 m) width of the room.

Figure 4-6 is the radar profile from the S-1736 traverse (see Figure 4-5 for the location of this traverse). The large continuous reflection at about 35 ns (6.5 ft), which extends across the roof of the room, is interpreted to be due to anhydrite "b" and clay G. Numerous subhorizontal fractures or bed separations below anhydrite "b"/clay G are also present. These bed separations occur from about 25 to 35 ns (4.7 to 6.5 ft) above the roof surface. Some subhorizontal fracturing above anhydrite "b"/clay G is present as well. These fractures occur at about 35 to 45 ns (6.5 to 8.4) into the roof's surface. On the east side of the profile, a fracture starts at the east edge of the radar profile at about 15 ns (2.8 ft) and angles upward deeper into the roof, towards the center of the room and intersects numerous bed separations below clay G at about 30 ns (5.6 ft). A second, smaller fracture below the above-mentioned fracture also angles upward from the east edge of the profile to about 13 ns (2.4 ft) into the roof. No fractures are present on the west side of the radar profile.

Figure 4-7 is the radar image from the S-1798 traverse (see Figure 4-5 for the location). This traverse is similar to the S-1736 traverse described above (Figure 4-6). Reflections interpreted to be due to anhydrite "b"/clay G occur at about 33 ns (6.2 ft). Numerous bed separations also occur between 25 and 33 ns (4.7 and 6.2 ft) below anhydrite "b"/clay G. On the east end of the profile, a fracture starts at about 10 ns (1.9 ft) and angles upward into the roof and intersects bed separations below clay G at about 27 ns (5.0 ft). Again, no fractures were present on the west side of the radar profile.

Figure 4-8 from the S-1807 traverse is also similar in appearance to the S-1736 and the S-1798 traverses (Figures 4-6 and 4-7); however, Figure 4-8 has a fracture located near the west rib. This fracture starts near the west rib at about 3 ns (0.6 ft) and angles deeper into the roof to about 10 ns (1.9 ft). Reflections due to anhydrite "b"/clay G occur at about 33 ns (6.3 ft). Bed separations occur below clay G between 25 and 33 ns (4.7 and 6.2 ft) and a fracture starting at the east end of the profile at about 6 ns (1.1 ft) angles upward into the roof and intersects bed separations below clay G at about 30 ns (5.6 ft).

4.5 Discussion of Room 6 Roof Results

The only other roof profile that has inclined fractures which angle upward deeper into the roof is the S-1811 traverse (Appendix C, Figure C-27). Because this profile was similar in appearance to Figure 4-8, it was not included in the body of this report. Appendix C contains radar profiles from the Room 6 roof that are not discussed above. Processing sequences for radar profiles from the Room 6 roof are also included in Appendix C. Other radar profiles from the Room 6 roof are relatively free from reflections for the first approximately 25 ns (4.7 ft). Thus, little brittle deformation has occurred in the roof in about the first 5 ft. From between 25 ns to 45 ns (4.7 to 8.4 ft), numerous reflections interpreted to be bed separations above and below anhydrite "b"/clay G extend across the Room 6 roof. Bed separations near clay G were presumably caused from the opposing directions of lateral movement of halite and anhydrite "b"/clay G.

Only four GPR surveys from the Room 6 roof have inclined fractures that start near the rib and angle deeper into the roof. The radar traverses that have inclined fractures are: the S-1736 traverse (Figure 4-6), the S-1798 traverse (Figure 4-7), the S-1807 traverse (Figure 4-8), and the S-1811 traverse (Appendix C, Figure C-27). Radar profiles from the S-1736 traverse and the S-1798 traverse have only fractures that start from near the east rib. There are no fractures that start near the west rib in these traverses. Radar profiles from the

S-1807 and the S-1811 traverses, however, do have fractures that start near both the west and east ribs and angle deeper into the roof. These traverses are both located near one another near the center of the room (see Figure 4-5 for the locations of roof traverses). More brittle deformation has been noted in the middle of the rooms compared with the room intersections (DOE, 1993). Near the center of the rooms, the pillars between the rooms move toward the opening, perpendicular to the ribs, and therefore exert pressure directly on the roof beam; in the intersections, however, the salt mass is less confined and has more freedom when creeping toward the openings, leading to less local concentration of stresses in the corners, and resulting in less creep and less failure in the roof beam at the intersections (DOE, 1993).

4.6 Summary of Room 6 Results

In Room 6, fractures develop diagonally in the floor from near the ribs and extend deeper into the floor. These fractures often cut across the presumed location of MB139. Subhorizontal reflections occur between 0.6 to 4.5 ft (0.2 to 1.4 m) into the floor and generally extend across the floor. These reflections are interpreted to be due to fractures or separations developed within the salt. Some subhorizontal fractures also occur within MB139. Large- amplitude reflections also occur along the lower contact of MB139, presumably due to clay E. These reflections are present in many of the radar profiles.

Most of the fractures in the Room 6 roof occur below anhydrite "b" and clay G. These fractures or bed separations occur about 5 to 6.5 ft (1.5 to 2.0 m) into the roof. The area between the roof surface and these fractures is relatively free from reflections. Some fracturing also occurs just above anhydrite "b" from about 6.5 to 8.4 ft (2.0 to 2.6 m); thus, anhydrite "b"/clay G has a pronounced effect on brittle deformation in the roof. This is probably due to opposing directions of lateral movement of salt and anhydrite "b"/clay G. Inclined fractures that extend up from near the ribs have been detected in four traverses near the middle of Room 6. Fractures that angle up from near both the west and east ribs are present in radar profiles from the S-1807 and the S-1811 traverses. The other two radar profiles exhibit fractures that angle up from the east side only (Figure 4-6, S-1736 traverse and Figure 4-7, S-1798 traverse). These profiles are all near the middle of Room 6. Additional radar surveys in this area could be used to monitor fracture development in the Room 6 roof.

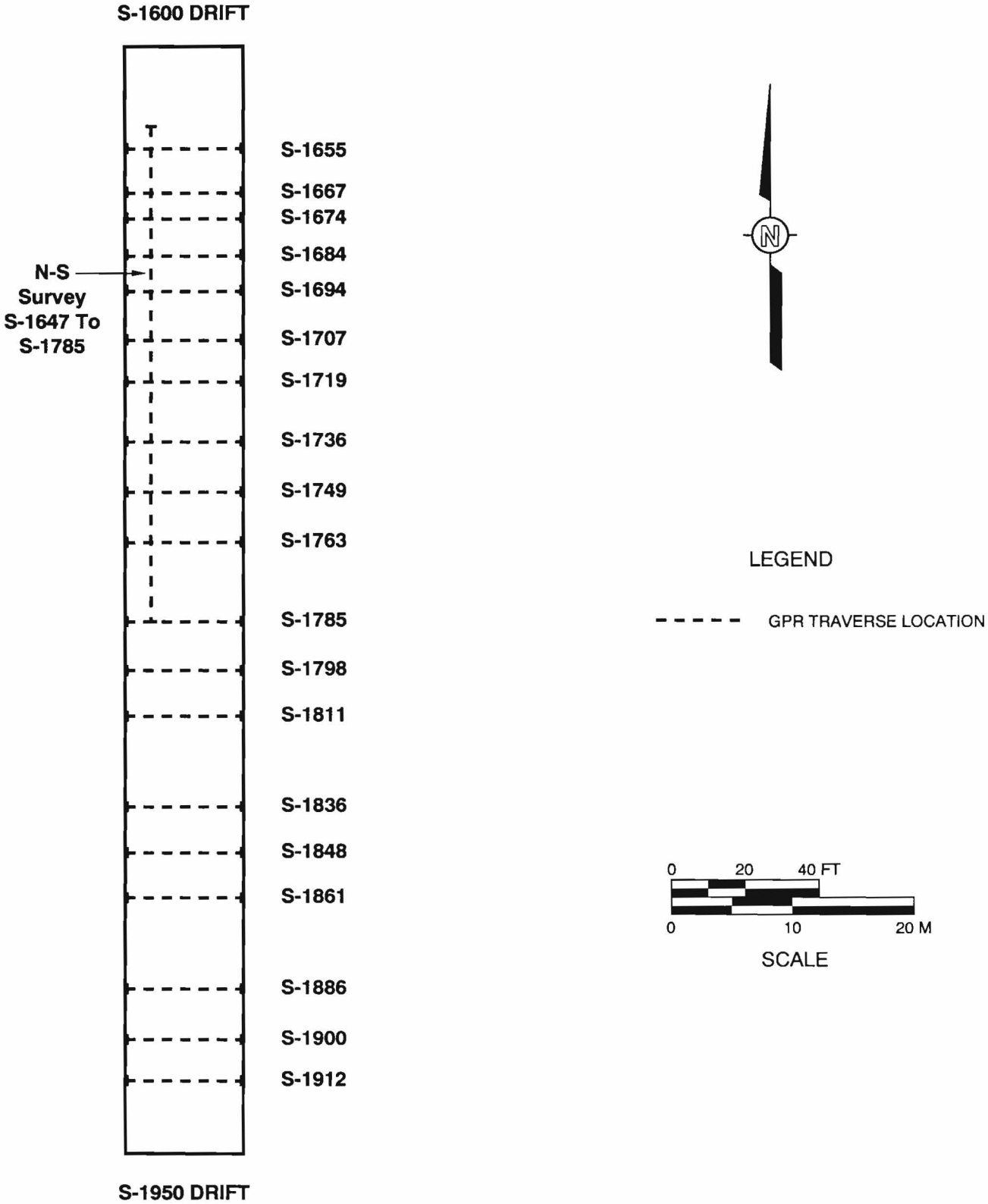

Figure 4-1
Locations of GPR Floor Traverses in Room 6, Panel 1

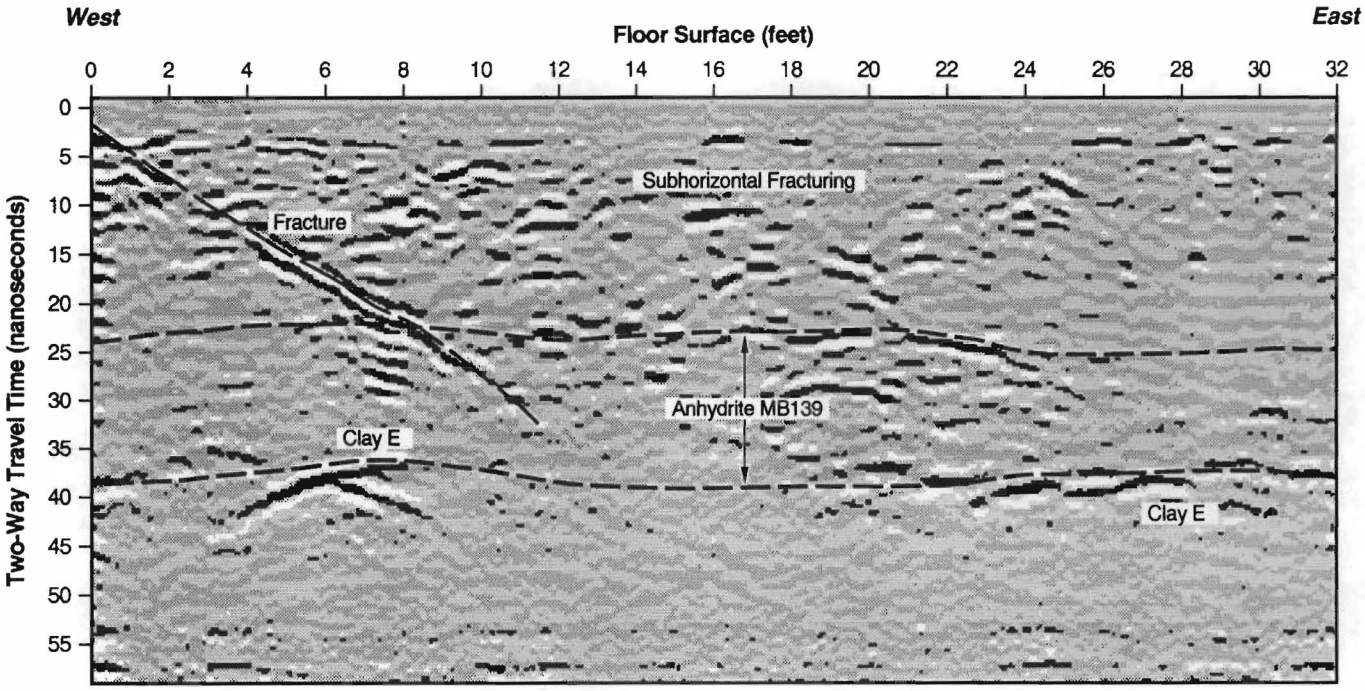

Figure 4-2
S-1667 Traverse, Room 6, Panel 1 Floor: January 1992

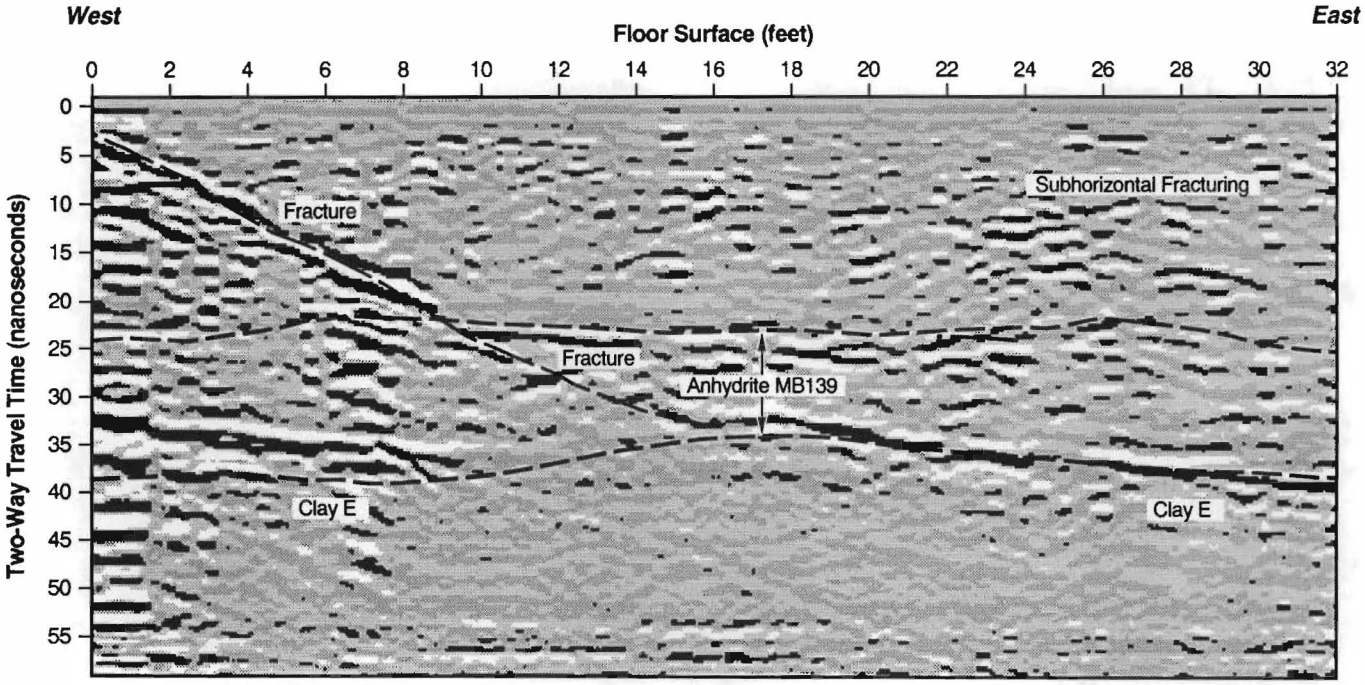

Figure 4-3
S-1674 Traverse, Room 6, Panel 1 Floor: January 1992

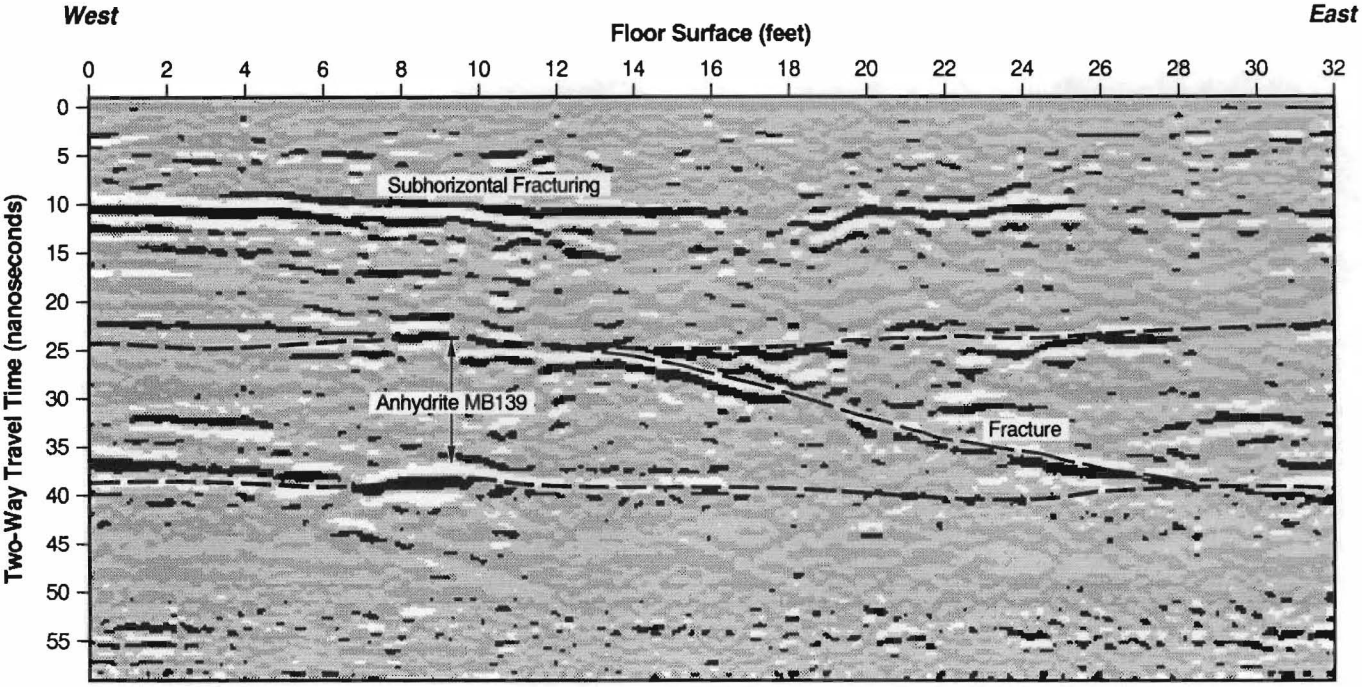

Figure 4-4
S-1811 Traverse, Room 6, Panel 1 Floor: January 1992

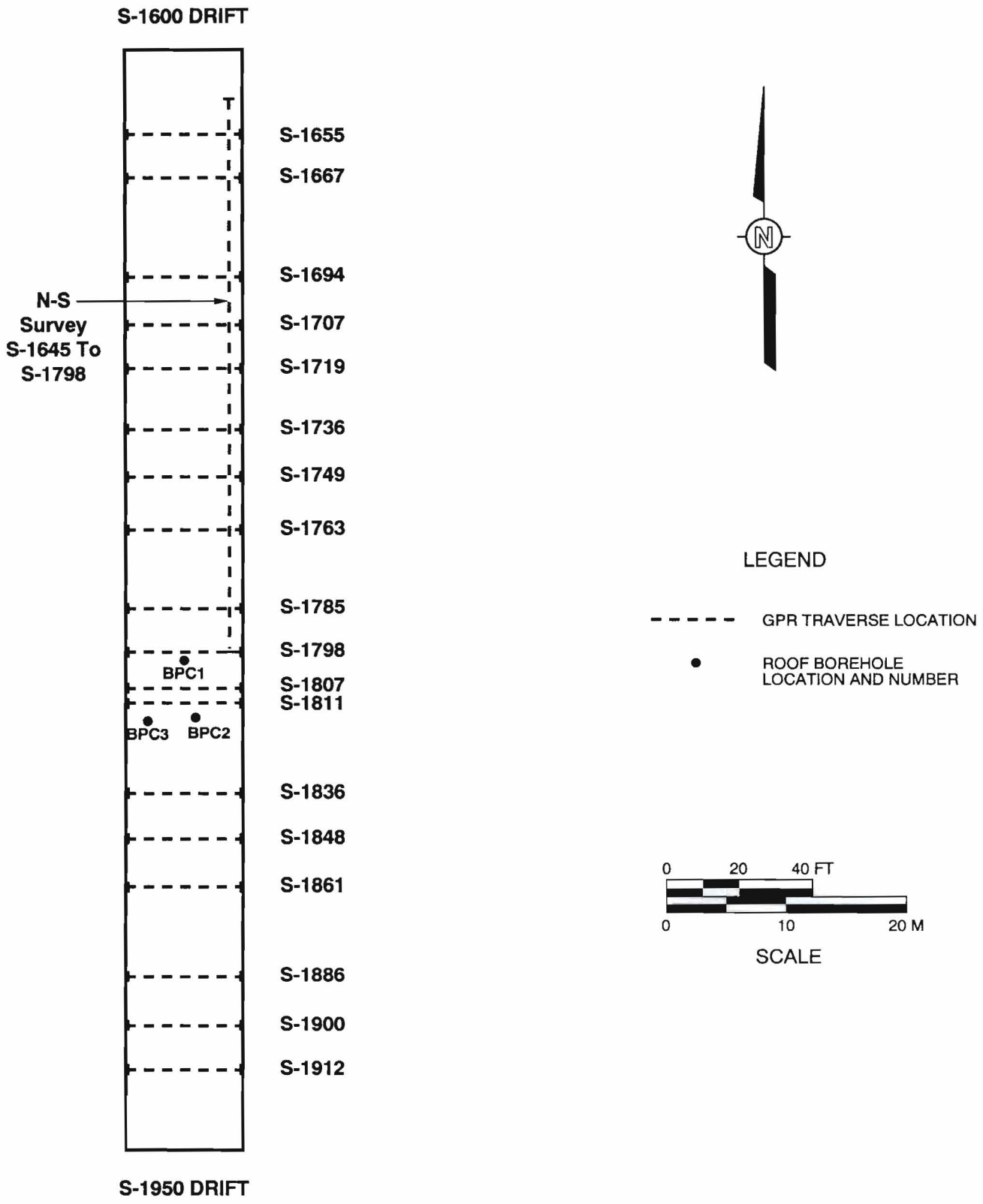

Figure 4-5
Locations of GPR Roof Traverses and Roof Boreholes in Room 6, Panel 1

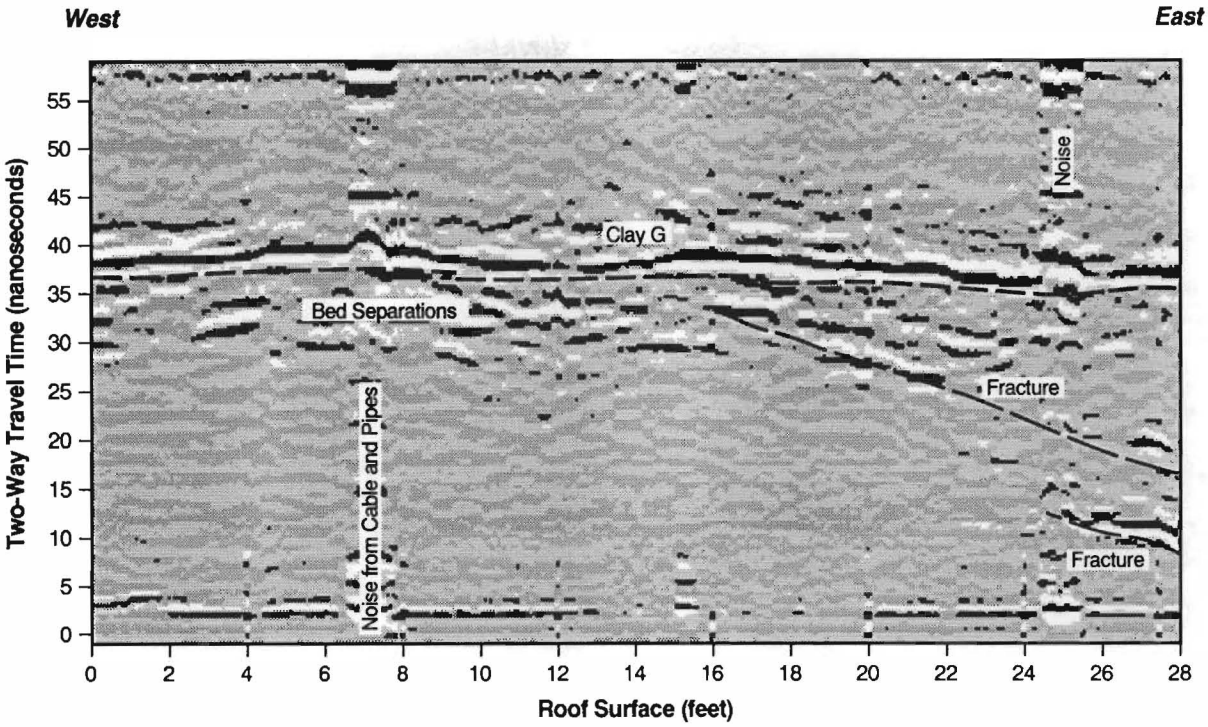

Figure 4-6
S-1736 Traverse, Room 6, Panel 1 Roof: January 1992

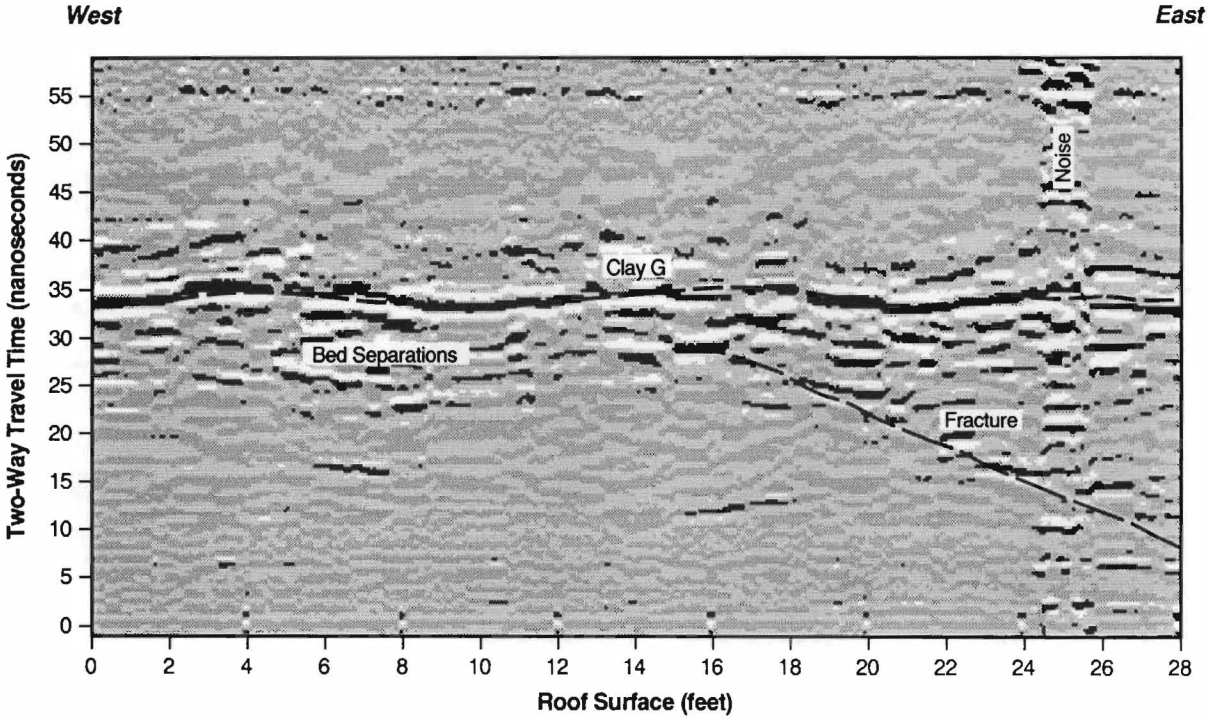

Figure 4-7
S-1798 Traverse, Room 6, Panel 1 Roof: January 1992

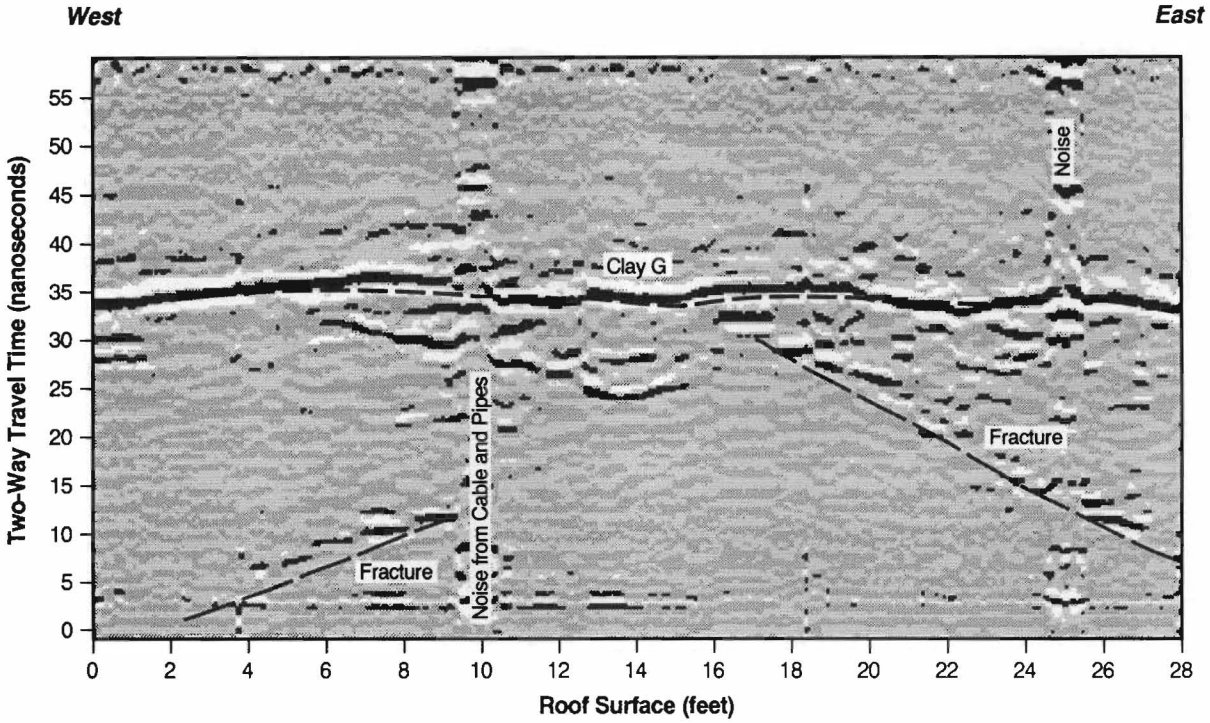

Figure 4-8
S-1807 Traverse, Room 6, Panel 1 Roof: January 1992

5.0 GPR Surveys of the S-1950 Drift Roof

5.1 Introduction

Forty-one GPR surveys were conducted on the S-1950 Access Drift roof on February 4, February 5, and February 6, 1992. The S-1950 Drift is one of the primary access drifts for Panel 1 (see Figure 1-2 for the location of the S-1950 Drift). The locations of roof GPR surveys in the S-1950 Drift are shown in Figure 5-1. Thirty-two radar surveys were conducted from north to south perpendicular to the long axis of the S-1950 Drift. Six axial radar surveys (traverses B through G) were conducted from west to east along the center line of the S-1950 Drift. An additional three surveys (traverses A, H, and I) were conducted in waste storage rooms near the intersection of the rooms and the S-1950 Drift. (See Figure 5-1 for the locations of radar surveys.)

5.2 S-1950 Drift Surveys

Radar traverses conducted in the S-1950 Drift are labeled using the WIPP descriptive mine coordinates. Since the radar profiles along the S-1950 Access Drift roof are all similar in appearance, only three profiles are discussed in the body of this report. The remaining radar profiles are included in Appendix D. The instrumentation settings used to conduct the radar traverses as well as the processing sequences used to process the radar data are also included in Appendix D.

Lights, cables, and pipes were suspended from the S-1950 Drift roof. These metallic objects presented obstacles that required successively lowering and raising the GPR antenna. Reflections from both the objects and from the roof when the antenna was being lowered or raised caused multiple reflections to be reverberated throughout the 60-ns time range at these particular locations. These multiple reflections appear as vertical bands of noise in the radar profiles.

The GPR surveys conducted at E-0660, E-0854, E-1060, E-1062, traverse I, and traverse G, (Figure 5-1) were used in part to determine the 500-MHz wave velocity in the halite (see section 1-3). The distances to anhydrite "b"/clay G from the roof surface were taken from the logs of the roof boreholes. The one-way travel for the reflection from clay G was determined from the radar profiles, and the velocity was calculated (see Section 1-3). The average wave velocity of 0.37 ft/ns was used to convert two-way travel times to the reflectors in ns into

distance to the reflectors in ft. The two-way travel time to the reflector can be divided by 5.35 ns/ft to give the distance to the reflector in ft.

5.3 S-1950 Drift Results

Figure 5-2 shows the radar profile from the E-0606 traverse located between Room 1 and Room 2 in the S-1950 Drift (see Figure 5-1 for location). This profile is typical for radar profiles from the S-1950 Drift. A continuous reflector that extends across the entire profile is located at about 38 ns (7.1 ft) into the roof. This reflector is interpreted to be anhydrite "b" and clay G. Below clay G, numerous reflections occur from about 23 to 38 ns (4.3 to 7.1 ft) into the roof. These are interpreted to be due to subhorizontal fractures or bed separations that occur below anhydrite "b"/clay G. Some subhorizontal fracturing also occurs above anhydrite "b"/clay G between 40 and 47 ns (7.5 and 8.8 ft). Above 47 ns (8.8 ft), the profile is relatively free from reflections. The radar profile is also relatively free from reflections between 0 and 23 ns (0 to 4.3 ft). Thus, the halite near anhydrite "b" and clay G contains numerous subhorizontal fractures or bed separations.

Figure 5-3 is the north to south radar profile from the E-0920 traverse that is located at the intersection of Room 4 and the S-1950 Drift (see Figure 5-1 for location). A continuous reflector that extends across the entire profile is located about 43 to 35 ns (8.0 to 6.5 ft) into the roof. This reflector is interpreted to be anhydrite "b"/clay G. Below clay G, numerous reflections interpreted to be subhorizontal fractures or bed separations occur from about 40 to 25 ns (7.5 to 4.7 ft) into the roof. An inclined fracture also is present in the E-0920 traverse. This fracture starts near the roof surface at about 10 ft (3.05 m) from the north side of the traverse. The fracture angles upward to about 15 ns (2.8 ft) at the north end of the radar profile. This fracture probably angles upward deeper into the Room 4 roof; however, it is not known how far the fracture extends into Room 4.

Figure 5-4 is the radar profile from traverse E, an axial profile that was collected west to east from E-0920 to E-1060 along the center of the S-1950 Drift (see Figure 5-1 for the location of the radar traverse). The vertical exaggeration of this profile is 3.5 times the horizontal length for purposes of displaying the entire traverse. The continuous reflector at about 35 ns (6.5 ft) is interpreted to be anhydrite "b"/clay G. Below clay G, there are numerous reflections interpreted to be due to bed separations. These occur between about 25 to 35 ns (4.7 to 6.5 ft) into the roof. Some fracturing has occurred just above anhydrite "b"/clay G as well. These fractures occur at about 37 to 43 ns (6.9 to 8.0 ft) into the roof. The halite

above 43 ns (8.0 ft) is relatively free from reflections. Additionally, the area below about 25 ns (4.7 ft) is also free from reflections. Thus, fracturing of the halite has occurred near anhydrite "b"/clay G.

5.4 Discussion and Summary of the S-1950 Drift Results

Most GPR reflections in the S-1950 Drift roof are associated with anhydrite "b" and clay G at about 35 to 40 ns (6.5 to 7.5 ft) into the roof. Numerous small subhorizontal fractures or bed separations occur just below clay G from about 25 to 35 ns (4.7 to 6.5 ft) into the roof. Some subhorizontal fractures occur just above anhydrite "b"/clay G as well. Above about 40 ns (7.5 ft) and below about 25 ns (4.7 ft) reflectors are generally absent in the radar profiles. Thus, most of the fracture development in the S-1950 Drift roof appears to occur just above and below clay G and anhydrite "b." Reflections that occur near clay G are presumably due to the opposing directions of lateral movement of salt and anhydrite "b"/clay G.

An inclined fracture was detected in the E-0920 radar profile, which passes through the center of a drift intersection (Figure 5-3). No other inclined fractures were observed in the radar profiles from the S-1950 Drift. However, one small inclined fracture was observed in traverse H (Appendix D, Figure D-37). This traverse is at the south end of Room 7 near the intersection of Room 7 and the S-1950 Drift (see Figure 5-1 for the location of traverse H). The small fracture from traverse H starts near the roof of the west rib and extends upward to about 17 ns (3.2 ft) into the roof. The fracture is similar to inclined fractures in Room 1 and Room 6, which start near the rib and angle deeper into the roof.

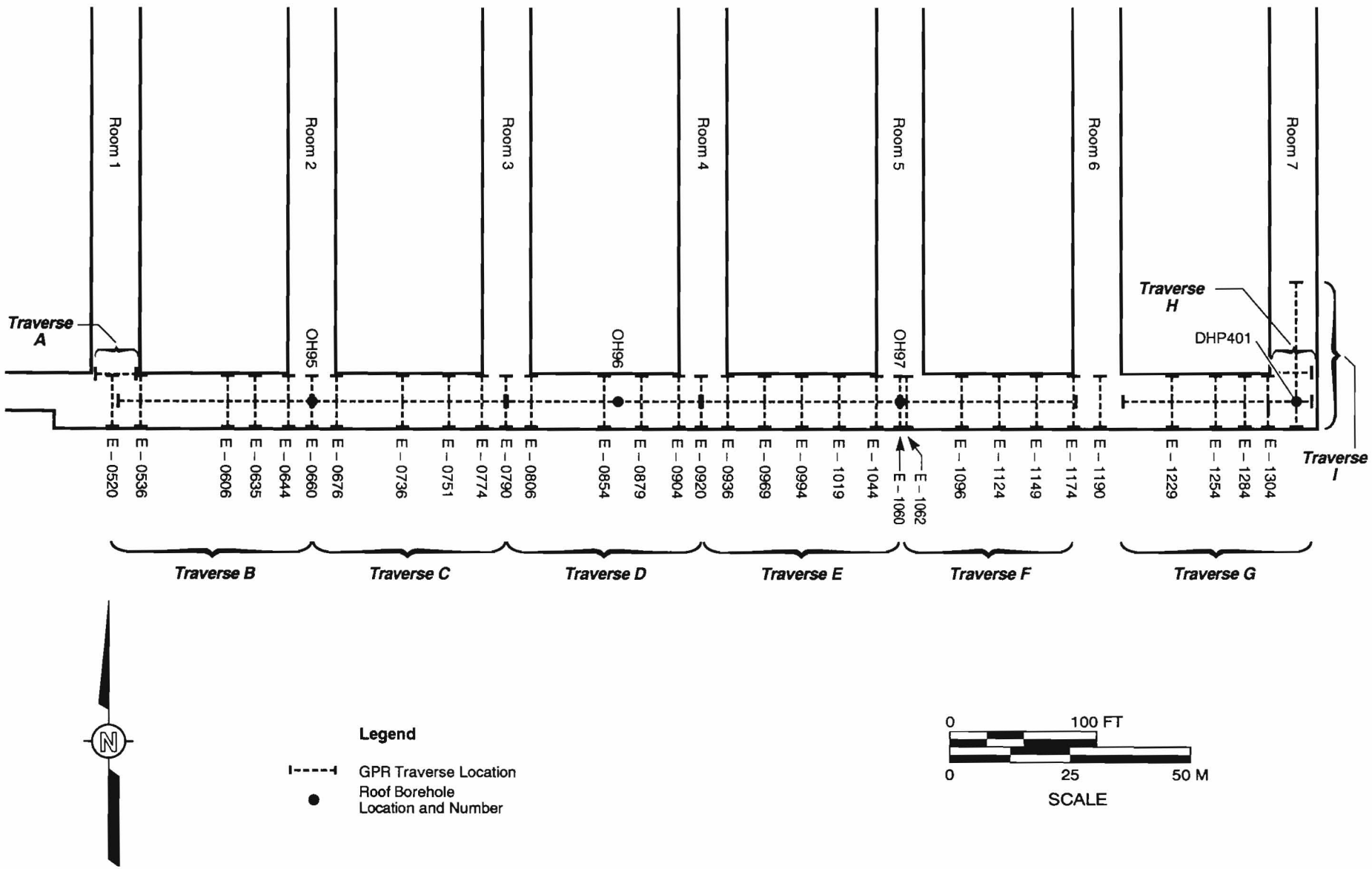

Figure 5-1
Locations of GPR Roof Traverses and Roof Boreholes in the S-1950 Drift, Panel 1

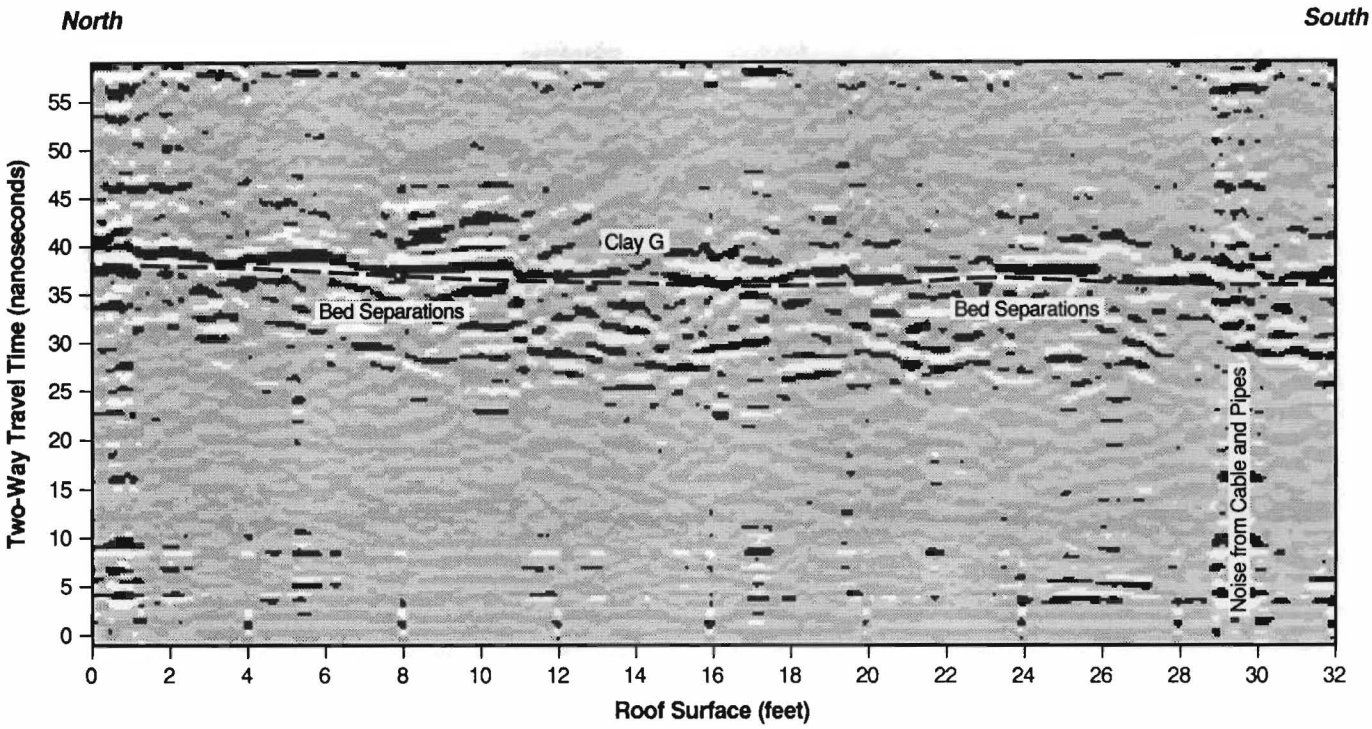

Figure 5-2
E-0606 Traverse, S-1950 Drift Roof: February 1992

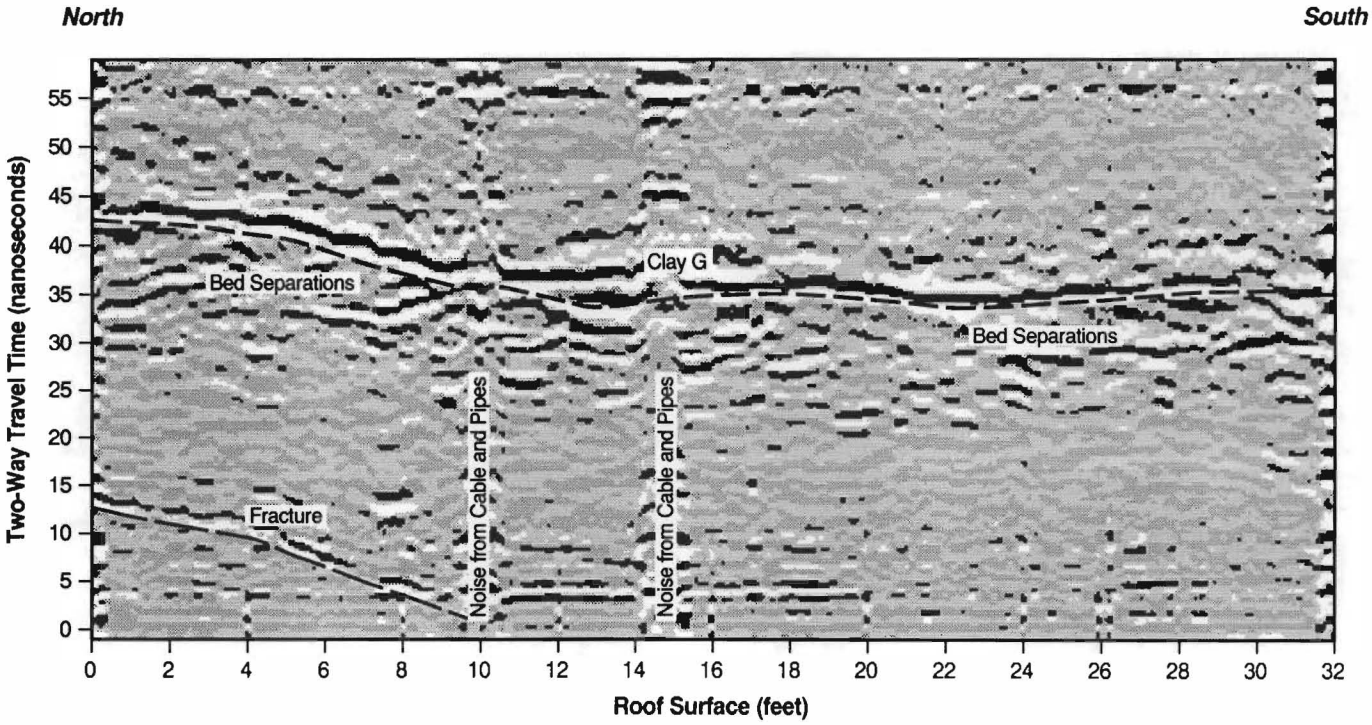

Figure 5-3
E-0920 Traverse, S-1950 Drift Roof: February 1992

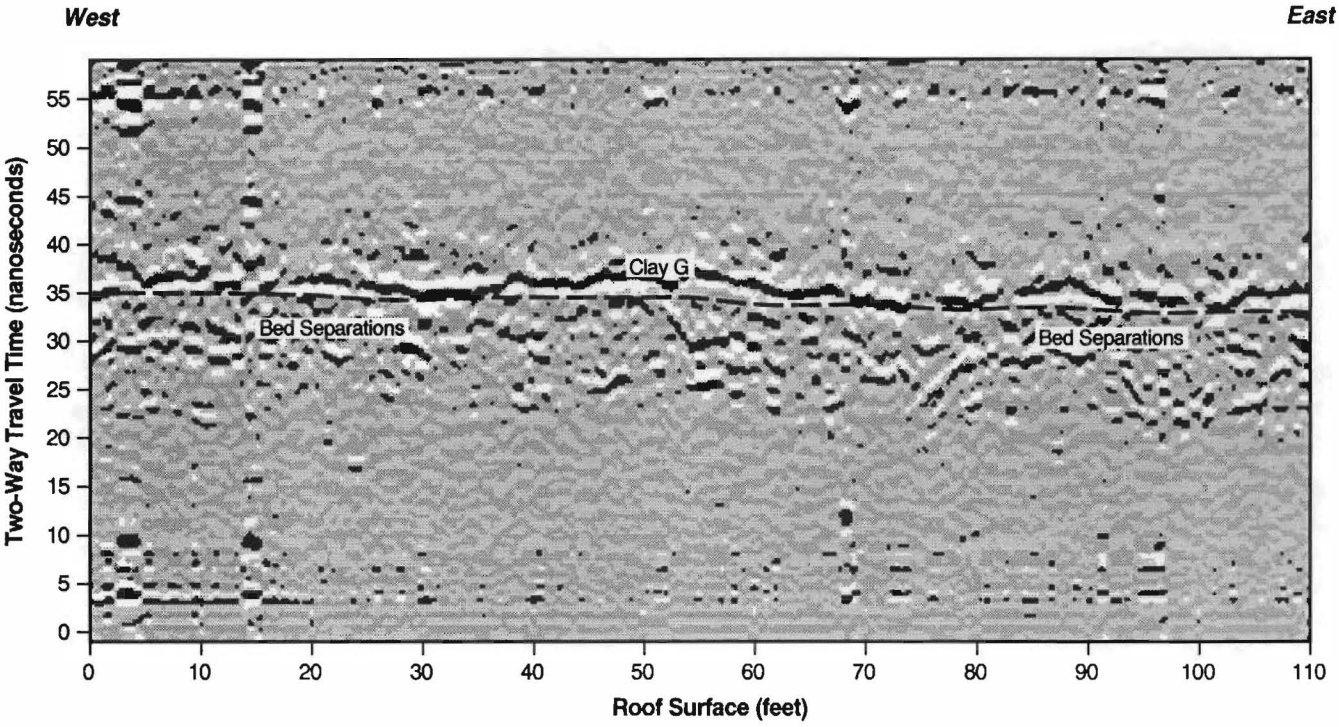

Figure 5-4
Traverse E, E-0920 to E-1060, S-1950 Drift Roof: February 1992
Vertical Exaggeration 3.5x

6.0 N-1420 Drift Roof; Room B to Room D

6.1 Introduction

Forty GPR surveys of the N-1420 Drift roof were conducted on June 17 and June 19, 1991. The surveys were conducted in the eastern portion of N-1420, between Room B and Room D (see Figure 1-1 for the location of the N-1420 Drift). The surveys were taken both across the width of the drift and along the center line of the drift. Roof boreholes from three Excavation Effects Program (EEP) arrays were used to determine the wave velocity of the transmitted 500-MHz wave in the salt above the roof surface. The locations of the EEP arrays and the GPR surveys are shown in Figure 6-1.

The GPR surveys conducted at E-1100, E-1120, E-1380, and E-1480 (Figure 6-1) were used in part to determine the 500-MHz wave velocity in the halite (see Section 1-3). The distances to clay I from the roof surface were taken from the logs of the EEP roof boreholes. The one-way travel time of the reflection from clay I was determined from the radar profiles taken nearest the boreholes, and velocities were calculated (Section 1-3). The average wave velocity calculated was 0.37 ft/ns. This was used to convert two-way travel time to the reflectors in ns into distance to the reflectors in ft. The two-way travel time to a reflector can be divided by 5.35 ns/ft to give the distance to the reflector in ft.

Because of lights, cables, and pipes suspended from the N-1420 Drift roof, vertical bands of noise were introduced into the radar surveys. Metallic objects suspended from the roof presented obstacles that required successively lowering and raising the GPR antenna. Reflections from both the objects and from the roof when the antenna was being lowered or raised caused multiple reflections to be reverberated throughout the 60-ns time range. Therefore, the radar profiles of the N-1420 Drift roof contain a considerable amount of noise.

Since many of the radar profiles from the N-1420 Drift are similar in appearance, only five radar profiles are discussed below. Radar profiles not discussed in the body of this report are included in Appendix E, along with the processing sequences used to process the radar data.

6.2 Results of GPR Surveys in the N-1420 Drift

The excavation of this portion of N-1420 was completed in 1984 (DOE, 1991c). The drift is therefore a relatively old excavation, and the EEP data show numerous fractures developed

between the roof excavated surface and clay I (DOE, 1991c). Clay I is located between about 4.4 to 5.3 ft (1.3 to 1.6 m) into the roof.

Figure 6-2 is the radar profile from E-1480 radar traverse (see Figure 6-1 for the location of the radar traverse). Reflections from clay I are very large in amplitude and occur at about 25 ns (4.7 ft). Clay I is a brown to brownish clay that is about 1/4 to 5/8 inches (0.64 to 1.59 cm) thick. It is unlikely that a thin, dry, clay seam would produce the large amplitude reflections observed from clay I. However, a brine-saturated clay seam would provide a large contrast in the dielectric constant between halite and clay and produce large amplitude radar reflections. During drilling of the EEP array boreholes, it was observed that mud was dripping from the holes (Francke, 1992). Therefore, the large amplitude reflections from clay I are interpreted to be due to brine saturation of clay I.

In Figure 6-2 numerous fractures occur between the roof surface and clay I. An arcuate, or dish-shaped fracture, concave toward the opening, occurs near the center of the drift. The fracture starts at a distance of about 5 ns (0.9 ft) into the north and south side of the roof and extends to about 12 ns (2.2 ft) into the roof, near the center of the drift where it flattens (Figure 6-2). Relatively flat reflectors located above clay I, at 35 ns (6.5 ft), 42 ns (7.9 ft) and 50 ns (9.4 ft), are interpreted to be due to subhorizontal fractures.

Dish-shaped fractures, concave toward the opening, that have developed from about 1 ft into the roof and extend from near the north and south ribs and angle deeper into the roof toward the center of the drift, were observed only in radar profiles from the eastern portion of N-1420, between E-1480 and E-1620 (Figure 6-1). Figures 6-3 and 6-4, from E-1560 and E-1620 respectively, show dish-shaped fractures that generally occur with the first 3 to 4 ft of the roof. These fractures do not appear to intersect clay I.

The GPR surveys conducted across the width of Drift N-1420, at locations west of E-1480, generally do not have arcuate fractures and generally show less deformation than do the radar profiles from transects conducted east of E-1480. All radar profiles from the N-1420 Drift contained fracturing of some type.

Figure 6-5 shows a radar profile from the E-1120 traverse. This traverse is located about midway between Room B and Room A1 (Figure 6-1). The fractures observed in this radar profile, as well as other nearby radar profiles (Appendix E), display different geometries than

the dish-shaped fractures observed further east in the drift. In Figure 6-5, clay I is located at about 27 ns (5.0 ft) into the roof. Figure 6-5 also contains relatively flat or angled slightly upward, "stacked" fractures close to the roof surface. These fractures angle upward from about 8 ns (1.5 ft) into the roof near the north end of the profile to about 25 ns (4.7 ft) near the south end of the profile. Fractures that angle upward from the north to the south rib below clay I also occur in other radar profiles east of E-1480 (Appendix E).

Reflections extending across the entire roof span, at about 8 ns (1.5 ft) in Figure 6-5, are interpreted to be due to "drummy" ground in the roof. Relatively flat reflections within about the first 1 to 2 ft (0.30 to 0.61 m) into the roof are believed to be shallow, horizontal fractures of the type that have been found throughout the underground. Cook and Roggenthen (1991) describe this type of fracturing as causing "drummy" ground in the roof that generally develops within 1.5 ft (0.5 m) of the roof and comprises thin slabs with little separation between them.

Reflections from fractures and stratigraphy above clay I in Figure 6-5 display small amplitudes relative to reflections from fractures below clay I and reflections from clay I itself. This is probably due to two factors: (1) clay I is such a strong reflector that little energy is left for transmission deeper into the roof, and (2) greater amounts of deformation could be expected to occur in the horizon between the roof and clay I.

Figure 6-6 is an axial survey, conducted along the center line of Drift N-1420, from Room C-1 to EEP #32 (E-1589 to E-1470, see Figure 6-1). At an area between 88 to 108 ft (27 to 33 m) from the west end of the survey, the reflections from clay I are much smaller in amplitude. Therefore, this is interpreted as a location where clay I may contain less amounts of brine than the remaining areas shown in the axial survey (Figure 6-6).

Figure 6-6 also shows that most of the fracturing in the N-1420 roof occurs between the roof and clay I. Many reflections above clay I are due to vertical bands of noise caused by pipes, cables, and lights suspended from the roof surface. Subhorizontal, relatively large amplitude reflections immediately above clay I are echoes of the strong reflections from clay I due to the presence of brine. Deeper into the roof, at about 50 ns (9.4 ft), are subhorizontal reflections believed to be due to clay J. This interpretation is based on the horizontal aspect of the reflections and the distance of the reflections from clay I.

6.3 Summary of N-1420 GPR Survey Results

The horizon between the roof and clay I, in all areas surveyed, contains many fractures. This would be expected, given that the excavation is much older and smaller (14-ft wide) than the newer waste storage rooms and access drifts.

Fewer fractures were observed in the roof above clay I than below clay I, with the exception of E-1480. Clay I returns strong amplitude reflections, and based on these strong amplitude reflections and physical observations made during drilling of the EEP arrays, it is believed that clay I is saturated with brine in most of the surveyed areas.

In general, the most deformation observed in the N-1420 roof was in the areas between E-1480 and E-1620 (see Figures 6-2 through 6-4), where several dish-shaped fractures occur. The dish-shaped fractures are concave toward the opening and generally extend from about 1 ft (0.3 m) into the roof, near the north and south side of the drift, and angle deeper into the roof to about 3 to 4 ft (0.9 to 1.2 m). The dish-shaped fractures flatten near the center of the drift and do not appear to intersect clay I.

The fractures in profiles west of E-1480 display a "stacked" fracture geometry. In other words, numerous relatively flat fractures are developed at successively greater distances into the roof, beginning at about 1.5 ft (0.5 m) and continuing to clay I at about 4.4 to 5.3 ft (1.3 to 1.6 m). In some radar profiles these "stacked" fractures are angled slightly upward as in Figure 6-5. Reflections extending across the entire roof span, at about 1 to 2 ft (0.3 to 0.6 m) into the roof, are interpreted to be due to subhorizontal fracturing, which results in "drummy" ground in the roof.

In some areas, there are reflections from what is believed to be either a clay seam, or argillaceous halite (clay J), which is about 5 ft (1.5 m) above clay I (see Figure 6-6). This interpretation is based on the horizontal aspect of the reflections and the distance of the reflections from clay I. Reflections interpreted to be due to clay J are not present in many of the radar profiles from N-1420. Clay J may only be detected when it is either saturated with brine or contains greater percentages of clay. Additionally, radar energy must be able to penetrate far enough into the roof such that reflections from clay J may be detected. The presence of brine or greater amounts of clay could increase the relative dielectric constant contrast between clay J and the surrounding salt to allow detectable reflections from the unit.

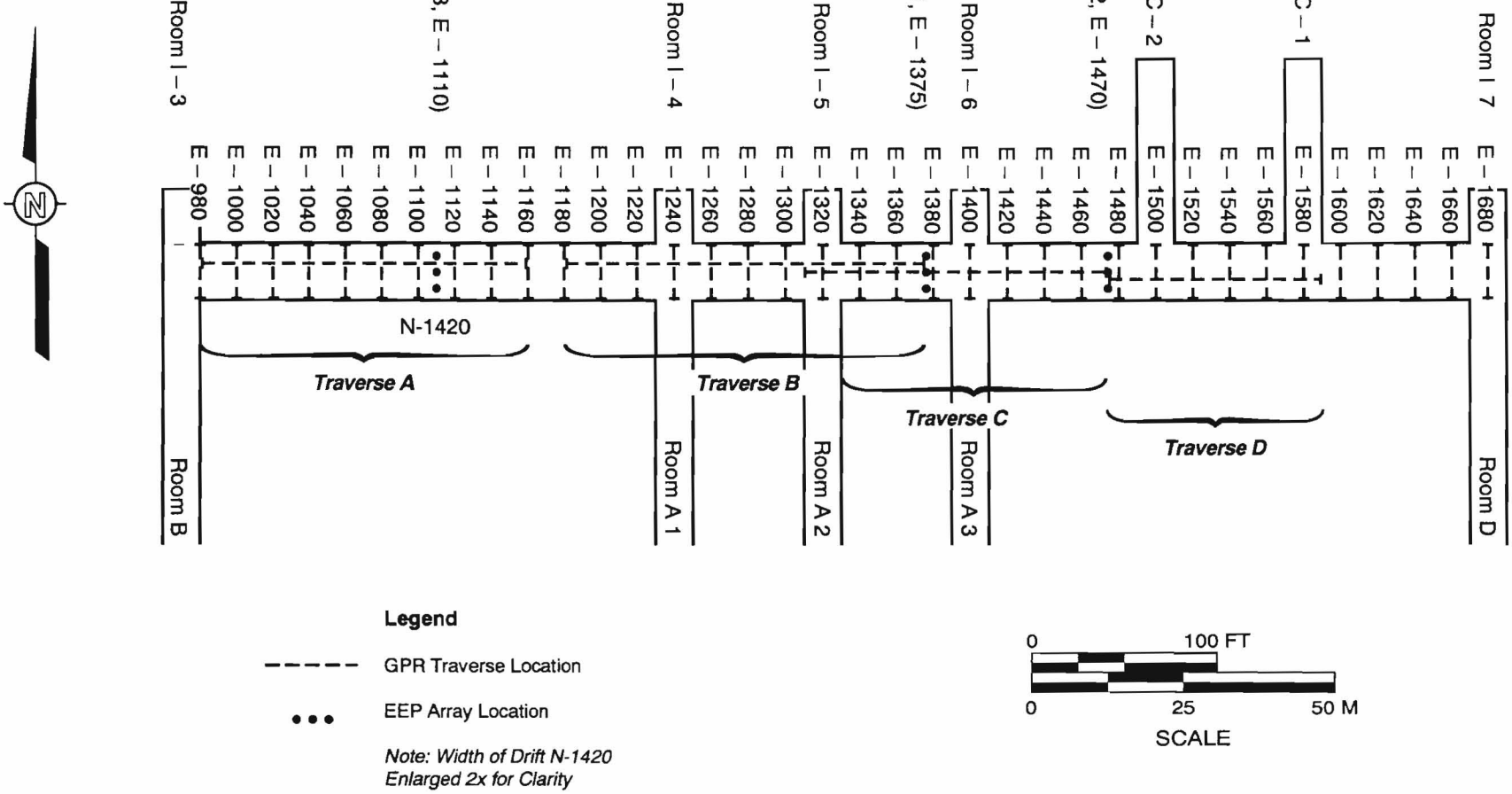

Figure 6-1
Locations at GPR Surveys on Roof of N-1420 Drift and EEP Arrays #31, 32, and 33

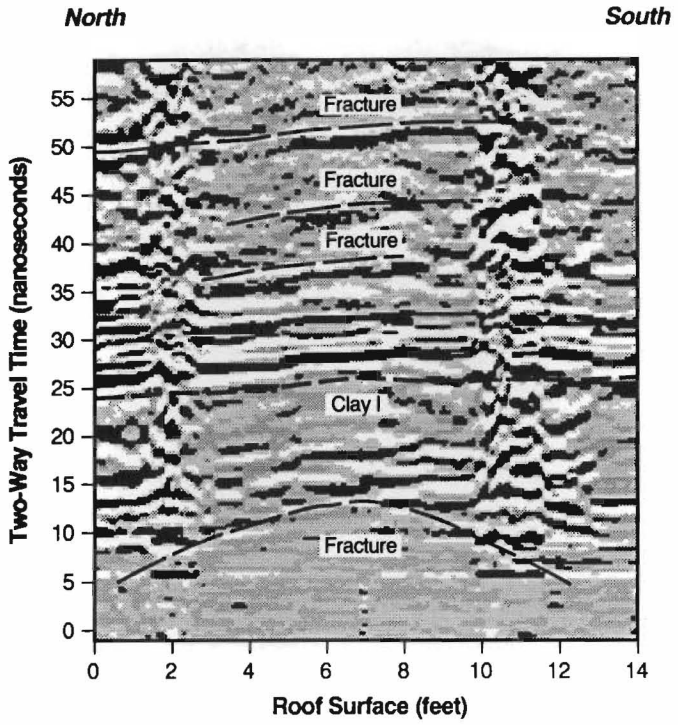

Figure 6-2
E-1480 Traverse, N-1420 Drift Roof: June 1991

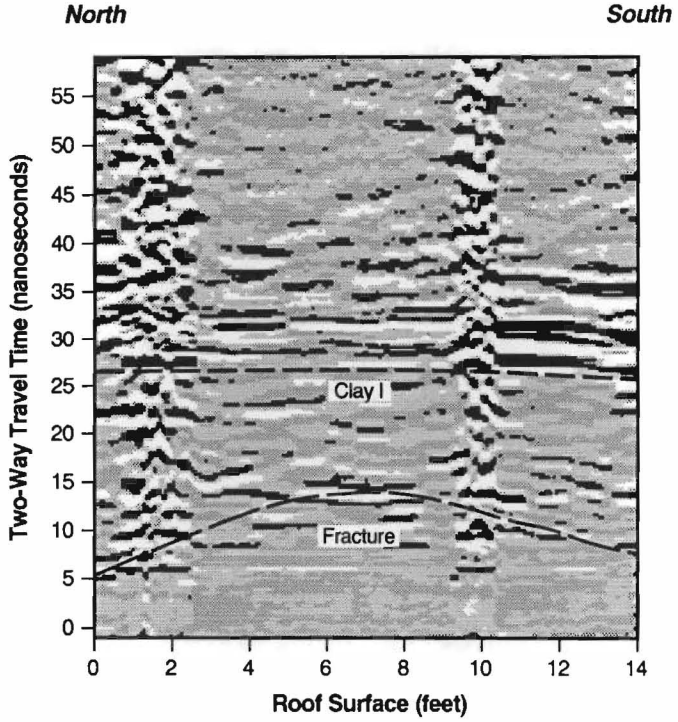

Figure 6-3
E-1560 Traverse, N-1420 Drift Roof: June 1991

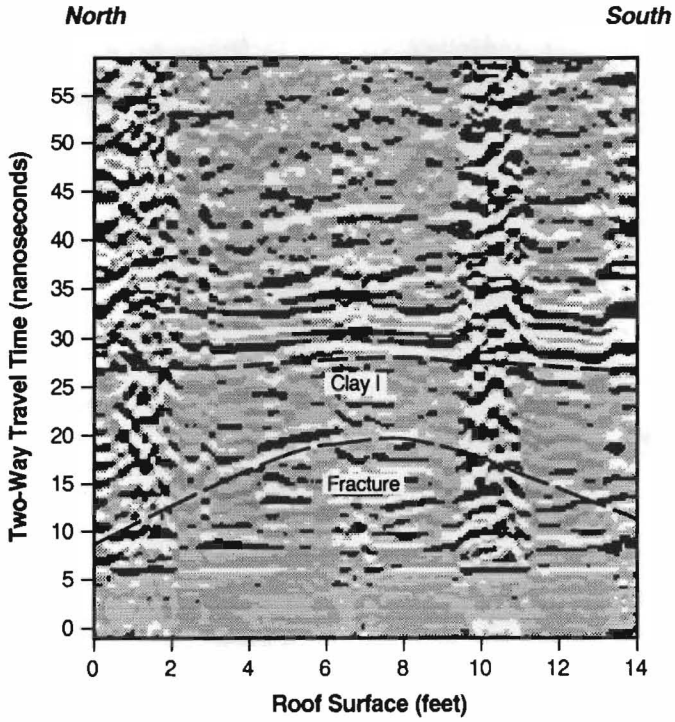

Figure 6-4
E-1620 Traverse, N-1420 Drift Roof: June 1991

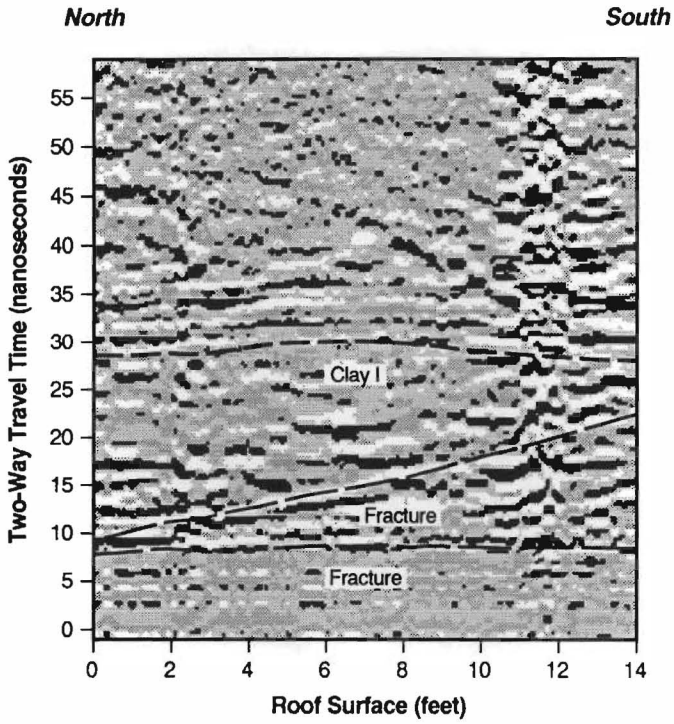

Figure 6-5
E-1120 Traverse, N-1420 Drift Roof: June 1991

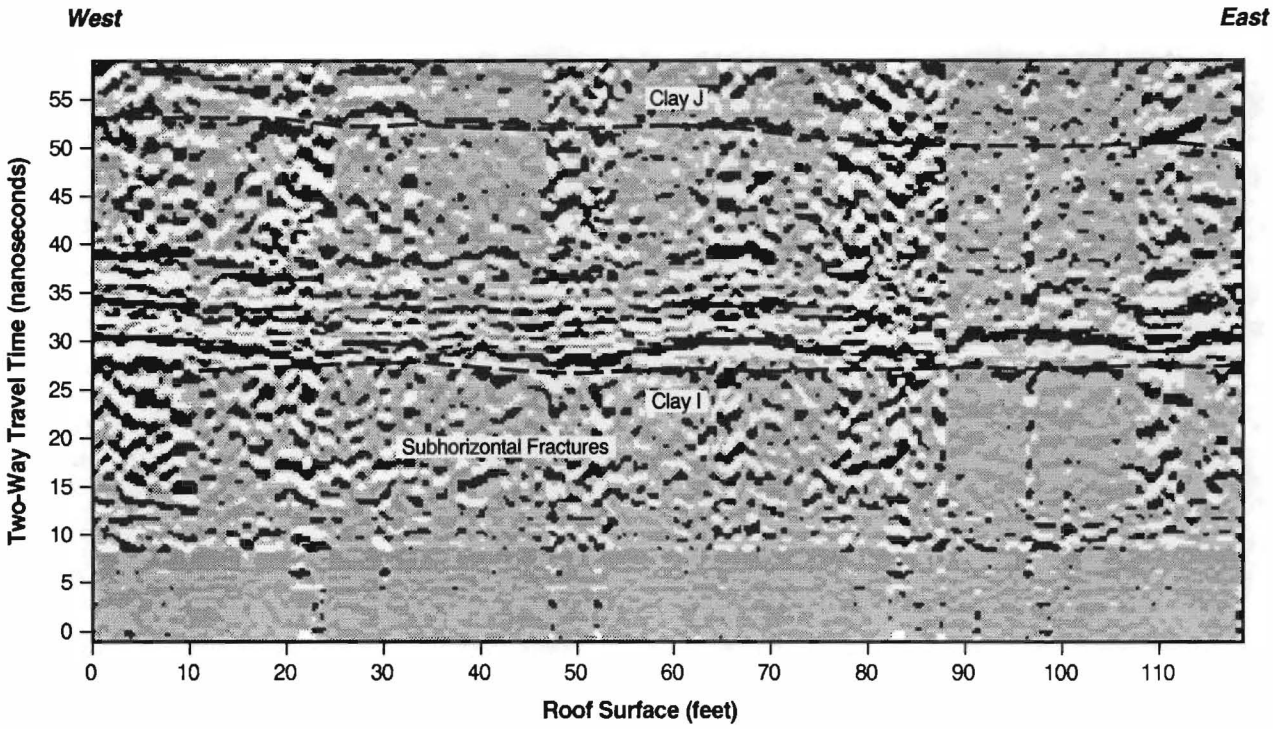

Figure 6-6
Traverse D, E-1470 to E-1589, N-1420 Drift Roof: June 1991
Vertical Exaggeration 4x

7.0 GPR Surveys in Room Q and Room Q Access Drift

7.1 Introduction

Ten GPR surveys were conducted in Room Q on March 3, 1991. Room Q is an experimental room used by Sandia National Laboratories/New Mexico (SNL/NM). Room Q is different from other experimental rooms in the WIPP underground and is shaped like a hollow cylinder with a diameter of 9.5 ft (2.9 m) and a total length of 355.5 ft (108.4 m). The surveys conducted in Room Q included eight circumferential surveys and two axial surveys (see Figure 1-2 for the location of Room Q).

During the collection of radar data in Room Q, the GPR instrumentation controls were located outside of the room and were operated by personnel from the WIPP geotechnical engineering group and personnel from IT Corporation (IT). Personnel with confined-space training from the WIPP Experimental Operations group operated the antenna within the room and recorded the locations of the surveys within the room. The antenna and instrumentation settings used to conduct the radar surveys in Room Q are included in Appendix F, along with processing sequences used to produce the radar profiles, and additional radar profiles not discussed in the body of this report.

Seven radar surveys were also conducted in the Room Q Access Drift (S-90 Drift) on March 3, 1991 (see Figure 1-2 for the location of the Room Q Access Drift). Surveys were conducted near an array of five boreholes (QPB05, QPB04, QPB03, QPB02, and QPB01). The boreholes were drilled as part of an experiment conducted by SNL/NM personnel. Information on stratigraphy was not available from these boreholes; thus, the radar surveys were not used for calculation of the 500-MHz wave velocity.

The average wave velocity of 0.37 ft/ns was used to convert two-way travel times from reflectors in Room Q and in Room Q Access into distance (see Section 1.3 for calculation of average wave velocity). Two-way travel times to a reflector may be divided by 5.35 ns/ft to give the distance to the reflector in ft.

7.2 Results of Room Q Surveys

The intersection of Room Q with the wall in the instrumentation area (i.e., west wall of the Room Q Access Drift) is called the Room Q collar (Figure 7-1). Both axial and circumferential surveys were conducted between 43 ft to 80 ft (13.1 to 24.4 m) west of the

collar. The circumferential radar surveys in Room Q were conducted beginning at the center of the floor and rotated around the room from south to north (i.e., clockwise, when looking west into the room). The center of the floor was designated as 0 degrees, and degrees of arc were measured in a clockwise direction. One axial survey (Survey 9) was conducted along the center of the floor, and the other (Survey 10) was conducted along a line at about 20 degrees of arc. Figure 7-1 shows the locations of the GPR surveys conducted in Room Q in plan view, and Figure 7-2 illustrates the orientation and locations of the surveys in cross section.

Few reflections were recorded from the floor (0 or 360 degrees) in the circumferential surveys, and a relatively large amount of noise is present in the data taken near the roof of the room. This noise was generated by reflections from suspended cables, wires, and a ventilation tube. Most of the reflections in the circumferential surveys occur between 90 degrees and 270 degrees of arc.

Circumferential surveys were conducted at the following three locations: (1) 77 ft (23.5 m) from the collar, (2) 65 ft (19.8 m) from the collar, and (3) 43 ft (13.1 m) from the collar (Figure 7-1). A pore-pressure measurement array is located at 75 ft (22.9 m) from the collar (Figure 7-1). At this location the ends of the boreholes occur directly above the roof (180 degrees), directly to the north of the room (270 degrees), and directly beneath the floor (0 or 360 degrees). The boreholes originate at the room collar. These boreholes are believed to be the source of many of the reflections observed in the circumferential surveys conducted at 65 ft and 43 ft (19.8 and 13.1 m) from the collar. Figures 7-3 and 7-4, modified from Nowak and others (1990), show the orientation of the pore-pressure test boreholes.

7.2.1 Circumferential Survey at 77 Ft from Collar

In the circumferential surveys, planar or point-source reflectors generate curved, concave-down reflections. This was due to the room's circular geometry, and any reflections from concentric fractures would appear as horizontal reflectors. Figure 7-5 is the radar profile from a circumferential survey conducted 77 ft (23.5 m) from the collar (see Figure 7-1 for survey location). Because the boreholes from the room's collar terminate at the pore-pressure gage array at 75 ft (22.9 m) from the collar, there should be no reflections from boreholes in this radar profile. In Figure 7-5, reflections occur near 180 degrees at about 35 ns (6.5 ft). These reflections occur about 6.5 ft (2.0 m) above the roof and display a curved, concave-

down shape, indicating a planar reflector. These reflections are interpreted to be due to clay G. The stratigraphic horizon of Room Q would place clay G about 7 ft (2.1 m) above the roof of the room.

7.2.2 Circumferential Survey at 65 Ft from Collar

Figure 7-6 is the radar profile from a circumferential survey conducted 65 ft (19.8 m) from the collar. At this location, reflections from boreholes could be expected to occur near 0 and 360 degrees (i.e., beneath the floor), at about 180 degrees (i.e., above the roof), and at about 270 degrees of arc (i.e., in the north wall) (Figure 7-4). There are no coherent reflections beneath the floor, but reflections do occur near 180 degrees and 270 degrees.

The distances to the boreholes from the room's surface at 65 ft (19.8 m) from the collar were calculated based on the angles of the boreholes, and these estimated distances are shown in Table 7-1. Because there are few reflections from beneath the floor (0 and 360 degrees) in the circumferential surveys, the estimated depths to boreholes beneath the floor are not shown in Table 7-1.

Table 7-1
Estimated Distance to Boreholes from Room Q
Excavated Surface at 65 Feet from the Room Collar

Borehole Number	Estimated Location in Profile (degrees)	Distance to Borehole (feet)
QPP05	~180	2.6
QPP04	~180	5.6
QPP03	~180	8.5
QPP25	~270	3.1
QPP24	~270	5.2
QPP23	~270	9.6

A curved, concave-down reflector is present in Figure 7-6, at slightly less than 180 degrees. Based on the average wave velocity of 0.37 ft/ns, it is about 12 ns or 2.2 ft from the room surface. This coincides with the estimated distance to borehole QPP05. Also near

180 degrees, a curved reflector occurs that steepens to the right at about 26 ns, or 4.9 ft. The shape of the reflections suggests a planar target; however, the reflections occur at approximately the same location as the estimated distance to borehole QPP04. Although the GPR-determined distances do not precisely agree with the estimated distances listed in Table 1, it is believed that the reflections at 2.2 ft and 4.9 ft are due to reflections from boreholes QPP05 and QPP04, respectively.

Reflections at about 270 degrees occur about 16 ns (3.0 ft) from the room's surface and are believed to be due to borehole QPP25 (Figure 7-6). These distances from the room's surface determined by the wave velocity agree well with the estimated distance to borehole QPP25 (Table 7-1).

7.2.3 Circumferential Survey at 43 Ft from Collar

The radar profile from a survey conducted at 43 ft (13.1) from the collar is shown in Figure 7-7, and the reflections are interpreted to be due primarily to boreholes near the excavation surface (Figure 7-4). Table 7-2 contains the estimated distances to boreholes at 43 ft (13.1 m) from the collar, determined from the angles of the boreholes. Because there are few reflections from beneath the floor (0 and 360 degrees) in the circumferential surveys, the estimated depths to boreholes beneath the floor are not shown in Table 7-2.

Table 7-2
Estimated Distance to Boreholes from Room Q
Excavated Surface at 43 Feet from the Room Collar

Borehole Number	Estimated Location in Profile (degrees)	Distance to Borehole (feet)
QPP05	~180	1.7
QPP04	~180	3.7
QPP03	~180	5.6
QPP02	~180	11.8
QPP25	~270	3.1
QPP24	~270	5.2
QPP23	~270	8.8

Reflections interpreted to be due to borehole QPP05 occur near 180 degrees at about 11 ns, or 2.0 ft. Smaller amplitude reflections that occur at about 19 ns, or 3.6 ft, from the room surface are believed to be due to borehole QPP04. The distances determined from the radar

profiles using the average wave velocity agree well with the estimated distances to the boreholes (Table 7-2). Also near 180 degrees are reflections at about 25 ns, or 4.7 ft, interpreted to be due to borehole QPP03. The distances from the room's surface determined by the wave velocity and the estimated distance to the borehole QPP03 (Table 7-2) differ by about 1 ft. Possible reasons for these differences will be discussed in a later section.

Reflections near 270 degrees occur at about 17 ns and 28 ns, or 3.2 and 5.2 ft, respectively. These are believed to be reflections due to boreholes QPP25 and QPP24.

7.3 Results of Room Q Axial Surveys

Two axial surveys were conducted in Room Q parallel to the room's long axis and are labeled Survey 9 and Survey 10 in Figure 7-1. The left or west side of the axial radar profiles are at 80 ft (24.4 m) from the collar, and the right or east side is at 43 ft (13.1 m) from the collar.

The radar profile from the floor axial survey (Survey 9) is shown in Figure 7-8. Reflections that occur at about 12 ns (2.2 ft) are believed to be due to borehole QPP15 (Figure 7-4). The reflections that begin at about 30 ns (5.6 ft) and extend across the middle of the room, increasing in two-way travel time towards the west end of the radar profile, are believed to be due to borehole QPP14. Borehole QPP15 is about 2 to 3 ft (0.6 to 0.9 m) beneath the floor of Room Q, and borehole QPP14 is about 5.5 to 6.5 ft (1.7 to 2.0 m) beneath the floor of the room. The estimated position of the test region (75 ft from the collar) is located at about 5 ft (1.5 m) from the west side of the radar profile.

The radar profile from axial Survey 10 is shown in Figure 7-9. The profile contains no interpretable reflections. Because of the location of the survey, no reflections from boreholes would be expected, and there does not appear to be any significant fracture development.

7.4 Discussion of Room Q Radar Survey Results

The reflections in the circumferential surveys are interpreted to be due to boreholes and stratigraphy located in the halite surrounding Room Q. Reflections from clay G, however, were absent in Figures 7-6 and 7-7. Some discrepancies also existed in the estimated distances to boreholes and the distances converted from the two-way travel times of the reflections. Possible reasons for these discrepancies are discussed below.

The circumferential surveys at each location were conducted at least twice, and the radar-determined distances to reflectors present in two or more surveys from the same location often varied within 0.2 to 0.3 of a ft. This is probably due to differences in the operation or movement of the antenna around the room's circumference. For example, the antenna was not coupled with, or in physical contact with, the room's surface near 180 degrees of arc (i.e., the roof) because of the limited reach of the personnel operating the antenna. Also, although efforts were made to perform each survey in an identical manner, the spacing between the roof and antenna, the locations (in degrees of arc) where the antenna left and returned to the excavation surface, and the rotation speed of the surveys undoubtedly varied.

The data, especially data taken from near the roof of Room Q, contain a significant amount of noise due to various objects suspended from the roof of Room Q. This noise complicated the interpretation of the surveys and could have interfered with reflections from boreholes and from clay G. This could be the reason that reflections from clay G at surveys conducted at 43 ft (13.1 m) and 65 ft (19.8 m) from the collar are not readily apparent.

Distances to reflections interpreted to be due to boreholes and stratigraphy were calculated using an average wave velocity of 0.37 ft/ns, whereas the actual wave velocity in Room Q could be somewhat different from that value. Nevertheless, despite these uncertainties the interpretations are believed to be reasonably accurate, based on the general agreement between the estimated locations (in degrees of arc) and distances and the observed locations and distances of the reflections.

The circumferential surveys did not contain any reflections that could positively be identified as reflections from fractures. It is possible that fracture development has not progressed sufficiently to produce fractures with apertures large enough to generate interpretable reflections.

7.5 Room Q Access Results

Seven radar surveys were conducted in the Room Q Access Drift (S-90 Drift) on March 3, 1991. The surveys were conducted near an array of five boreholes (QPB05, QPB04, QPB03, QPB02, and QPB01). The location of the radar surveys and boreholes are shown in Figure 7-10 (see Figure 1-2 for the location of the Room Q Access Drift). Four radar surveys were conducted west to east along the long axis of the Access Drift, and three radar surveys

were conducted north to south perpendicular to the long axis of the Access Drift. Radar surveys were performed to determine the most likely migration paths of brine. These migration paths are probably fractures within the floor of the Access Drift. Fracturing would tend to greatly enhance the porosity of the halite, providing a potential migration path for brine.

Since the radar profiles from the GPR traverses conducted on the floor of Room Q Access Drift are similar in appearance, only one profile is included and discussed. The remaining radar profiles are included in Appendix F, along with the instrumentation settings used to conduct the traverses and the processing sequences used to produce the radar profiles.

Figure 7-11 is the radar profile from traverse 5, which is located near boreholes QPB01, QPB02, and QPB03 in the Room Q Access Drift. Traverse 5 was conducted perpendicular to the long axis of the Access Drift (see Figure 7-10). Large-amplitude undulatory reflections occur at about 26 ns (4.9 ft) across the width of the drift. This is interpreted to be the upper contact of MB139. The continuous reflections across the width of the Access Drift at about 43 ns (8.0 ft) are interpreted to be clay E at the lower contact of MB139. Thus, MB139 is approximately 3 ft (0.9 m) thick at this location. The halite above MB139 is relatively free from reflections, except for continuous reflections at about 10 ns (1.9 ft). These large-amplitude reflections are believed to be subhorizontal fracturing below the floor in the Access Drift.

7.6 Discussion of Room Q Access Results

Fractures that extend down from the ribs and angle deeper into the floor as seen in the floor of Room 1 and Room 6 (sections 3.4 and 4.3) are not present in the Room Q Access Drift surveys. However, horizontally continuous, large-amplitude reflections above MB139 at about 2.0 ft (0.6 m) are present in many of the radar surveys from the Room Q Access Drift. These reflections are interpreted to be subhorizontal fracturing in the floor of the drift. This fracturing may provide a potential migration path for brine in the floor of the Access Drift.

7.7 Summary

The reflections from the Room Q GPR surveys are interpreted to be due to pore-pressure test boreholes and stratigraphy. Most of the reflections in the circumferential surveys occur between 90 and 270 degrees of arc, or the top half of the room.

Few reflections were recorded from the floor of the room in the circumferential surveys, although pore-pressure test boreholes are present beneath the floor (Figures 7-3 and 7-4). It is possible that the rotation speed of the antenna was too great in the vicinity of the floor to record any coherent reflections. Reflections from the floor of the room were recorded from the axial surveys and were attributed to boreholes QPP15 and QPP14.

Reflections in radar profiles from Room Q Access Drift are interpreted to be due to the upper and lower contact of MB139 and subhorizontal fracturing about 2 ft (0.6 m) into the floor of the Access Drift. These fractures may provide a potential migration path for brine.

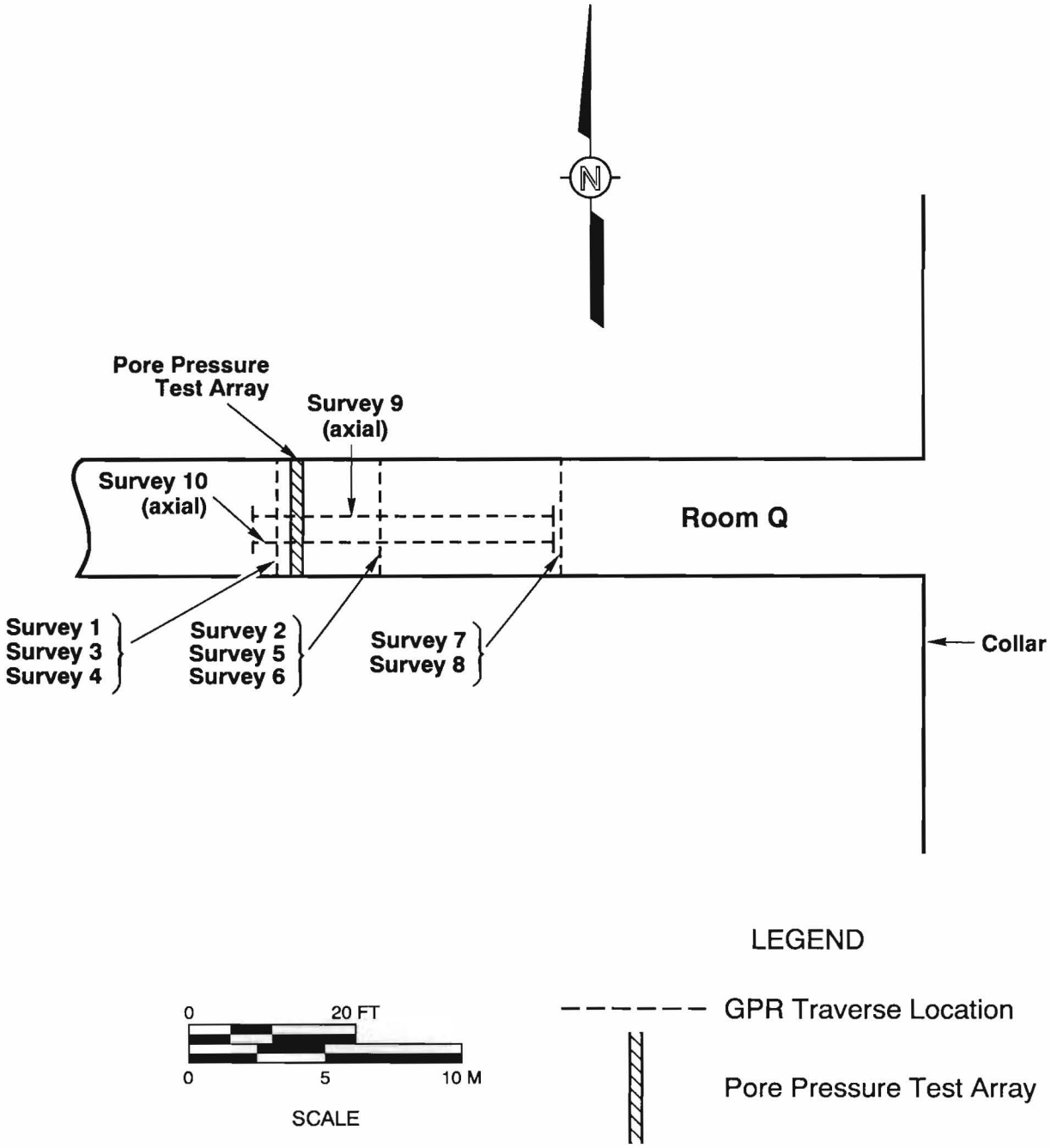

Figure 7-1
Plan View, Room Q Showing Locations of GPR Surveys

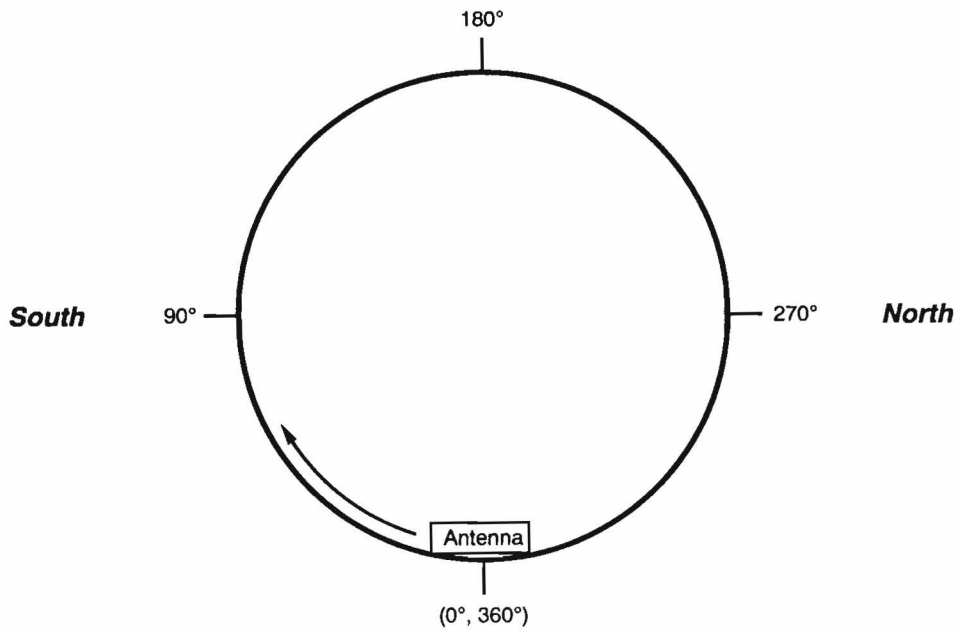

Circumferential Surveys

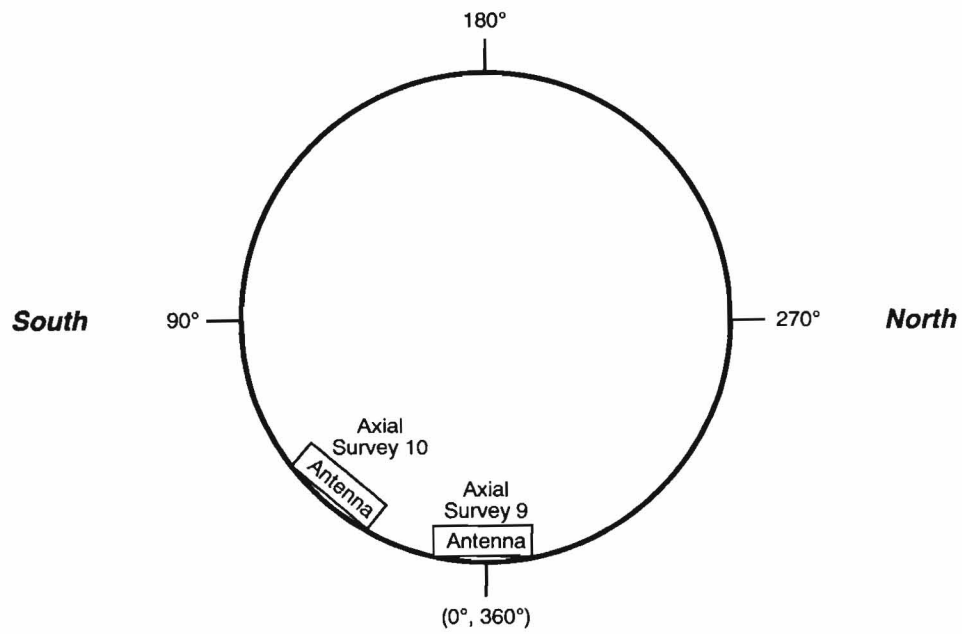

Axial Surveys

Figure 7-2
Room Q, GPR Surveys
Cross-Sectional View, Looking West *(not to scale)*

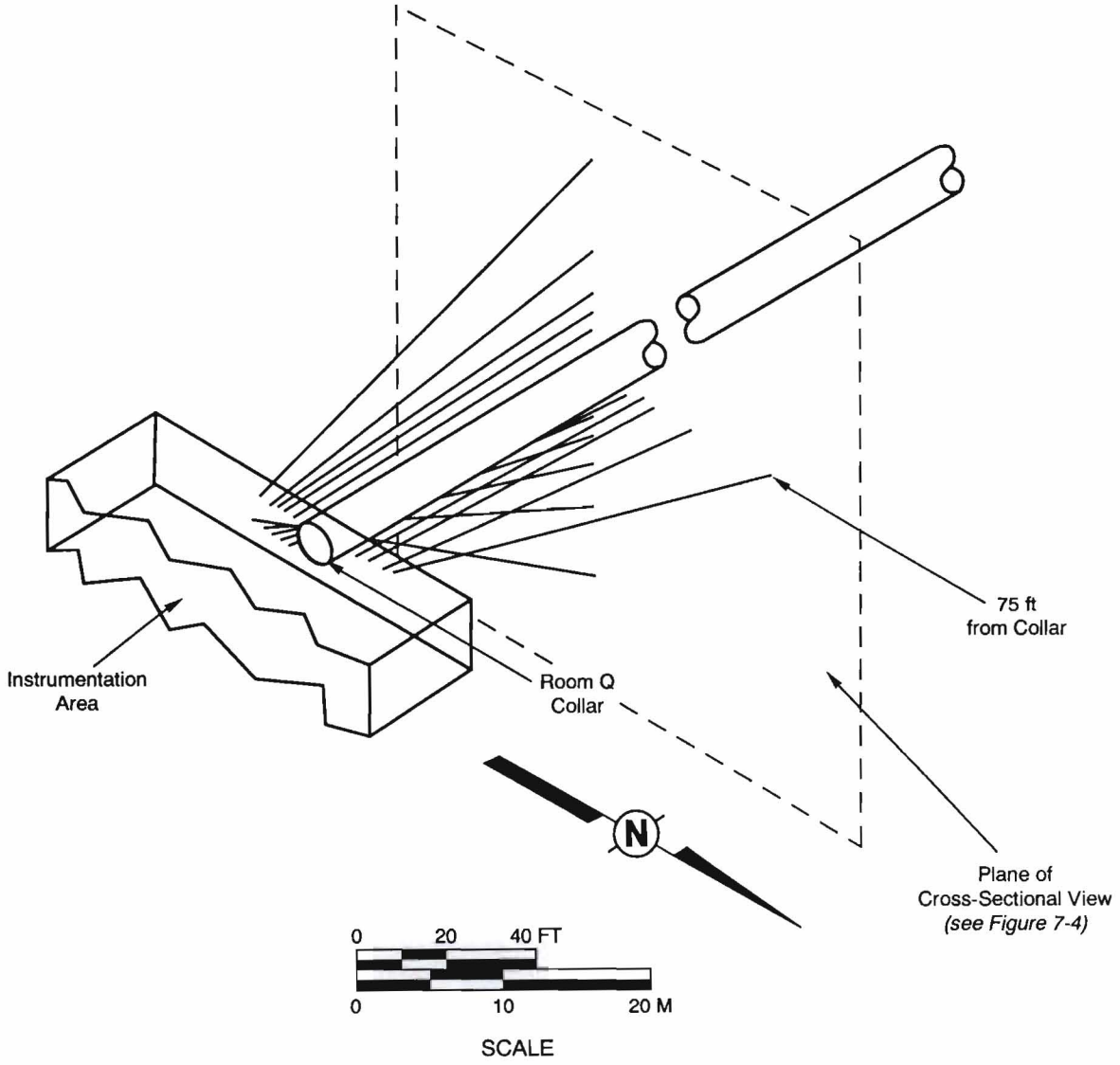

Figure 7-3
Isometric View of the Pore Pressure Test Boreholes Relative to the Instrumentation Area and Collar

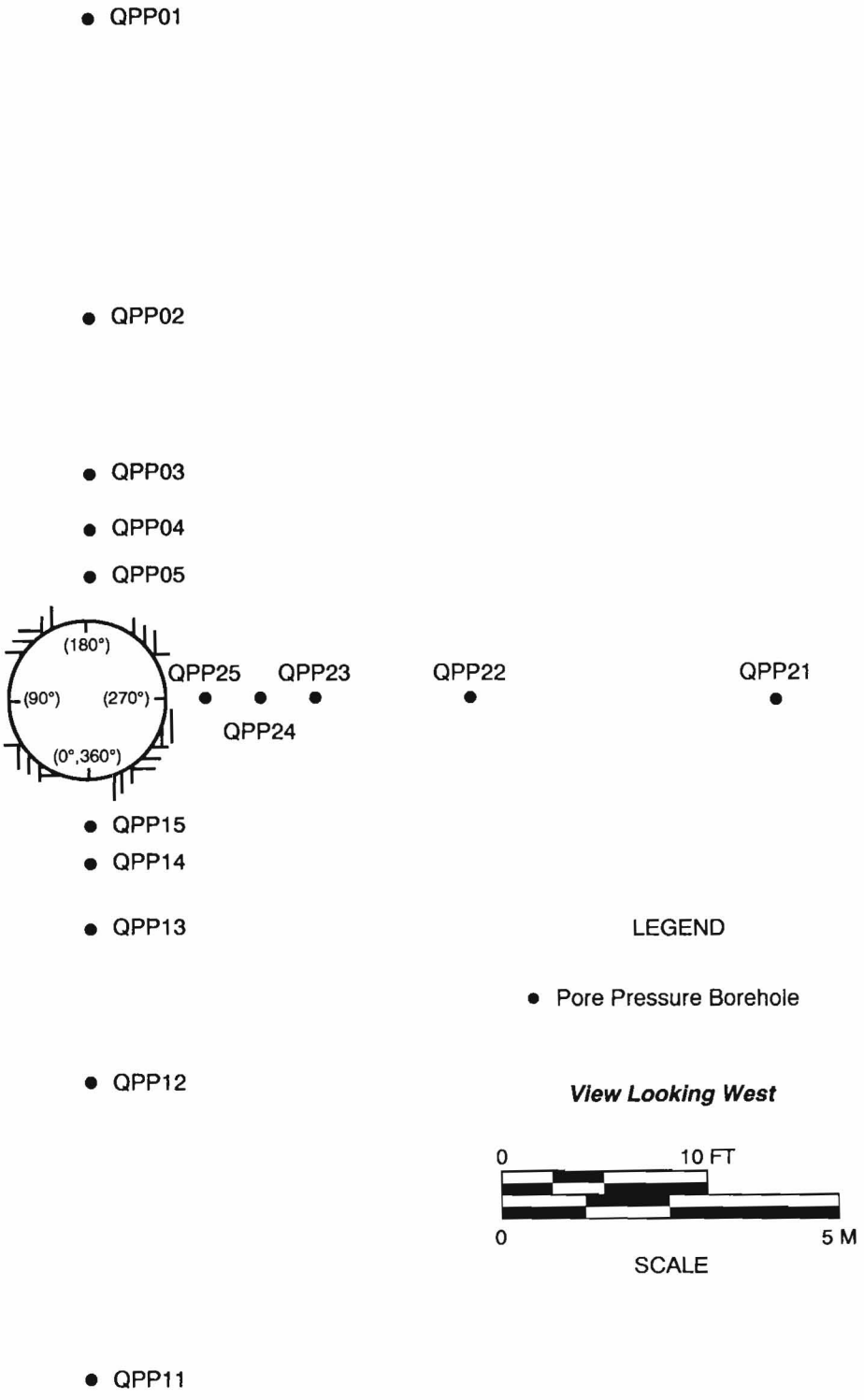

Figure 7-4
Cross-Sectional View of Room Q and the Borehole Array at 75 Feet from the Collar

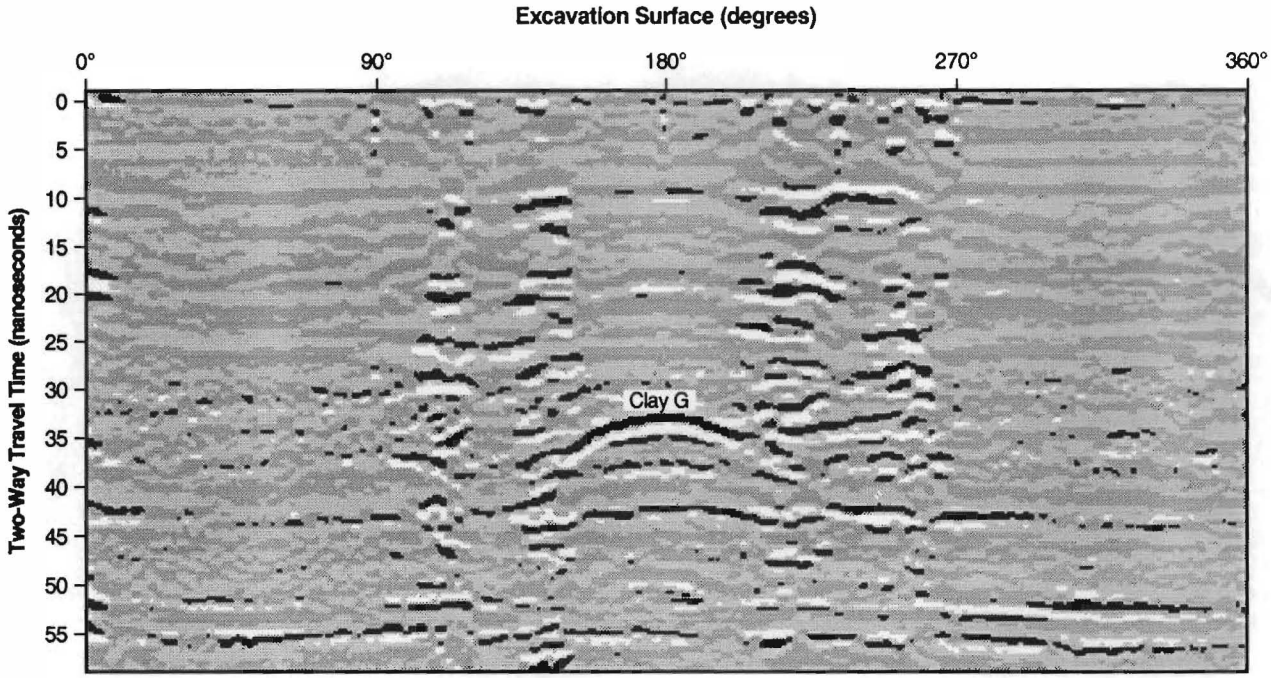

Figure 7-5
Survey 4, Room Q, Circumferential Survey, 77 Feet from the Collar: March 1991

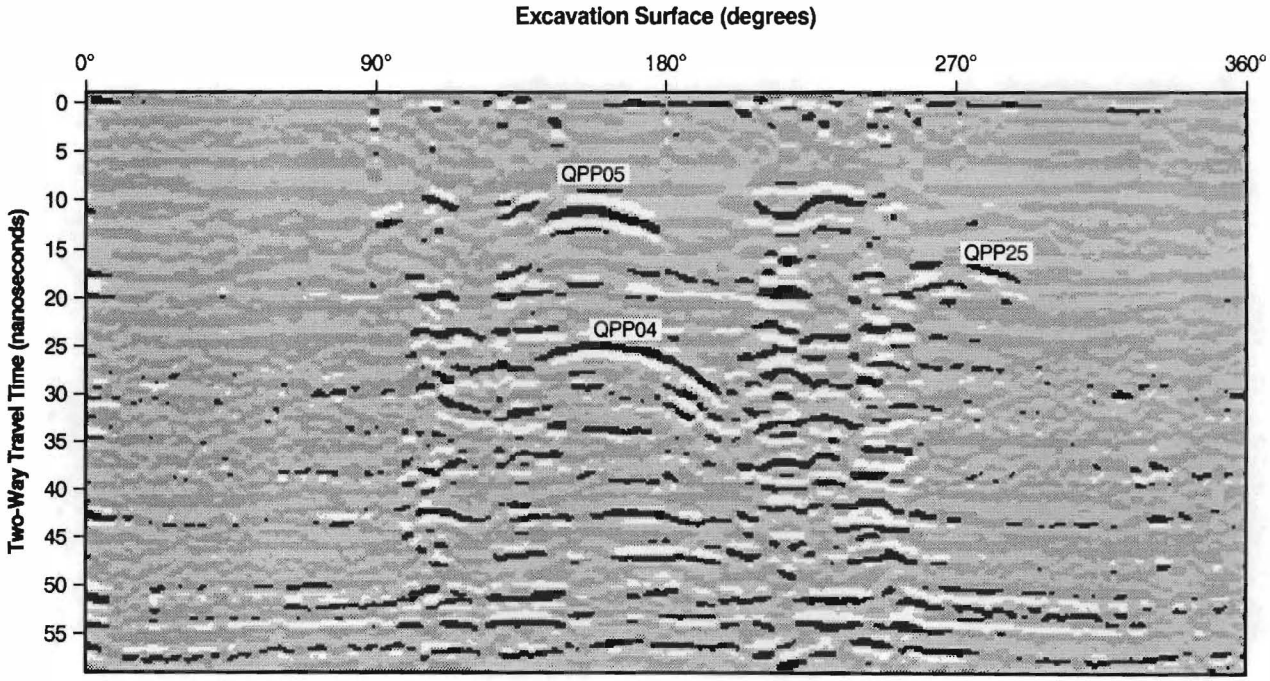

Figure 7-6
Survey 6, Room Q, Circumferential Survey, 65 Feet from the Collar: March 1991

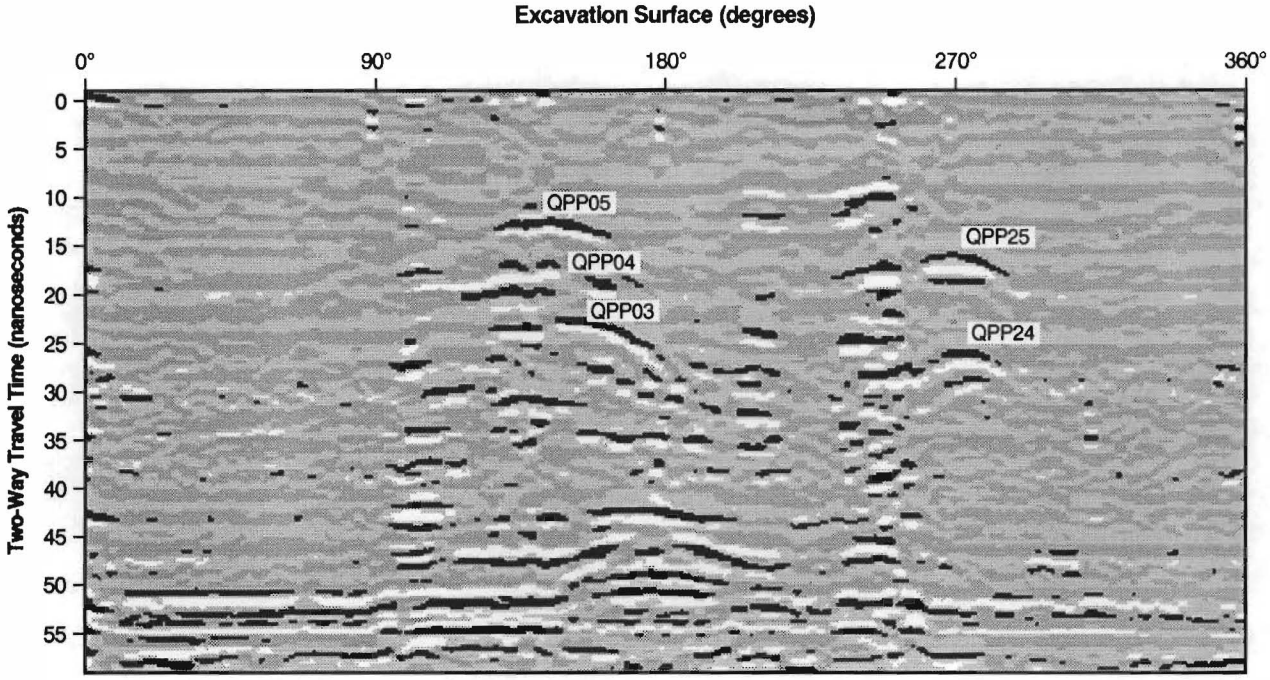

Figure 7-7
Survey 8, Room Q, Circumferential Survey, 43 Feet from the Collar: March 1991

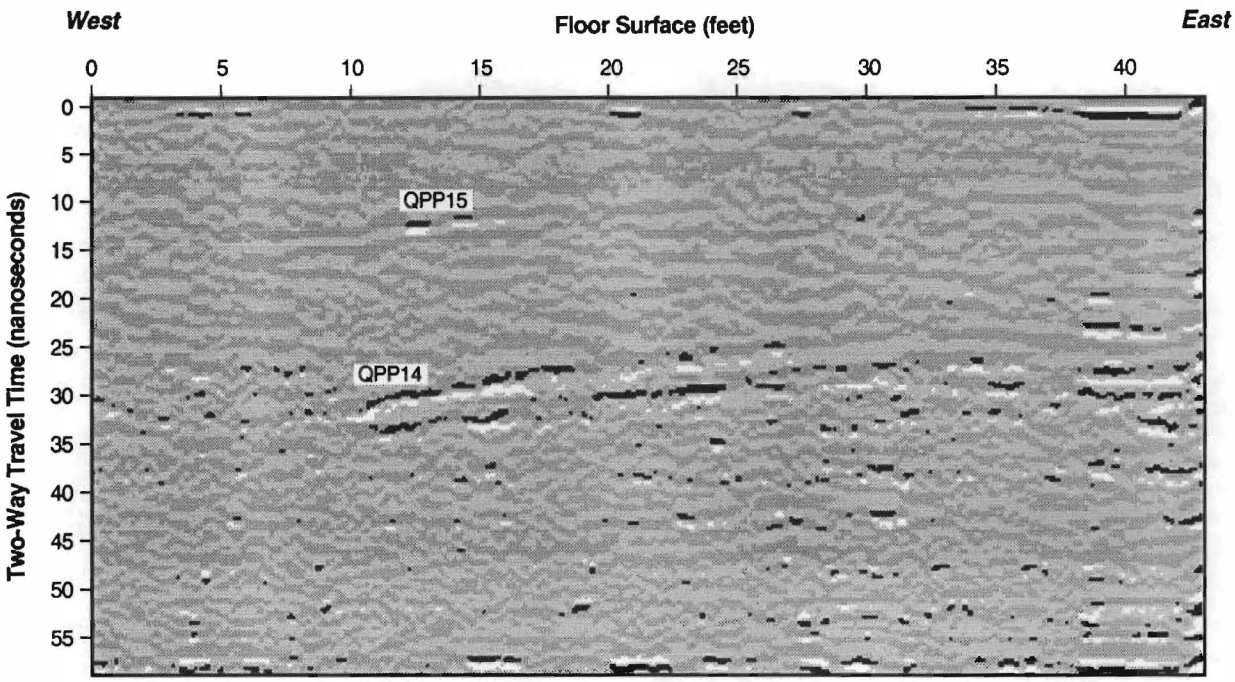

Figure 7-8
Survey 9, Room Q, Axial Survey: March 1991
Vertical Exaggeration 1.5x

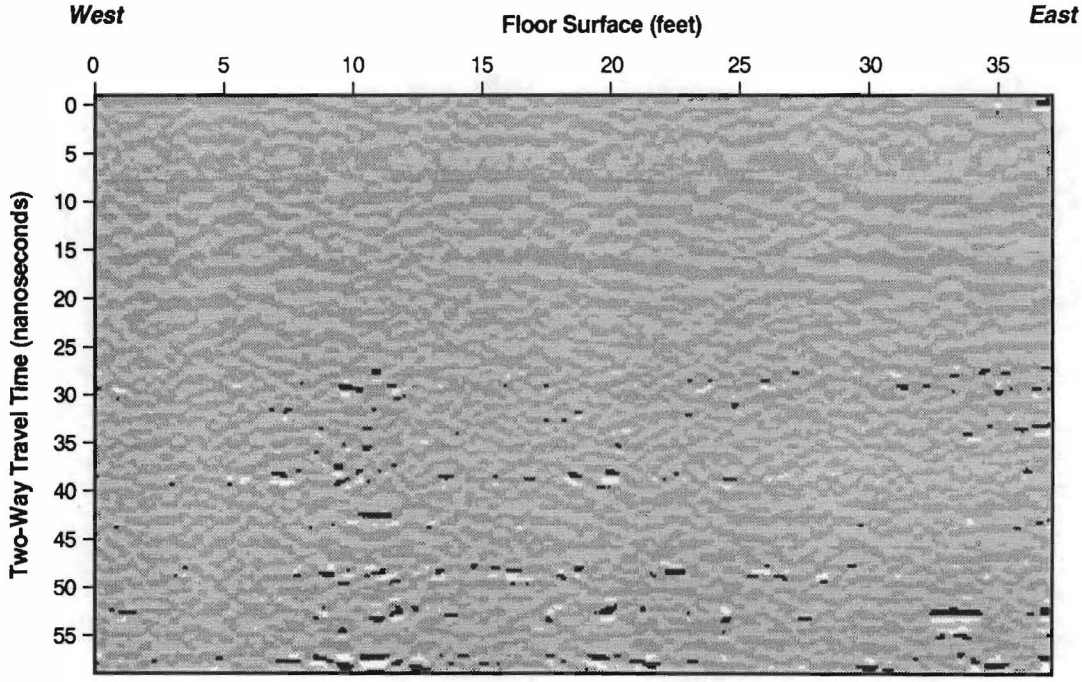

Figure 7-9
Survey 10 Room Q, Axial Survey: March 1991
Vertical Exaggeration 1.5x

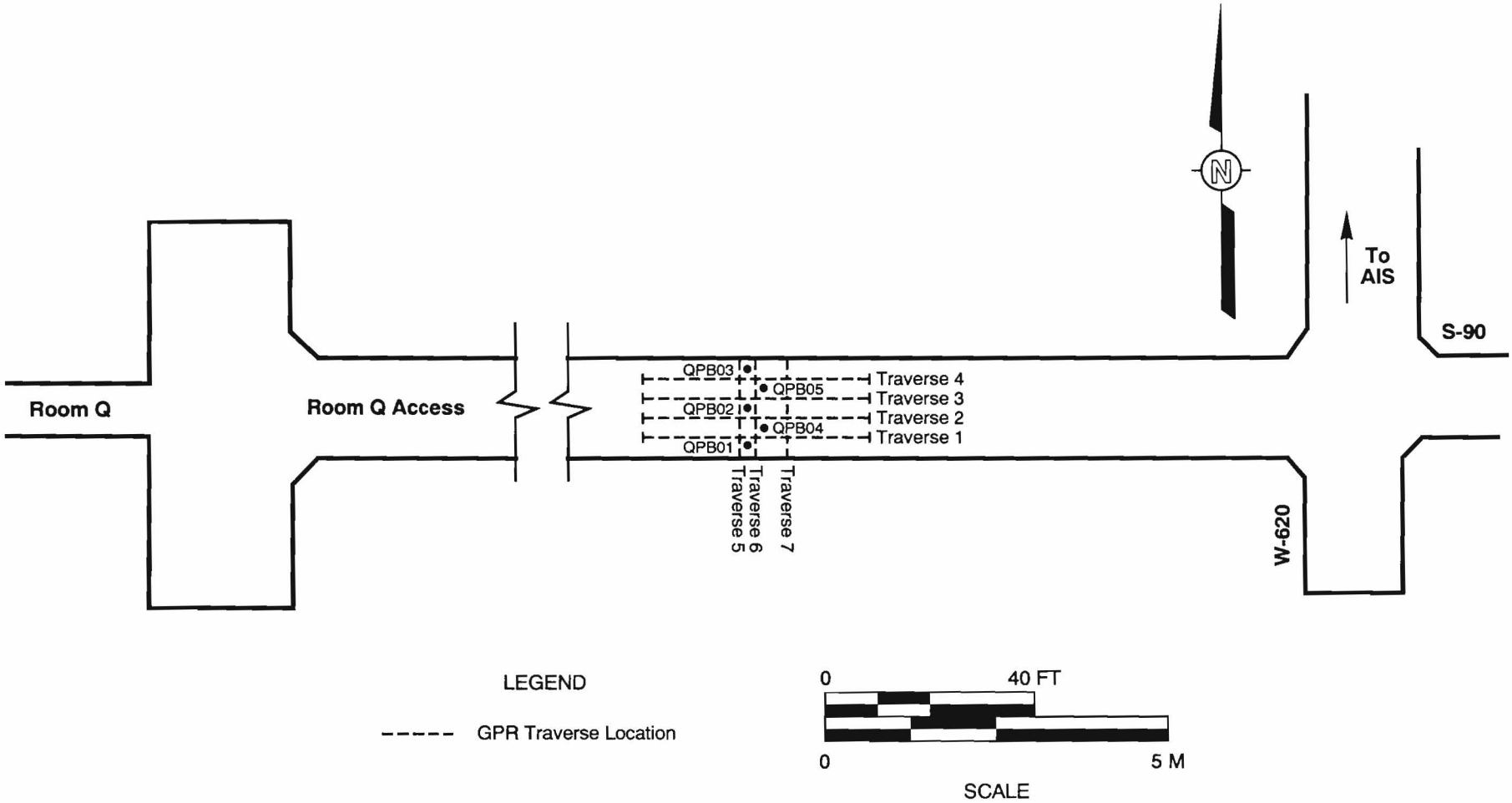

Figure 7-10
Locations of GPR Traverses in Room Q Access (S-90 Drift)

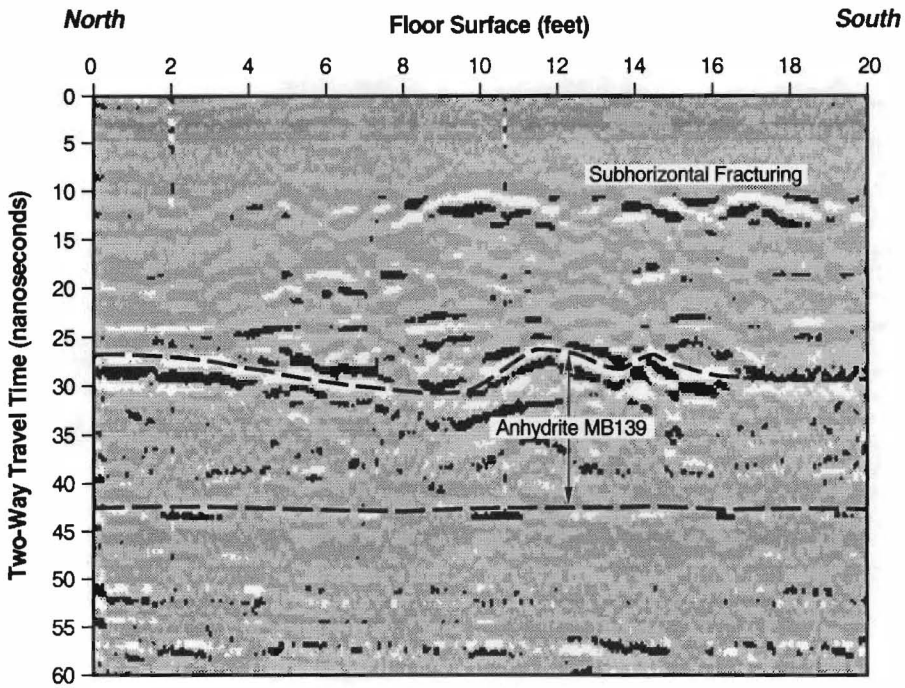

Figure 7-11
Traverse 5, Room Q Access: March 1991

8.0 References

Annan, A. P., J. L. Davis, and D. Gendzwill, 1988, "Radar Sounding in Potash Mines, Saskatchewan, Canada," *Geophysics*, Vol. 53, No. 12, pp. 1556-1564.

Cook, R. F., and W. M. Roggenthen, 1991, "Fracturing Around Excavations in Salt at the WIPP," *32nd U.S. Symposium of Rock Mechanics*, Norman, Olahoma, p. 889-898.

Davis, J. L., and A. P. Annan, 1989, "Ground-Penetrating Radar for High-Resolution Mapping of Soil and Rock Stratigraphy," *Geophysical Prospecting*, Vol. 37, pp. 531-551.

Dobrin, M. B., 1976, *Introduction to Geophysical Prospecting*, McGraw-Hill, New York, 630 pp.

DOE, see U.S. Department of Energy.

Francke, C. T., Westinghouse Corporation, 1992, Personal Communication.

Francke, C. T., 1990, "Results of Recent Demonstration of Ground Probing Radar Techniques for Fracture Characterization," attachment to the letter to V. Daub, April 3, 1990, Westinghouse Electric Corporation, Carlsbad, New Mexico.

Geophysical Survey Systems, Inc., 1989, "RADAN Instruction Manual," *MN43-101*, Rev. D, Release No. 3, Geophysical Survey Systems, Inc., North Salem, New Hampshire.

Geophysical Survey Systems, Inc., 1987, "Operations Manual for Subsurface Interface Radar (SIR) System-3," *Manual MN83-728*, Rev. A, Geophysical Survey Systems, Inc., North Salem, New Hampshire.

GSSI, see Geophysical Survey Systems, Inc.

Kannenberg, M. W., 1991, "Ground-Probing Radar Studies of the Underground Excavations at the Waste Isolation Pilot Plant, Near Carlsbad, New Mexico," unpublished M.S. thesis, South Dakota School of Mines and Technology, Rapid City, South Dakota.

Nowak, E. J., S. J. Finley, and C. L. Howard, 1990, "Implementation of Initial Tests in the Brine Inflow Room (Room Q) of the Waste Isolation Pilot Plant," *SAND90-0611*, Sandia National Laboratories, Albuquerque, New Mexico.

Stormont, J. C., 1990, "Discontinuous Behavior Near Excavations in a Bedded Salt Formation," *SAND89-2403*, Sandia National Laboratories, Albuquerque, New Mexico.

Terril, L., Westinghouse Corporation, 1991, Personal Communication.

U.S. Department of Energy (DOE), 1993, "The Current Bases for Roof Fall Prediction at WIPP and a Preliminary Prediction for SPDV Room 2," *DOE/WIPP 93-033*, Westinghouse Electric Corporation, Carlsbad, New Mexico.

U.S. Department of Energy (DOE), 1991a, "Evaluation of the Effectiveness and Feasibility of the Waste Isolation Pilot Plant Engineered Alternatives: Final Report of the Engineered Alternatives Task Force, Volume 1," *DOE/WIPP 91-007*, Westinghouse Electric Corporation, Carlsbad, New Mexico.

U.S. Department of Energy (DOE), 1991b, "Ground-Probing Radar Surveys of Rooms 1 and 6, Panel 1, and SPDV Test Rooms 3 and 4: March 1990 to March 1991," Draft Report, Prepared by IT Corporation for Westinghouse Electric Corporation, Carlsbad, New Mexico.

U.S. Department of Energy (DOE), 1991c, "Geotechnical Field Data and Analysis Report, Volume 2," *DOE/WIPP 91-012*, Westinghouse Electric Corporation, Carlsbad, New Mexico.

U.S. Department of Energy (DOE), 1991d, "Geotechnical Field Data and Analysis Report, Volume 1," *DOE/WIPP 91-012*, Westinghouse Electric Corporation, Carlsbad, New Mexico.

U.S. Department of Energy (DOE), 1990a, "Performing Underground Ground-Probing Radar Studies," *Document Number 07-318WP*, Westinghouse Electric Corporation, Carlsbad, New Mexico.

U.S. Department of Energy (DOE), 1990b, "Geotechnical Field Data and Analysis Report," *DOE/WIPP 90-006*, Westinghouse Electric Corporation, Carlsbad, New Mexico.

APPENDIX A

INSTRUMENTATION SETTINGS, PROCESSING SEQUENCES, AND RADAR PROFILES: E-0, N-150 OVERCAST

APPENDIX A

This appendix contains the following: (1) possible settings for the dual power/dual reciever amplification, 500-MHz antenna; (2) instrumentation settings used to conduct roof GPR surveys in the vicinity of the overcast at the E-0, N-150 intersection on 03/14/91, and 02/10/92; (3) processing sequences used to produce the radar profiles from the E-0 Drift roof near the E-0, N-150 intersection; and (4) radar profiles not contained in the body of this report (Figures A-1 to A-18).

A.1 Settings for the Dual Power/Dual Receiver Amplification

In February 1991, the 500-MHz antenna for the GPR system was modified to include a dual power/dual receiver amplification. The four possible settings for the 500-MHz antenna are shown in Table A-1.

Table A-1
Dual Power/Dual Receiver Amplification 500-MHz Antenna Settings

Transmitted Signal	Received Signal
High Power	High Amplification
High Power	Normal Amplification
Normal Power	High Amplification
Normal Power	Normal Amplification

A.2.1 Instrumentation Settings for E-0, N-150 Intersection, Roof Surveys (03/14/91)

Antenna settings:

Transmit = high power
Receiver = high amplification

Profiling recorder settings:

Surface gain = 3
Center gain = 2
Deep gain = 4
Threshold = 3
Signal position = manual
Print polarity = +/-
Range(dial) = 60 ns
Range multiplier = 1000
HP filter = 10
LP filter = 50
XMIT rate = 50 KHz
MODE = radar
Scans/sec = 16
Lines/in. = 200

A.2.2 Instrumentation Settings for E-0, N-150 Intersection, Roof Surveys (02/10/92)

Antenna settings:

Transmit = normal power
Receiver = normal amplification

Profiling recorder settings:

Surface gain = 3
Center gain = 2
Deep gain = 4
Threshold = 3
Signal position = manual
Print polarity = -/+/- (negative amplitudes stippled)
Range(dial) = 600 ns
Range multiplier = 100

HP filter = 10
LP filter = 50
XMIT rate = 50 KHz
MODE = radar
Scans/sec = 16
Lines/in. = 200

A.3.1 Processing Sequences for E-0, N-150 Intersection, Roof Surveys (03/14/91)

1. Horizontal scaling

2. Stack = 2

3. Finite impulse response filters

   Horizontal boxcar high pass = 255

4. Predictive deconvolution

   Operator length = 35
   Prediction lag = 17
   Prewhitening = 0.1%

5. Finite impulse response filters

   Vertical triangle high pass = 35
   Vertical triangle low pass = 7
   Horizontal triangle low pass = 7

A.3.2 Processing Sequences for E-0, N-150 Intersection, Roof Surveys (02/10/92)

1. LP compression, TC = 2

2. Horizontal scaling

3. Stack = 2

4. Finite impulse response filters

   Horizontal boxcar high pass = 255

5. Predictive deconvolution

   Operator length = 35
   Prediction lag = 17
   Prewhitening = 0.1%

6. Finite impulse response filters

   Vertical triangle high pass = 35
   Vertical triangle low pass = 7
   Horizontal triangle low pass = 7

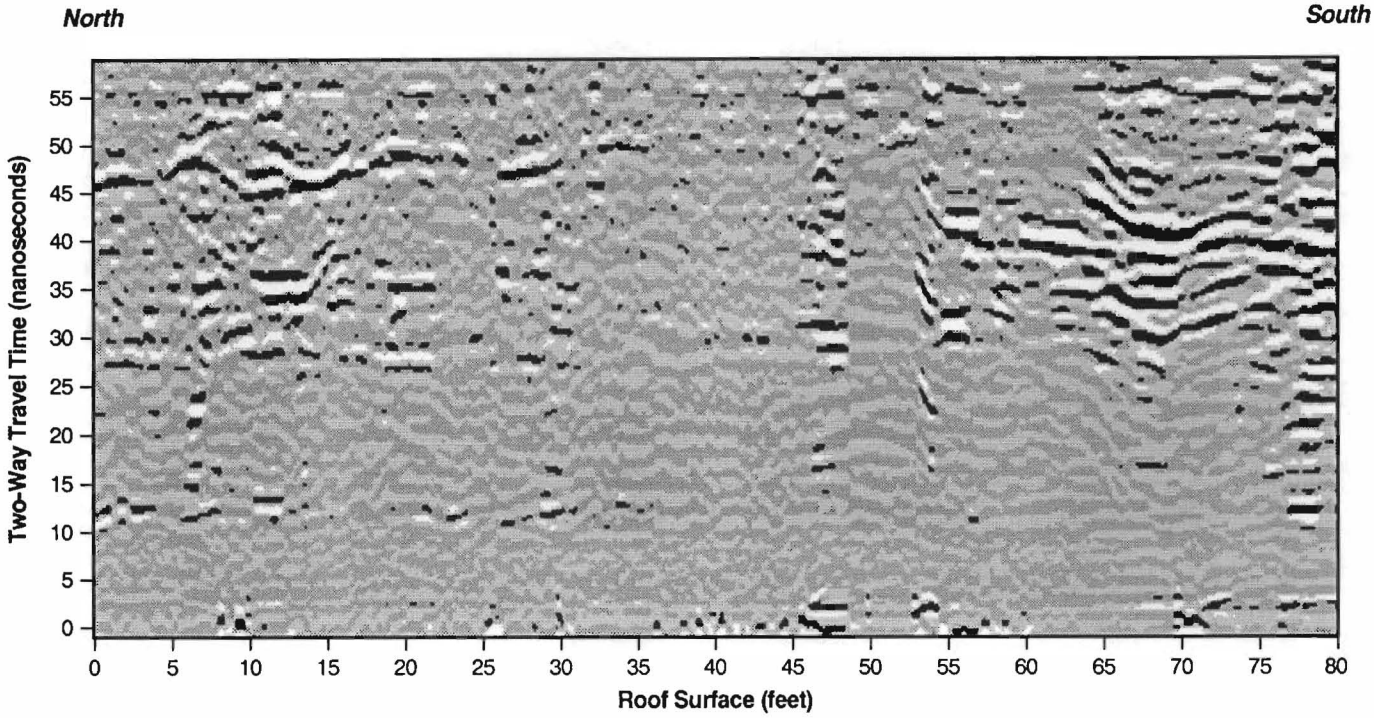

Figure A-1
Traverse 1; E-0, N-150 Overcast: March 1991
Vertical Exaggeration 2.5x

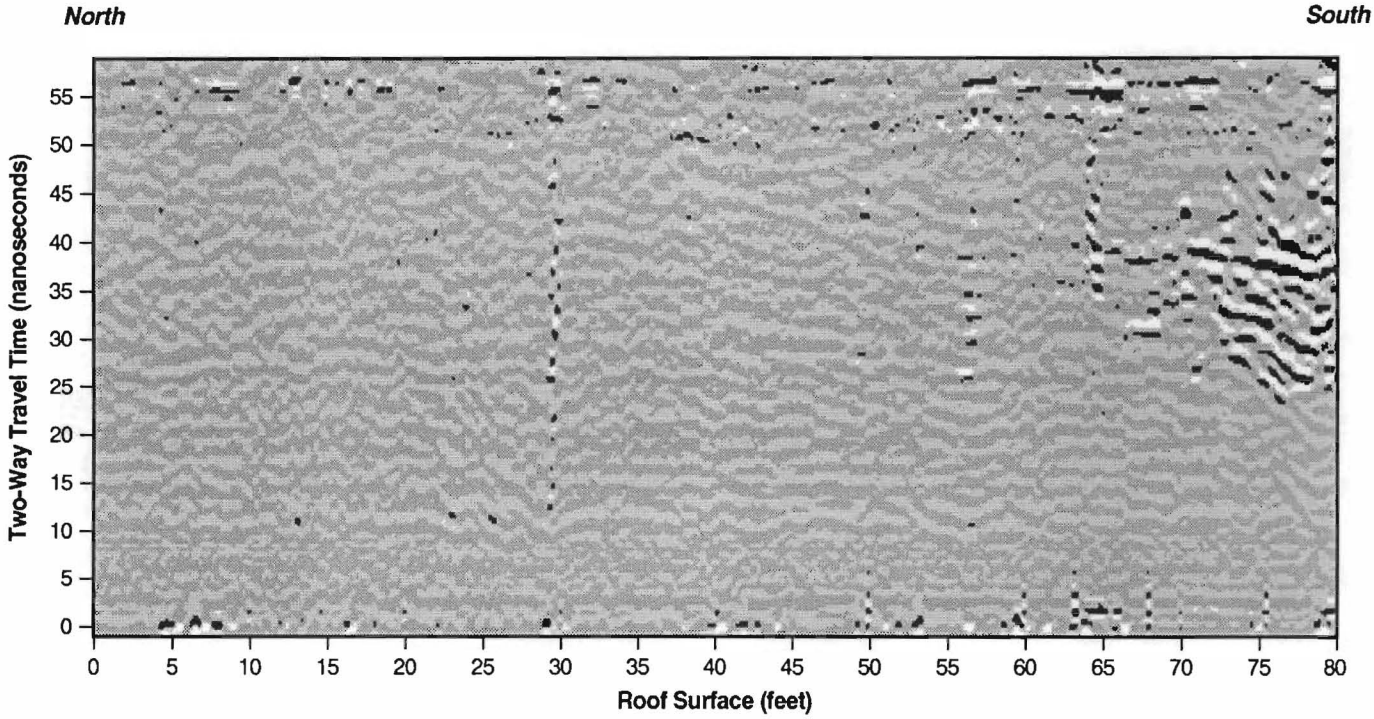

Figure A-2
Traverse 2; E-0, N-150 Overcast: March 1991
Vertical Exaggeration 2.5x

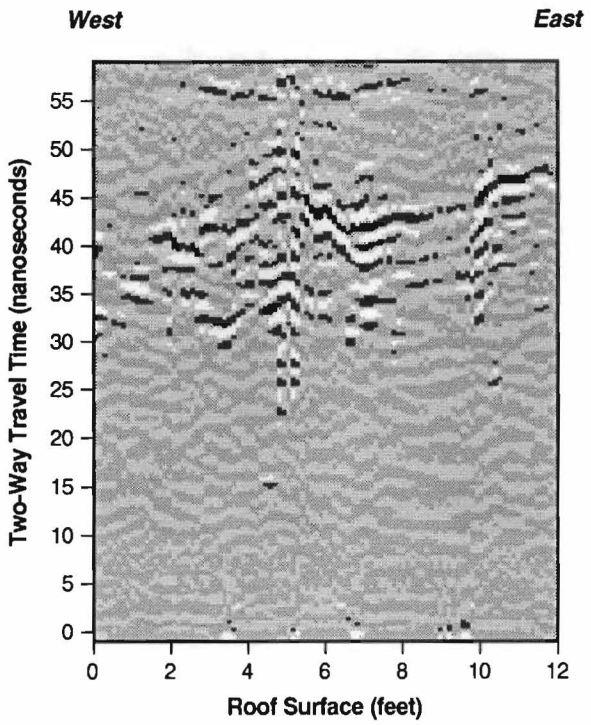

Figure A-3
Traverse 3; E-0, N-150 Overcast: March 1991

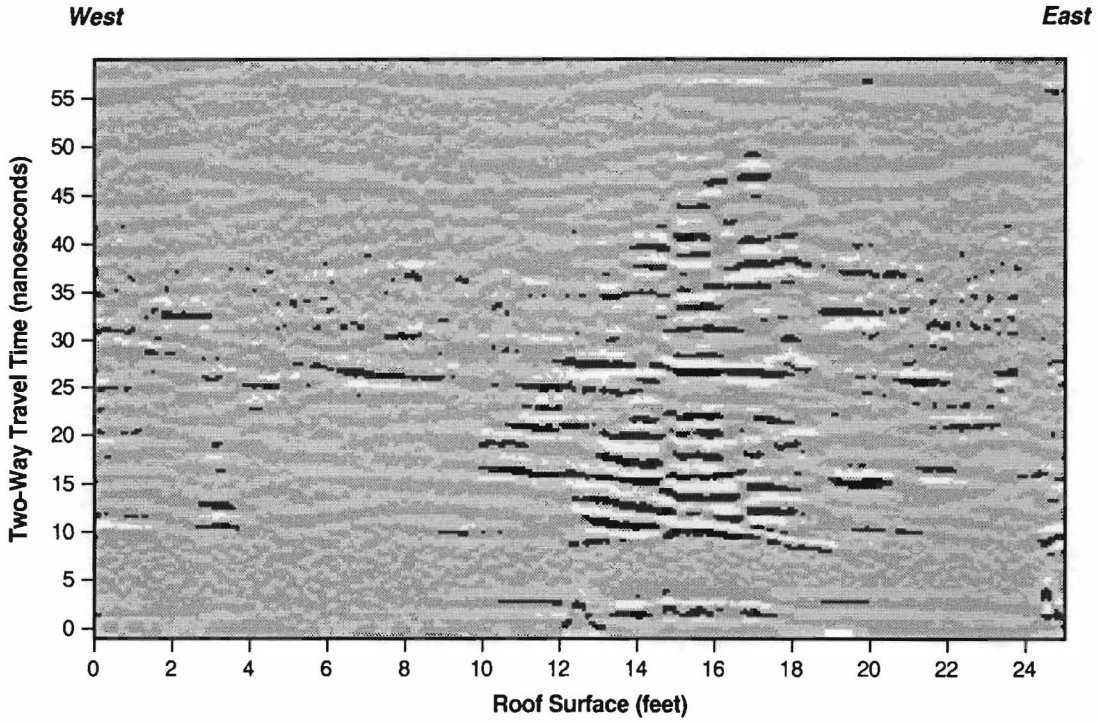

Figure A-4
Traverse 4; E-0, N-150 Overcast: March 1991

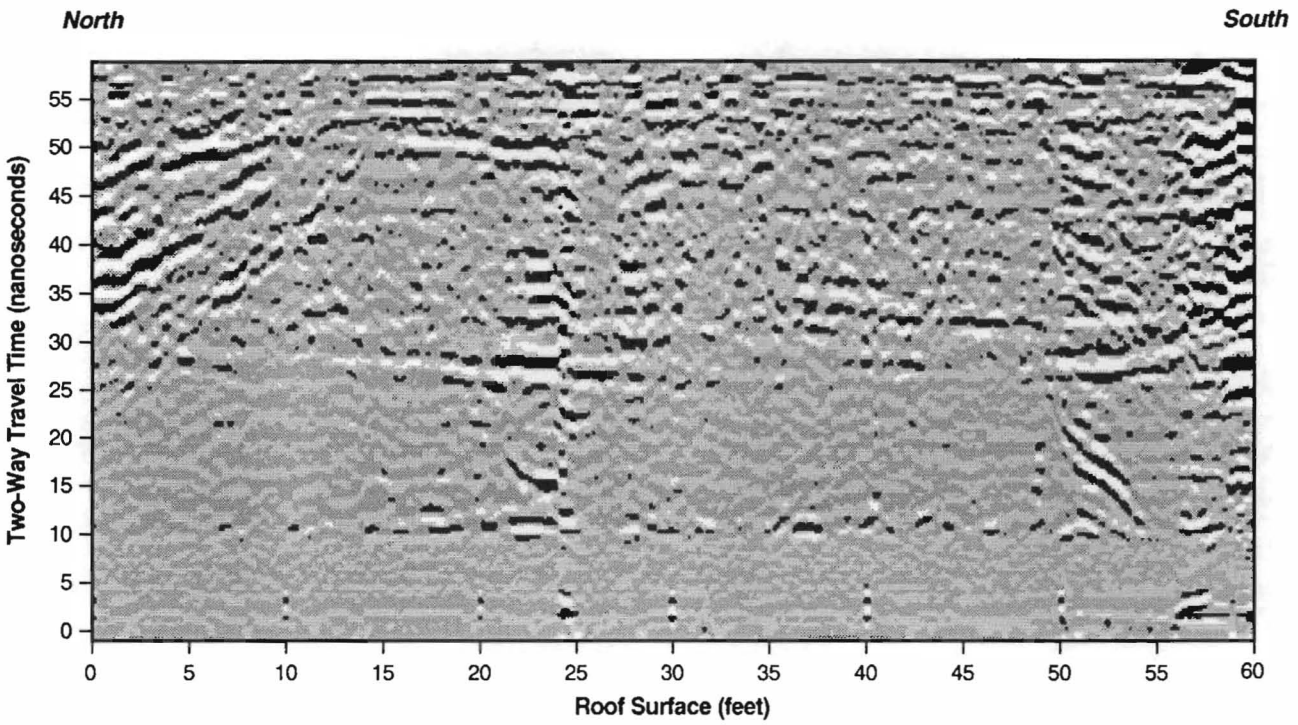

Figure A-5
Traverse 5; E-0, N-150 Overcast: March 1991
Vertical Exaggeration 2.0x

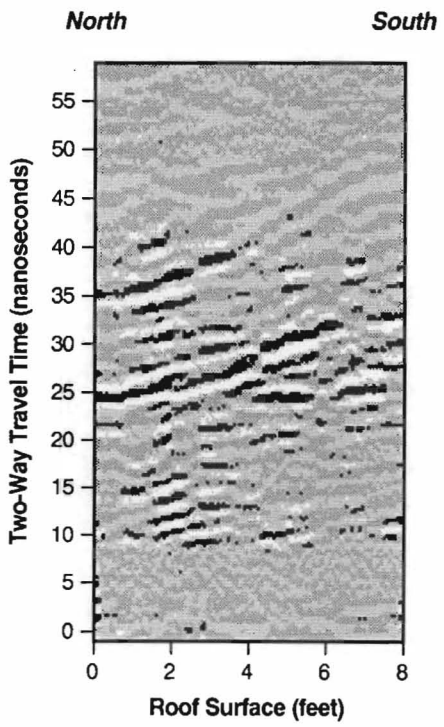

Figure A-6
Traverse 6; E-0, N-150 Overcast: March 1991

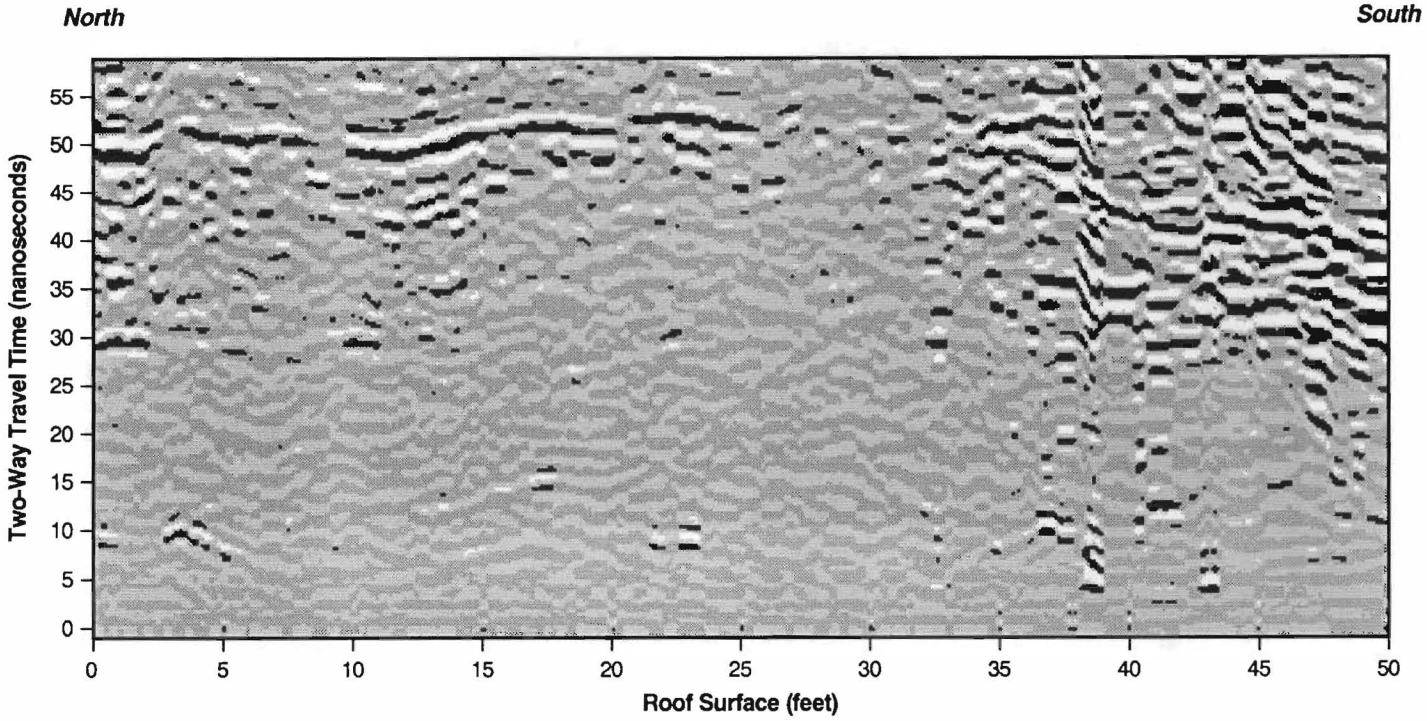

Figure A-7
Traverse A; E-0, N-150 Overcast: February 1992
Vertical Exaggeration 1.5x

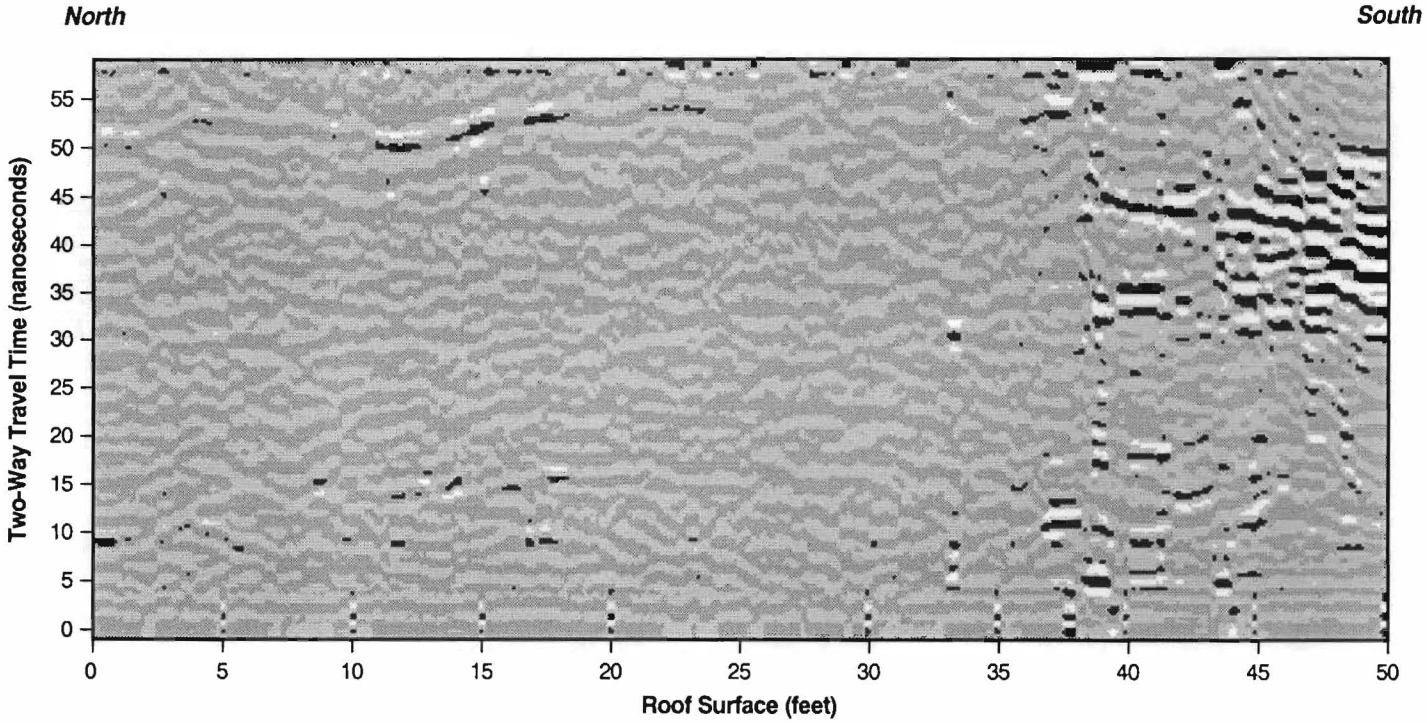

Figure A-8
Traverse C; E-0, N-150 Overcast: February 1992
Vertical Exaggeration 1.5x

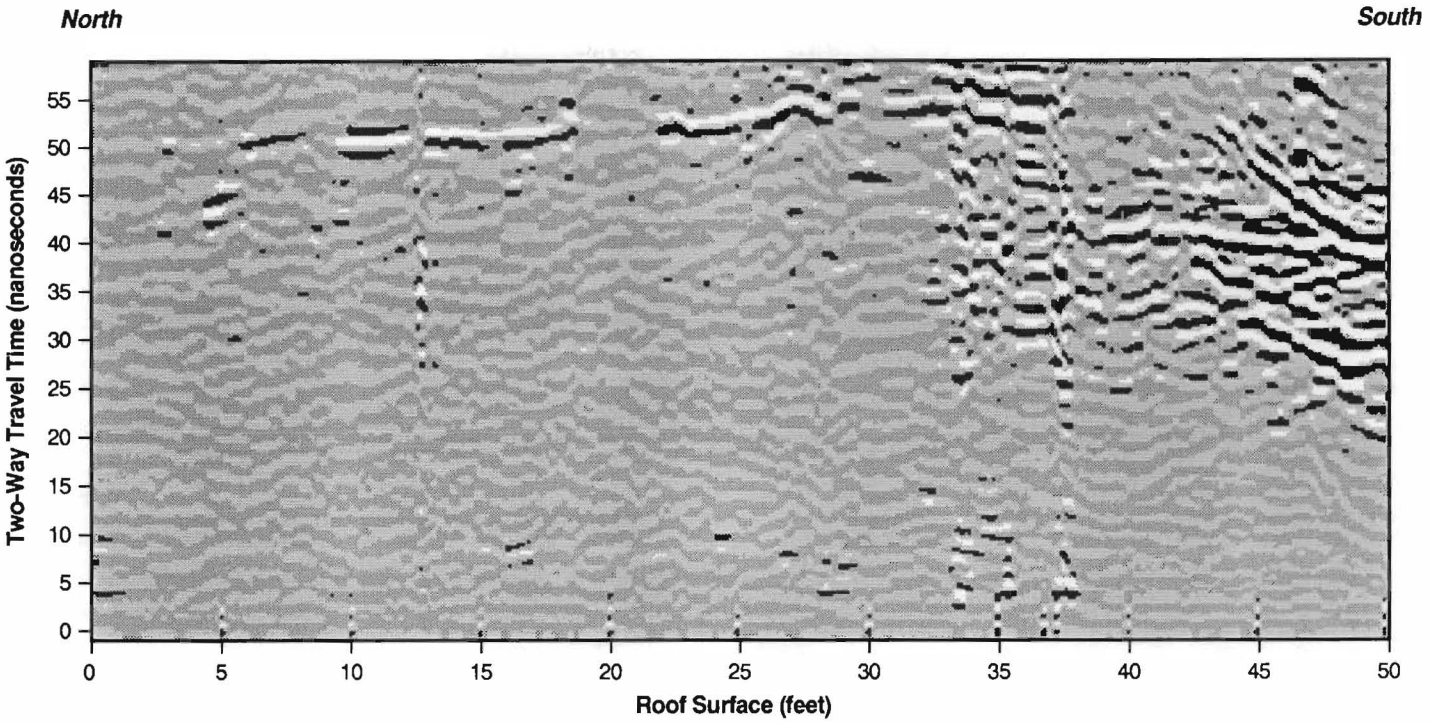

Figure A-9
Traverse D; E-0, N-150 Overcast: February 1992
Vertical Exaggeration 1.5x

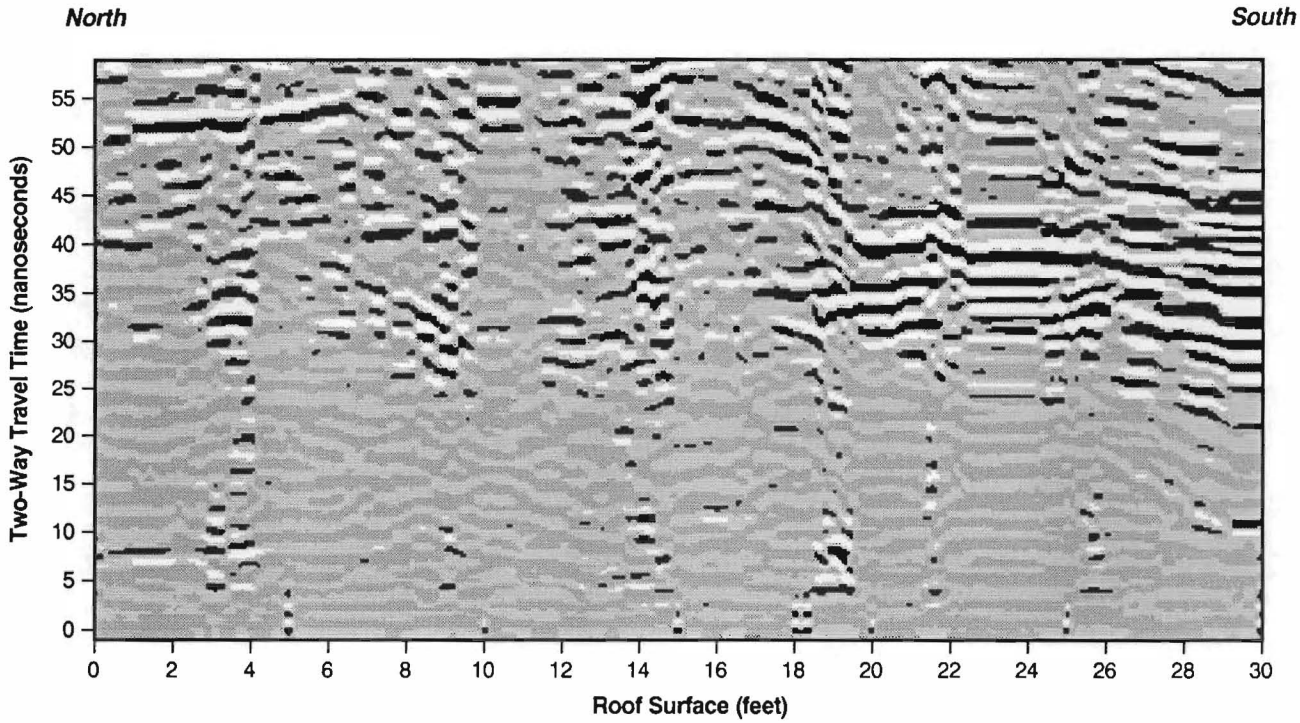

Figure A-10
Traverse E; E-0, N-150 Overcast: February 1992

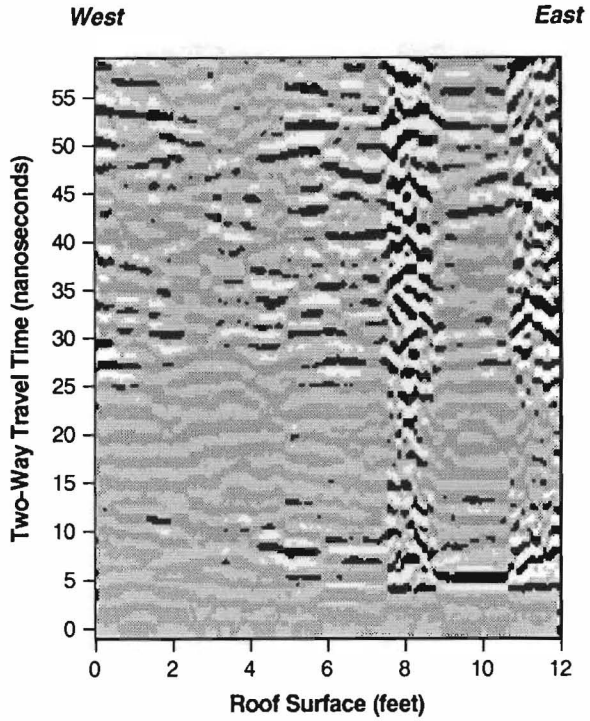

Figure A-11
Traverse F; E-0, N-150 Overcast: February 1992

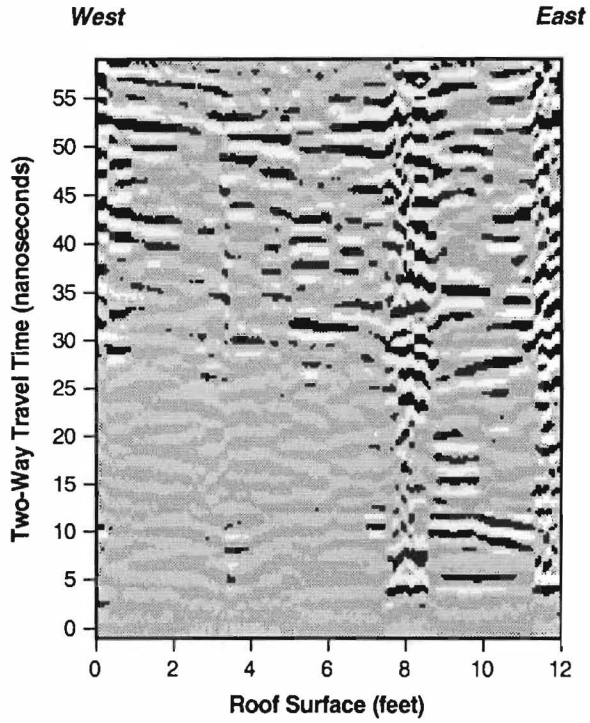

Figure A-12
Traverse G; E-0, N-150 Overcast: February 1992

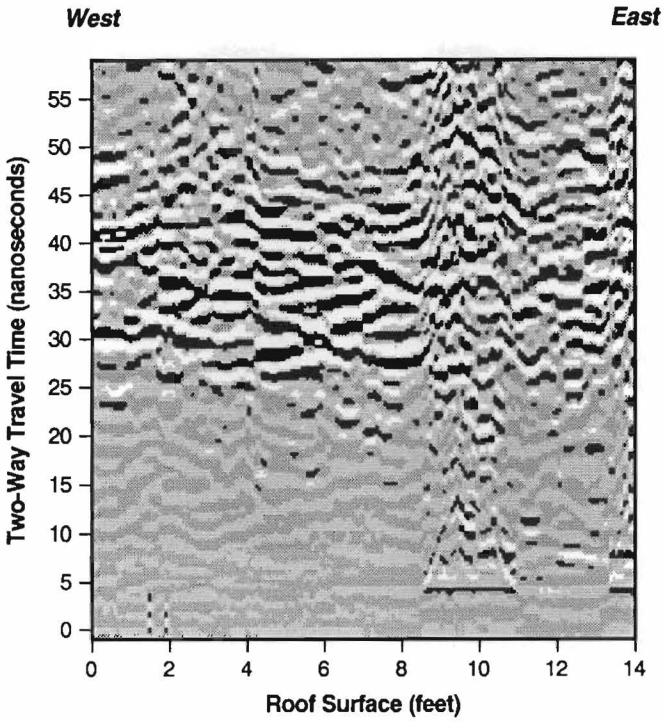

Figure A-13
Traverse H; E-0, N-150 Overcast: February 1992

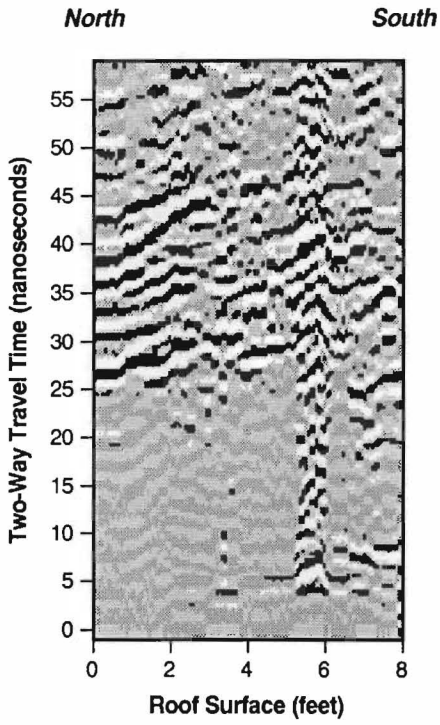

Figure A-14
Traverse J; E-0, N-150 Overcast: February 1992

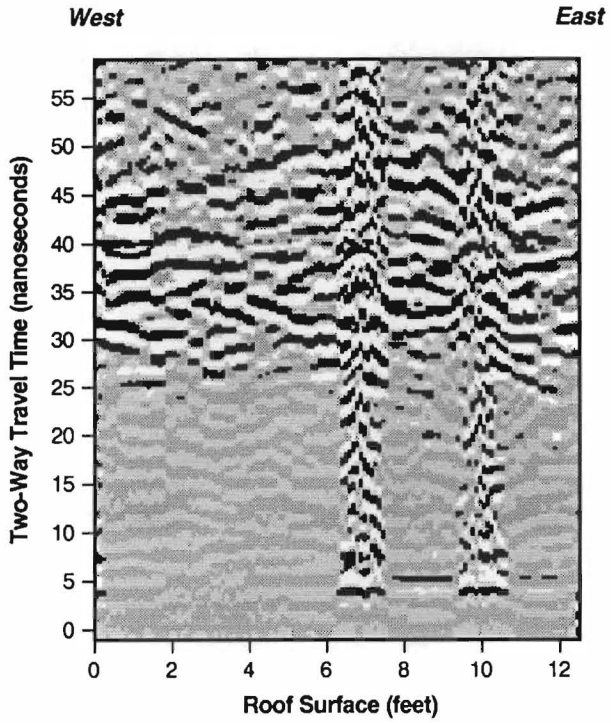

Figure A-15
Traverse K; E-0, N-150 Overcast: February 1992

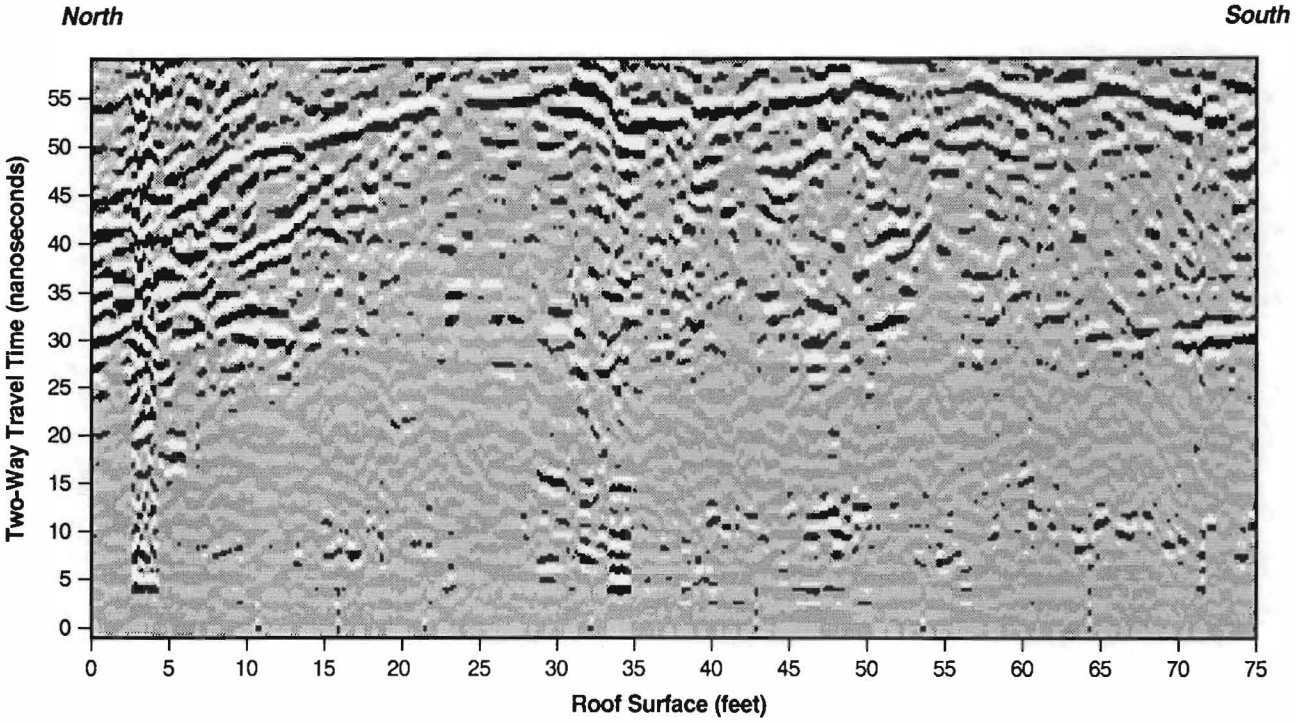

Figure A-16
Traverse L; E-0, N-150 Overcast: February 1992
Vertical Exaggeration 2.5x

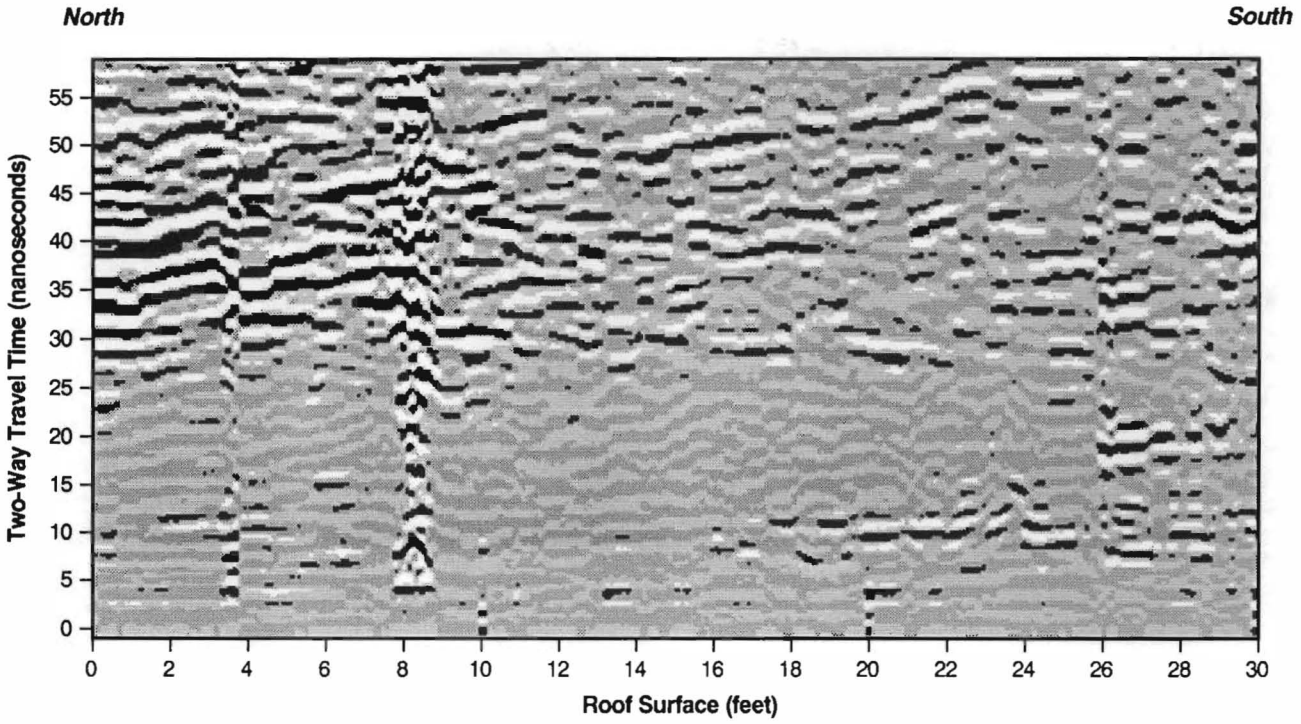

Figure A-17
Traverse M; E-0, N-150 Overcast: February 1992

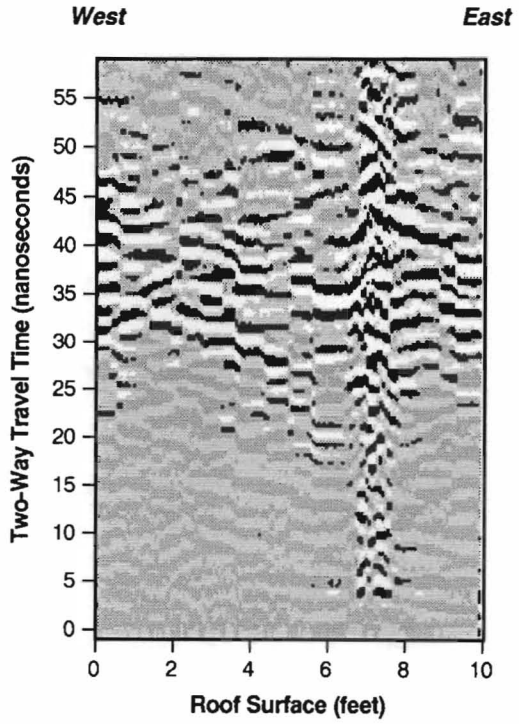

Figure A-18
Traverse N; E-0, N-150 Overcast: February 1992

APPENDIX B

INSTRUMENTATION SETTINGS, PROCESSING SEQUENCES, AND RADAR PROFILES: ROOM 1, PANEL 1

APPENDIX B

This appendix contains the following: (1) instrumentation settings used to conduct floor and roof GPR surveys in Room 1, Panel 1 on 06/19/91, 06/20/91 and 02/10/92; (2) processing sequences used to produce the radar profiles from the floor and roof of Room 1, Panel 1; and (3) radar profiles not contained in the body of this report (Figures B-1 to B-28).

B.1.1 Instrumentation Settings for Room 1, Panel 1, Floor and Roof Surveys (06/19/91 and 06/20/91)

Antenna settings:

Transmit = normal power
Receiver = normal amplification

Profiling recorder settings:

Surface gain = 4
Center gain = 3
Deep gain = 5.5
Threshold = 3
Signal position = auto
Print polarity = +/- - (negative amplitudes stippled)
Range(dial) = 600 ns
Range multiplier = 100
HP filter = 10
LP filter = 50
XMIT rate = 50 KHz
MODE = radar
Scans/sec = 16
Lines/in. = 200

B.1.2 Instrumentation Settings for Room 1, Panel 1, Floor Surveys (02/10/92)

Antenna settings:

Transmit = high power
Receiver = normal amplification

Profiling recorder settings:

Surface gain = 3
Center gain = 2
Deep gain = 4
Threshold = 3
Signal position = manual
Print polarity = -/+/- (negative amplitudes stippled)
Range(dial) = 600 ns
Range multiplier = 100
HP filter = 10
LP filter = 50
XMIT rate = 50 KHz
MODE = radar
Scans/sec = 16
Lines/in. = 200

B.2.1 Processing Sequences for Floor Radar Profiles from Room 1, Panel 1 (06/20/91)

1. LP compression, TC = 2

2. Horizontal scaling

3. Stack = 3

4. Finite impulse response filters

Horizontal boxcar high pass = 255

5. Predictive deconvolution

   Operator length = 45
   Prediction lag = 3
   Prewhitening = 0.1%
   Gain = 2

6. Finite impulse response filters

   Vertical triangle high pass = 19
   Vertical triangle low pass = 19
   Horizontal triangle low pass = 7

B.2.2 Processing Sequences for Floor Radar Profiles from Room 1, Panel 1 (02/10/92)

1. LP compression, TC = 2

2. LP compression, TC = 2

3. Horizontal scaling

4. Stack = 3

5. Finite impulse response filters

   Horizontal boxcar high pass = 255

6. Predictive deconvolution

   Operator length = 45
   Prediction lag = 3
   Prewhitening = 0.1%
   Gain = 9

7. Finite impulse response filters

   Vertical triangle high pass = 35
   Vertical triangle low pass = 10
   Horizontal triangle low pass = 7

B.2.3 Processing Sequences for Roof Radar Profiles from Room 1, Panel 1 (06/19/91)

1. LP compression, TC = 2

2. Horizontal scaling

3. Stack = 3

4. Finite impulse response filters

   Horizontal boxcar high pass = 255

5. Predictive deconvolution

   Operator length = 45
   Prediction lag = 3
   Prewhitening = 0.1%
   Gain = 3

6. Finite impulse response filters

   Vertical triangle high pass = 19
   Vertical triangle low pass = 15
   Horizontal triangle low pass = 7

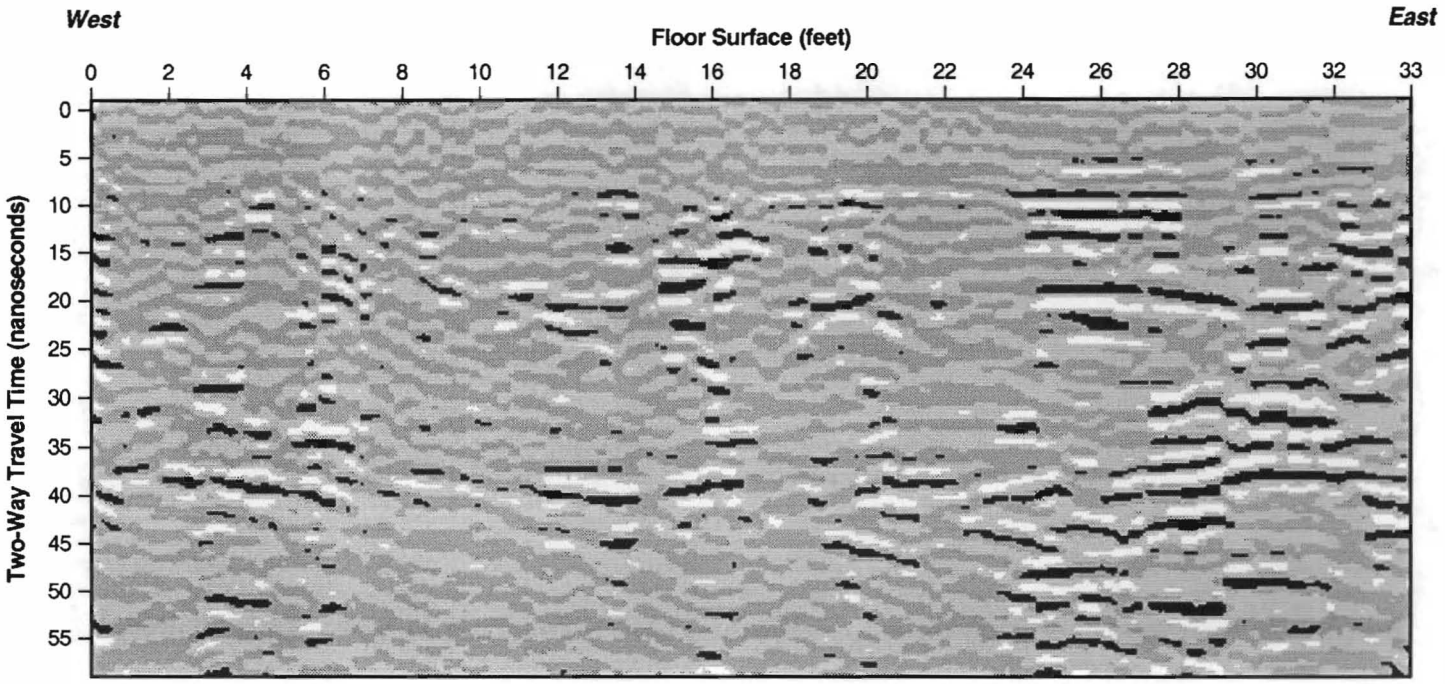

Figure B-1
S-1842 Traverse, Room 1, Panel 1 Floor: June 1991

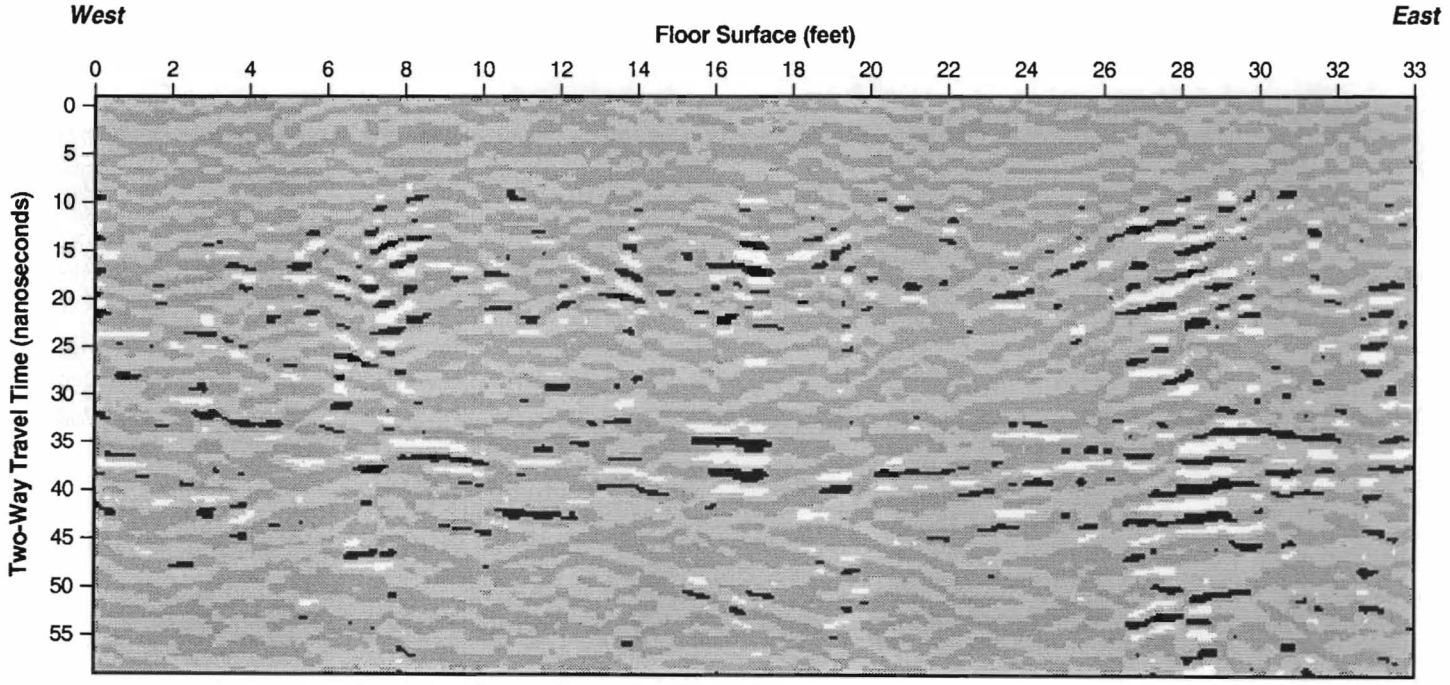

Figure B-2
S-1802 Traverse, Room 1, Panel 1 Floor: June 1991

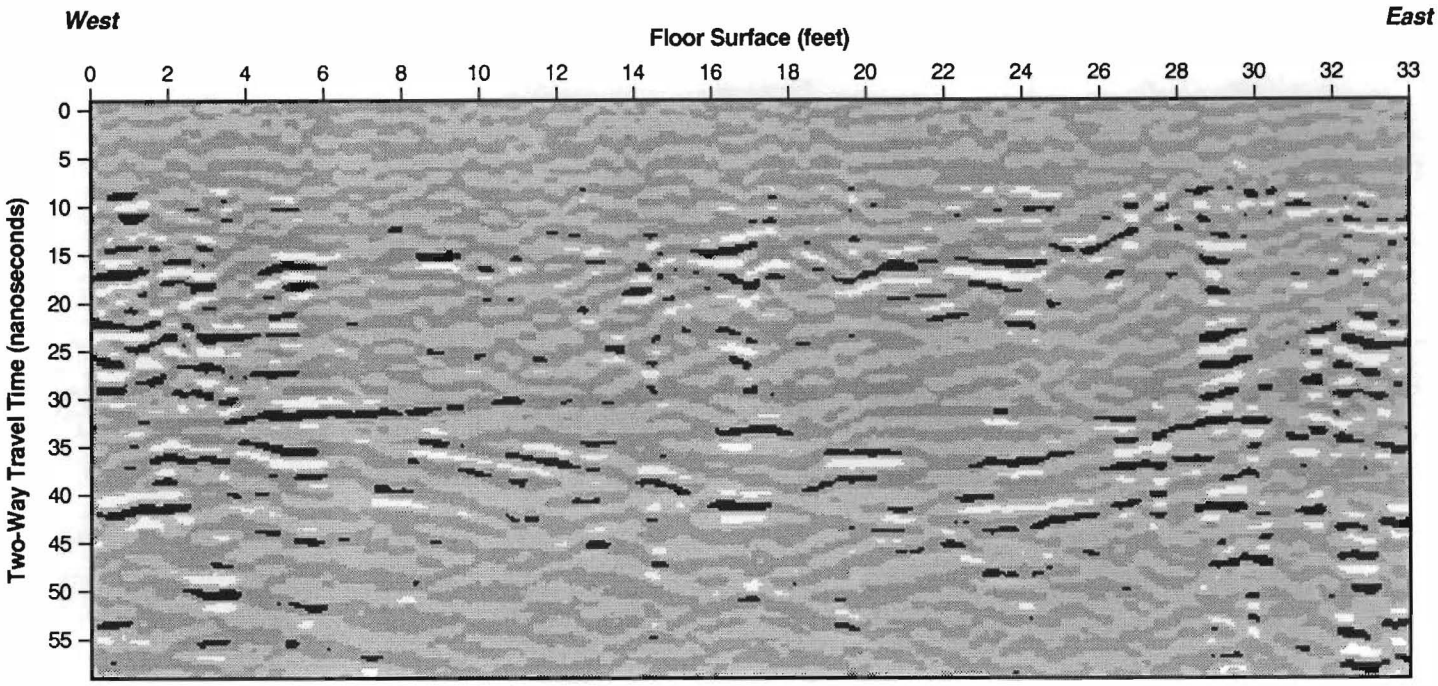

Figure B-3
S-1762 Traverse, Room 1, Panel 1 Floor: June 1991

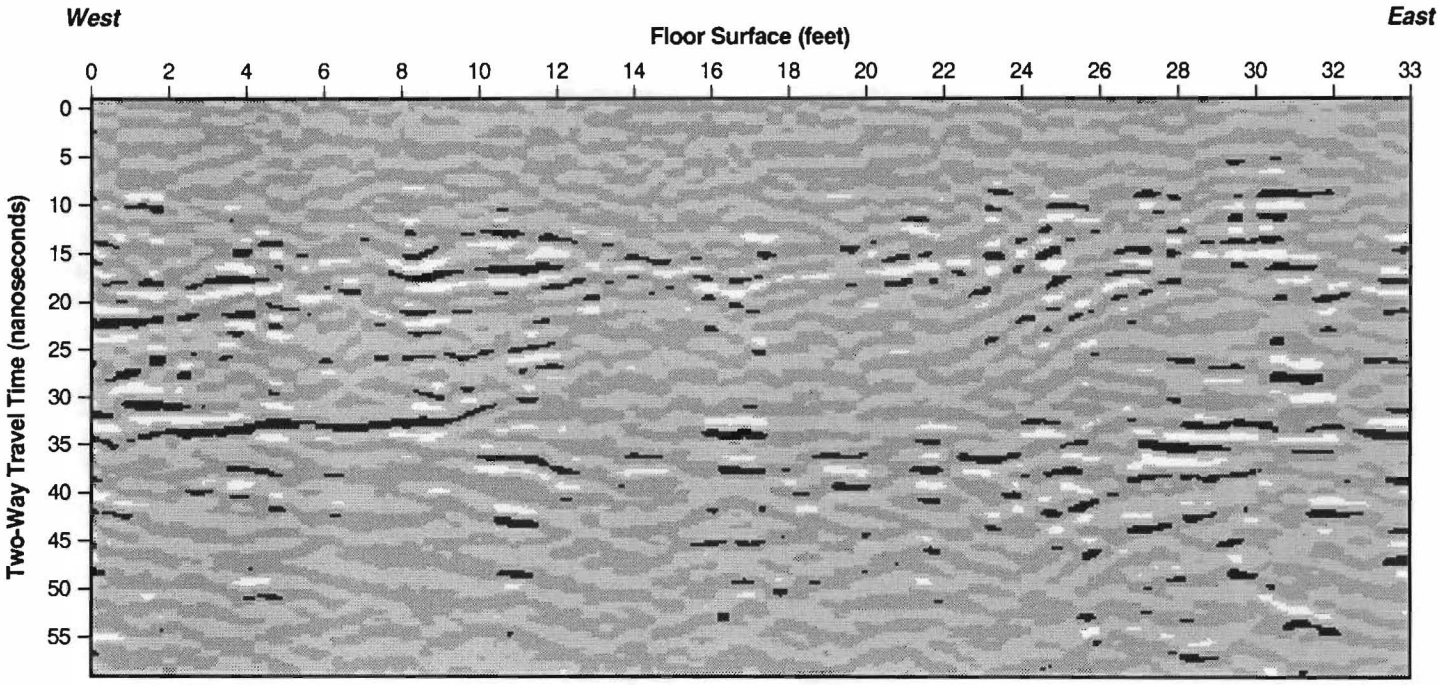

Figure B-4
S-1742 Traverse, Room 1, Panel 1 Floor: June 1991

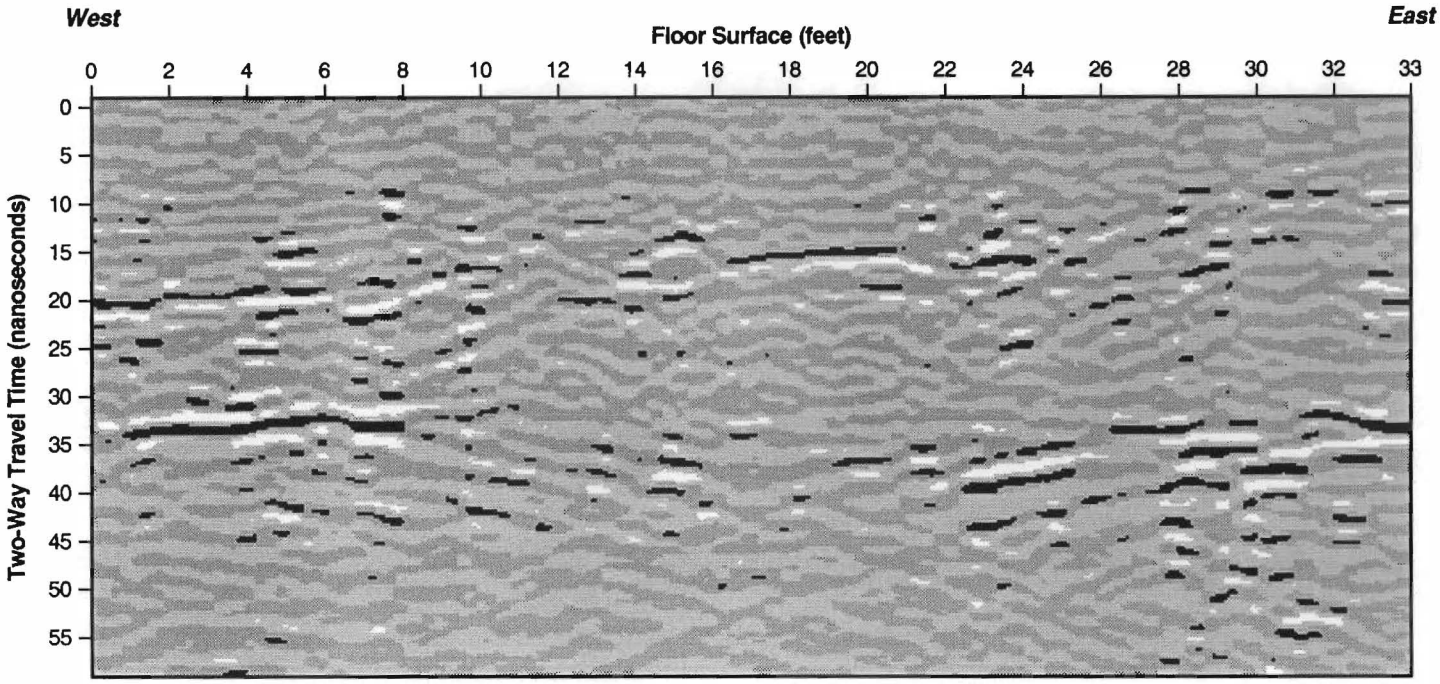

Figure B-5
S-1722 Traverse, Room 1, Panel 1 Floor: June 1991

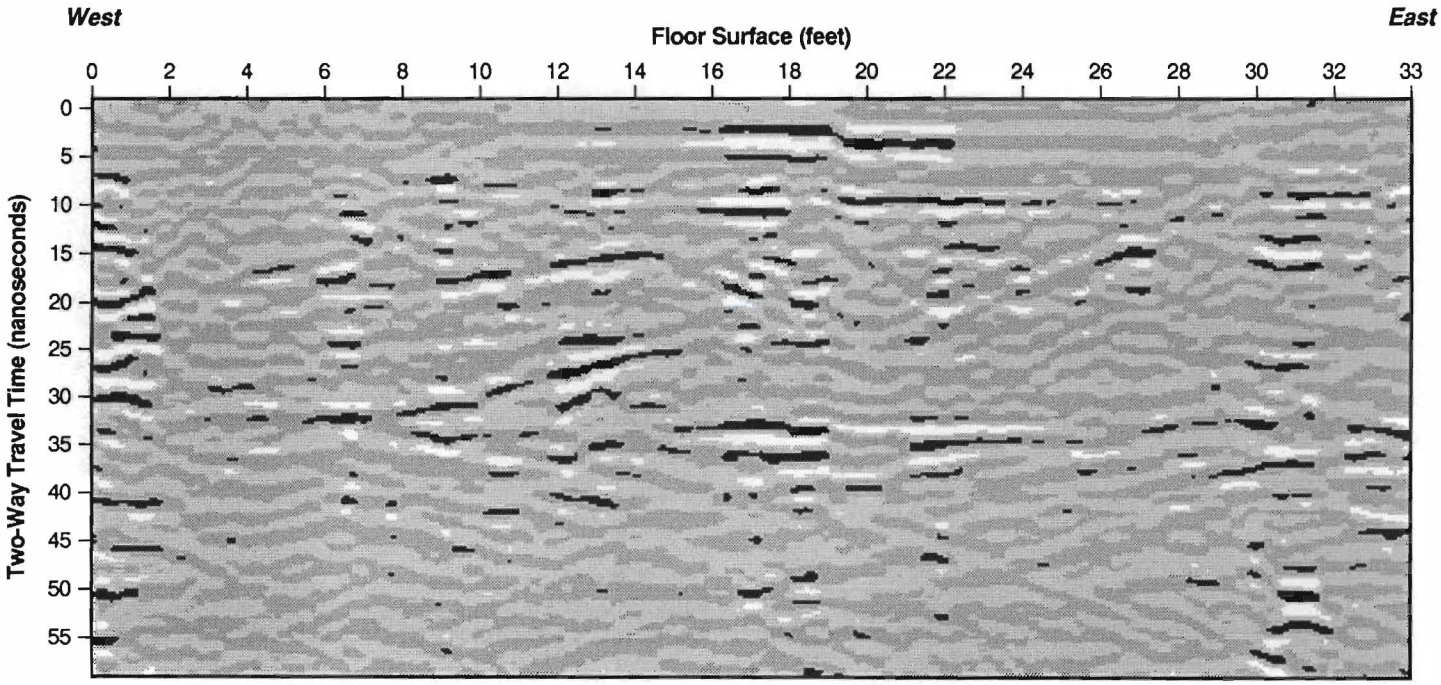

Figure B-6
S-1702 Traverse, Room 1, Panel 1 Floor: June 1991

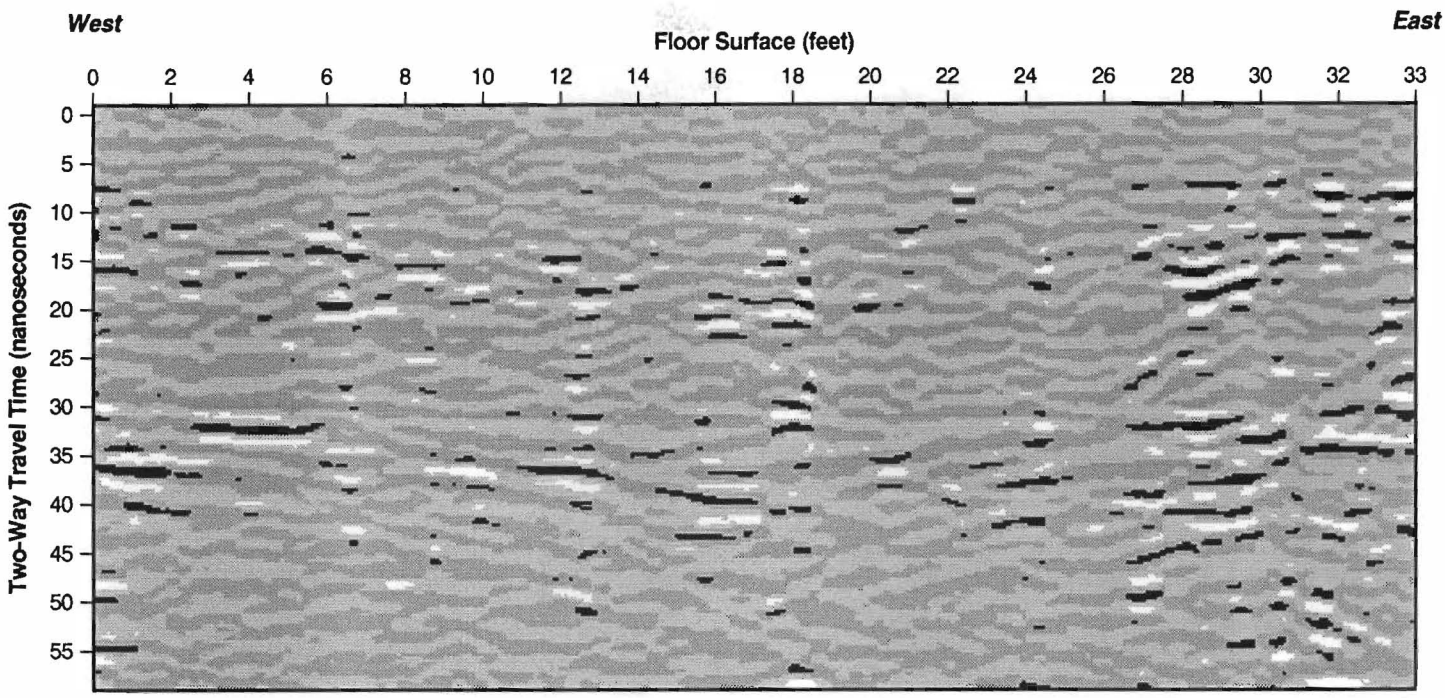

Figure B-7
S-1682 Traverse, Room 1, Panel 1 Floor: June 1991

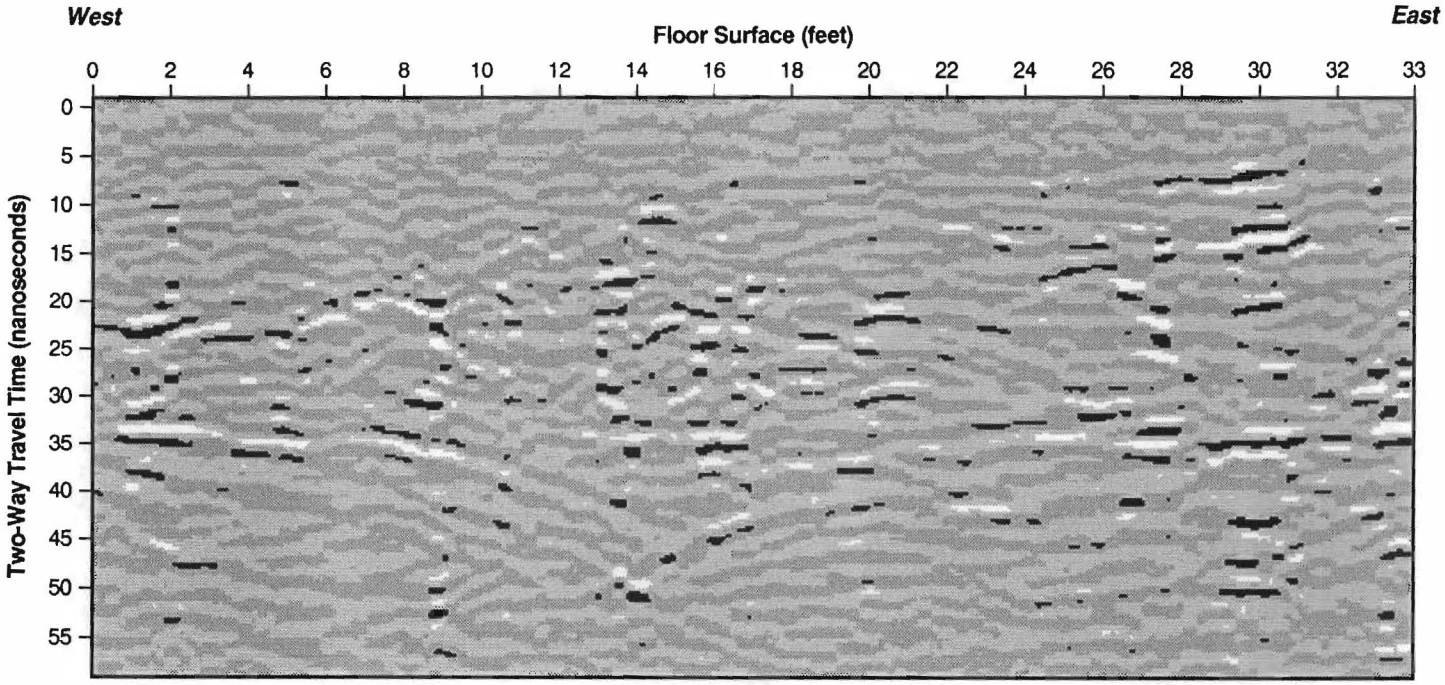

Figure B-8
S-1662 Traverse, Room 1, Panel 1 Floor: June 1991

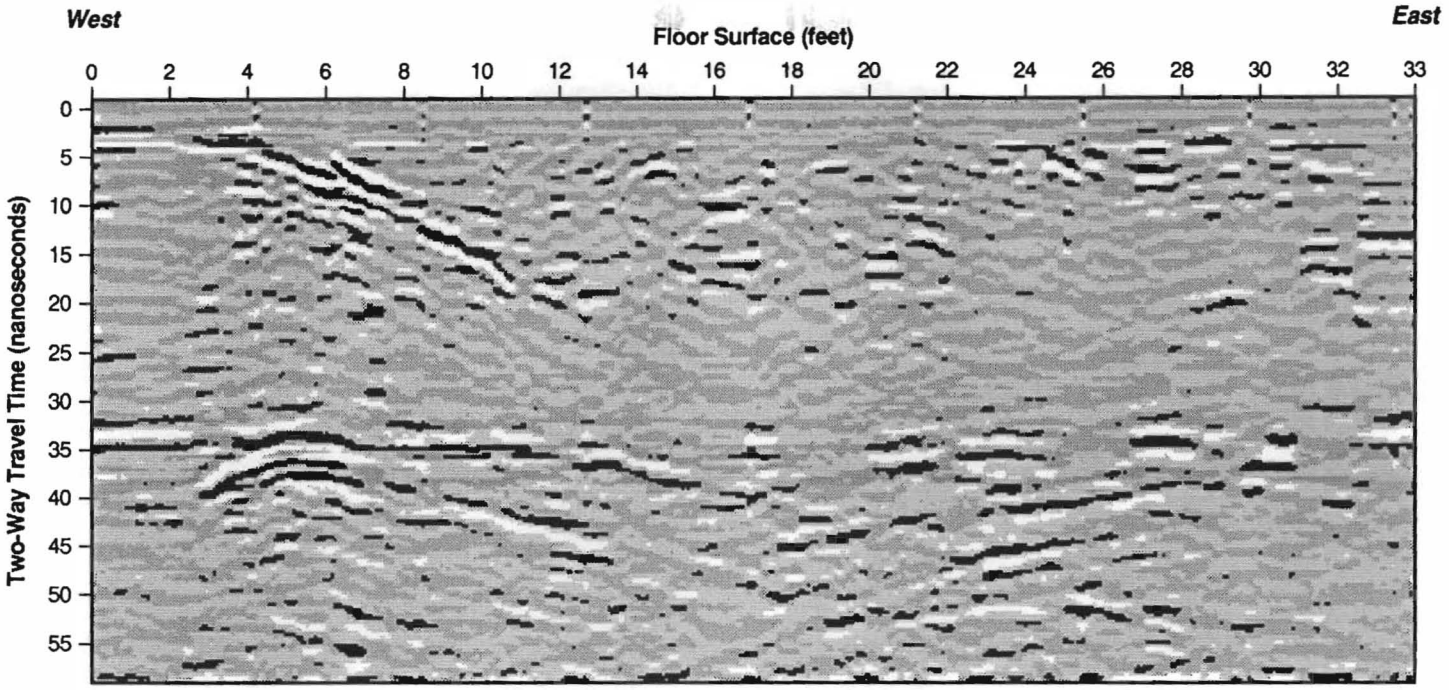

Figure B-9
S-1842 Traverse, Room 1, Panel 1 Floor: February 1992

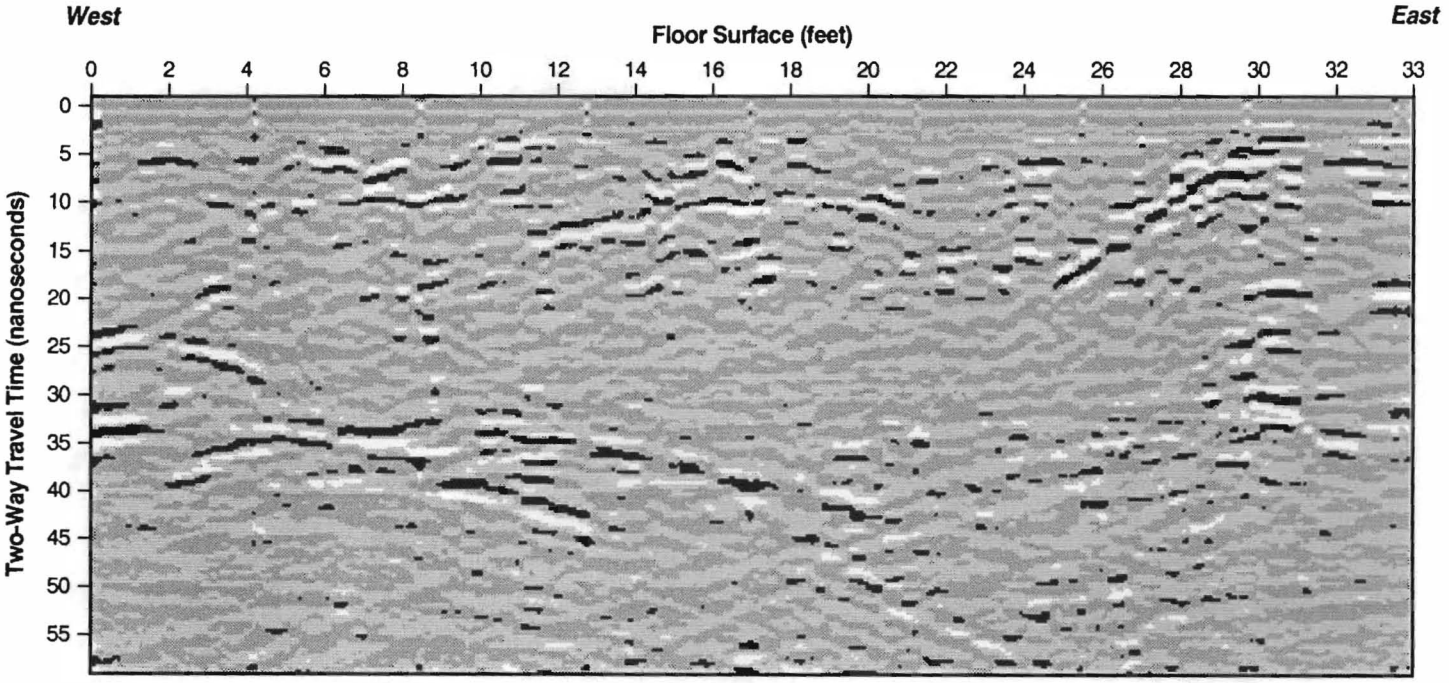

Figure B-10
S-1822 Traverse, Room 1, Panel 1 Floor: February 1992

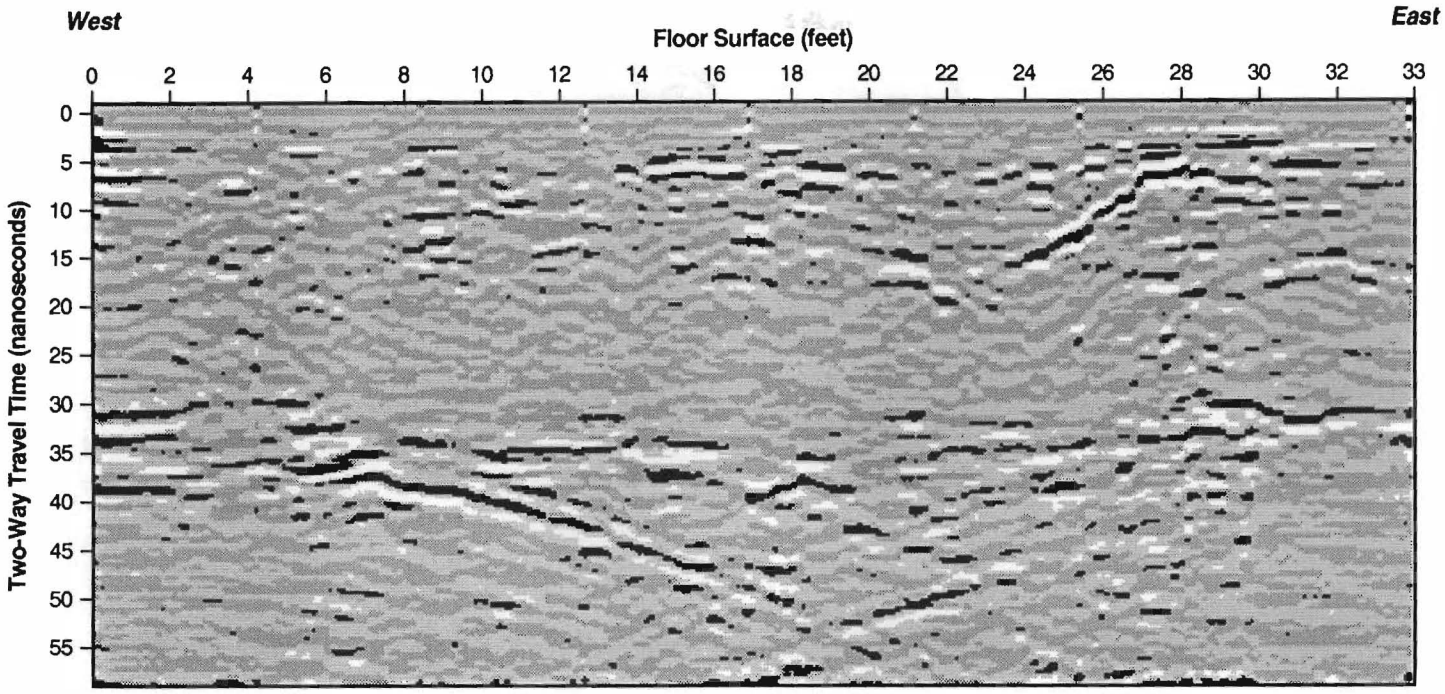

Figure B-11
S-1802 Traverse, Room 1, Panel 1 Floor: February 1992

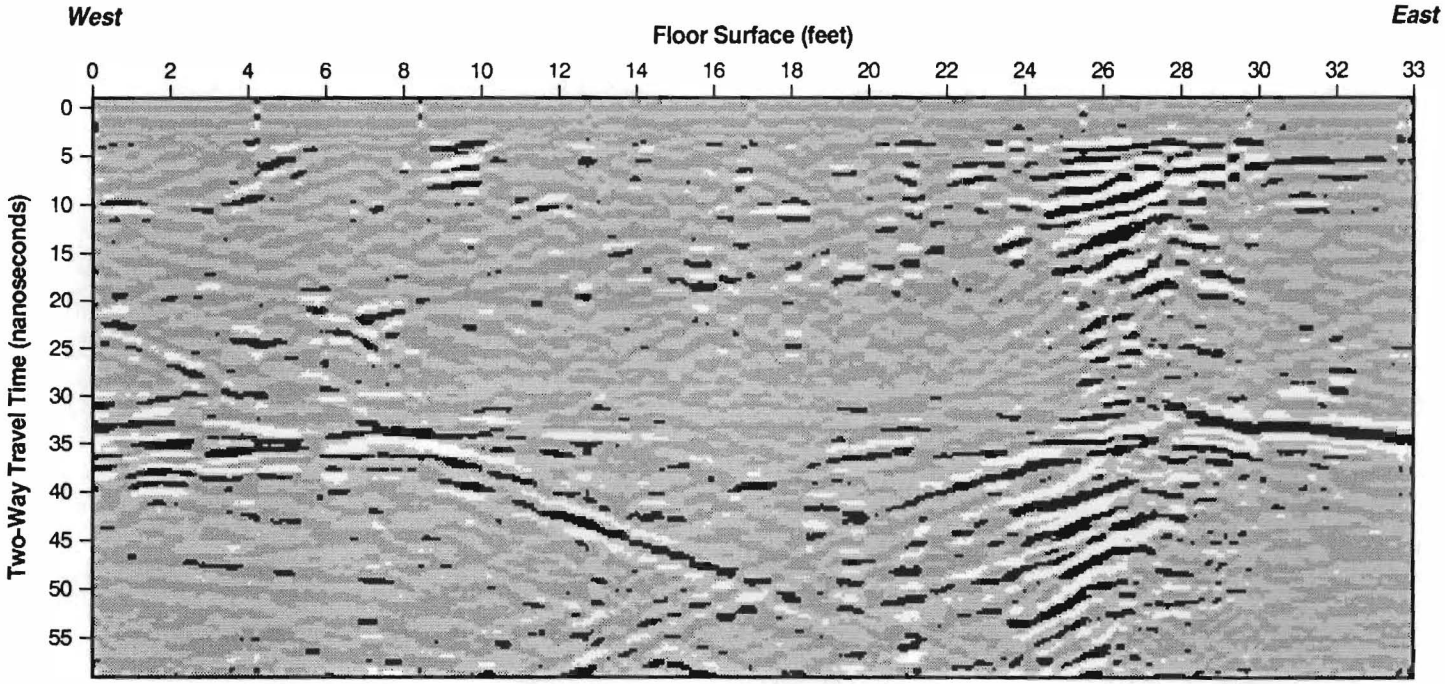

Figure B-12
S-1782 Traverse, Room 1, Panel 1 Floor: February 1992

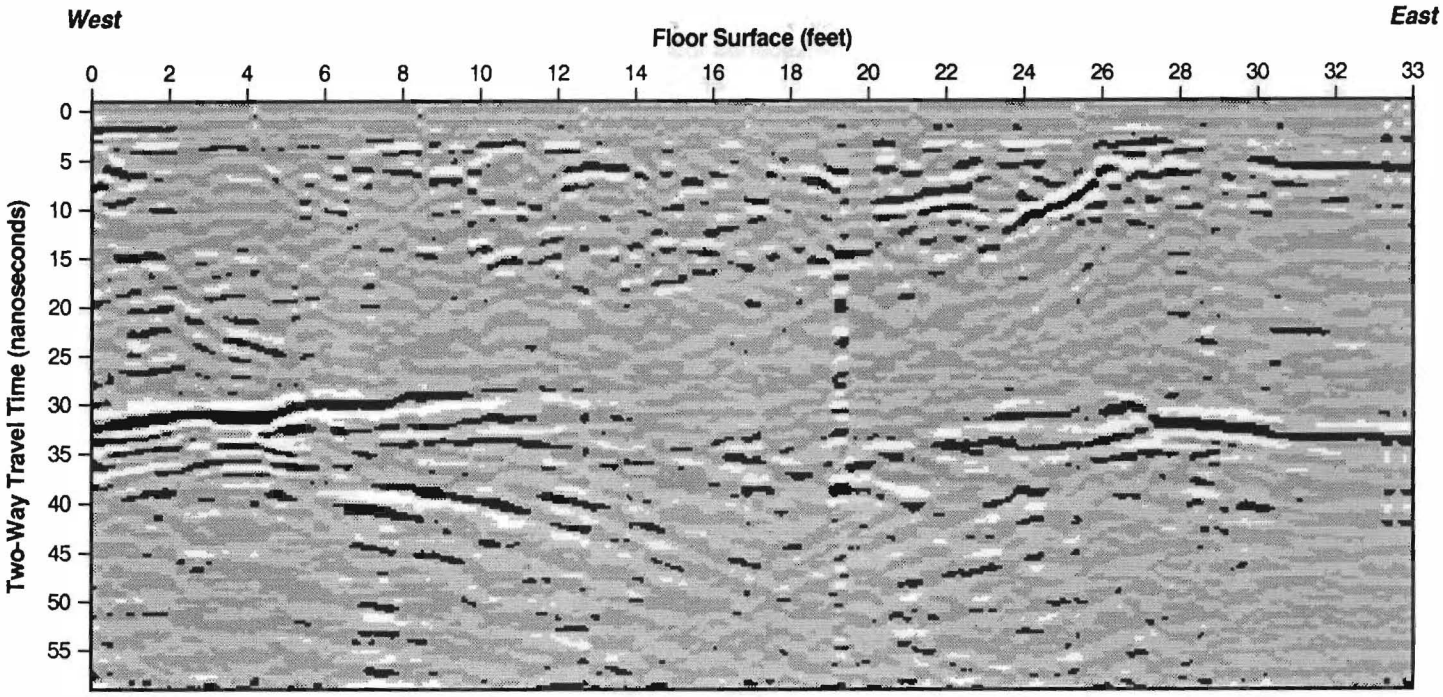

Figure B-13
S-1762 Traverse, Room 1, Panel 1 Floor: February 1992

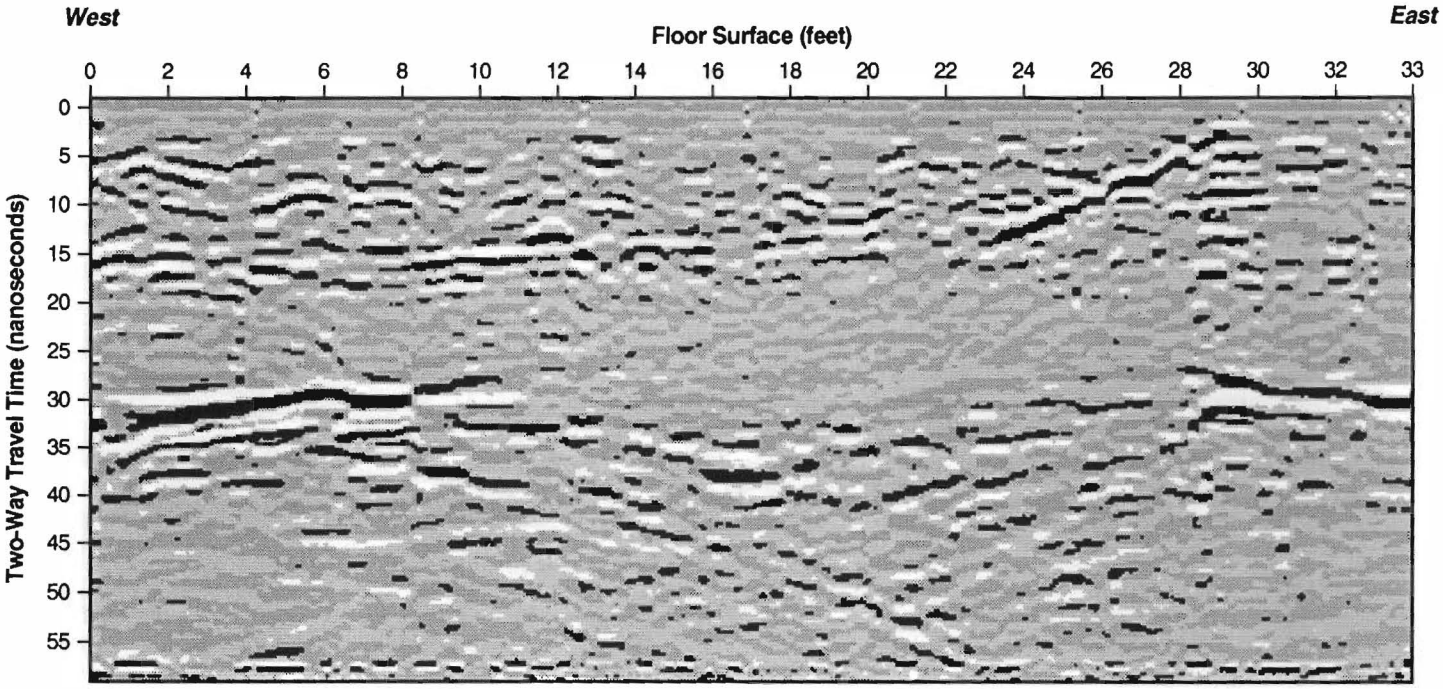

Figure B-14
S-1742 Traverse, Room 1, Panel 1 Floor: February 1992

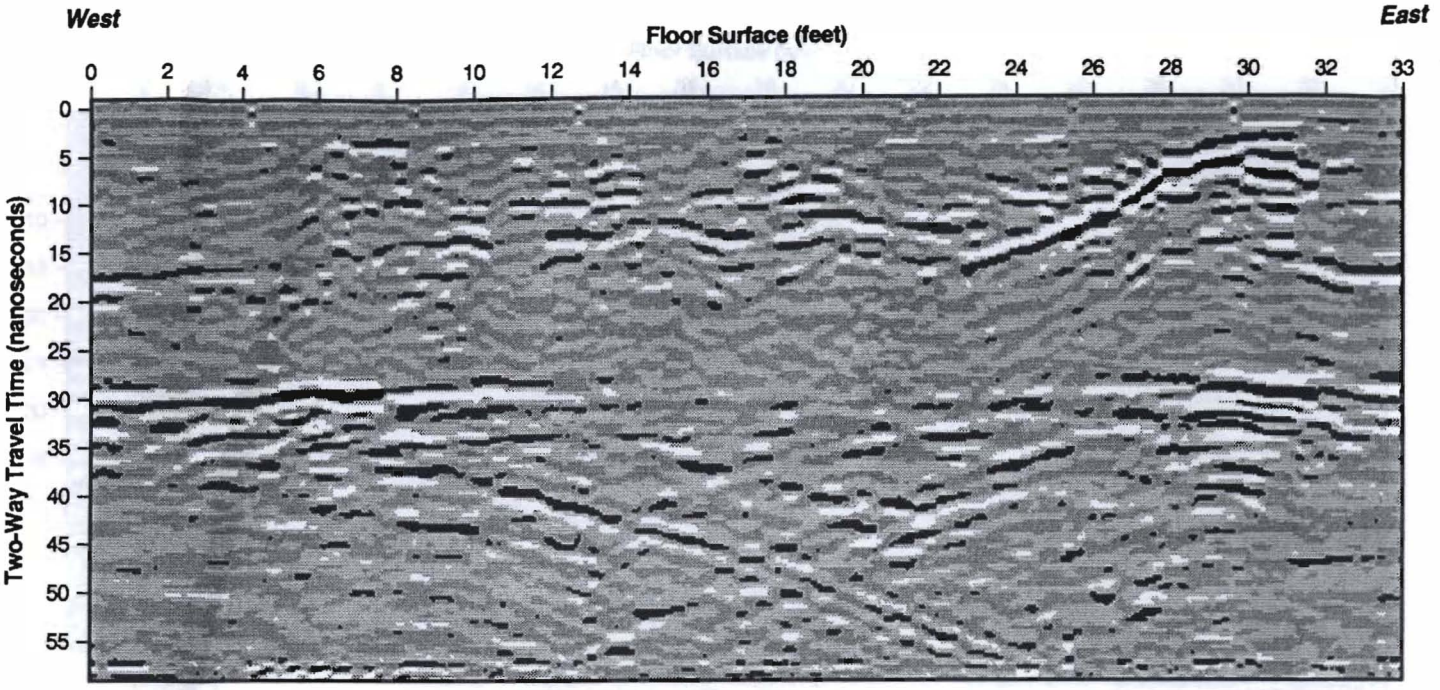

Figure B-15
S-1722 Traverse, Room 1, Panel 1 Floor: February 1992

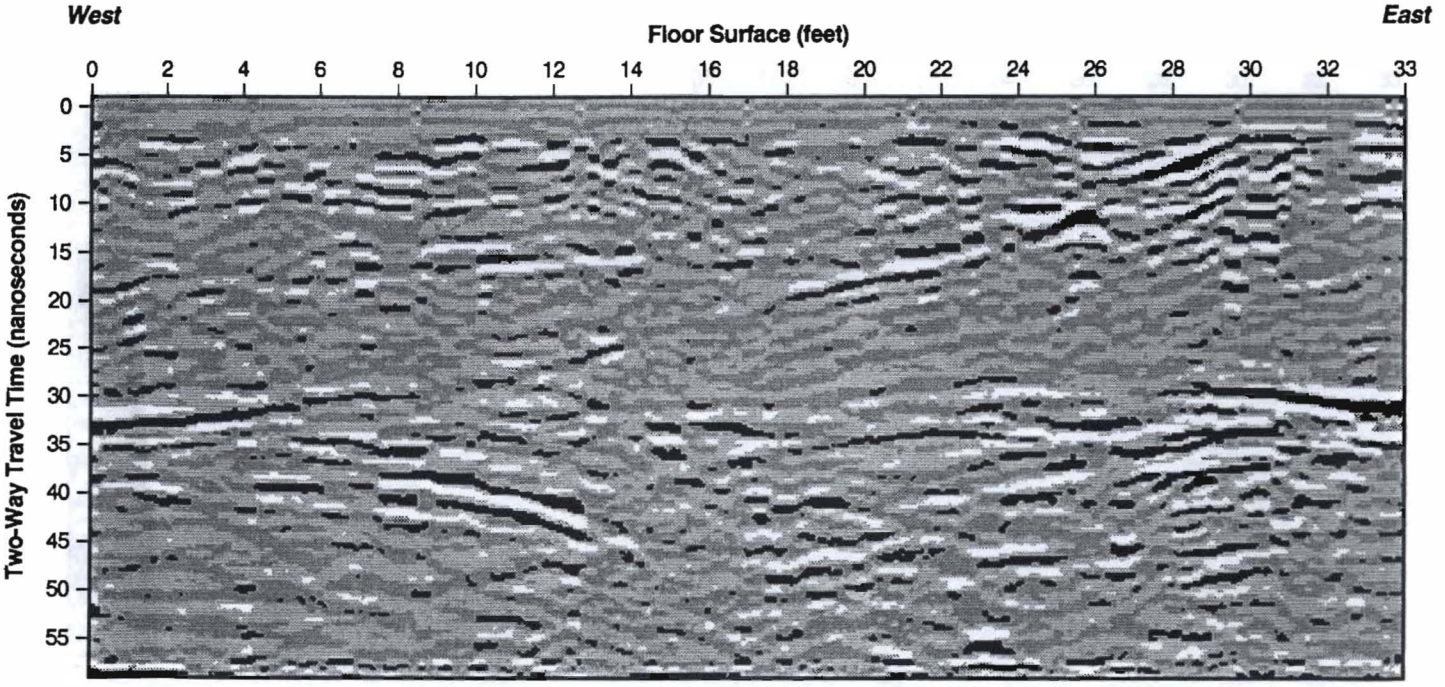

Figure B-16
S-1702 Traverse, Room 1, Panel 1 Floor: February 1992

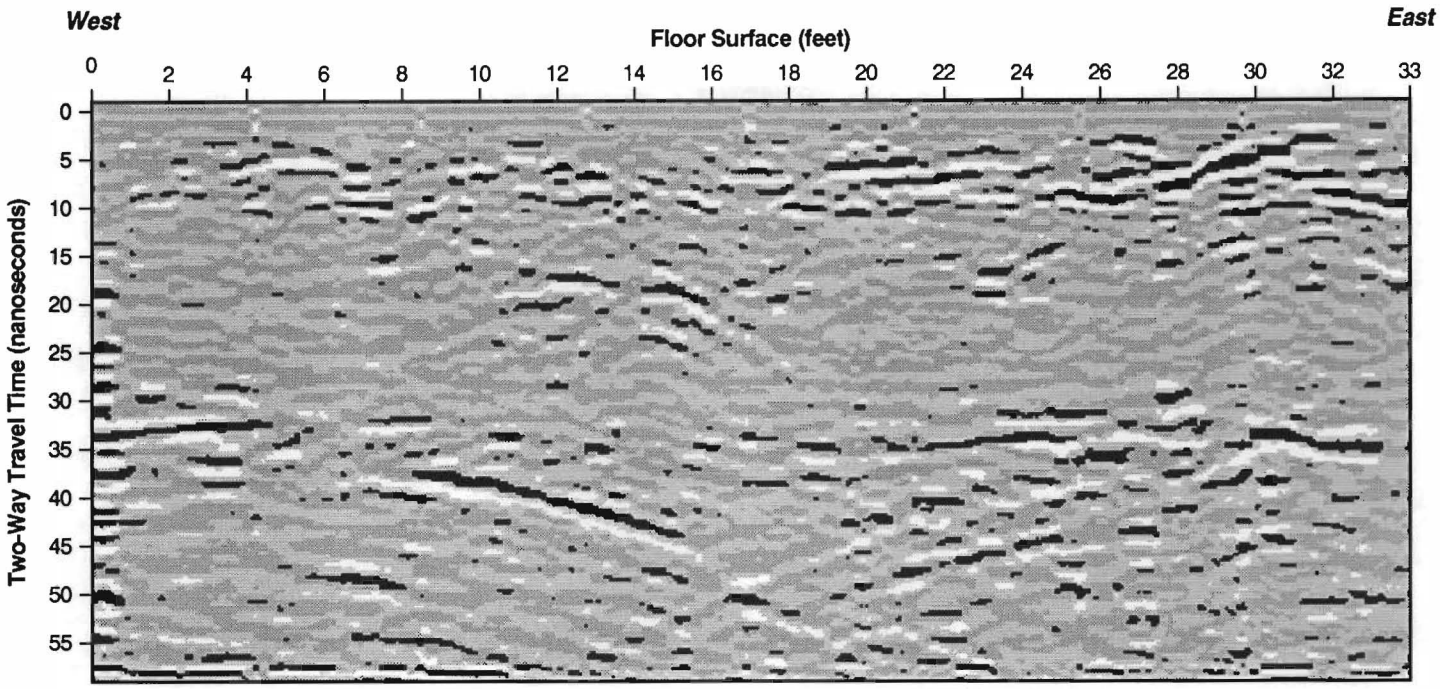

Figure B-17
S-1682 Traverse, Room 1, Panel 1 Floor: February 1992

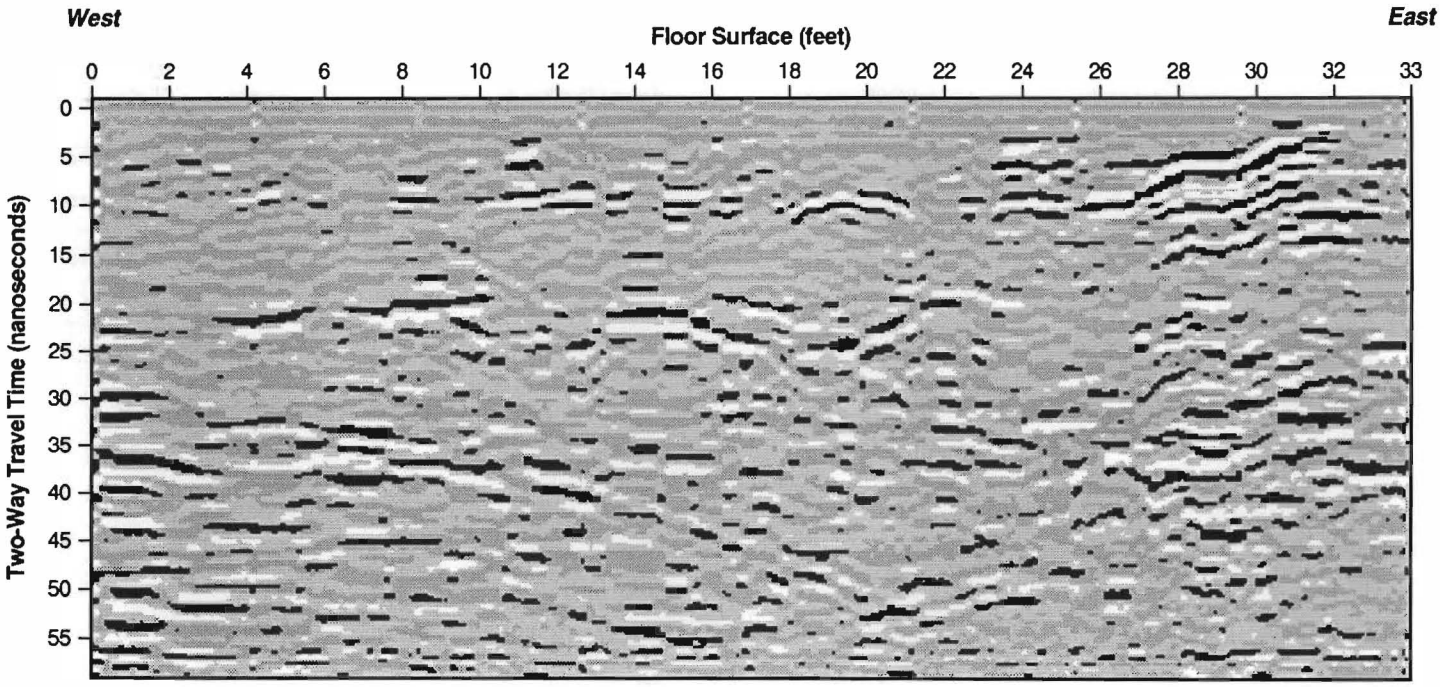

Figure B-18
S-1662 Traverse, Room 1, Panel 1 Floor: February 1992

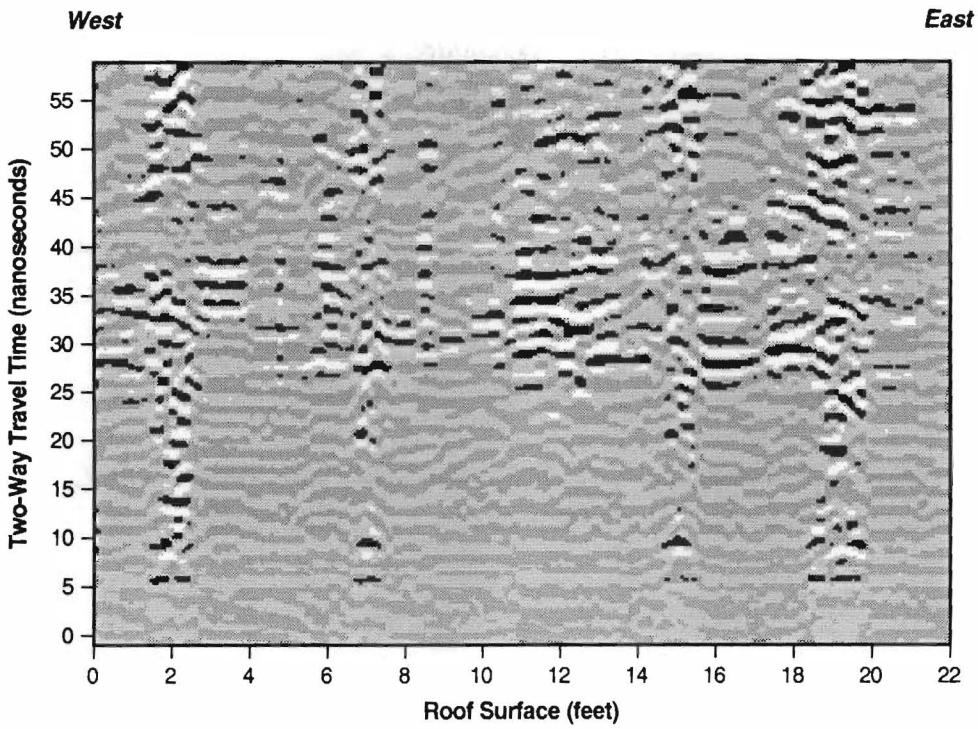

Figure B-19
S-1862 Traverse, Room 1, Panel 1 Roof: June 1991

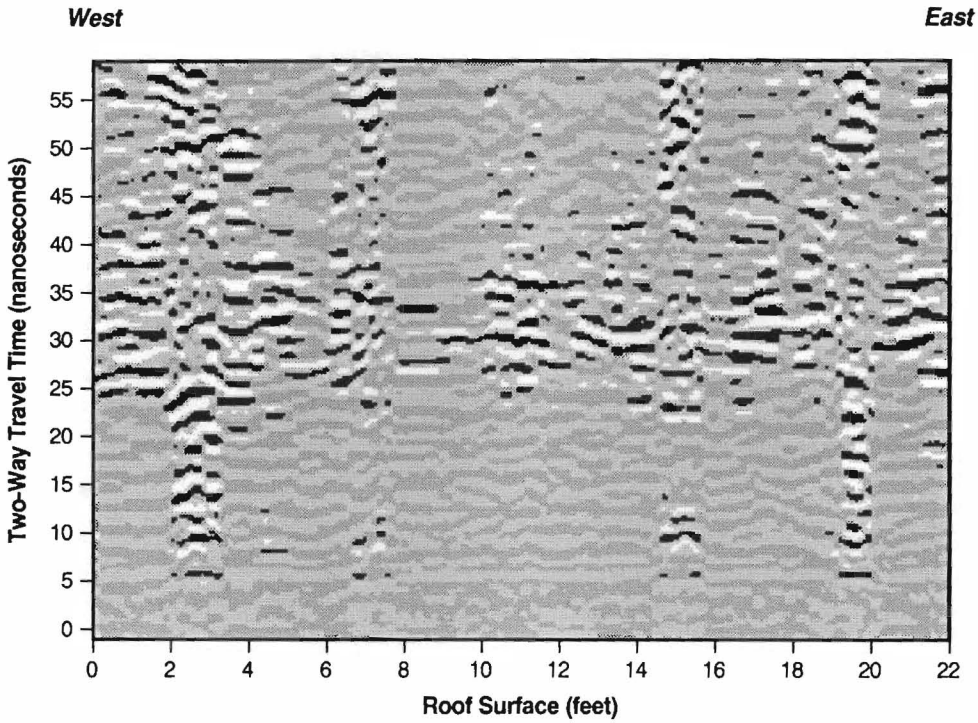

Figure B-20
S-1842 Traverse, Room 1, Panel 1 Roof: June 1991

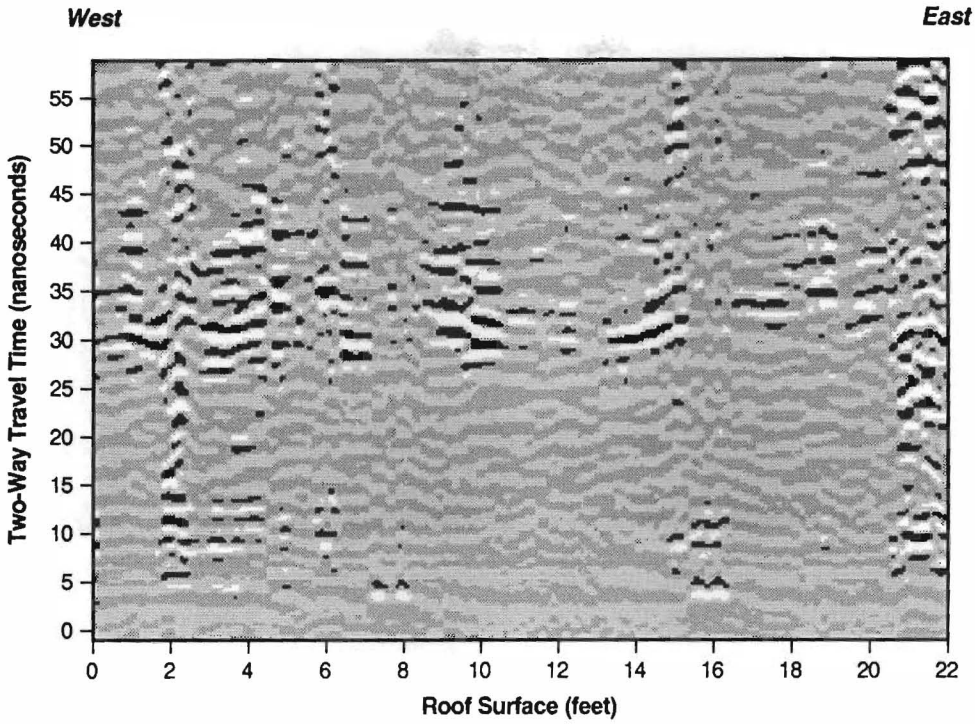

Figure B-21
S-1822 Traverse, Room 1, Panel 1 Roof: June 1991

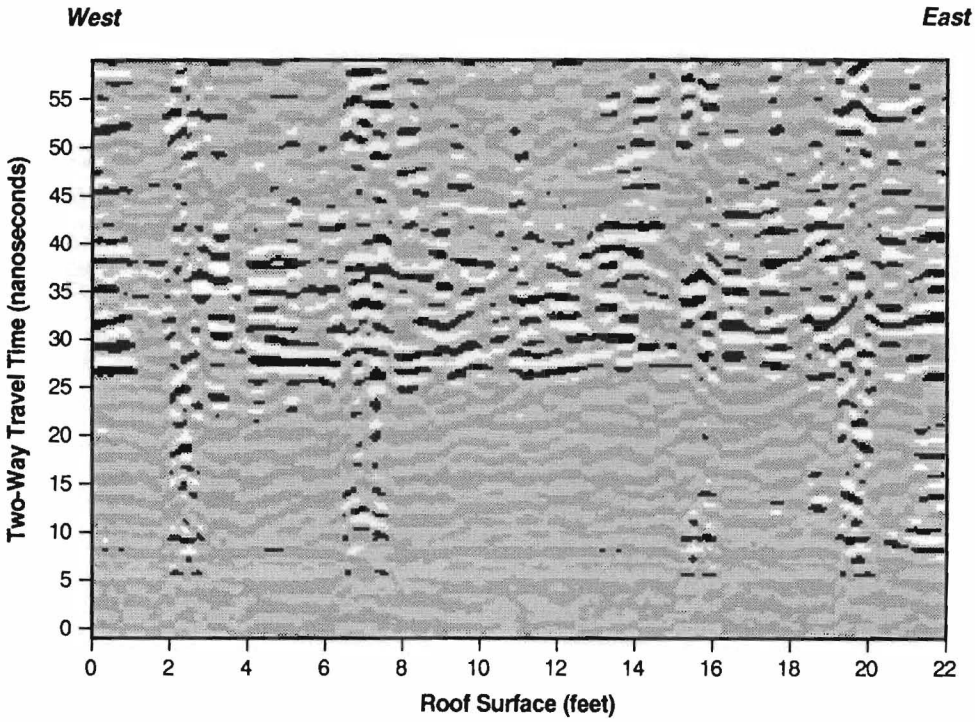

Figure B-22
S-1802 Traverse, Room 1, Panel 1 Roof: June 1991

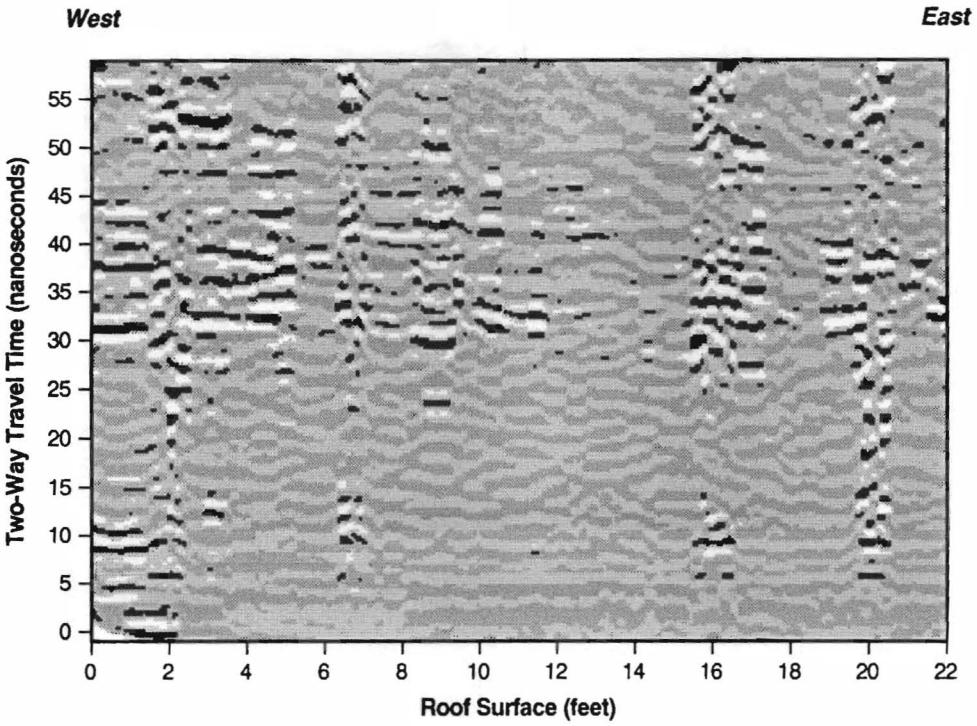

Figure B-23
S-1782 Traverse, Room 1, Panel 1 Roof: June 1991

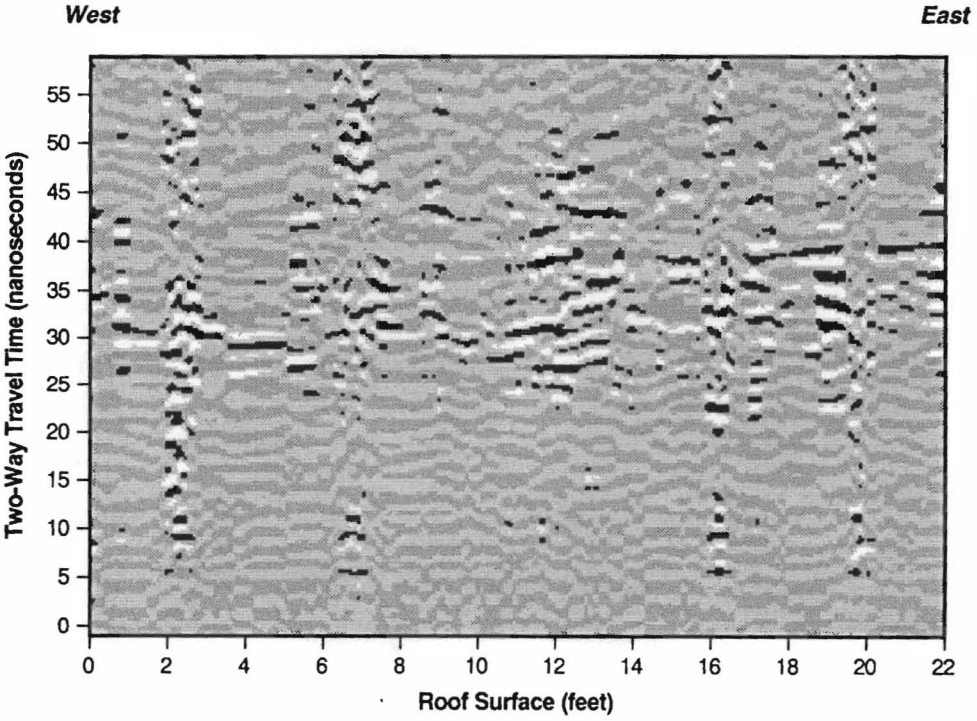

Figure B-24
S-1762 Traverse, Room 1, Panel 1 Roof: June 1991

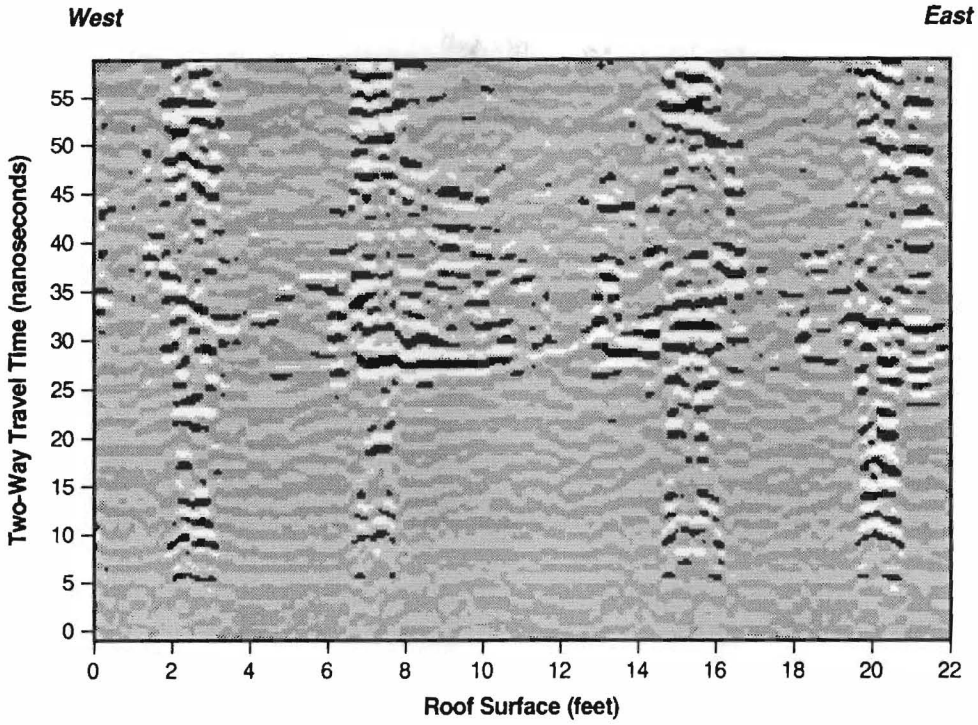

Figure B-25
S-1722 Traverse, Room 1, Panel 1 Roof: June 1991

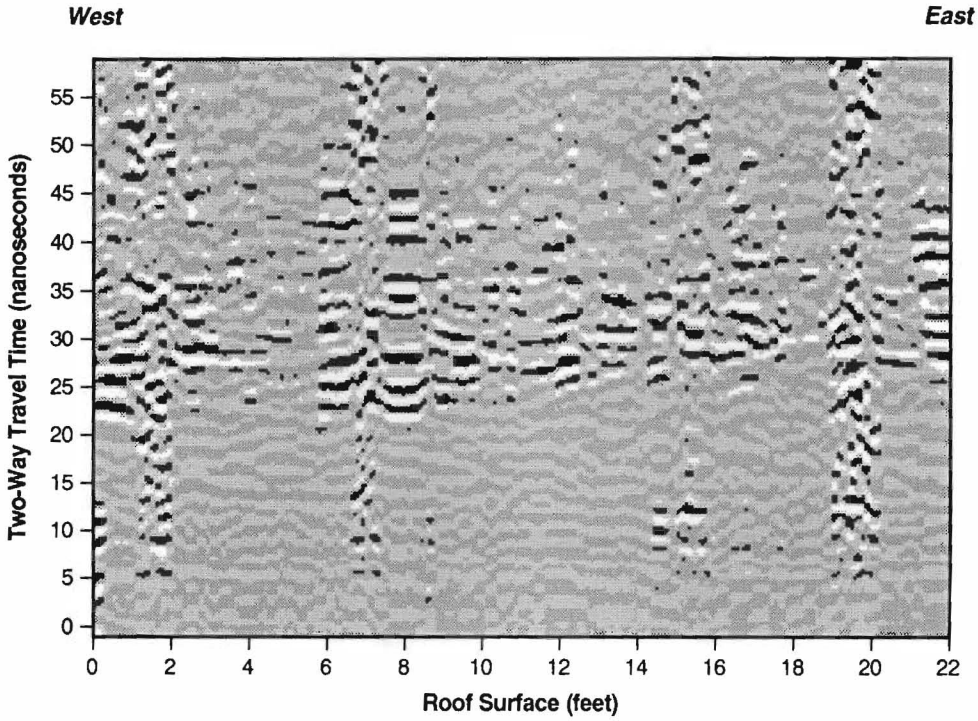

Figure B-26
S-1702 Traverse, Room 1, Panel 1 Roof: June 1991

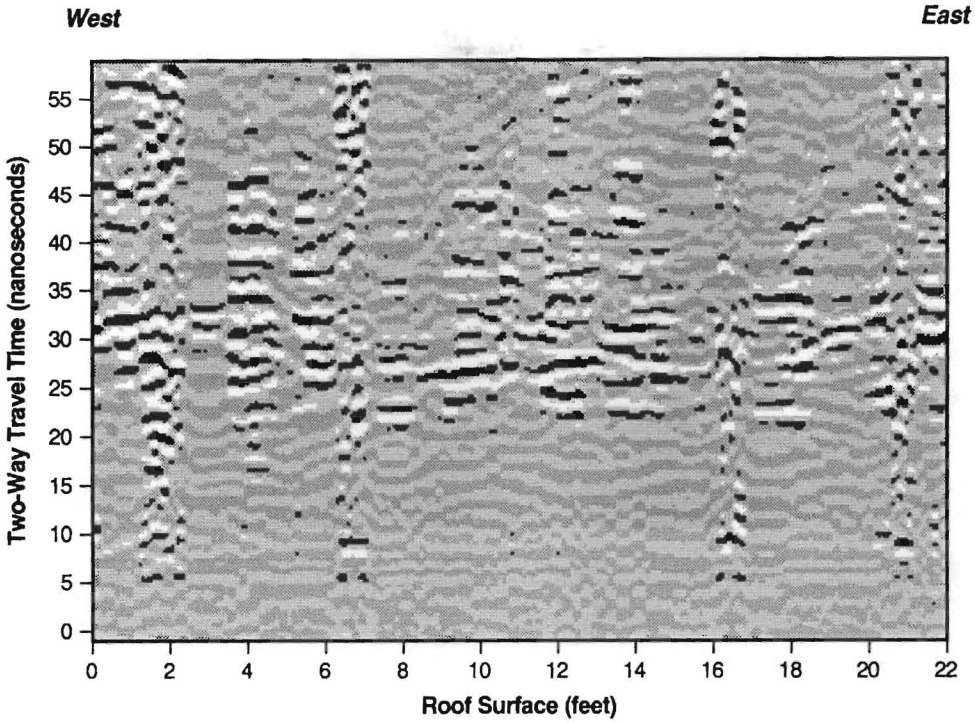

Figure B-27
S-1682 Traverse, Room 1, Panel 1 Roof: June 1991

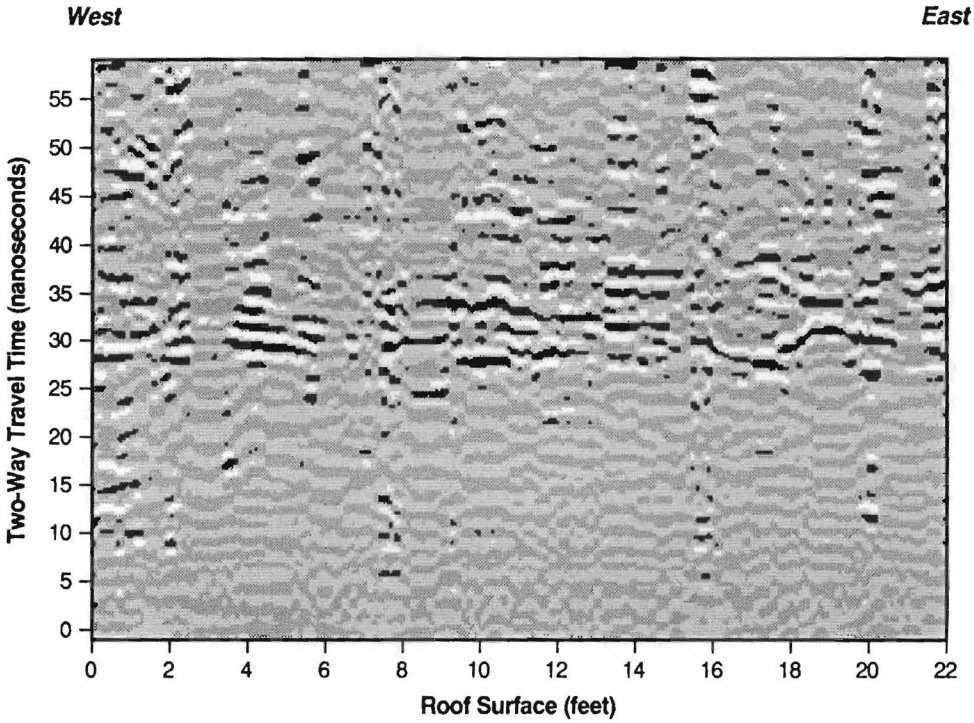

Figure B-28
S-1662 Traverse, Room 1, Panel 1 Roof: June 1991

APPENDIX C

INSTRUMENTATION SETTINGS, PROCESSING SEQUENCES, AND RADAR PROFILES: ROOM 6, PANEL 1

APPENDIX C

This appendix contains the following: (1) instrumentation settings used to conduct floor and roof GPR surveys in Room 6, Panel 1 on 01/29/92, 01/30/92 and 01/31/92; (2) processing sequences used to produce the radar profiles from the floor and roof of Room 6, Panel 1; and (3) radar profiles not contained in the body of this report (Figures C-1 to C-33).

C.1 Instrumentation Settings for Room 6, Panel 1, Floor and Roof Surveys (01/29/92, 01/30/92 and 01/31/92)

Antenna settings:

Transmit = high power
Receiver = normal and high amplification

Profiling recorder settings:

Surface gain = 3
Center gain = 2
Deep gain = 4
Threshold = 3
Signal position = manual
Print polarity = +/- - (negative amplitudes stippled)
Range(dial) = 600 ns
Range multiplier = 100
HP filter = 10
LP filter = 50
XMIT rate = 50 KHz
MODE = radar
Scans/sec = 16 and 8
Lines/in. = 200

C.2.1 Processing Sequences for Floor Radar Profiles from Room 6, Panel 1 (01/29/92 and 01/30/92)

1. LP compression, TC = 2

2. Horizontal scaling

3. Stack = 3

4. Finite impulse response filters

   Horizontal boxcar high pass = 255

5. Predictive deconvolution

   Operator length = 45
   Prediction lag = 3
   Prewhitening = 0.1%
   Gain = 6

6. Finite impulse response filters

   Vertical triangle high pass = 25
   Vertical triangle low pass = 10
   Horizontal triangle low pass = 7

C.2.2 Processing Sequences for Roof Radar Profiles from Room 6, Panel 1 (01/30/92 and 01/31/92)

1. LP compression, TC = 2

2. Horizontal scaling

3. Stack = 3

4. Finite impulse response filters

   Horizontal boxcar high pass = 255

5. Predictive deconvolution

   Operator length = 45
   Prediction lag = 3
   Prewhitening = 0.1%
   Gain = 6

6. Finite impulse response filters

   Vertical triangle high pass = 35
   Vertical triangle low pass = 9
   Horizontal triangle low pass = 5

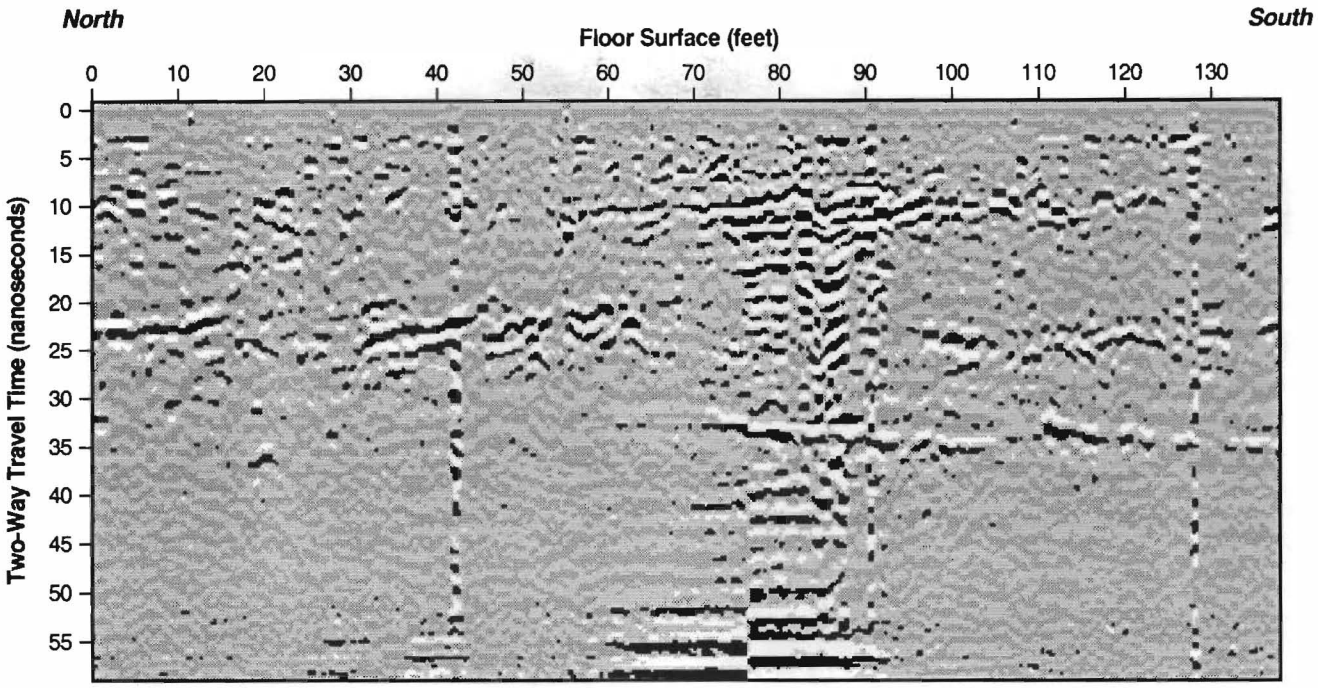

Figure C-1
S-1647 to S-1785 Traverse, Room 6, Panel 1 Floor: January 1992
Vertical Exaggeration 4.5x

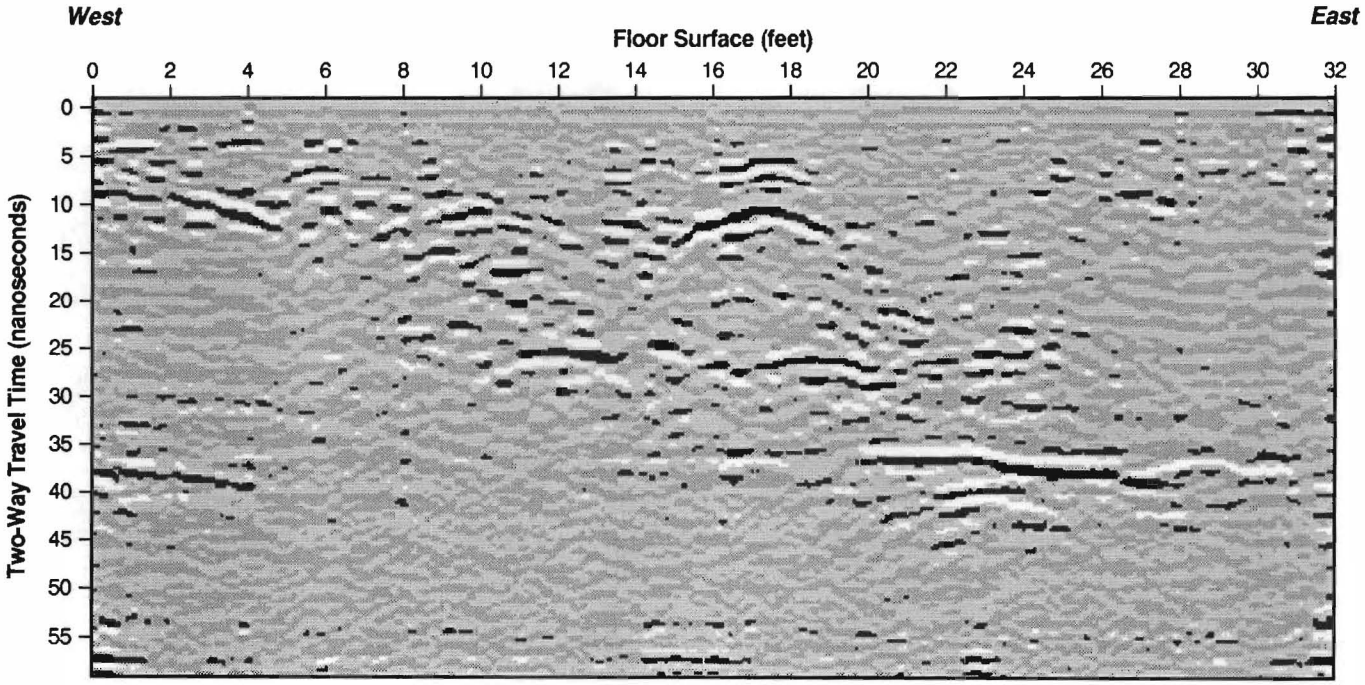

Figure C-2
S-1655 Traverse, Room 6, Panel 1 Floor: January 1992

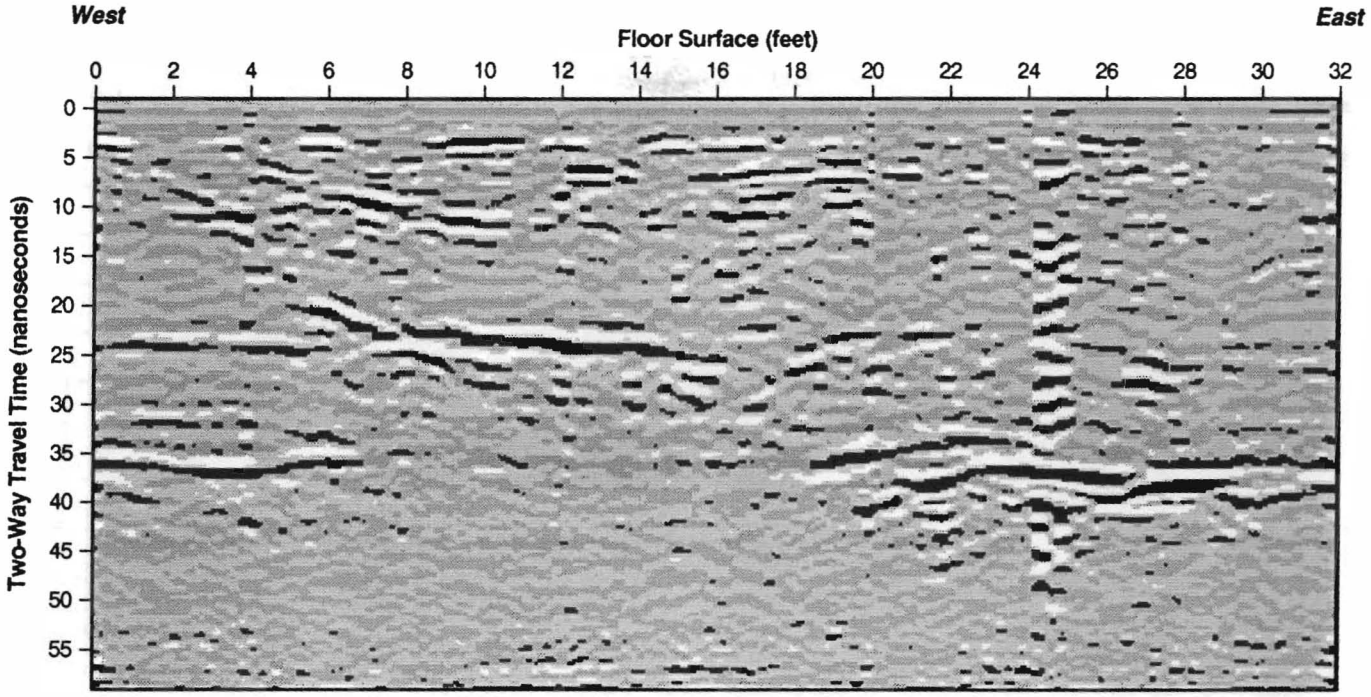

Figure C-3
S-1684 Traverse, Room 6, Panel 1 Floor: January 1992

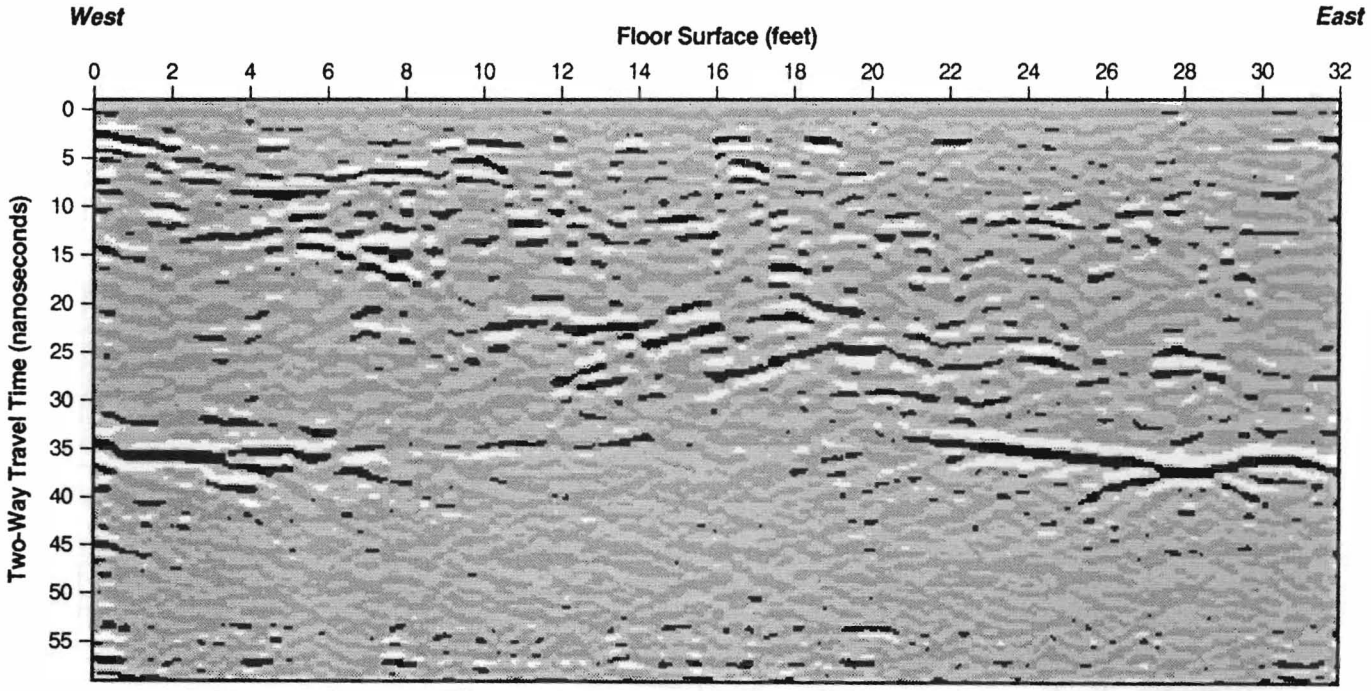

Figure C-4
S-1694 Traverse, Room 6, Panel 1 Floor: January 1992

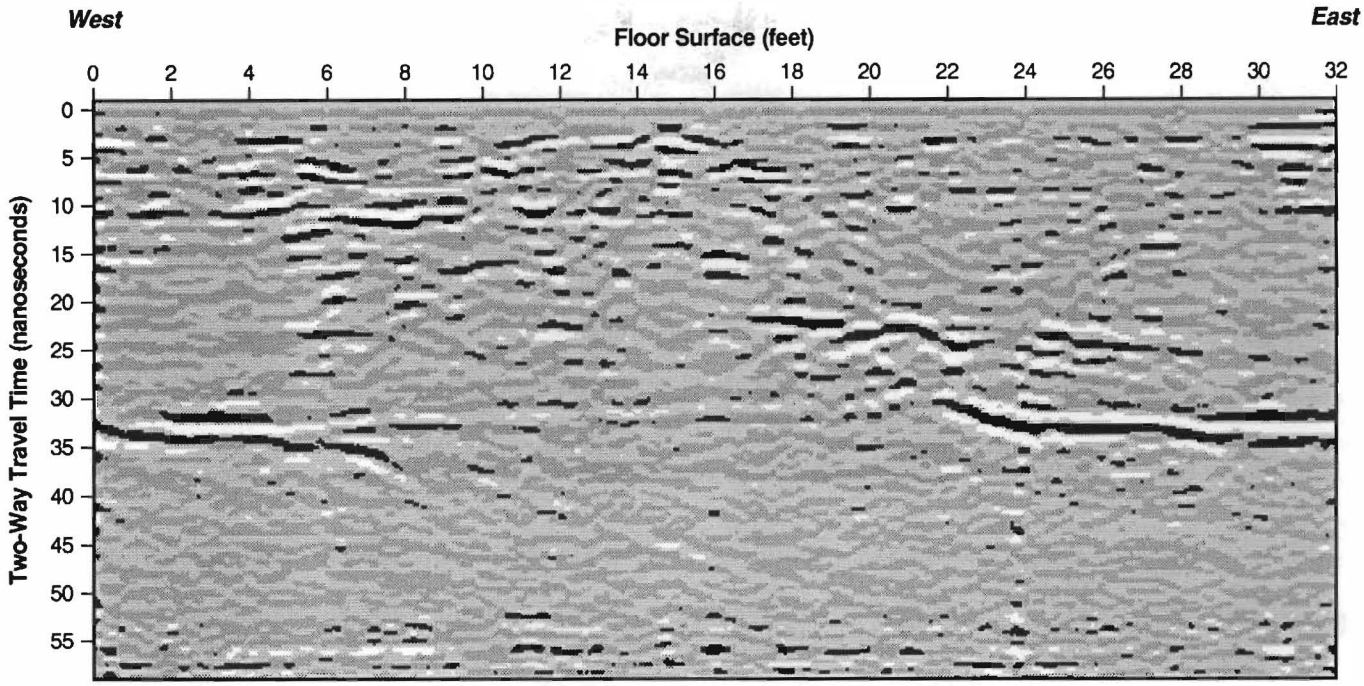

Figure C-5
S-1707 Traverse, Room 6, Panel 1 Floor: January 1992

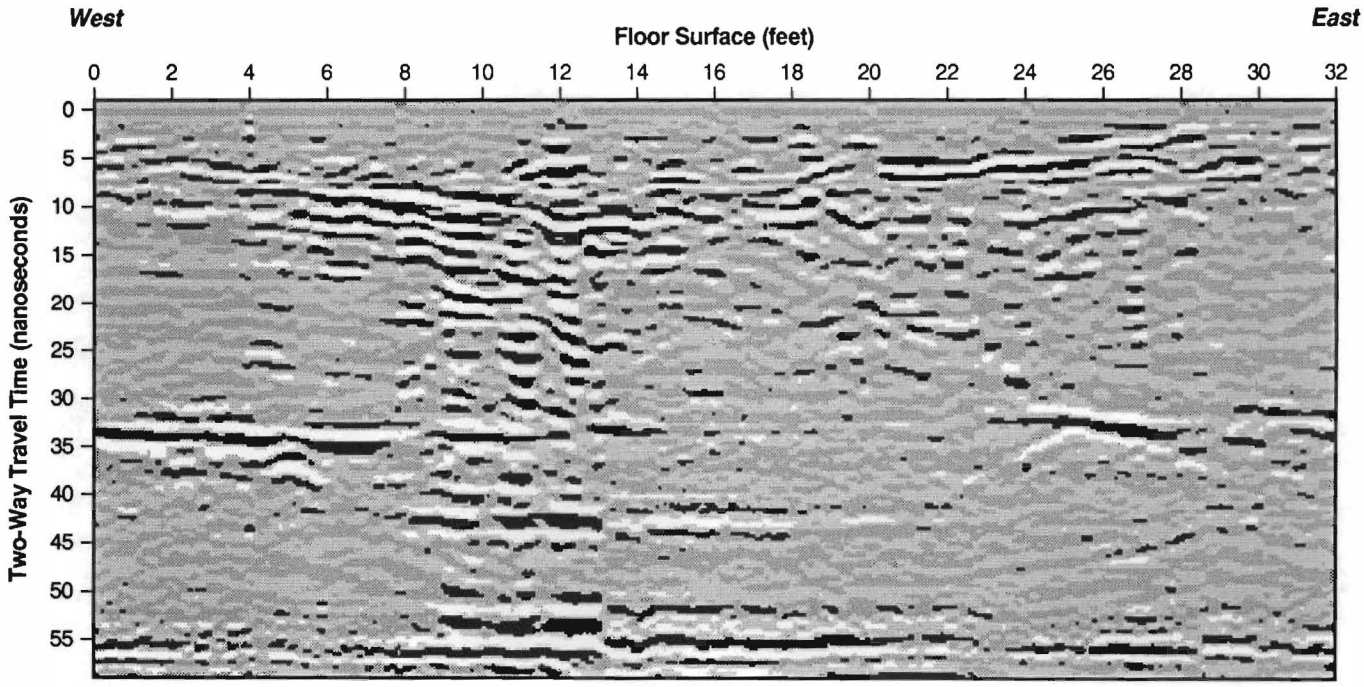

Figure C-6
S-1719 Traverse, Room 6, Panel 1 Floor: January 1992

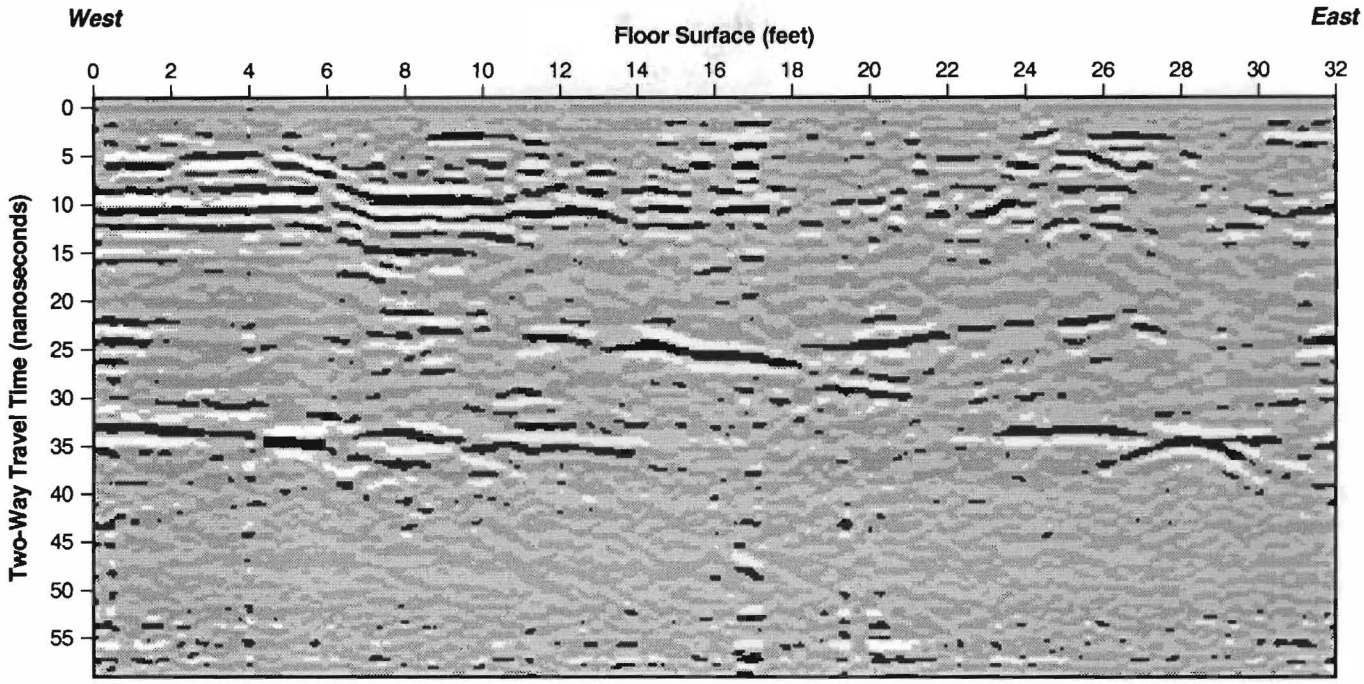

Figure C-7
S-1736 Traverse, Room 6, Panel 1 Floor: January 1992

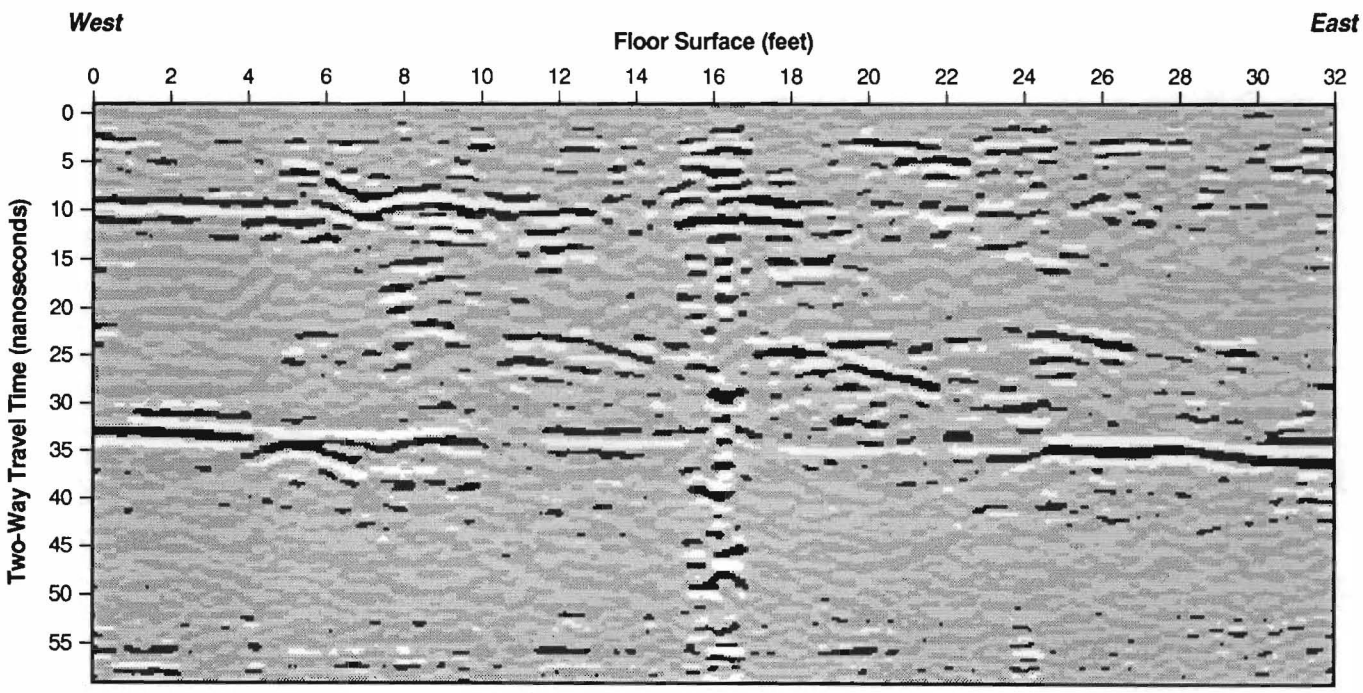

Figure C-8
S-1749 Traverse, Room 6, Panel 1 Floor: January 1992

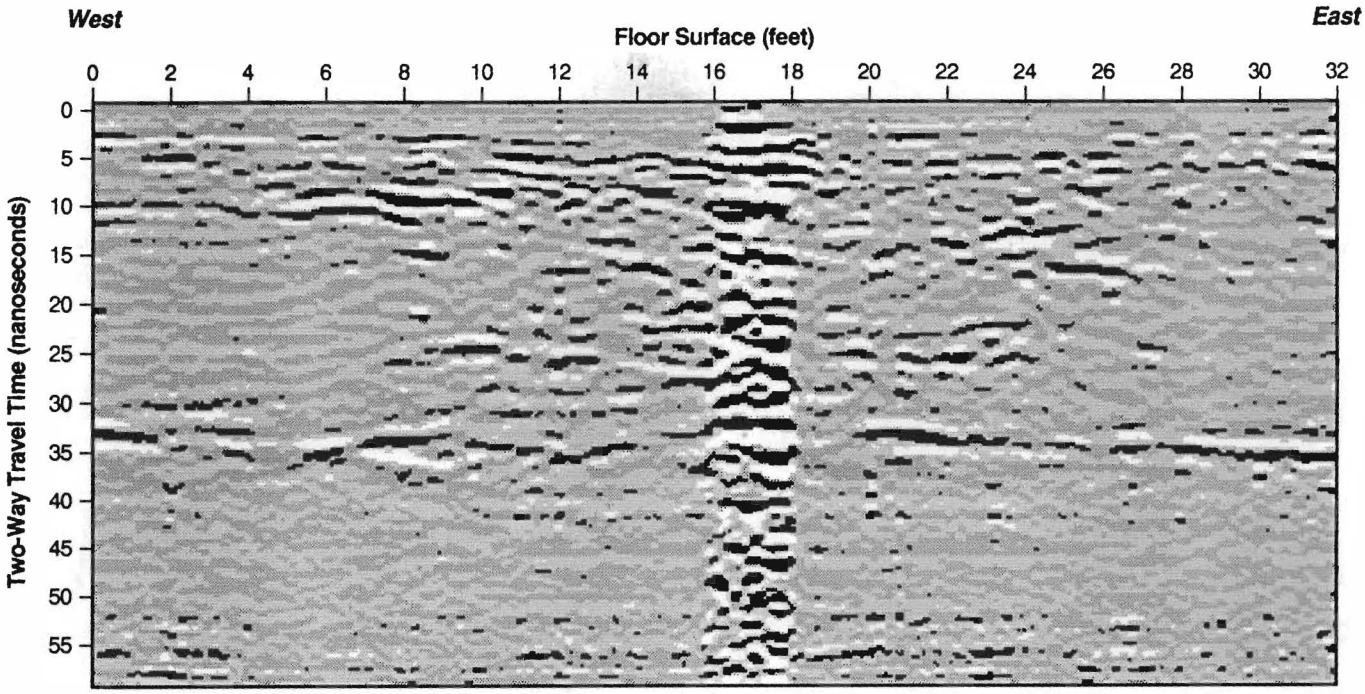

Figure C-9
S-1763 Traverse, Room 6, Panel 1 Floor: January 1992

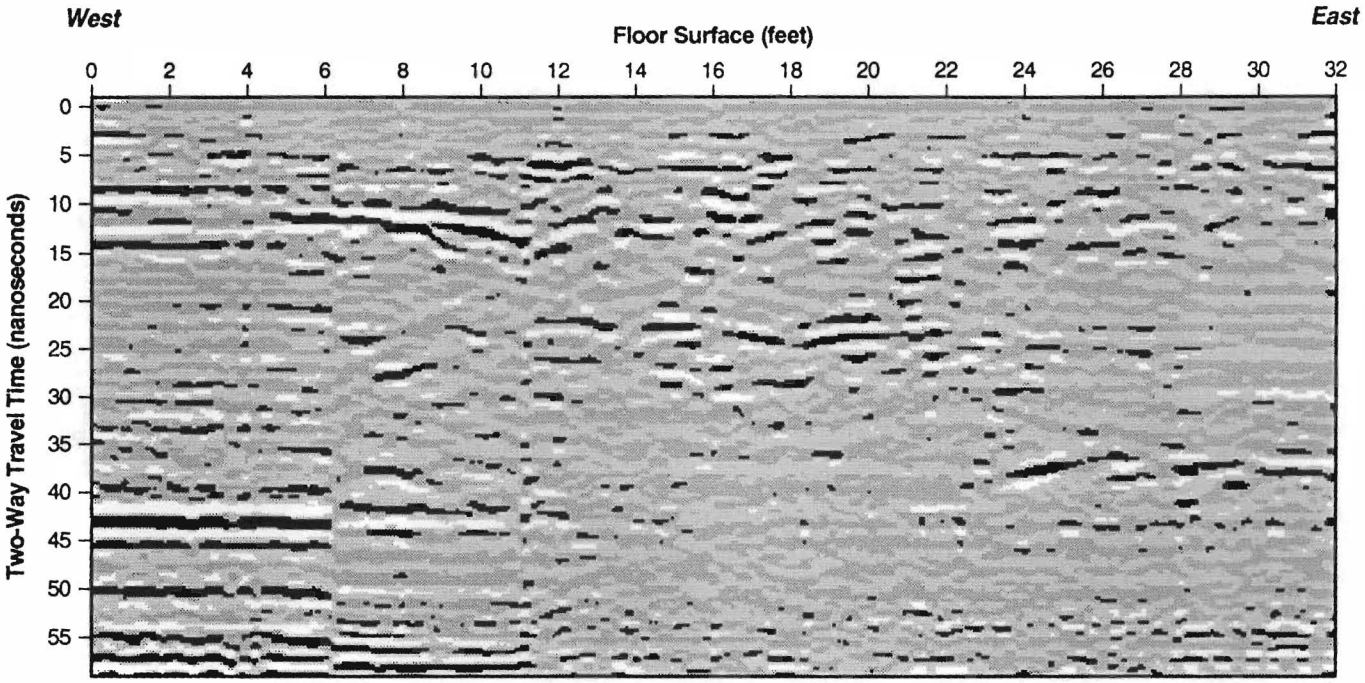

Figure C-10
S-1785 Traverse, Room 6, Panel 1 Floor: January 1992

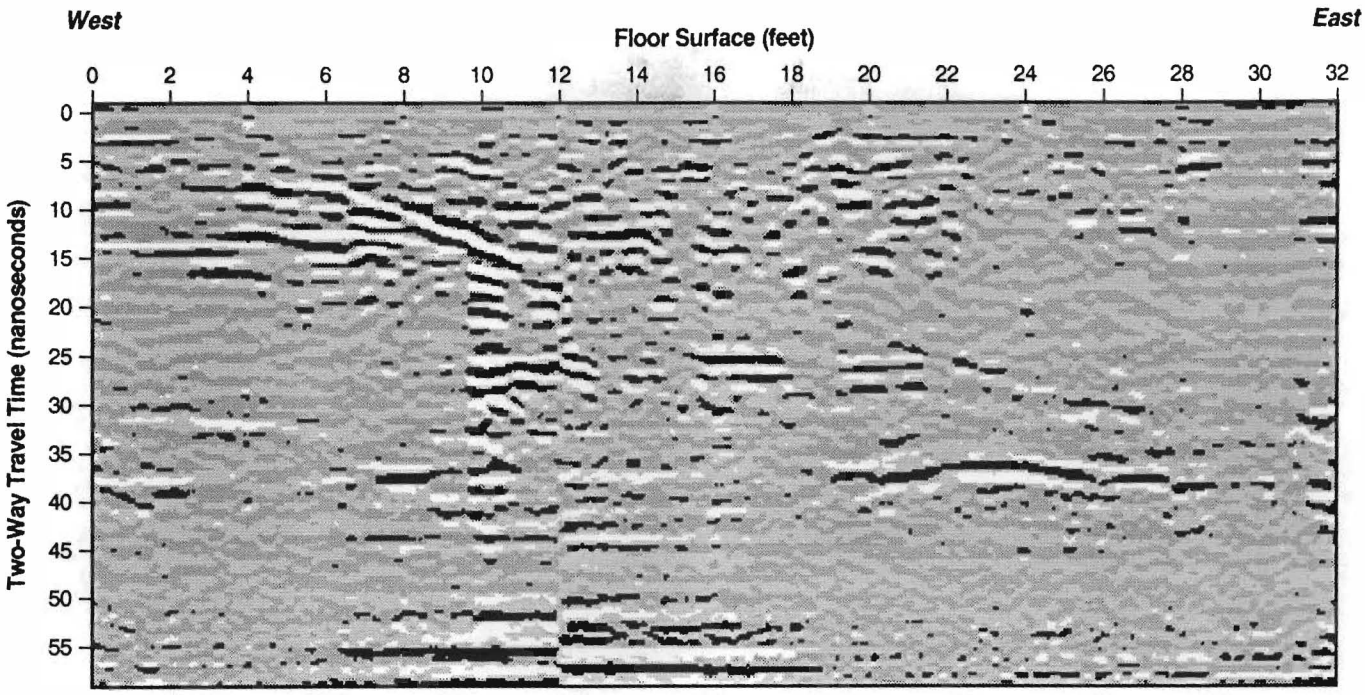

Figure C-11
S-1798 Traverse, Room 6, Panel 1 Floor: January 1992

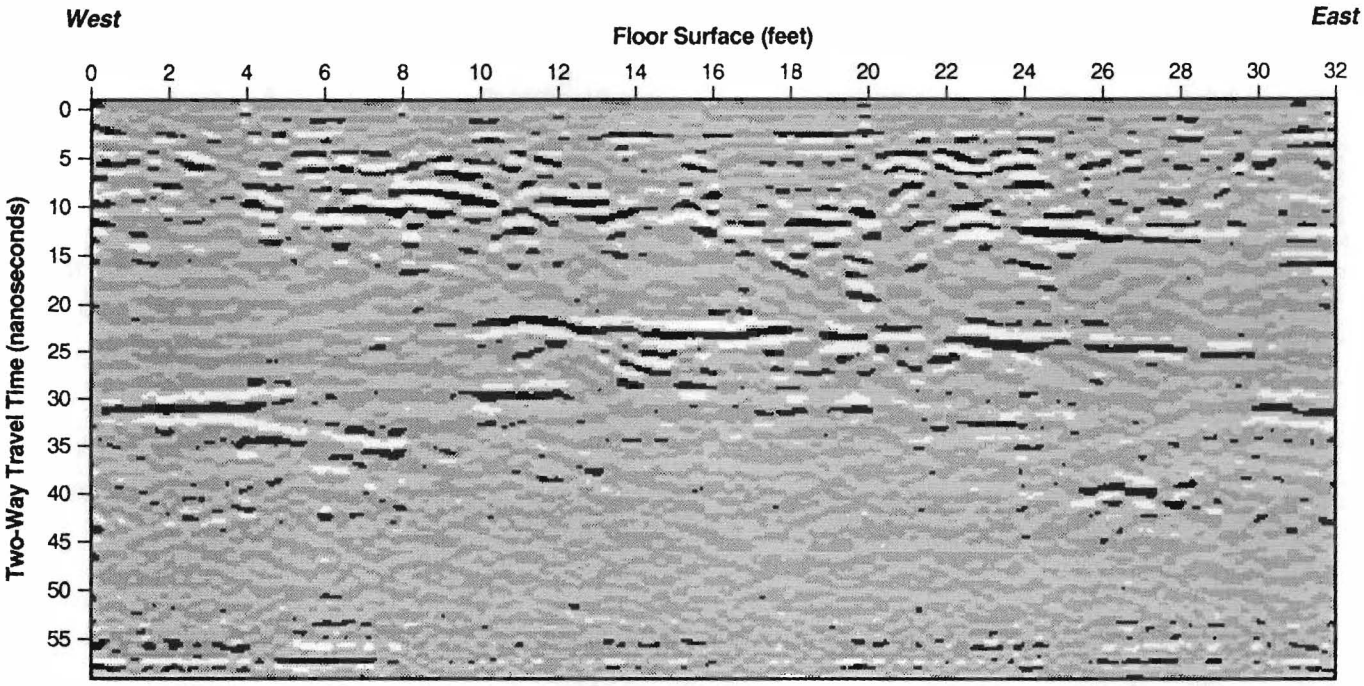

Figure C-12
S-1836 Traverse, Room 6, Panel 1 Floor: January 1992

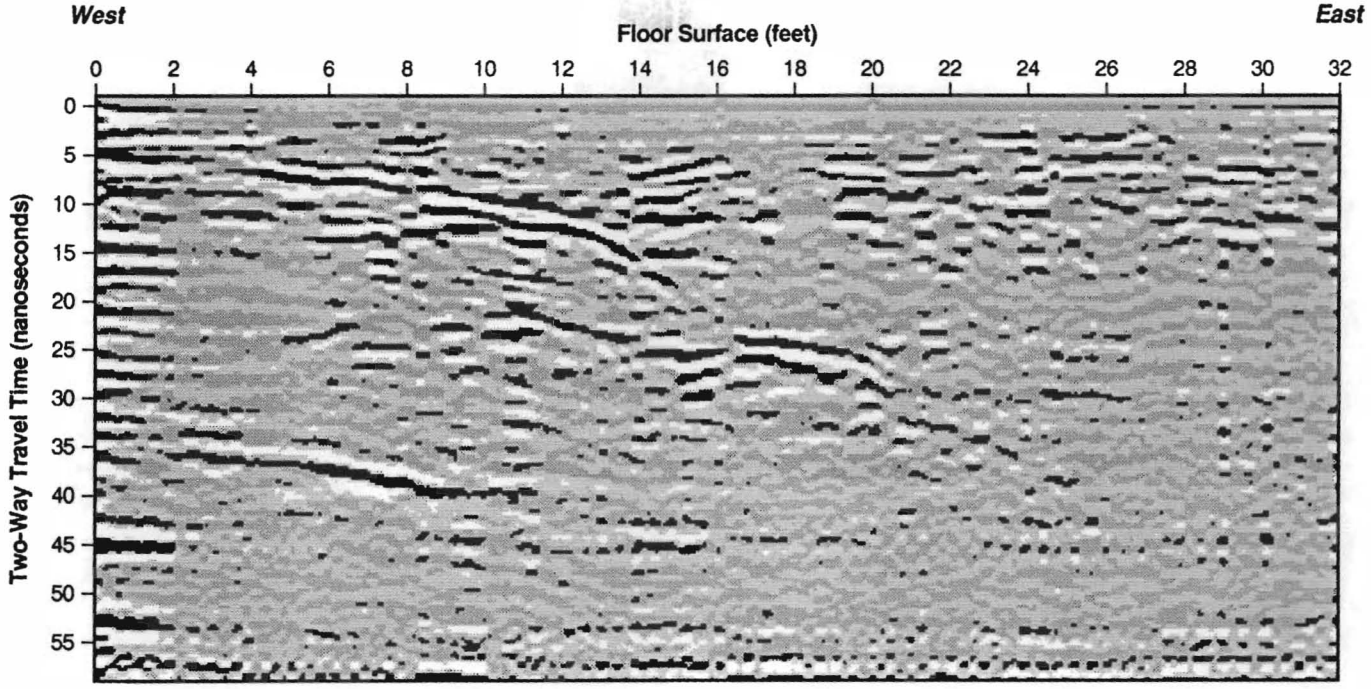

Figure C-13
S-1848 Traverse, Room 6, Panel 1 Floor: January 1992

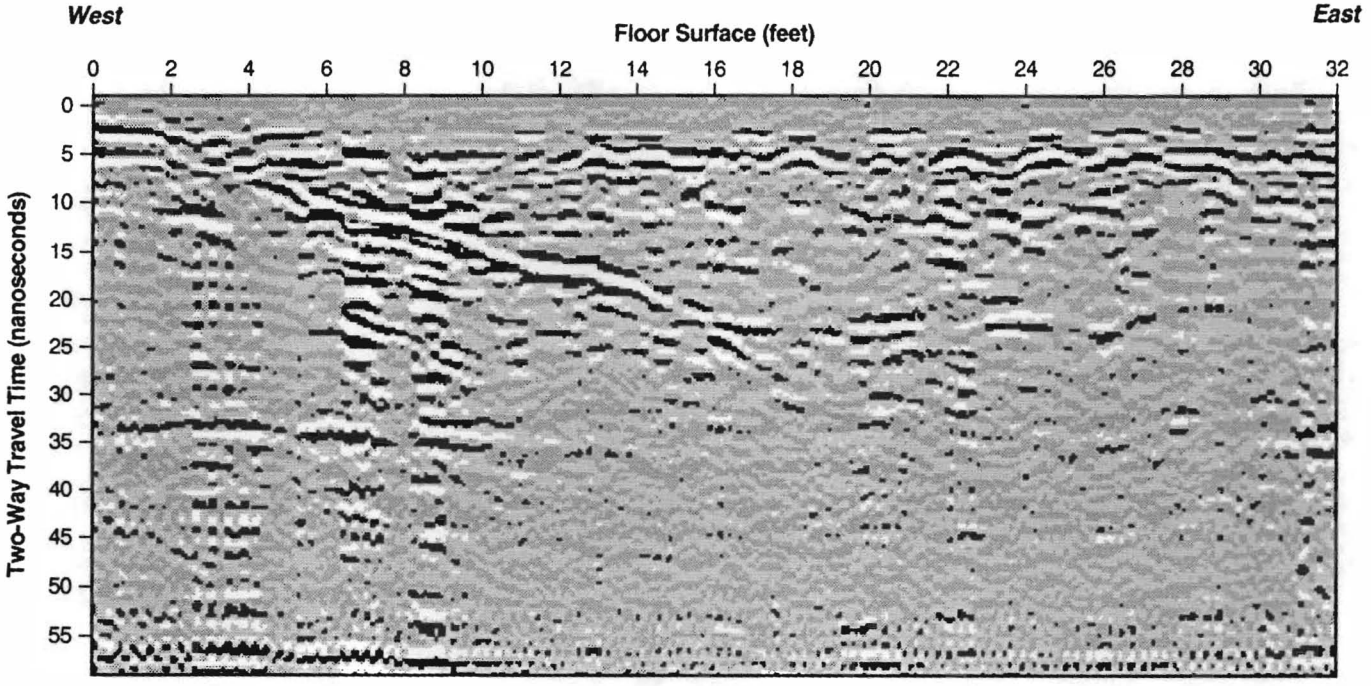

Figure C-14
S-1861 Traverse, Room 6, Panel 1 Floor: January 1992

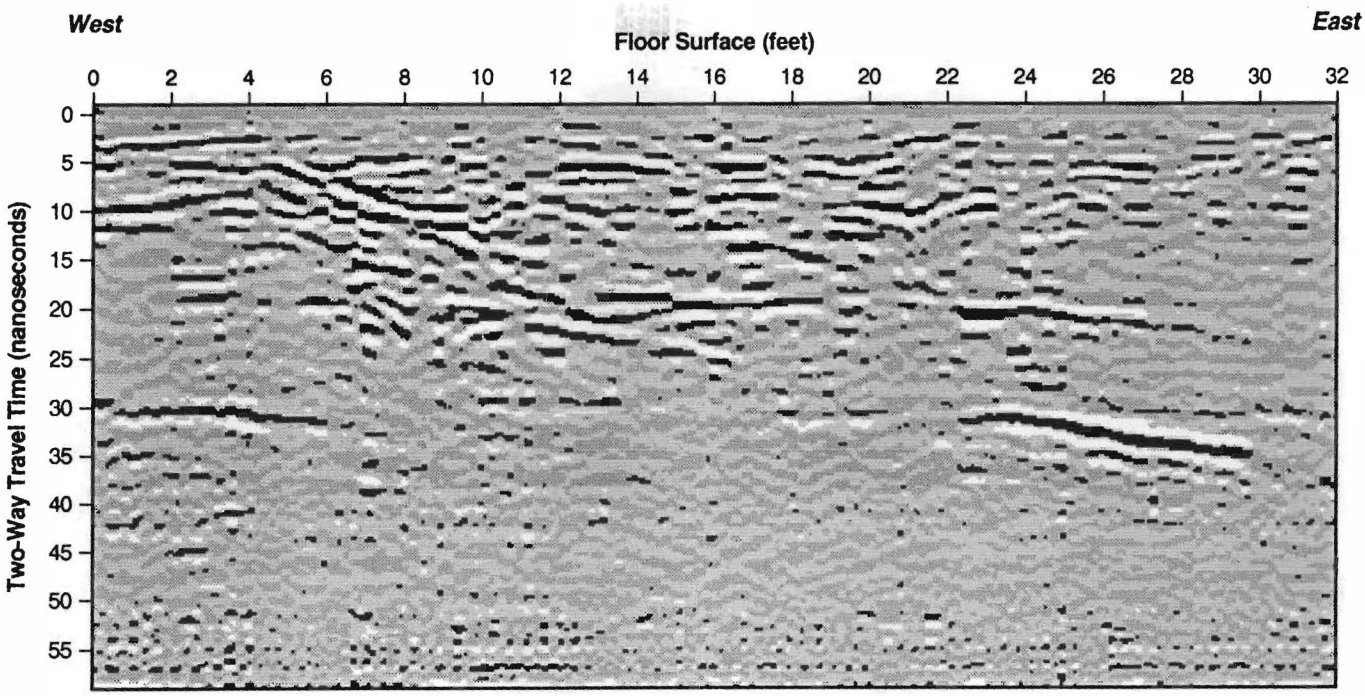

Figure C-15
S-1886 Traverse, Room 6, Panel 1 Floor: January 1992

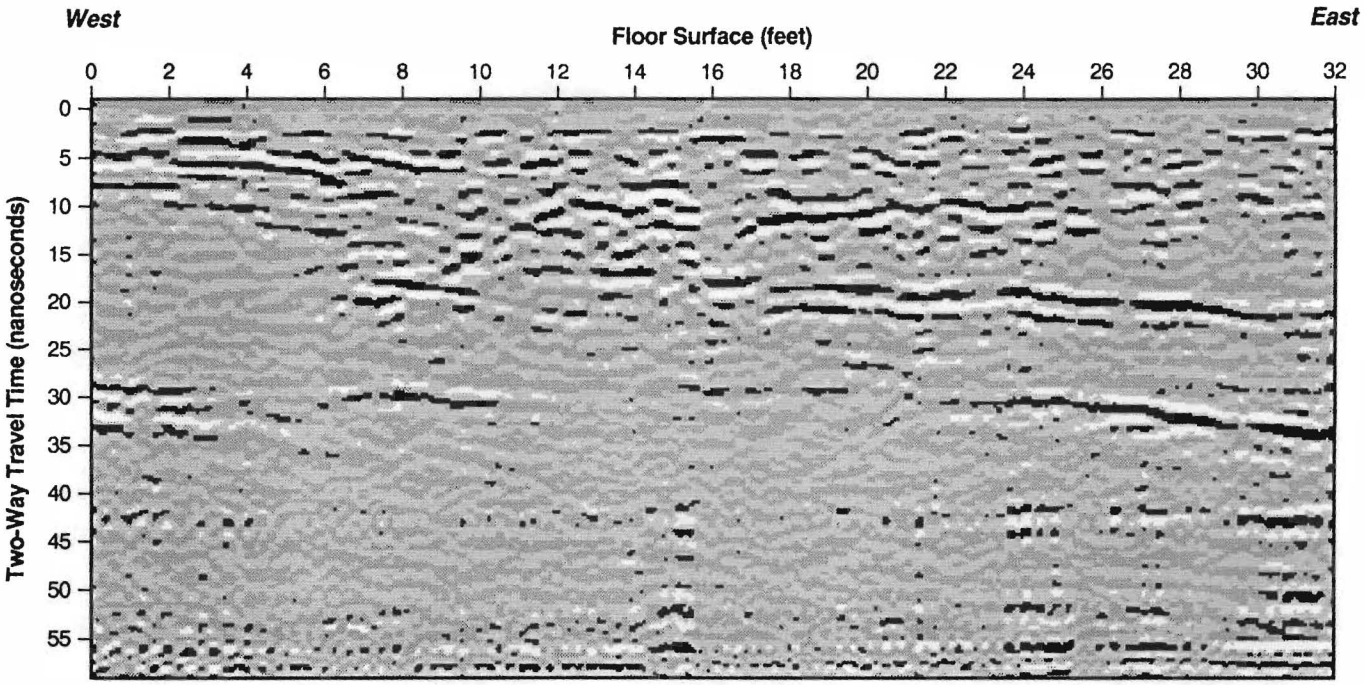

Figure C-16
S-1900 Traverse, Room 6, Panel 1 Floor: January 1992

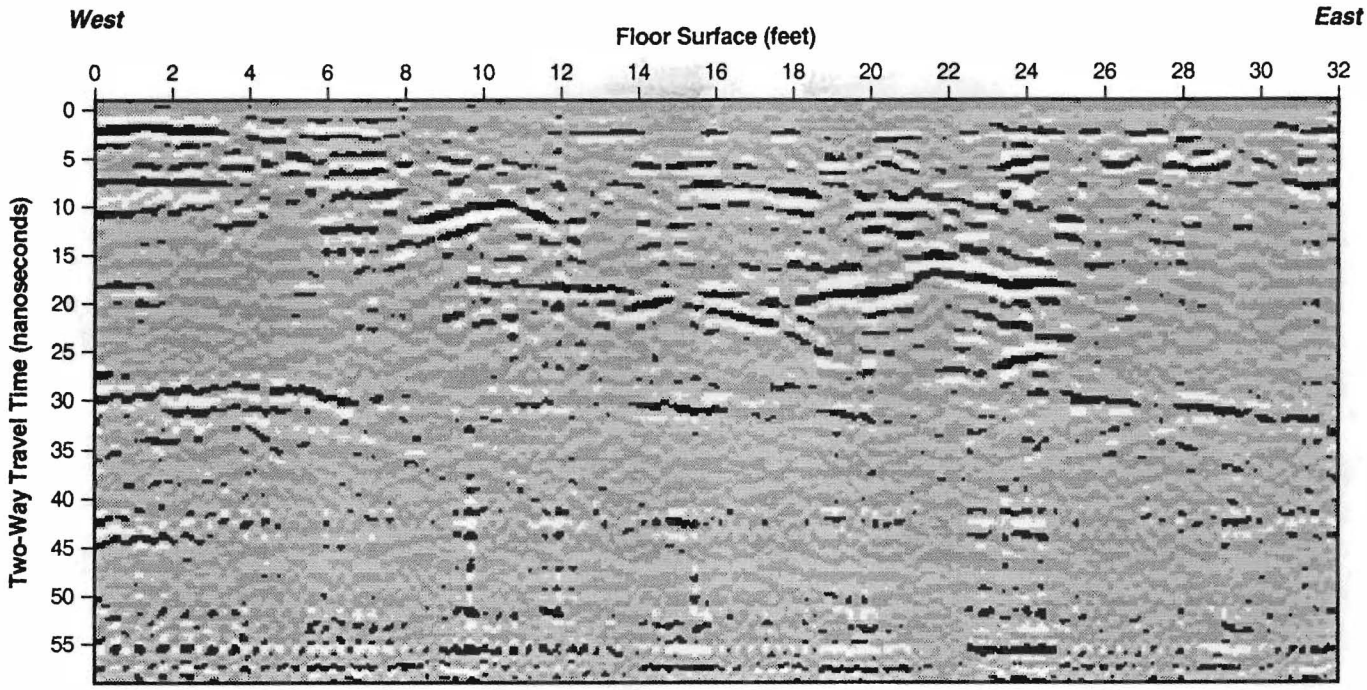

Figure C-17
S-1912 Traverse, Room 6, Panel 1 Floor: January 1992

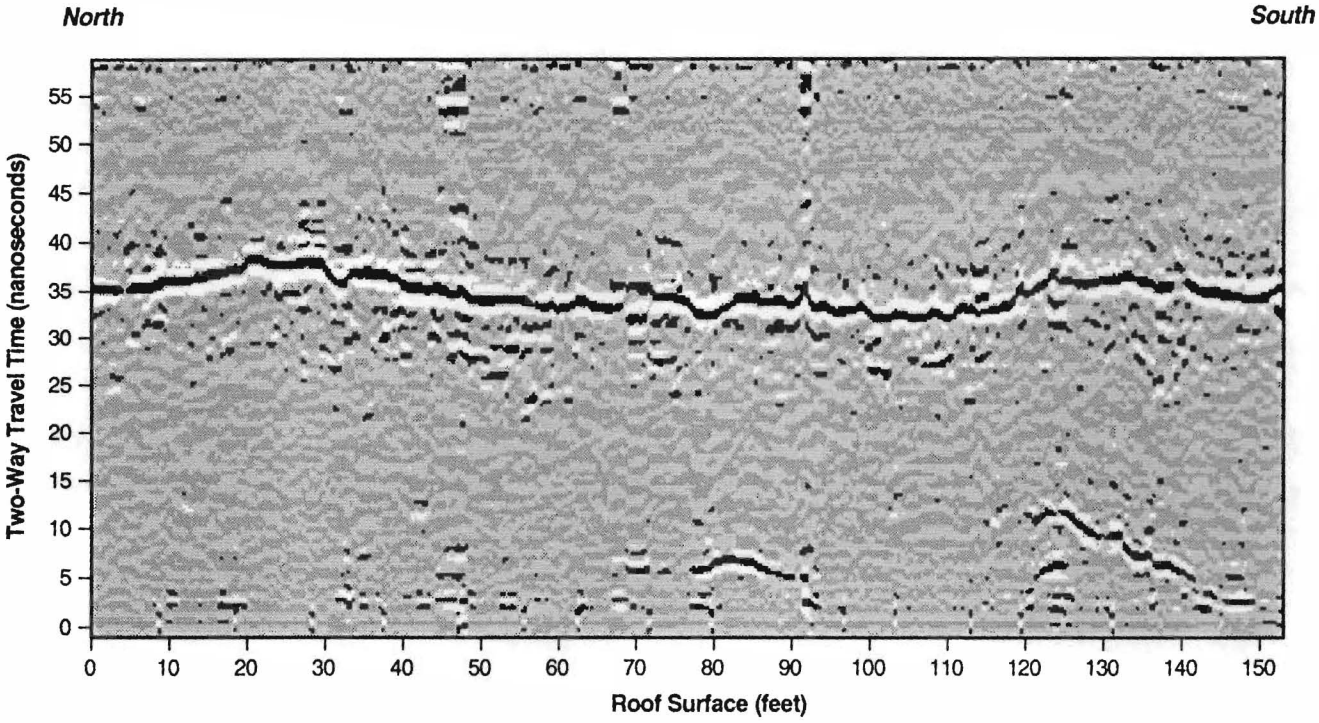

Figure C-18
S-1645 to S-1798 Traverse, Room 6, Panel 1 Roof: January 1992
Vertical Exaggeration 5.0x

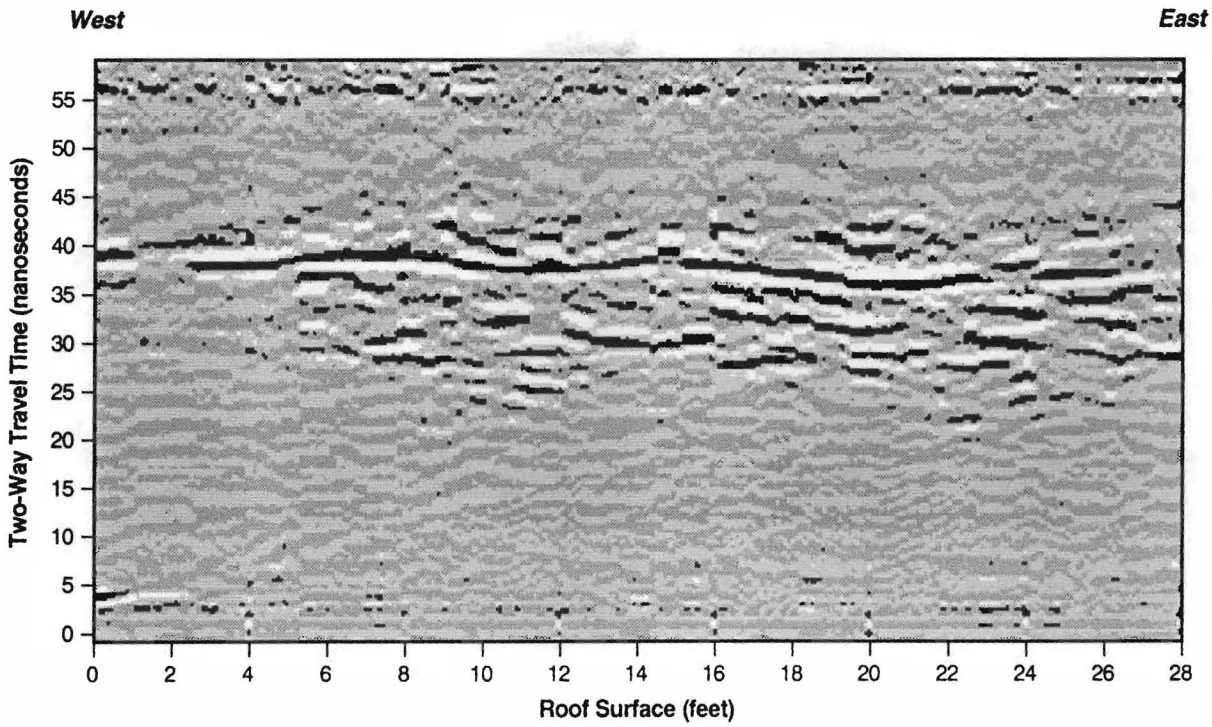

Figure C-19
S-1655 Traverse, Room 6, Panel 1 Roof: January 1992

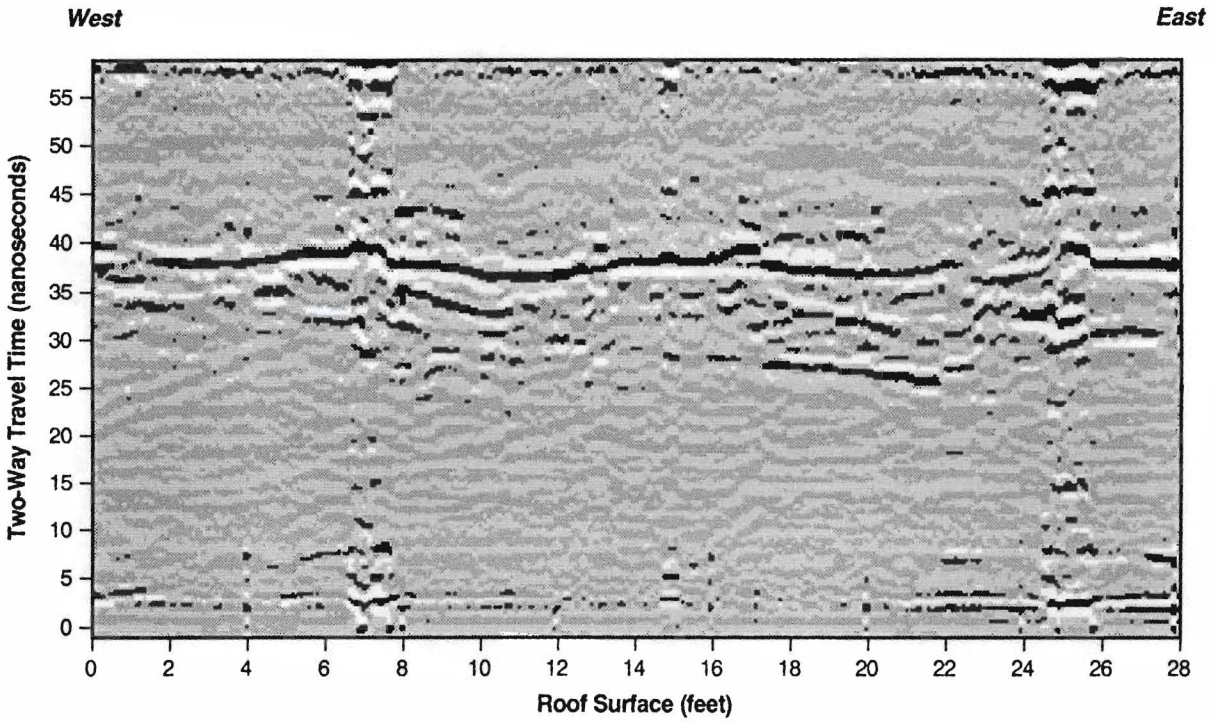

Figure C-20
S-1667 Traverse, Room 6, Panel 1 Roof: January 1992

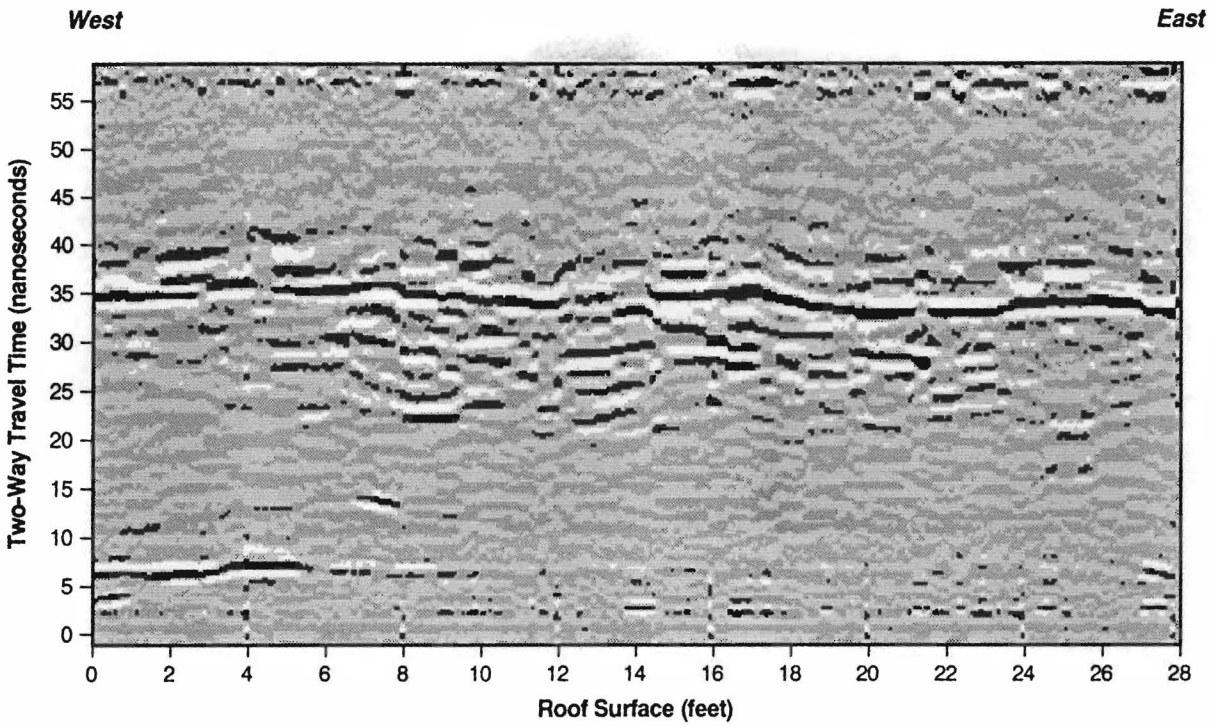

Figure C-21
S-1694 Traverse, Room 6, Panel 1 Roof: January 1992

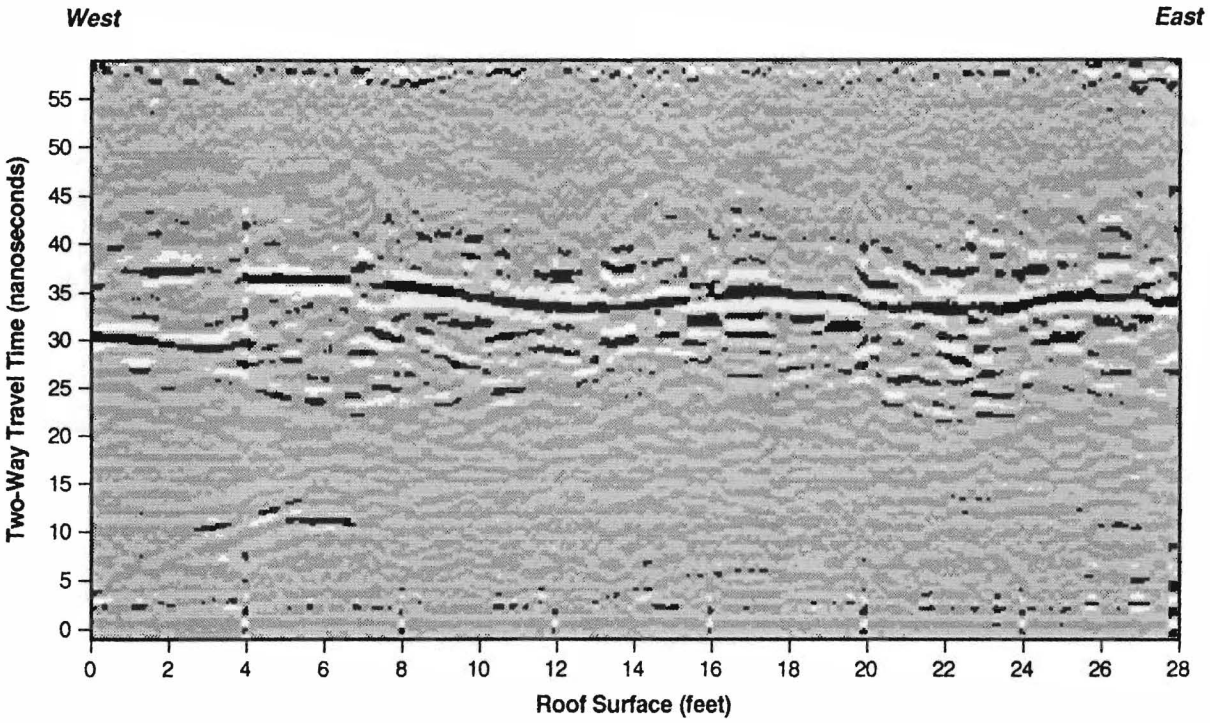

Figure C-22
S-1707 Traverse, Room 6, Panel 1 Roof: January 1992

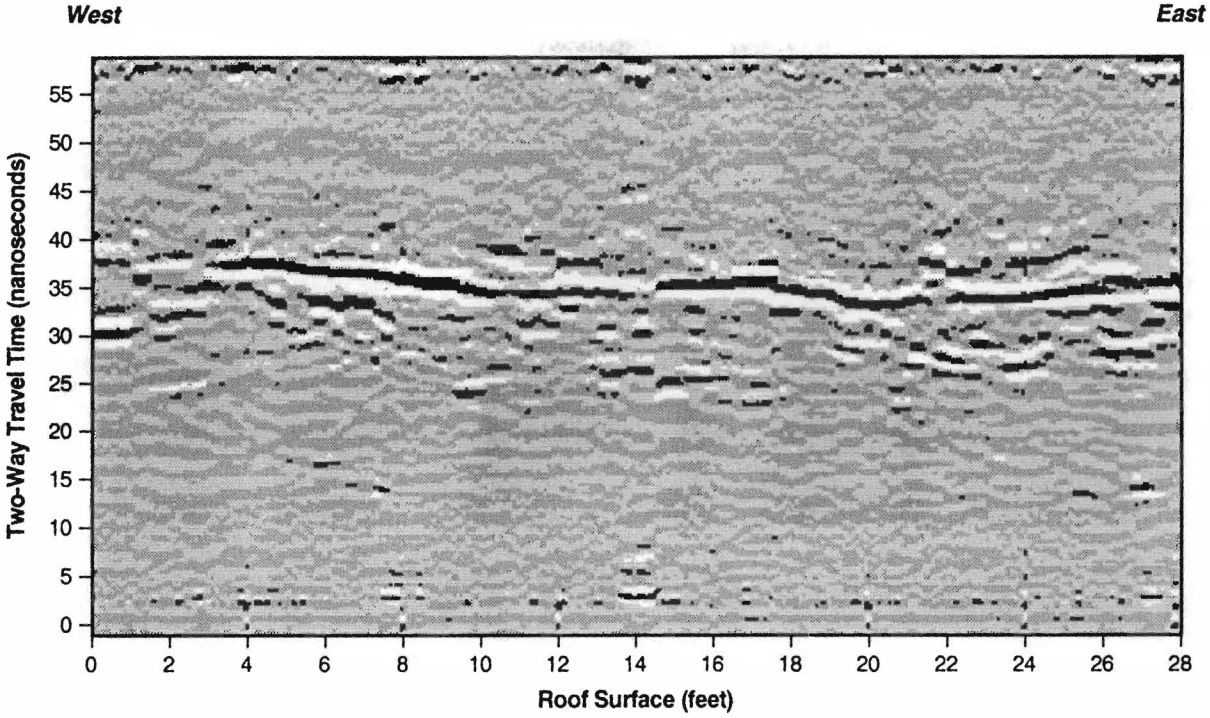

Figure C-23
S-1719 Traverse, Room 6, Panel 1 Roof: January 1992

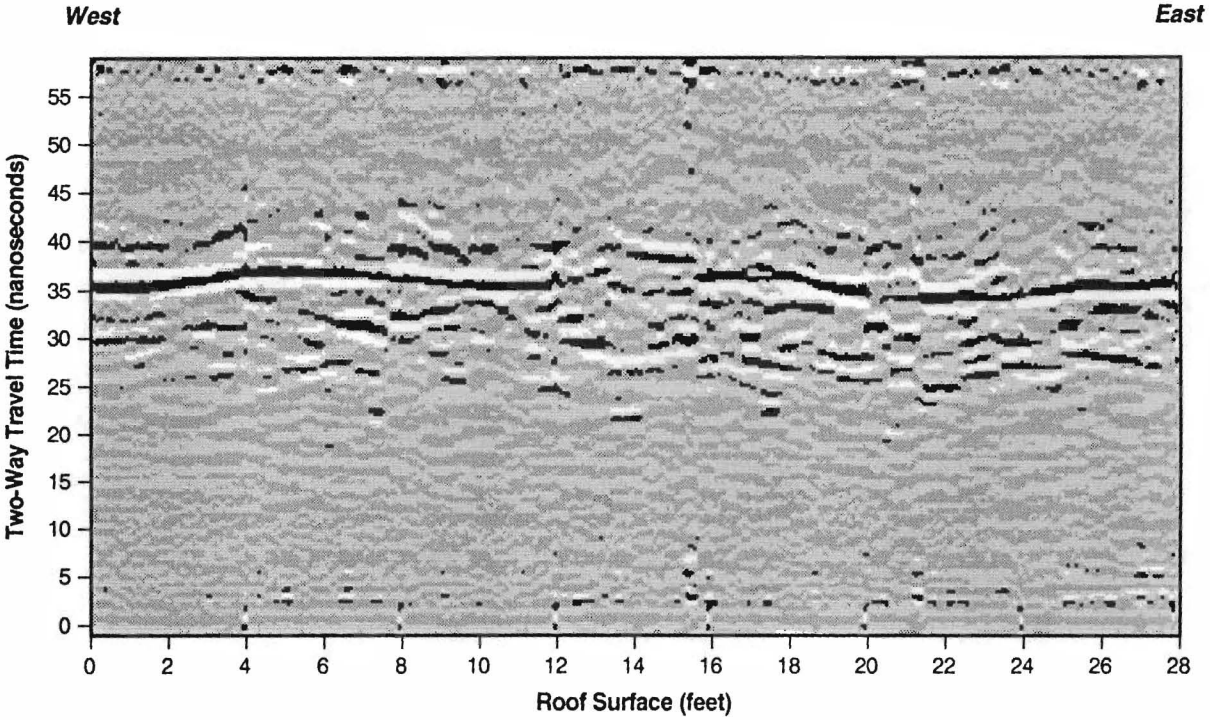

Figure C-24
S-1749 Traverse, Room 6, Panel 1 Roof: January 1992

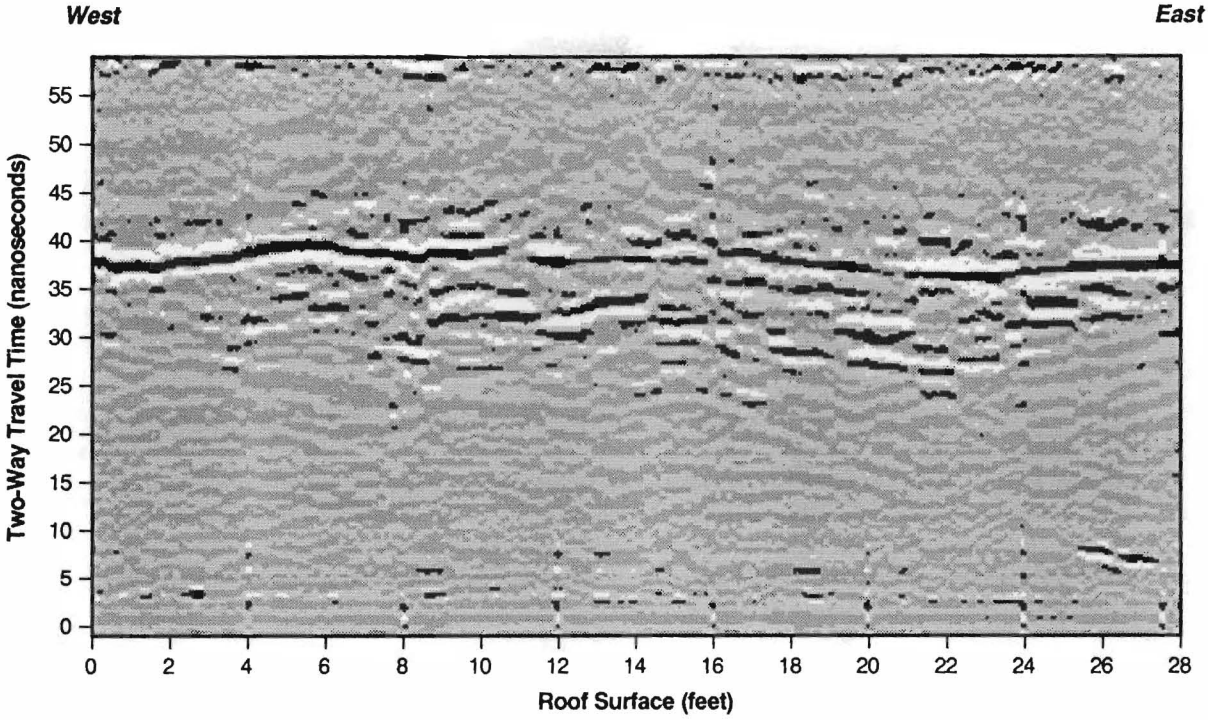

Figure C-25
S-1763 Traverse, Room 6, Panel 1 Roof: January 1992

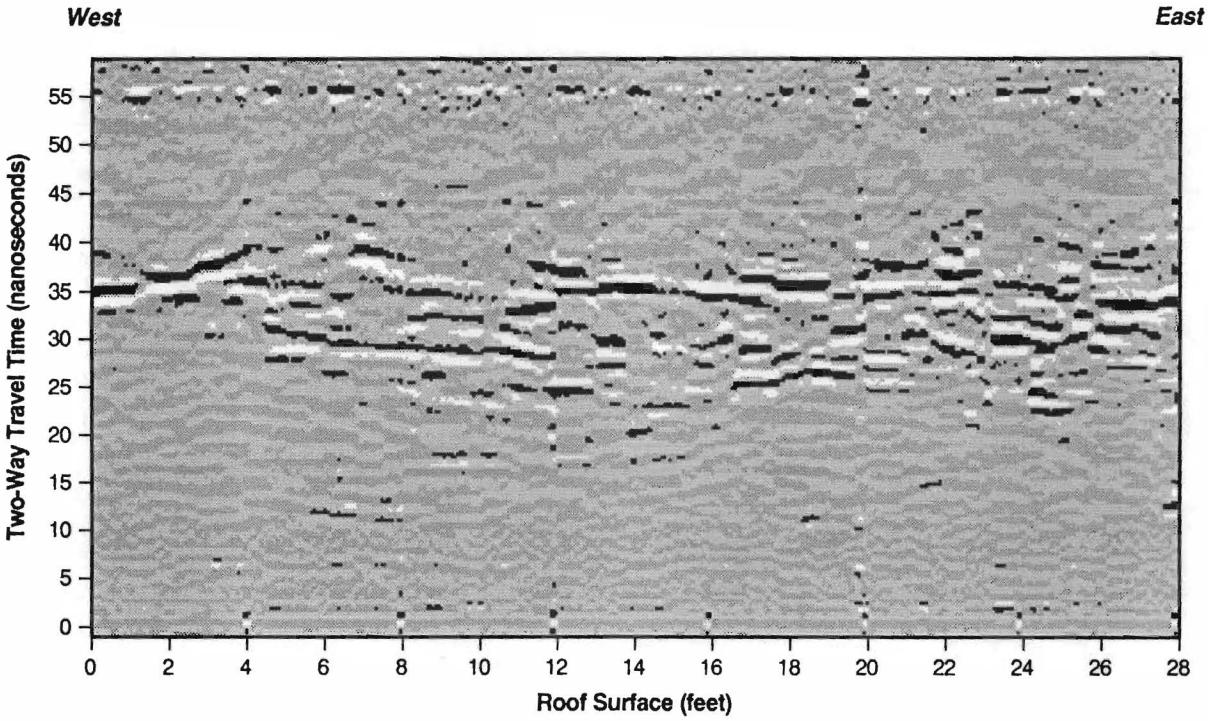

Figure C-26
S-1785 Traverse, Room 6, Panel 1 Roof: January 1992

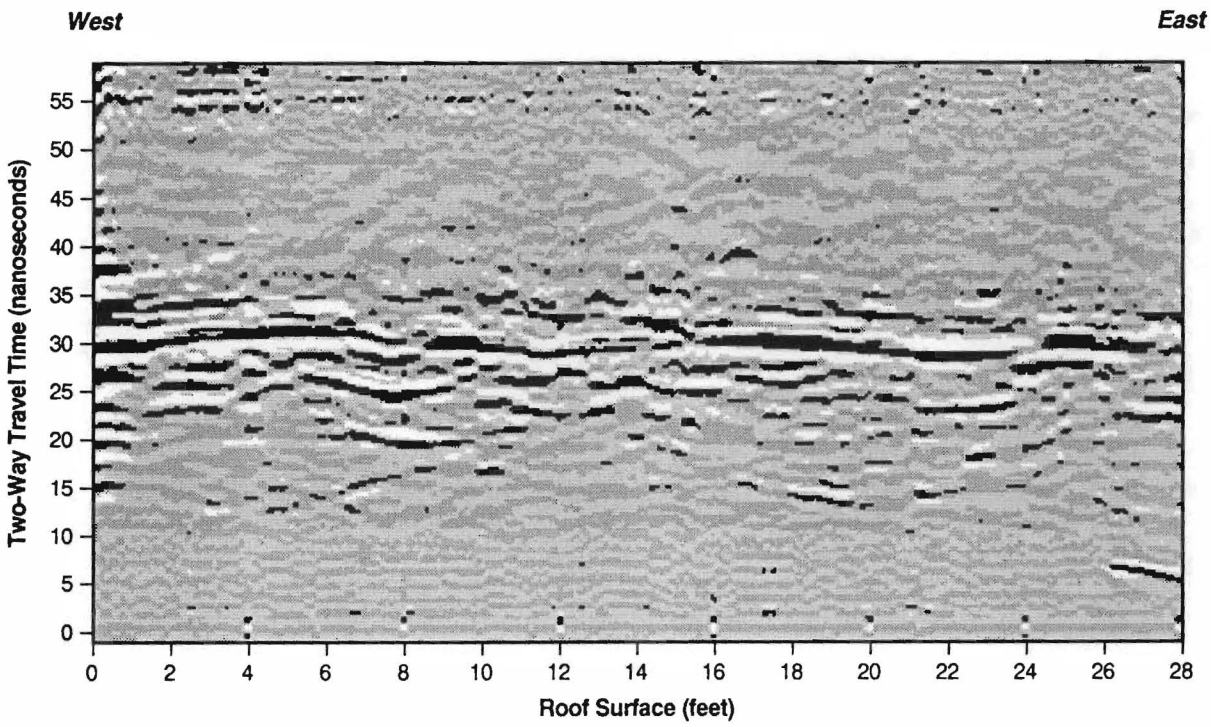

Figure C-27
S-1811 Traverse, Room 6, Panel 1 Roof: January 1992

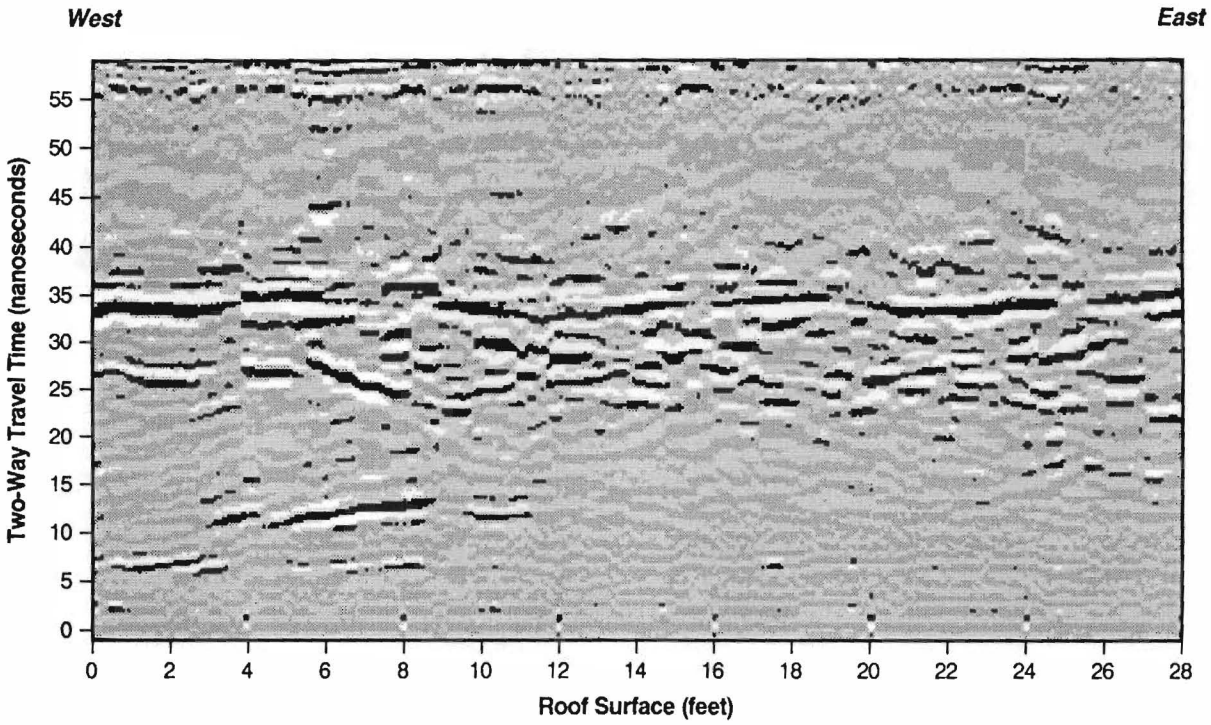

Figure C-28
S-1836 Traverse, Room 6, Panel 1 Roof: January 1992

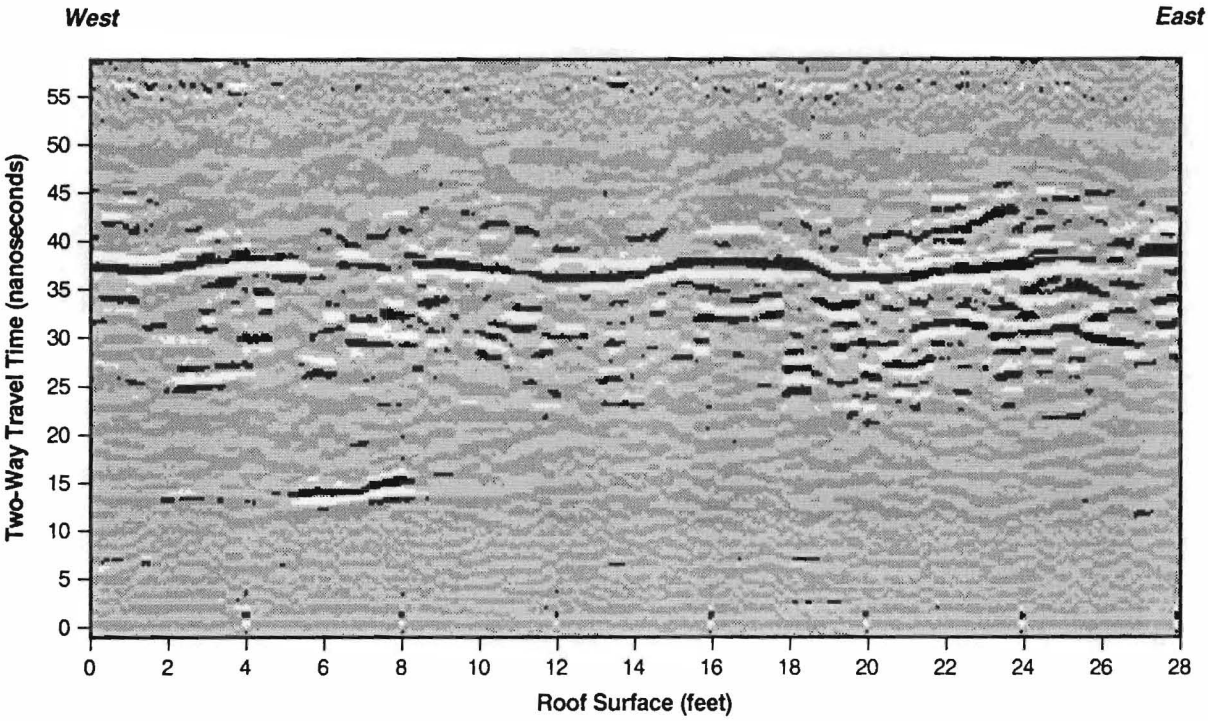

Figure C-29
S-1848 Traverse, Room 6, Panel 1 Roof: January 1992

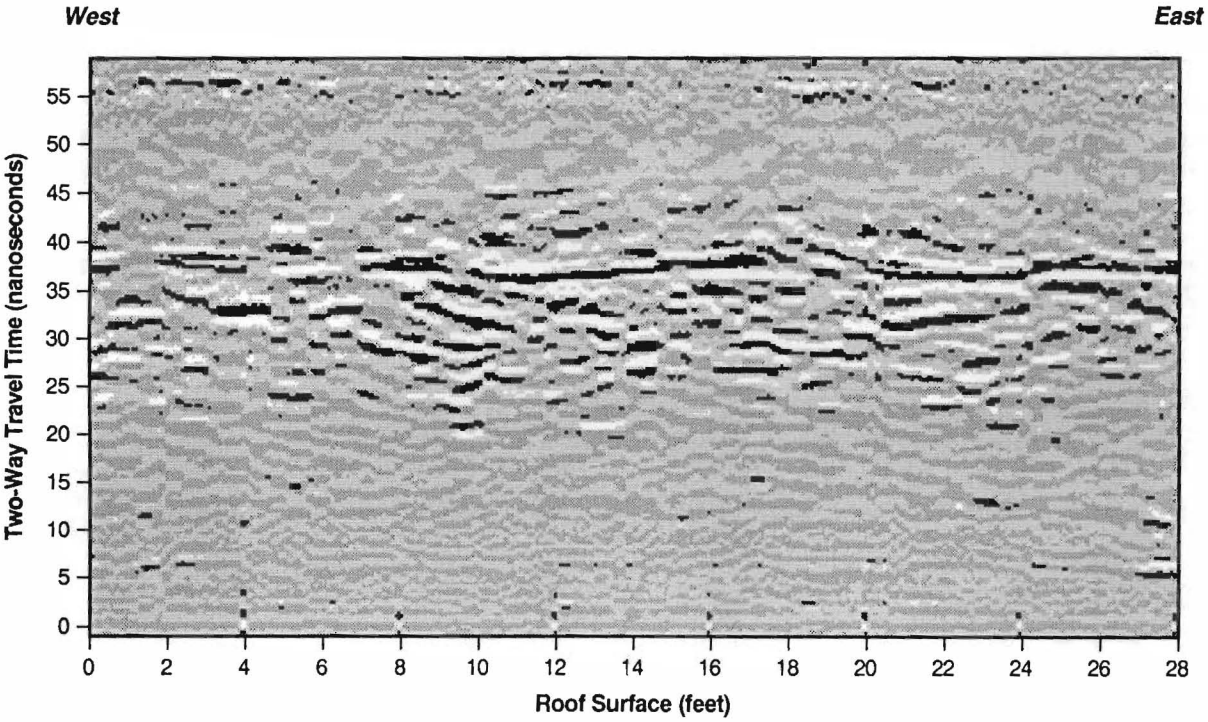

Figure C-30
S-1861 Traverse, Room 6, Panel 1 Roof: January 1992

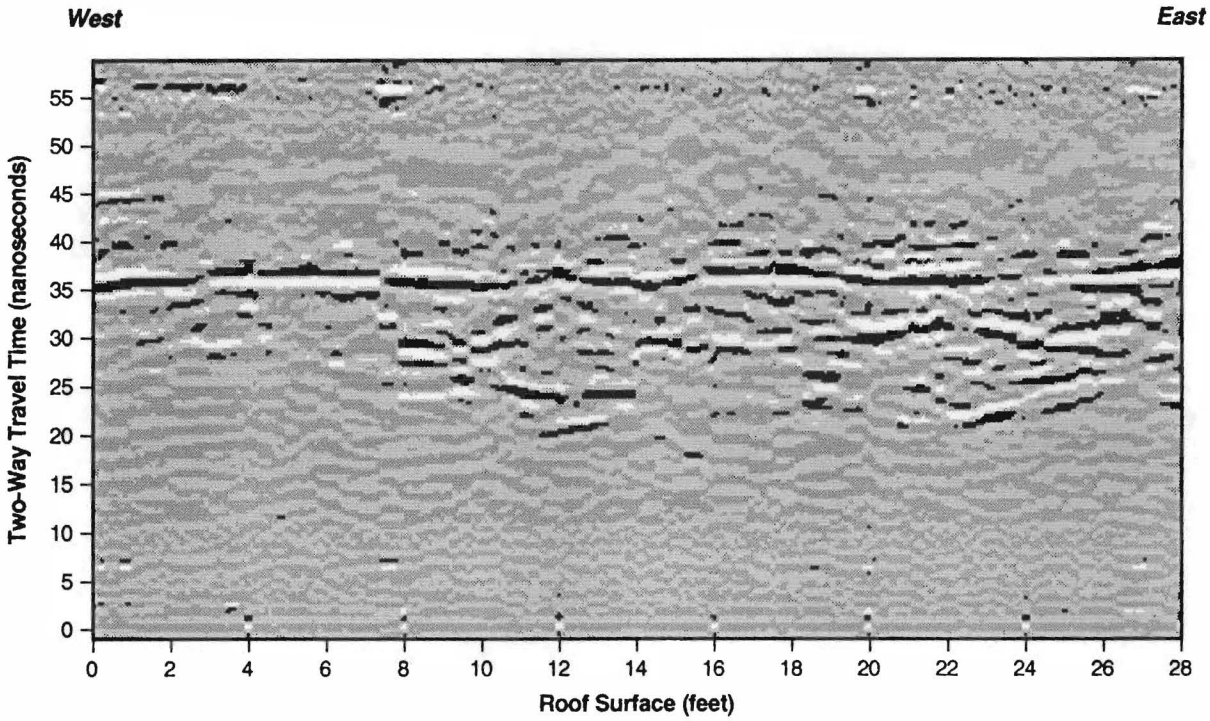

Figure C-31
S-1886 Traverse, Room 6, Panel 1 Roof: January 1992

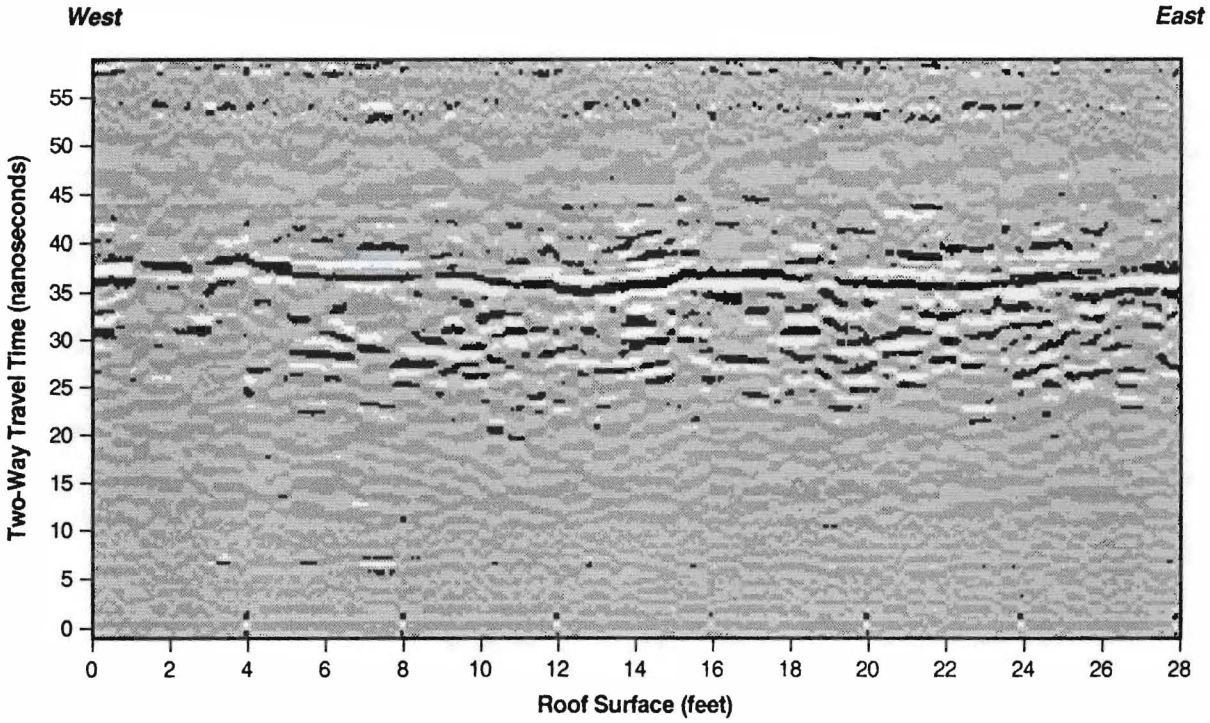

Figure C-32
S-1900 Traverse, Room 6, Panel 1 Roof: January 1992

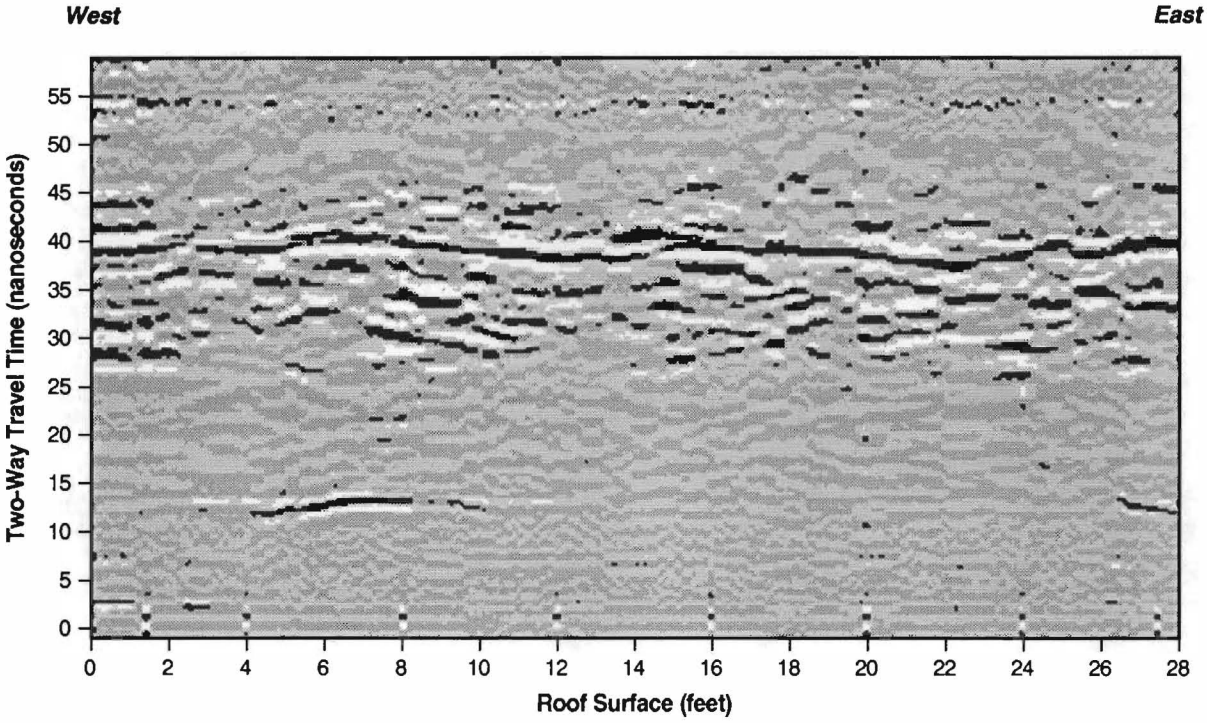

Figure C-33
S-1912 Traverse, Room 6, Panel 1 Roof: January 1992

APPENDIX D

INSTRUMENTATION SETTINGS, PROCESSING SEQUENCES, AND RADAR PROFILES: S-1950 DRIFT ROOF

APPENDIX D

This appendix contains the following: (1) instrumentation settings used to conduct GPR surveys on the S-1950 Drift roof on 02/04/92, 02/05/92 and 02/06/92; (2) processing sequences used to produce the radar profiles from the S-1950 Drift roof; and (3) radar profiles not contained in the body of this report (Figures D-1 to D-38).

D.1 Instrumentation Settings for the S-1950 Drift Roof Surveys (02/04/92, 02/05/92, and 02/06/92)

Antenna settings:

Transmit = high power
Receiver = normal amplification

Profiling recorder settings:

Surface gain = 3
Center gain = 2
Deep gain = 4
Threshold = 3
Signal position = manual
Print polarity = +/- - (negative amplitudes stippled)
Range(dial) = 600 ns
Range multiplier = 100
HP filter = 10
LP filter = 50
XMIT rate = 50 KHz
MODE = radar
Scans/sec = 16
Lines/in. = 200

D.2 *Processing Sequences for the S-1950 Drift Roof Surveys (02/04/92, 02/05/92, and 02/06/92)*

1. LP compression, TC = 2

2. Horizontal scaling

3. Stack = 3

4. Finite impulse response filters

   Horizontal boxcar high pass = 255

5. Predictive deconvolution

   Operator length = 45
   Prediction lag = 3
   Prewhitening = 0.1%
   Gain = 10

6. Finite impulse response filters

   Vertical triangle high pass = 35
   Vertical triangle low pass = 10
   Horizontal triangle low pass = 7

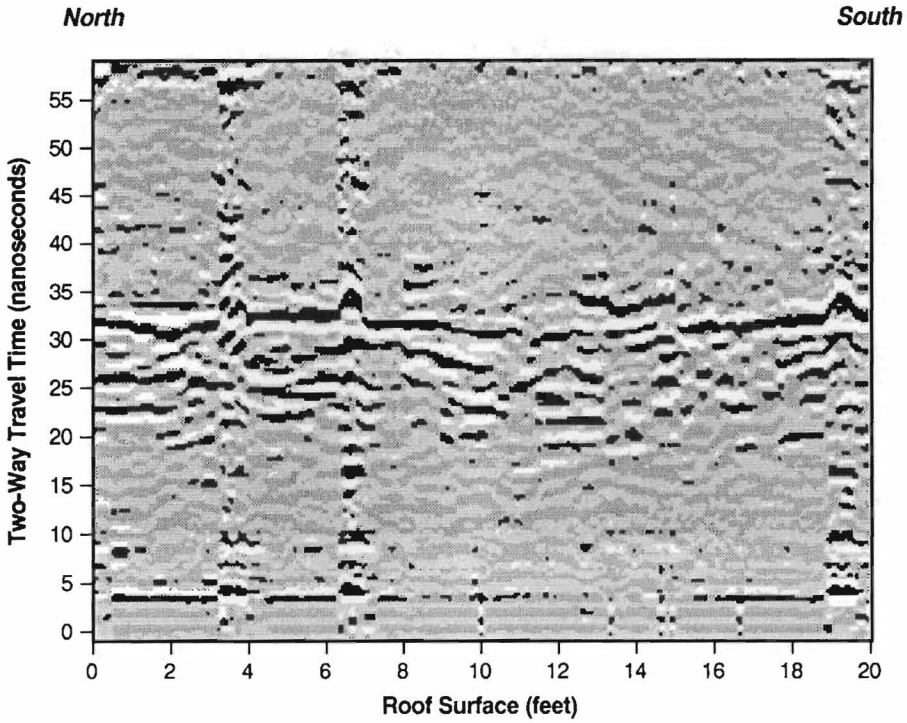

Figure D-1
E-0520 Traverse, S-1950 Drift Roof: February 1992

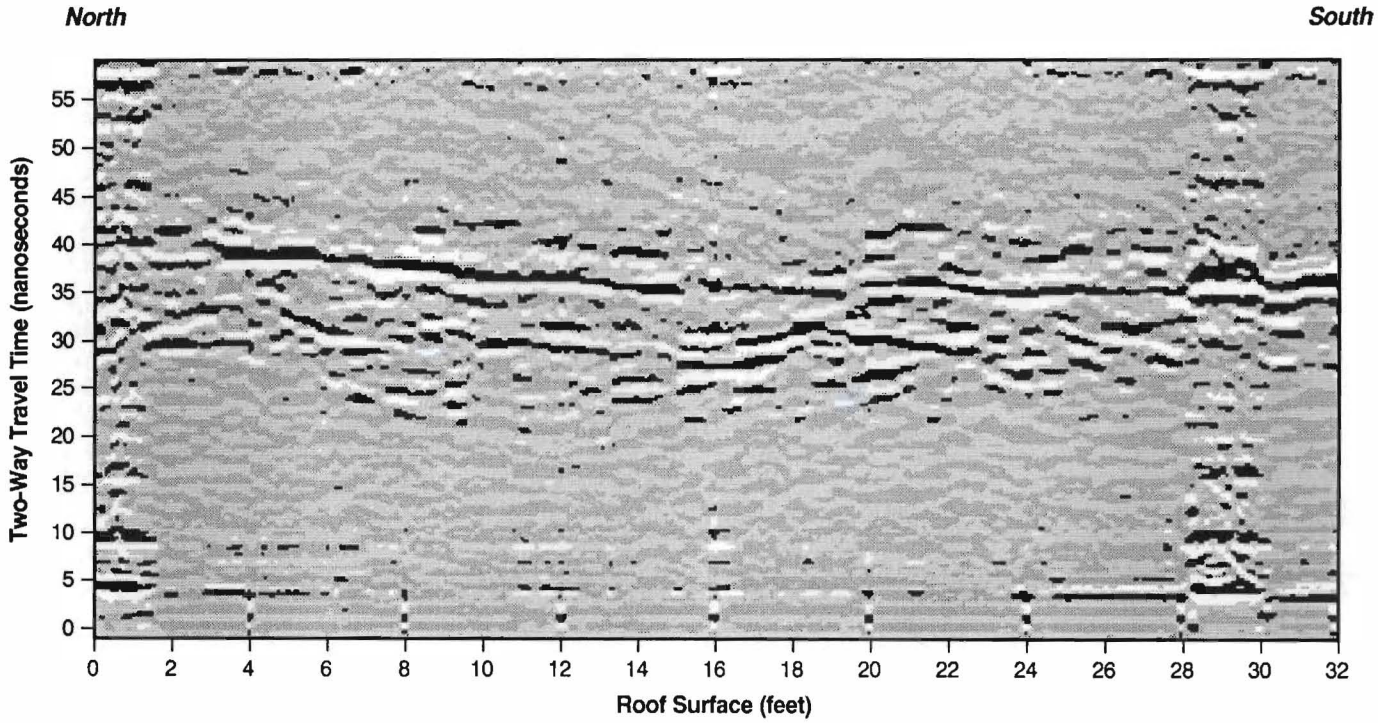

Figure D-2
E-0536 Traverse, S-1950 Drift Roof: February 1992

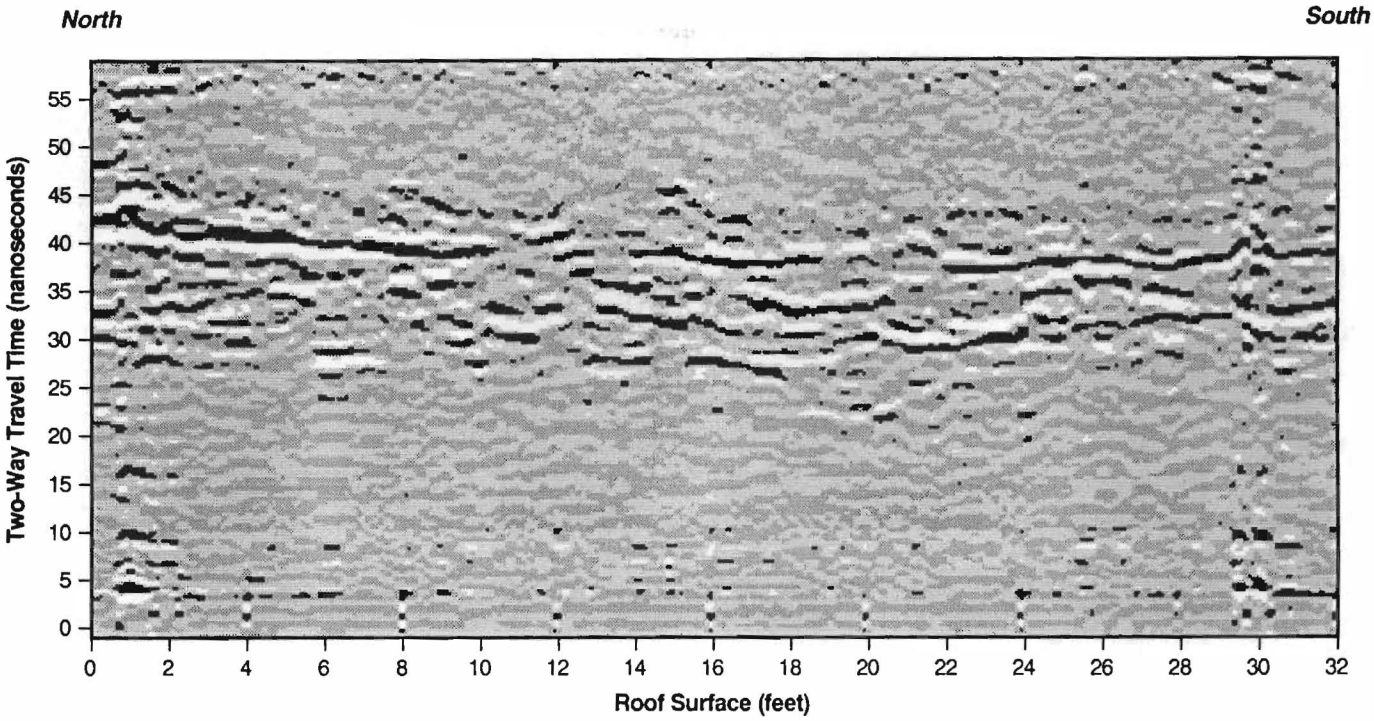

Figure D-3
E-0635 Traverse, S-1950 Drift Roof: February 1992

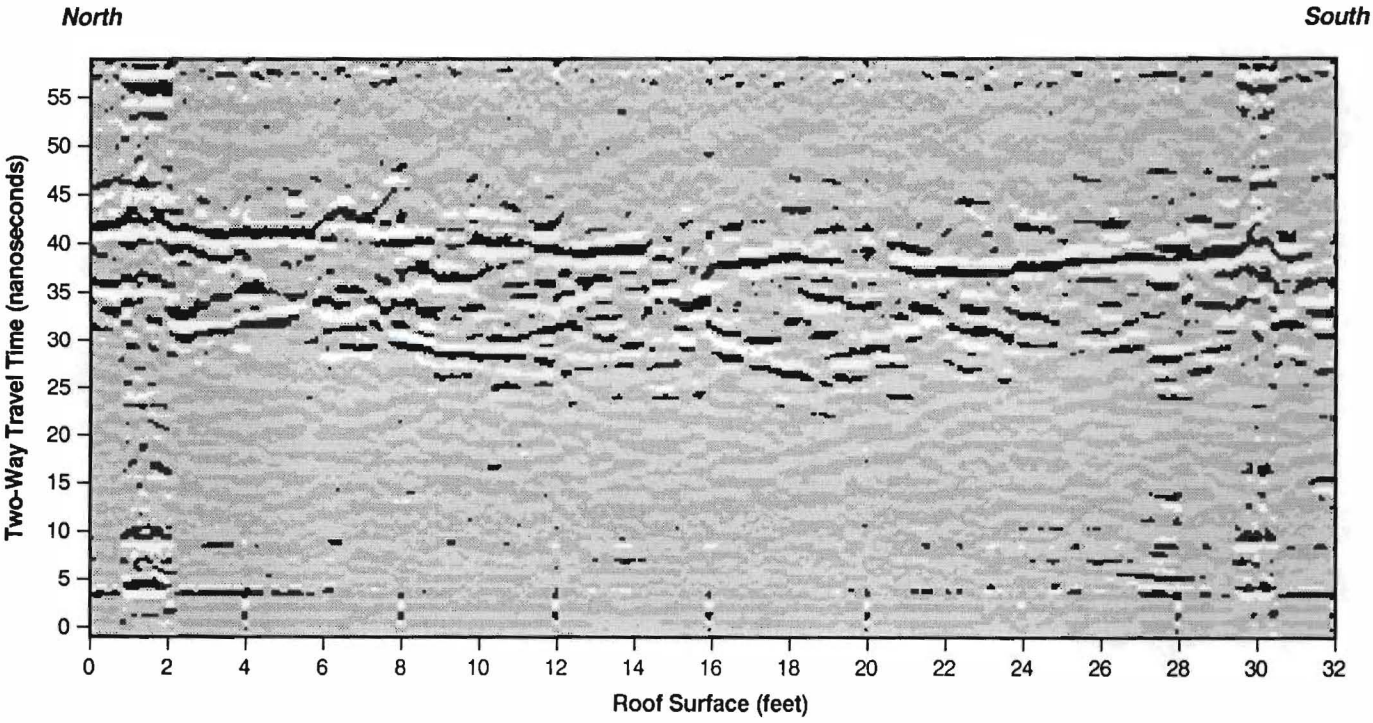

Figure D-4
E-0644 Traverse, S-1950 Drift Roof: February 1992

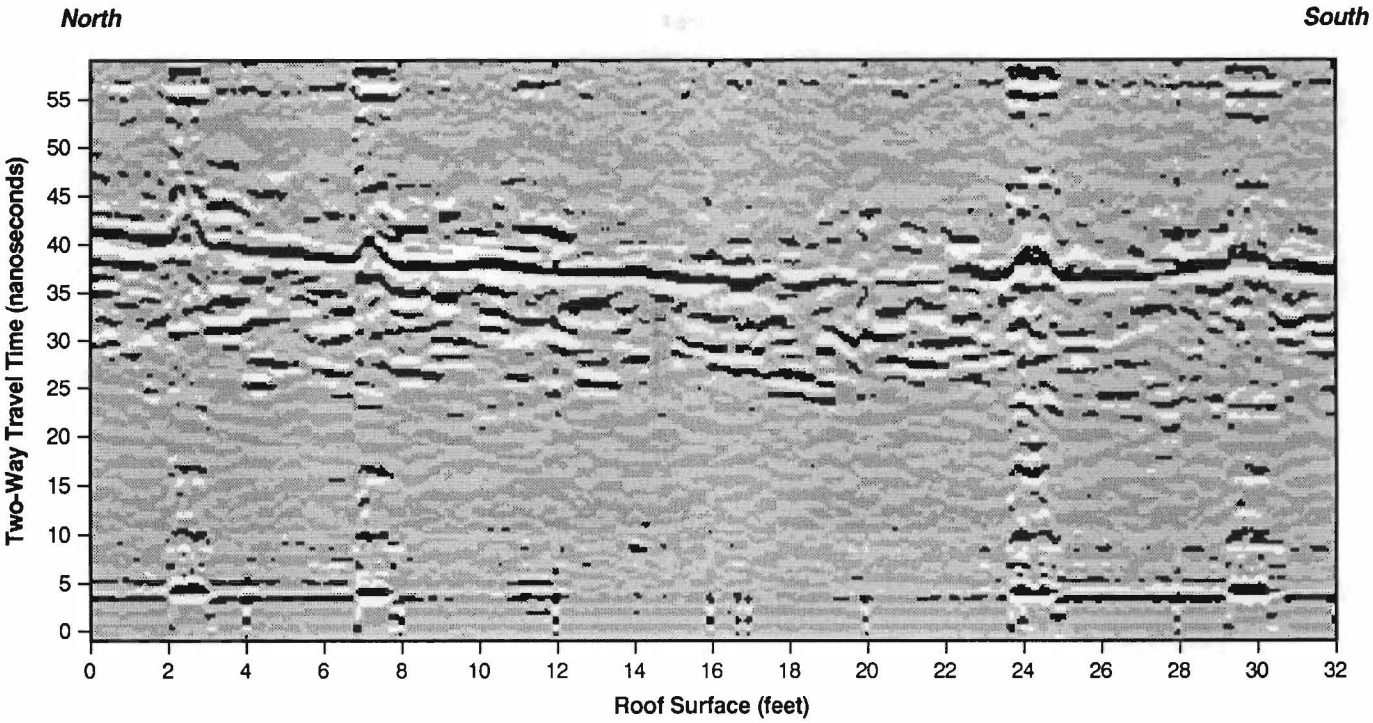

Figure D-5
E-0660 Traverse, S-1950 Drift Roof: February 1992

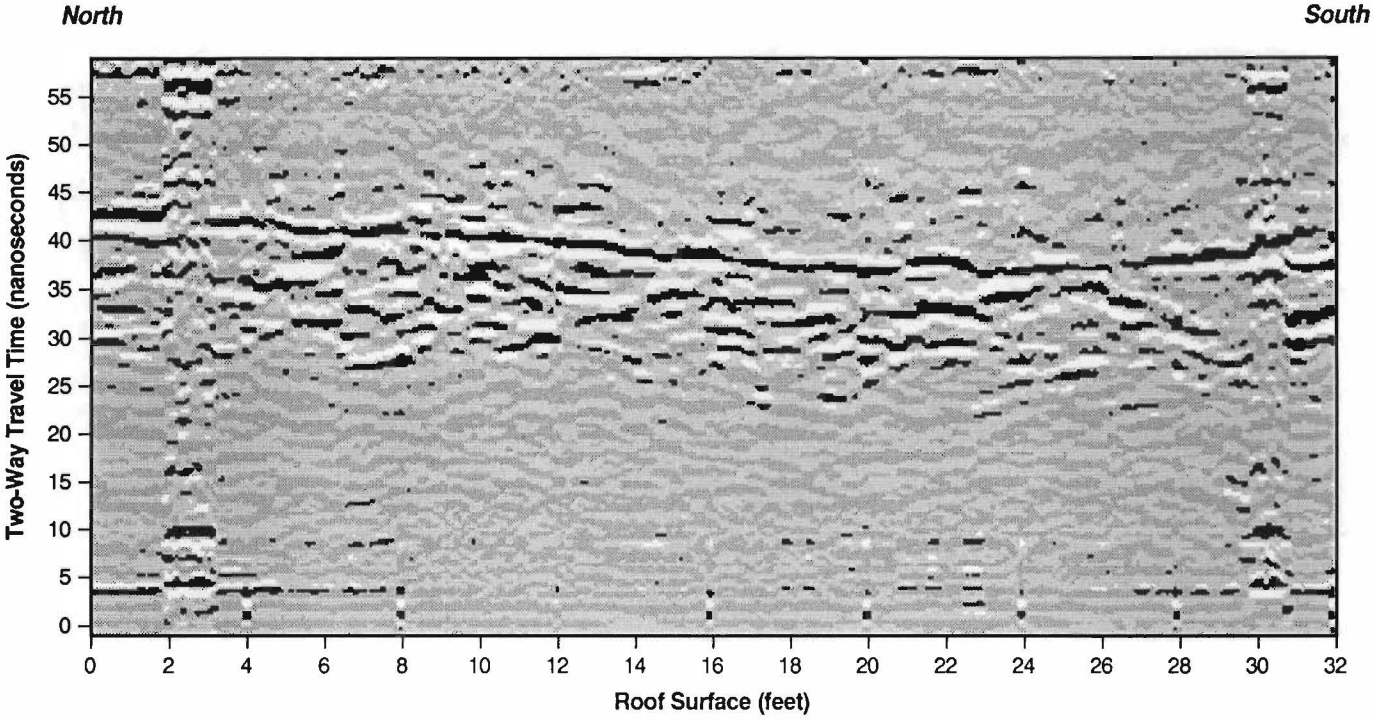

Figure D-6
E-0676 Traverse, S-1950 Drift Roof: February 1992

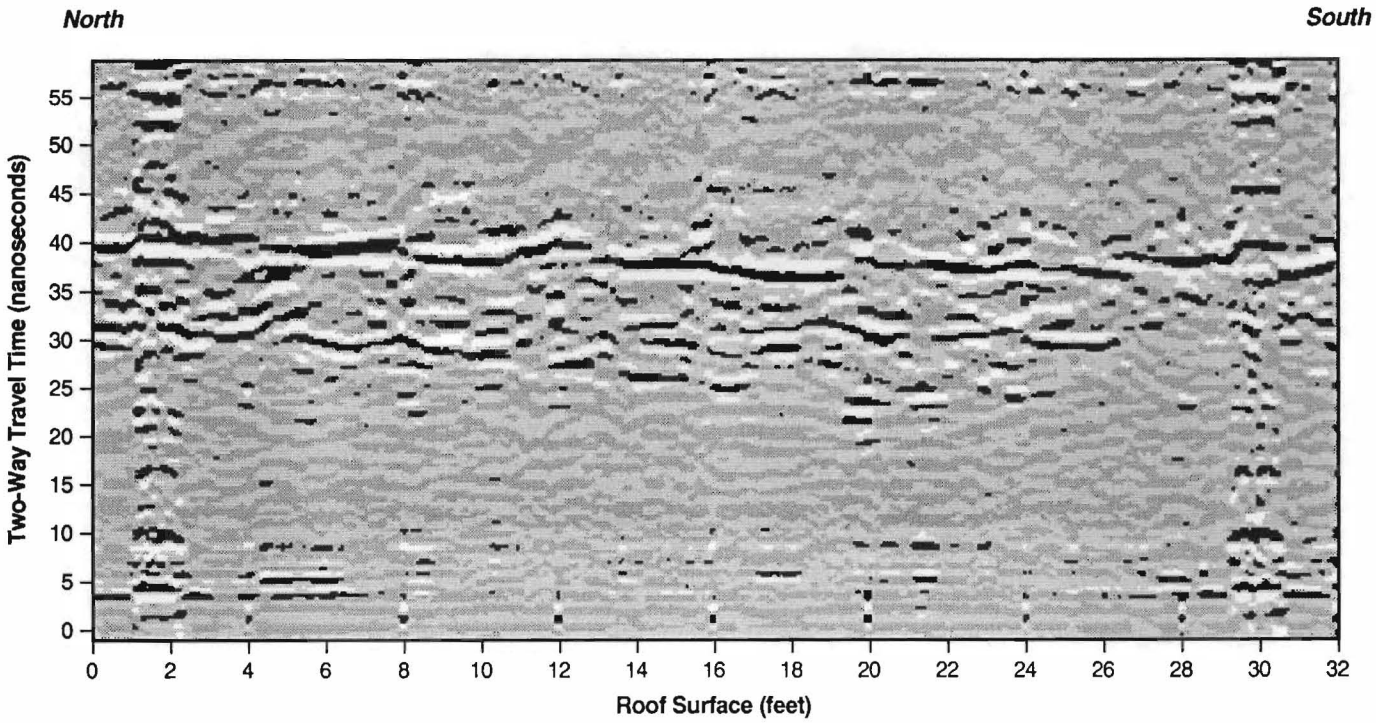

Figure D-7
E-0736 Traverse, S-1950 Drift Roof: February 1992

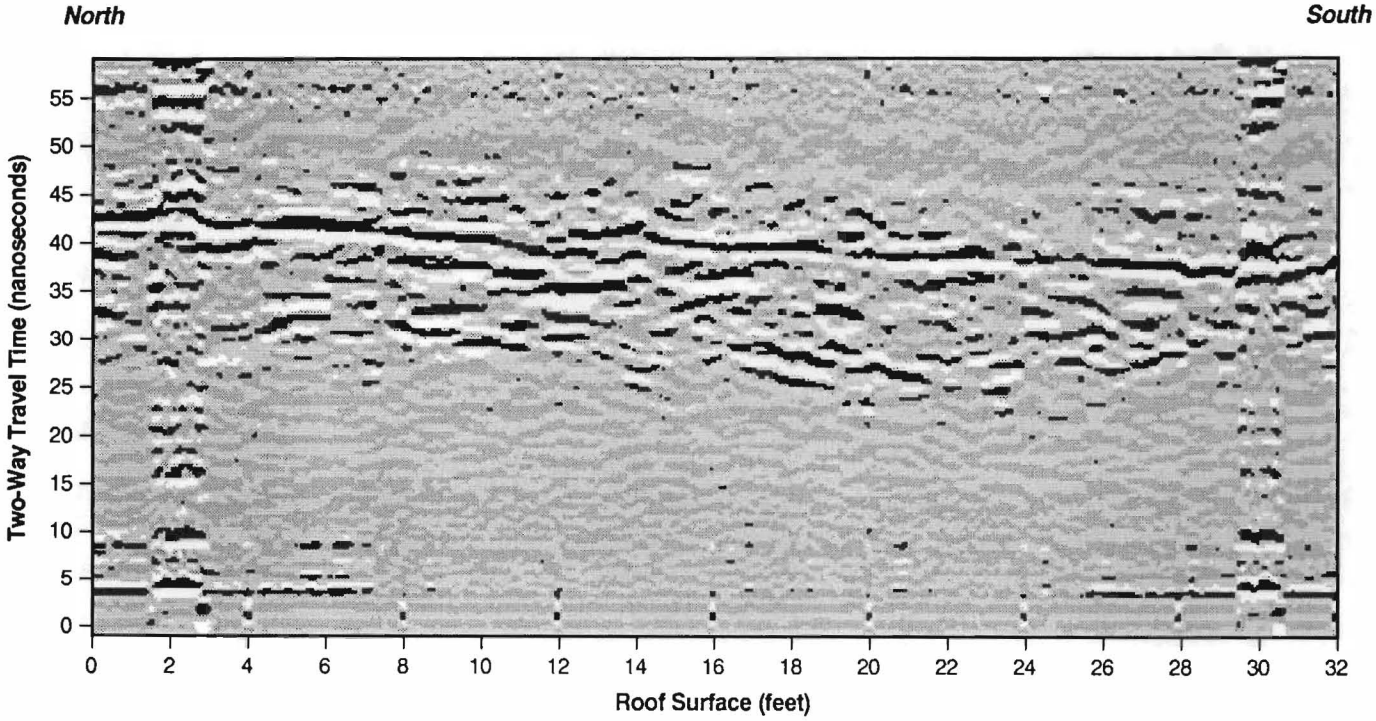

Figure D-8
E-0751 Traverse, S-1950 Drift Roof: February 1992

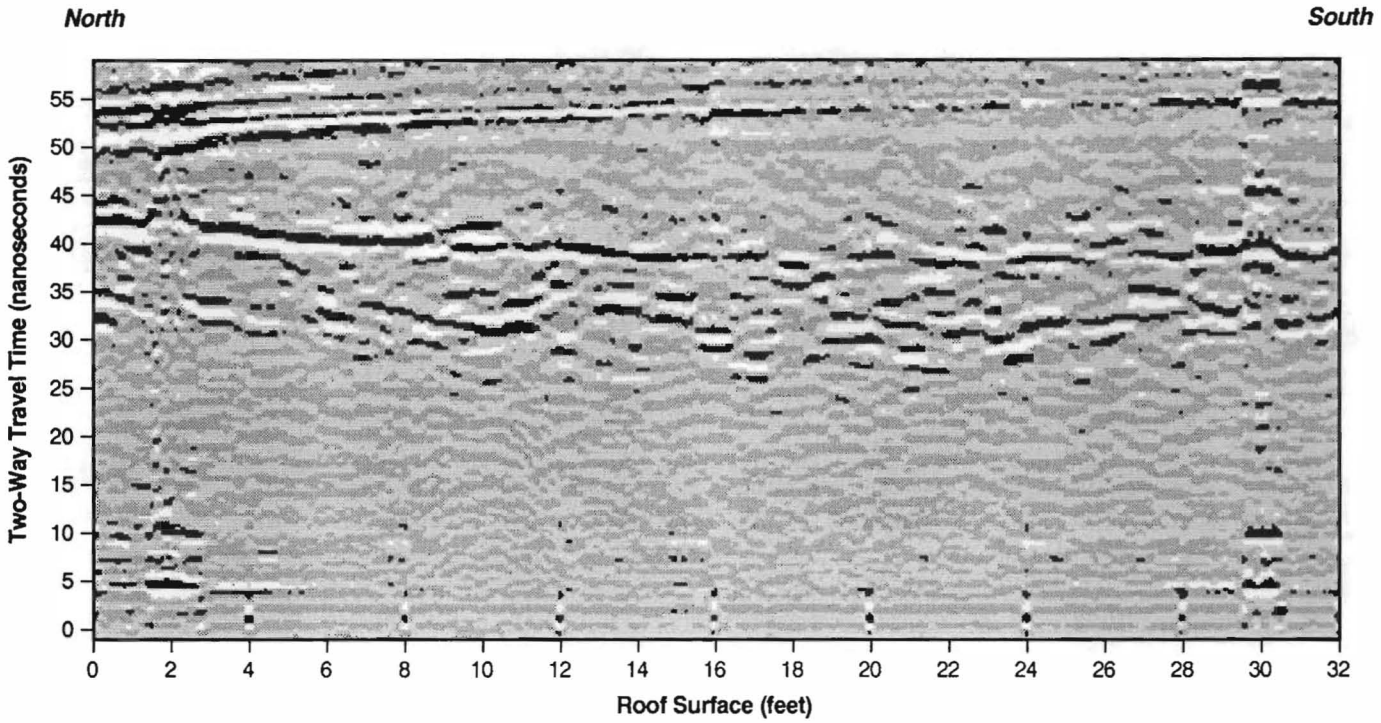

Figure D-9
E-0774 Traverse, S-1950 Drift Roof: February 1992

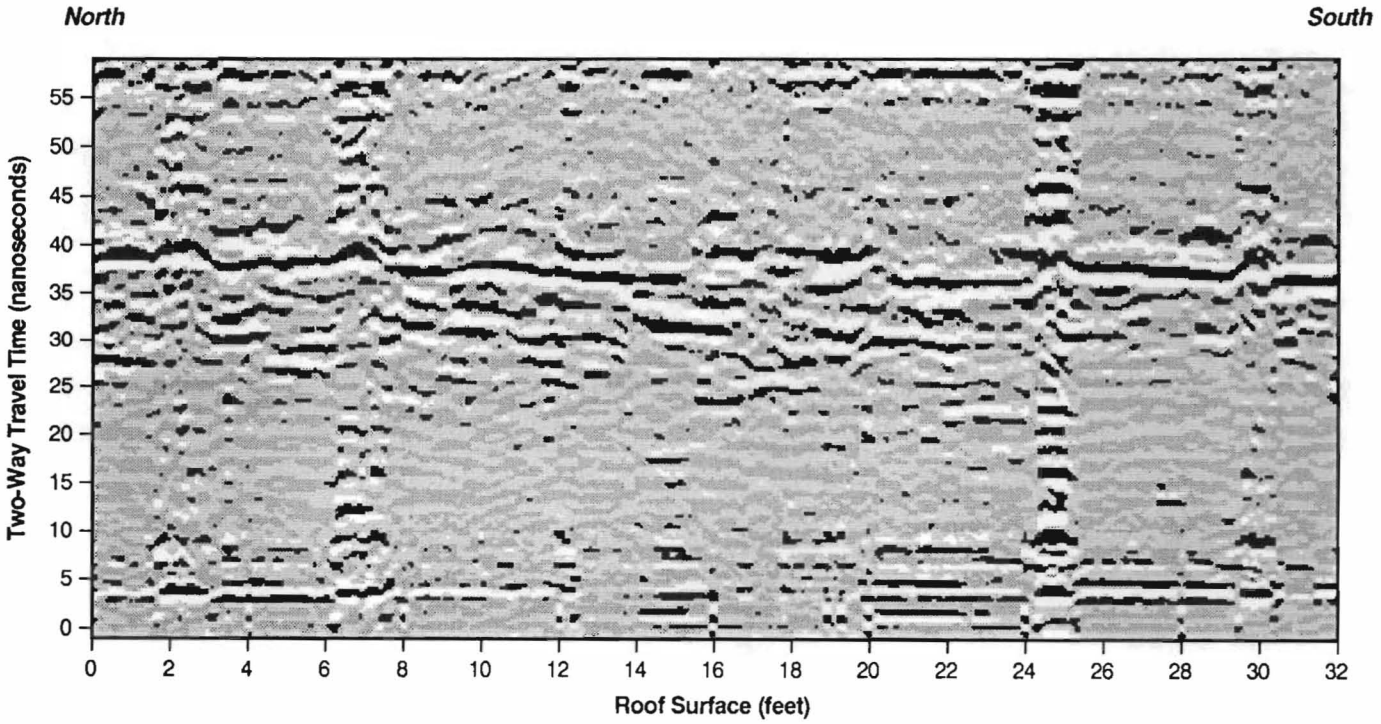

Figure D-10
E-0790 Traverse, S-1950 Drift Roof: February 1992

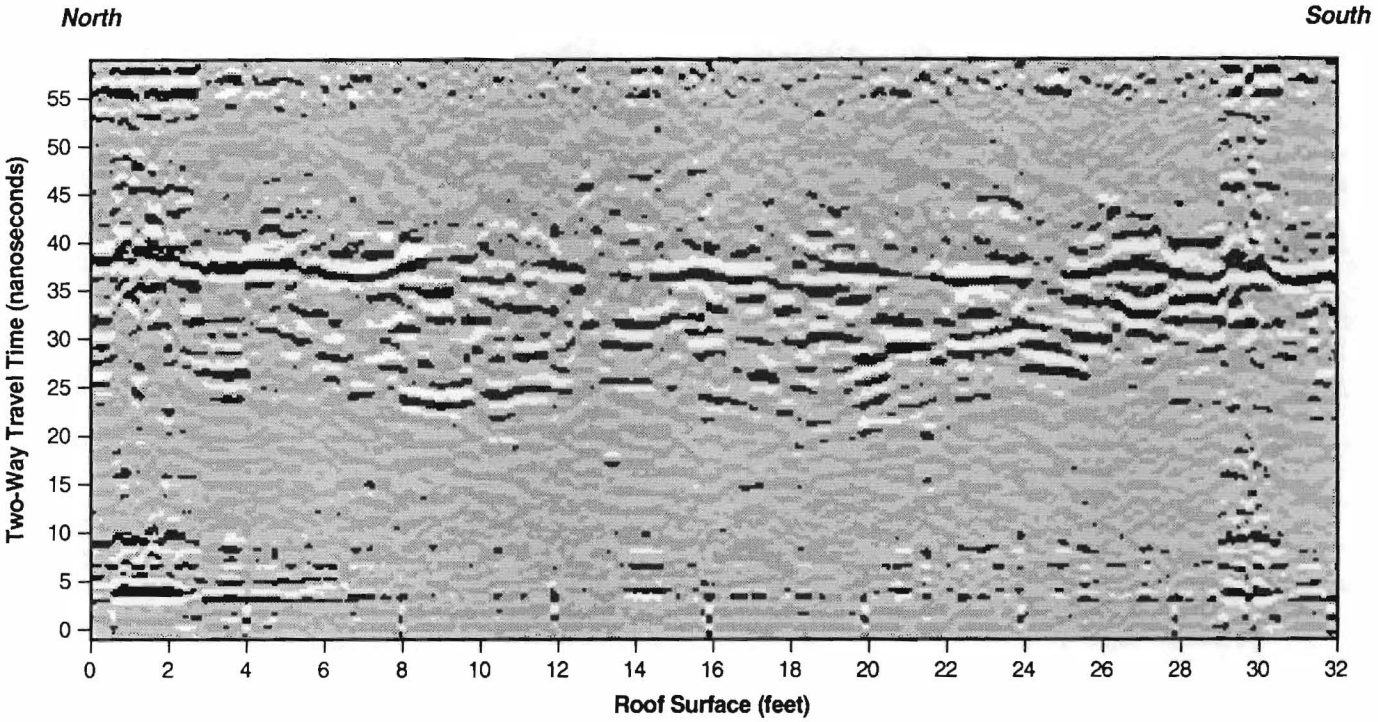

Figure D-11
E-0806 Traverse, S-1950 Drift Roof: February 1992

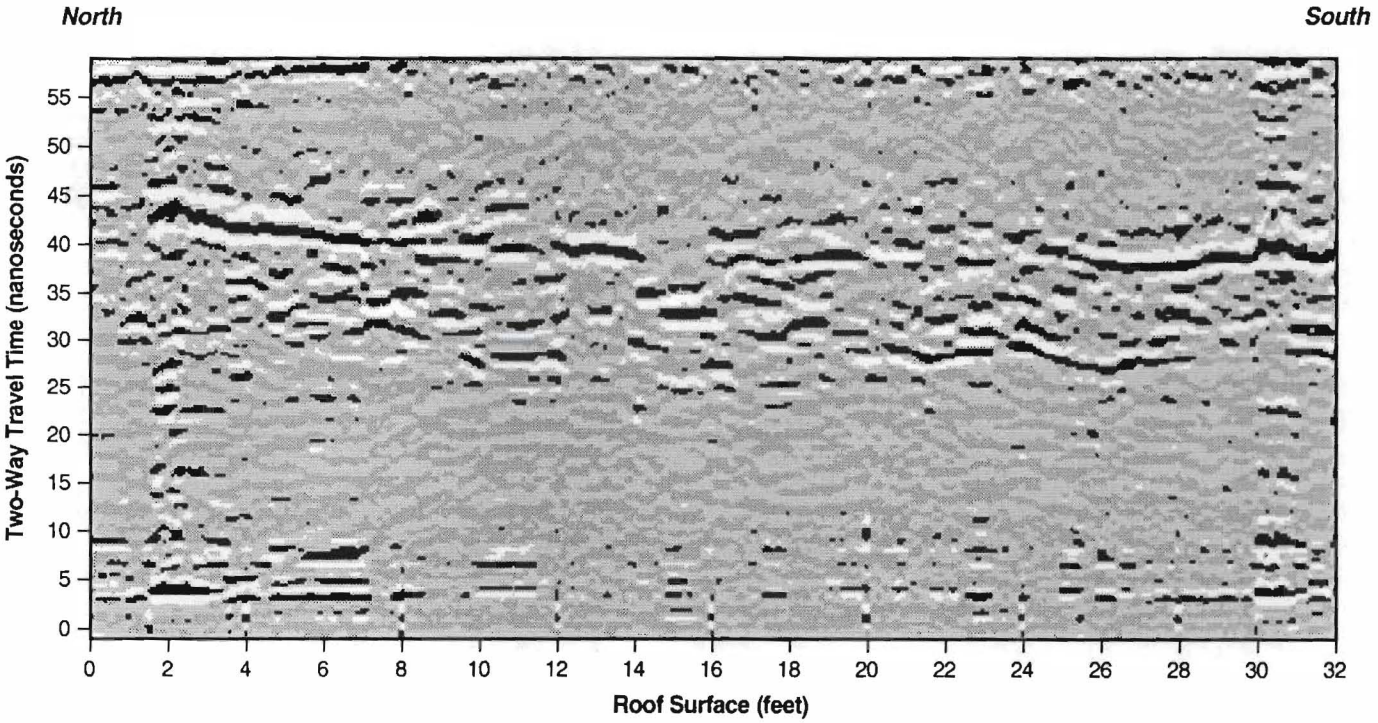

Figure D-12
E-0854 Traverse, S-1950 Drift Roof: February 1992

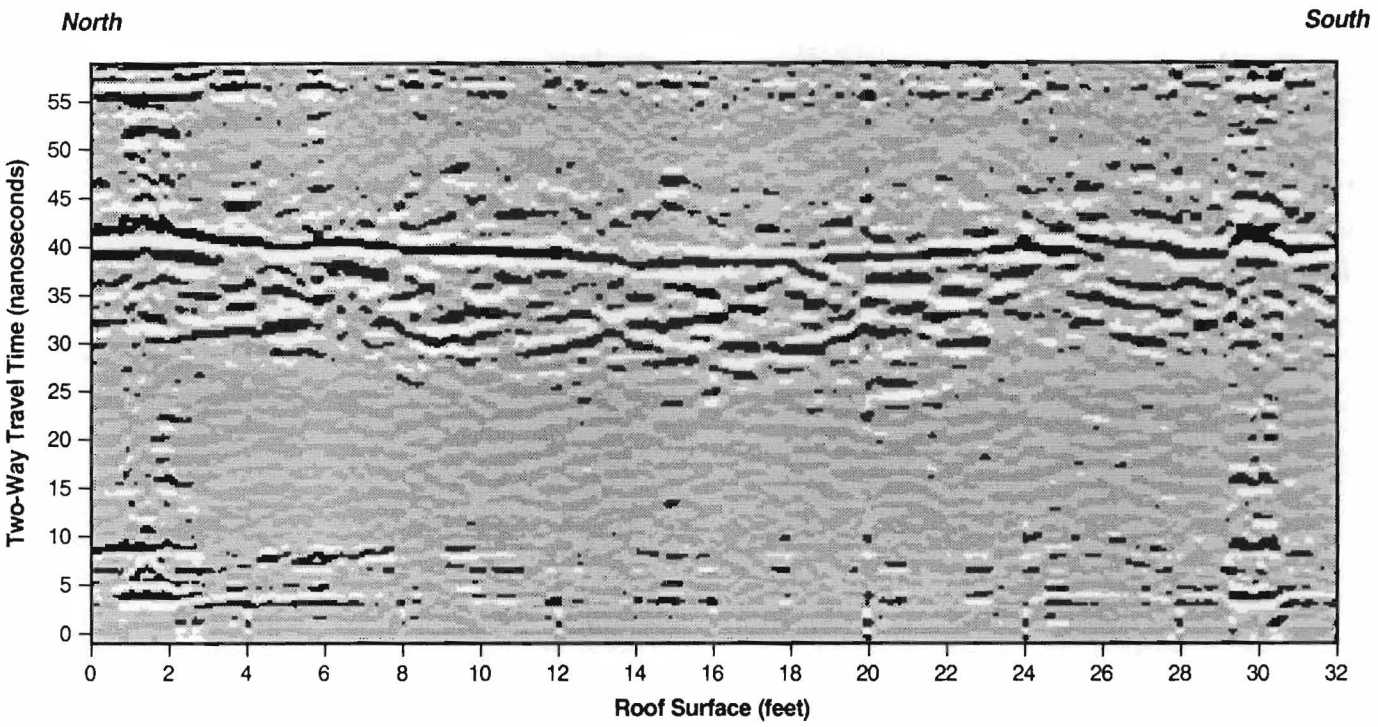

Figure D-13
E-0879 Traverse, S-1950 Drift Roof: February 1992

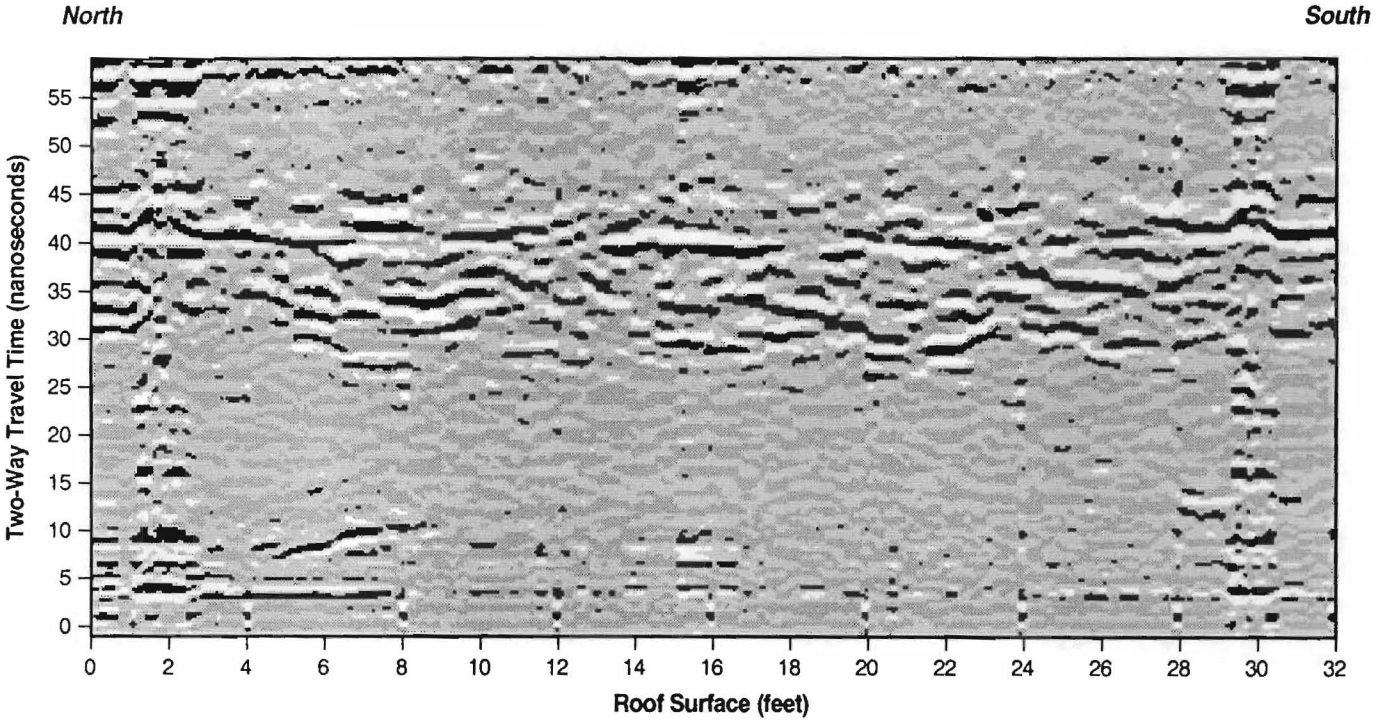

Figure D-14
E-0904 Traverse, S-1950 Drift Roof: February 1992

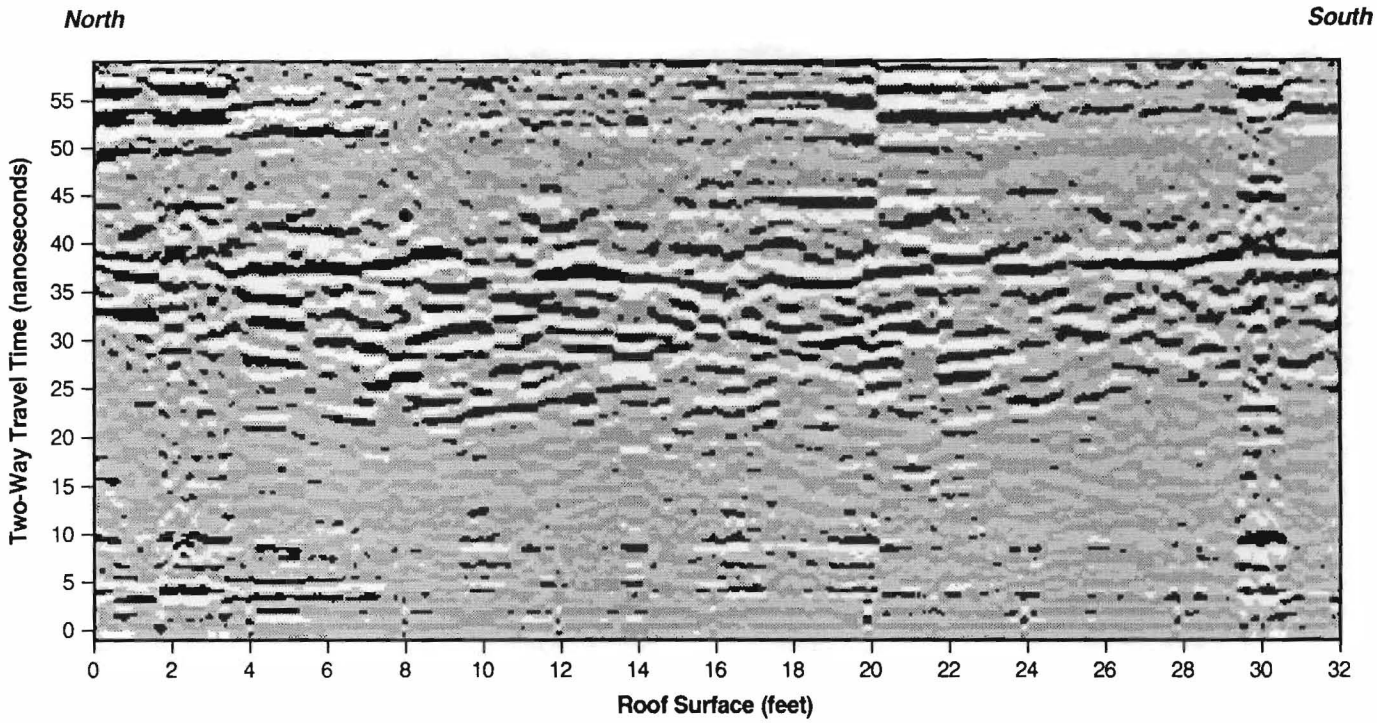

Figure D-15
E-0936 Traverse, S-1950 Drift Roof: February 1992

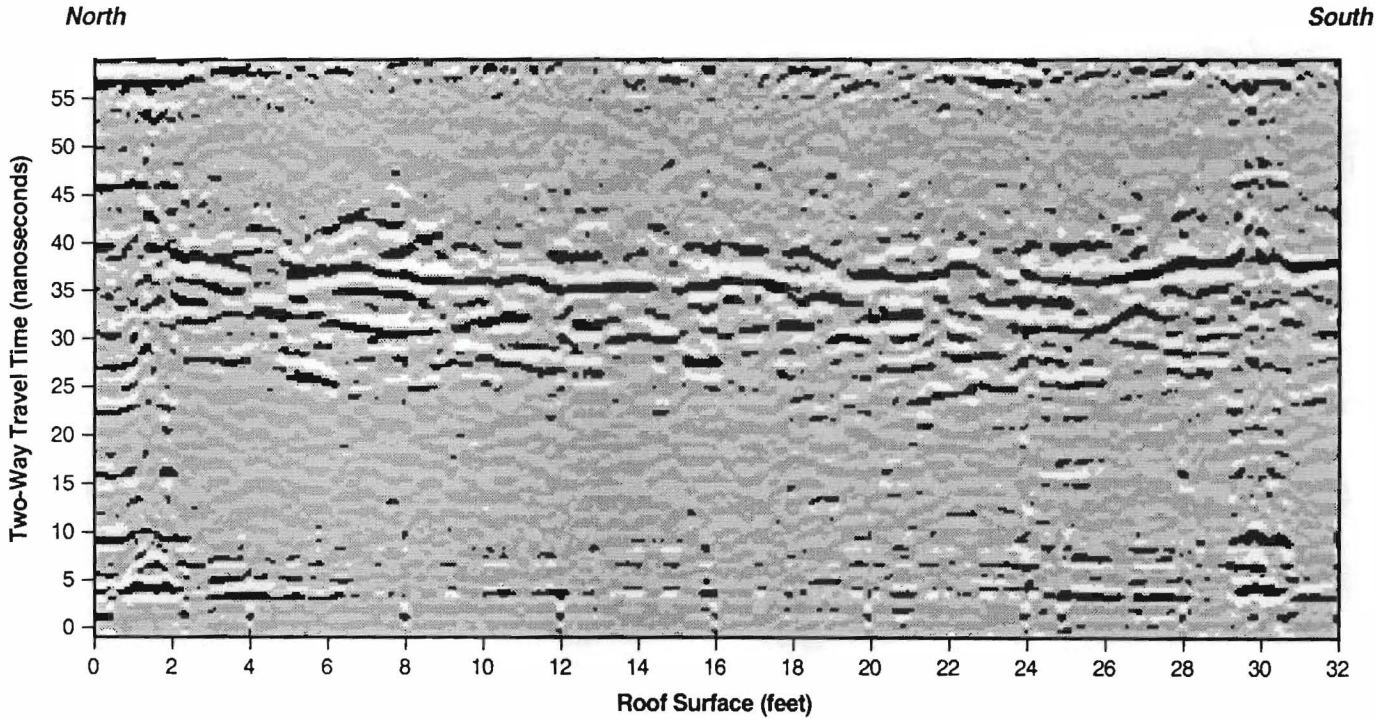

Figure D-16
E-0969 Traverse, S-1950 Drift Roof: February 1992

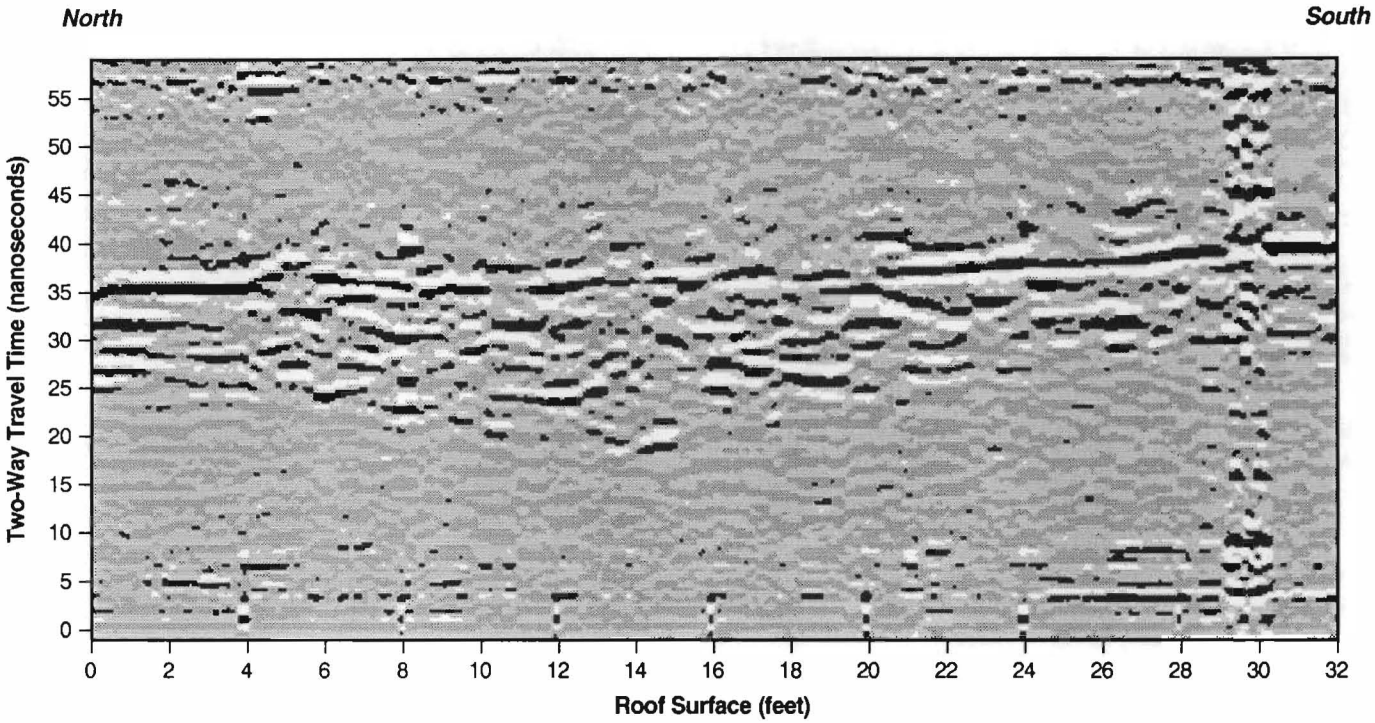

Figure D-17
E-0994 Traverse, S-1950 Drift Roof: February 1992

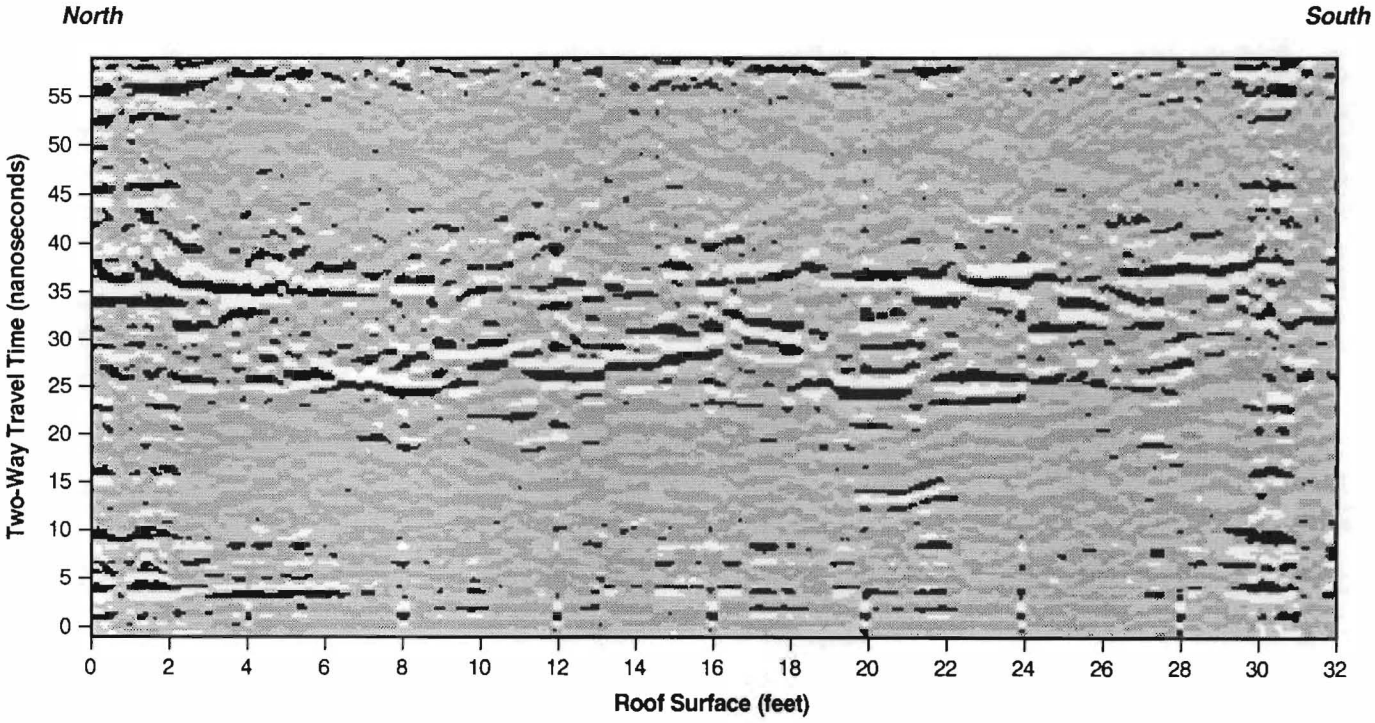

Figure D-18
E-1019 Traverse, S-1950 Drift Roof: February 1992

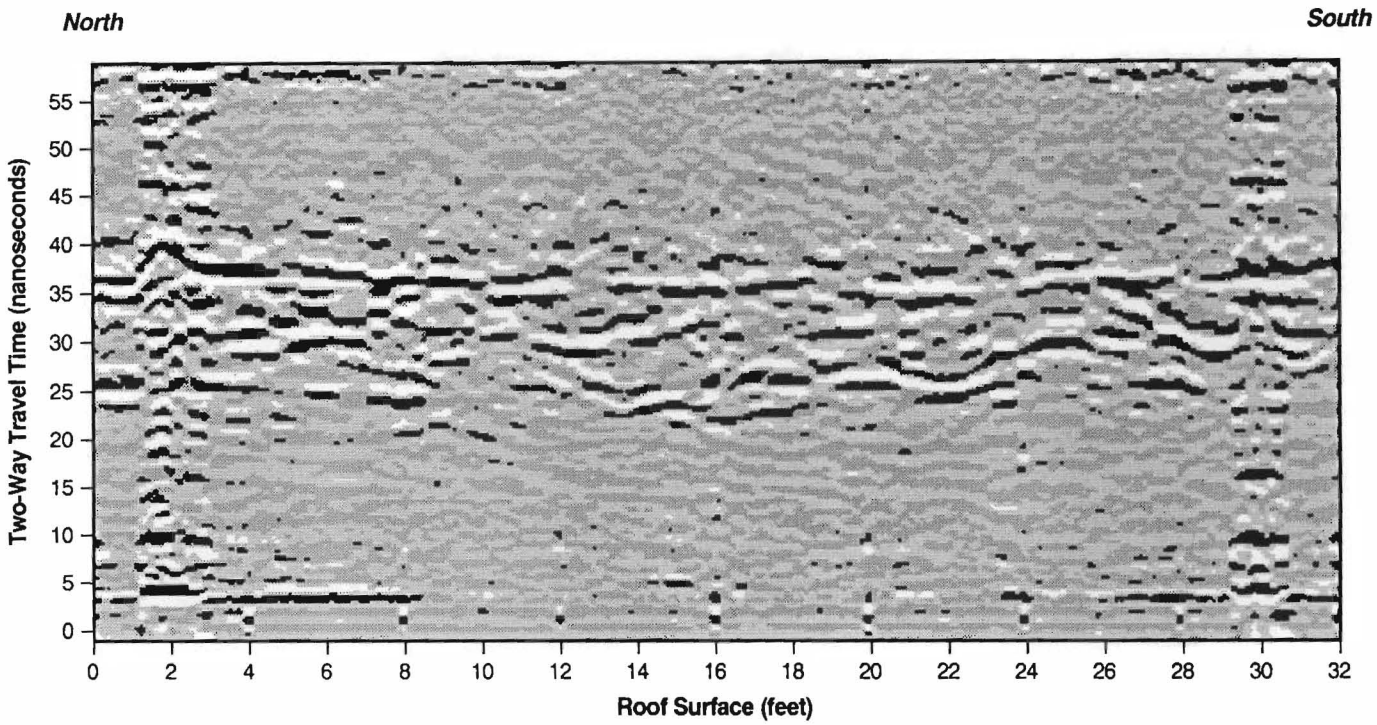

Figure D-19
E-1044 Traverse, S-1950 Drift Roof: February 1992

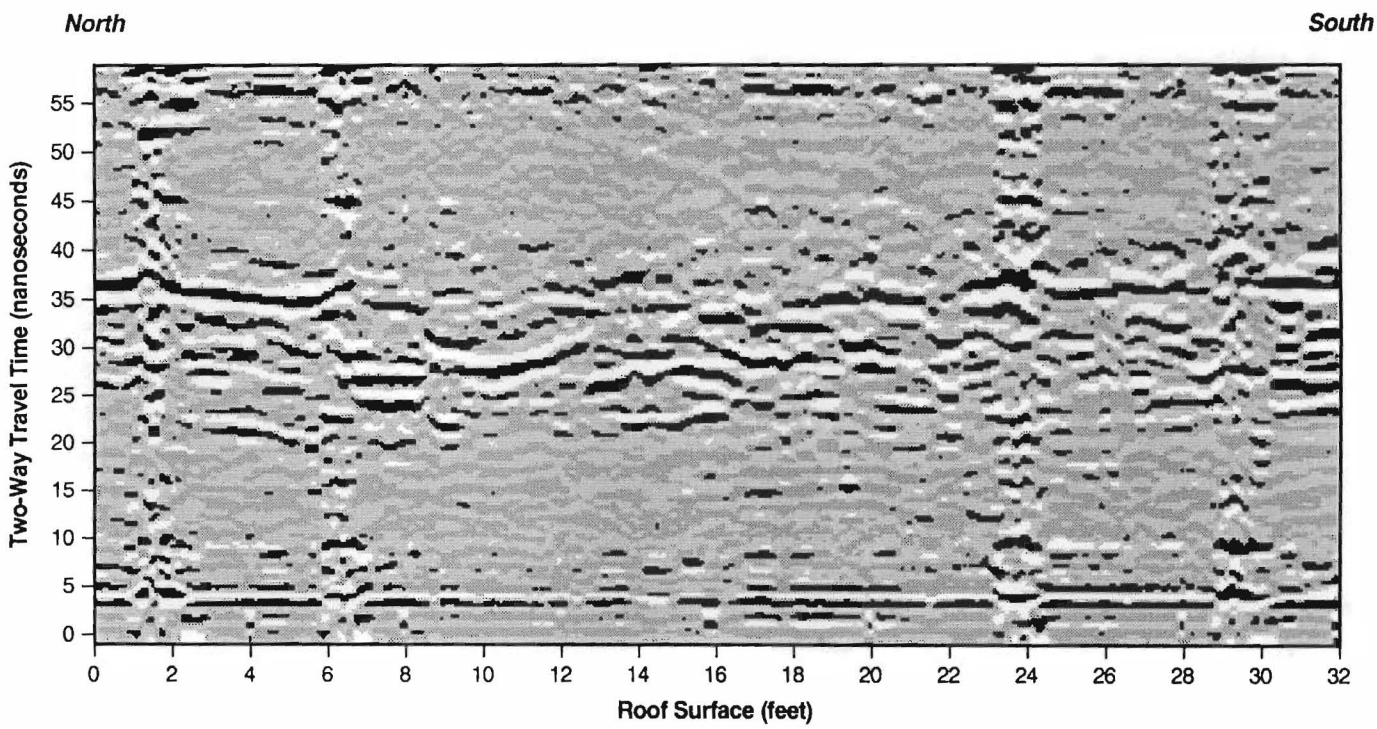

Figure D-20
E-1060 Traverse, S-1950 Drift Roof: February 1992

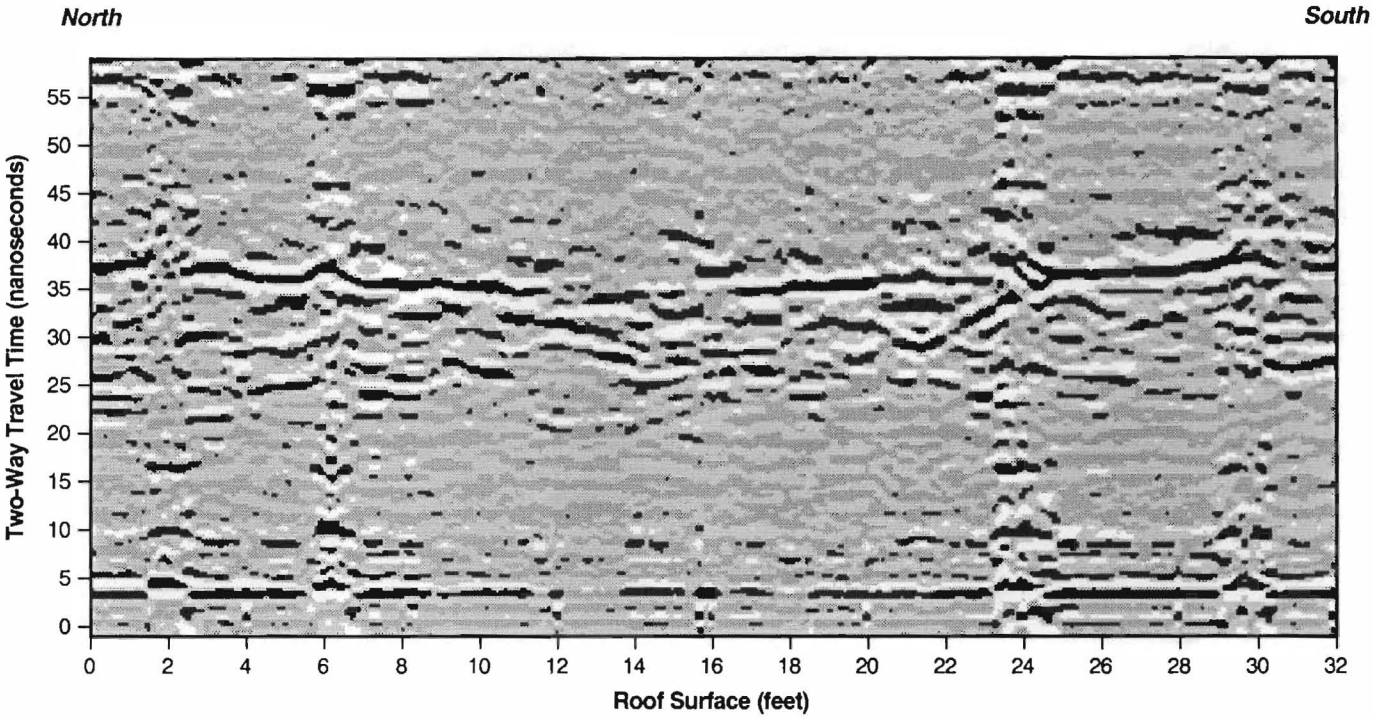

Figure D-21
E-1062 Traverse, S-1950 Drift Roof: February 1992

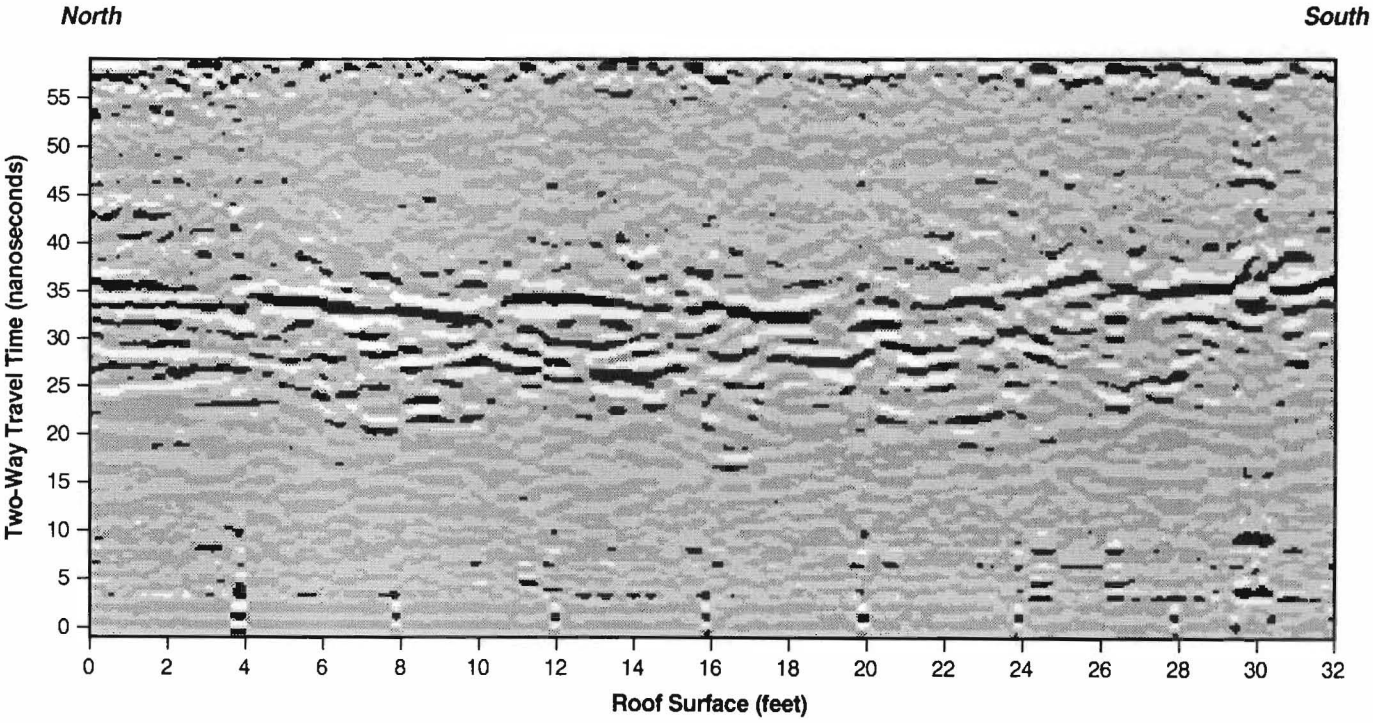

Figure D-22
E-1096 Traverse, S-1950 Drift Roof: February 1992

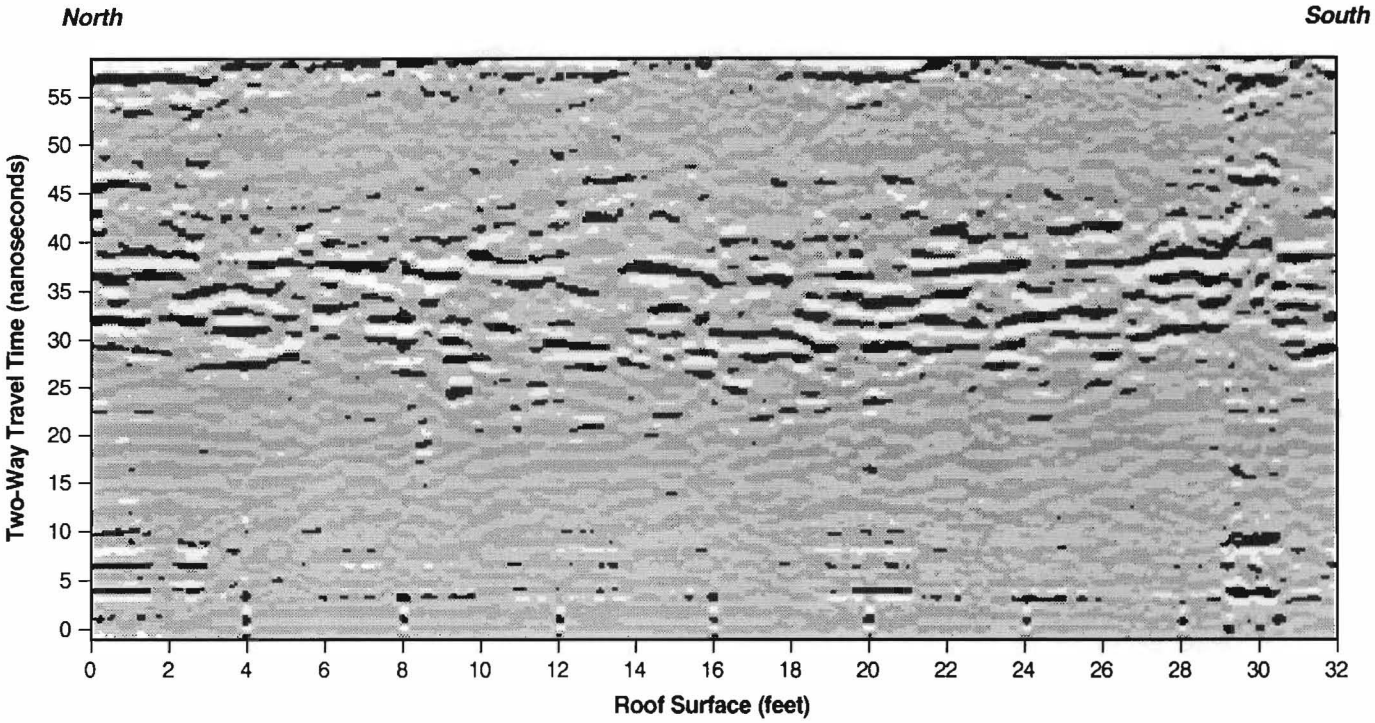

Figure D-23
E-1124 Traverse, S-1950 Drift Roof: February 1992

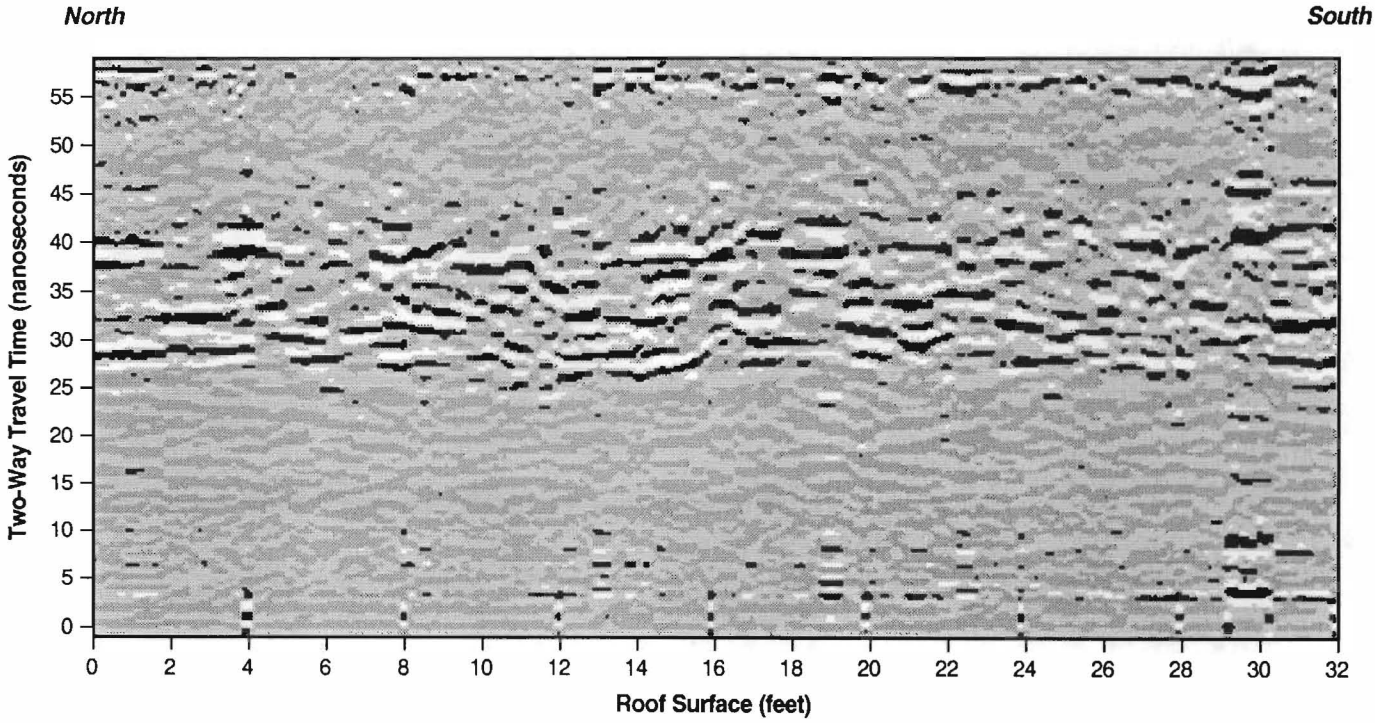

Figure D-24
E-1149 Traverse, S-1950 Drift Roof: February 1992

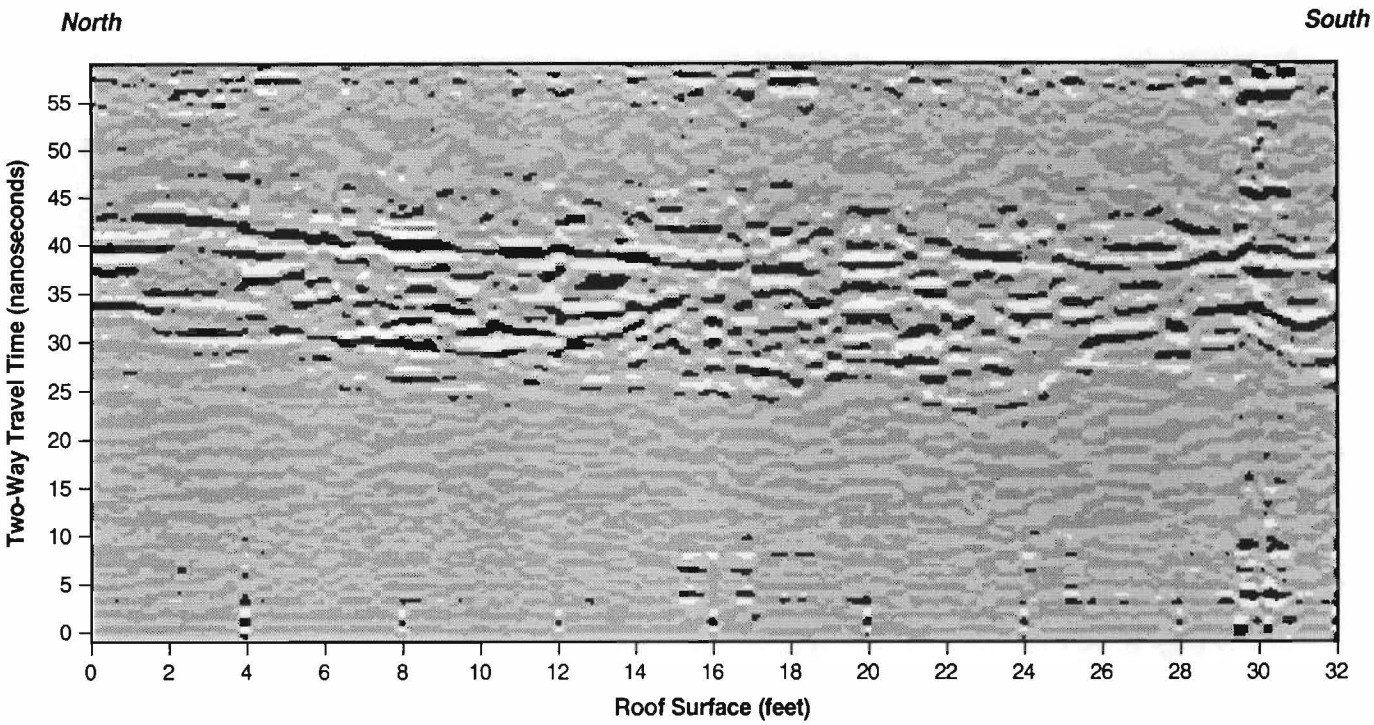

Figure D-25
E-1174 Traverse, S-1950 Drift Roof: February 1992

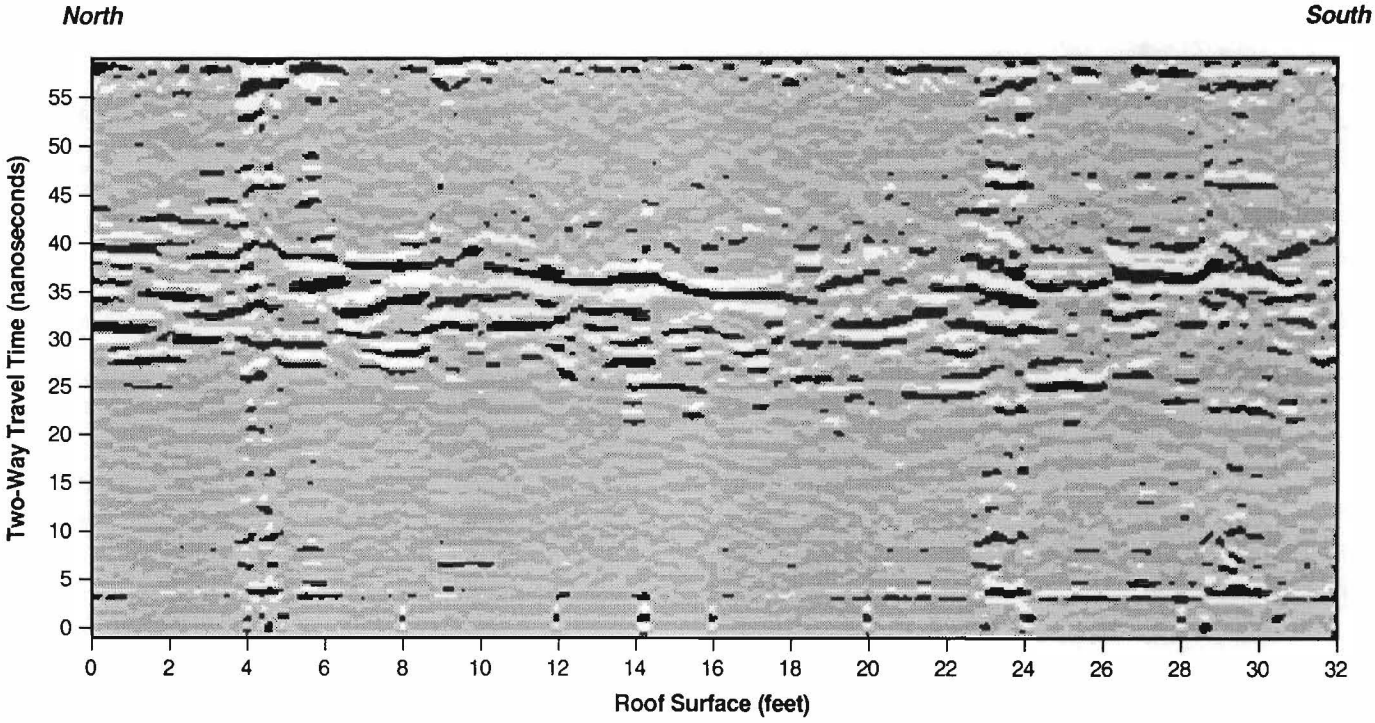

Figure D-26
E-1190 Traverse, S-1950 Drift Roof: February 1992

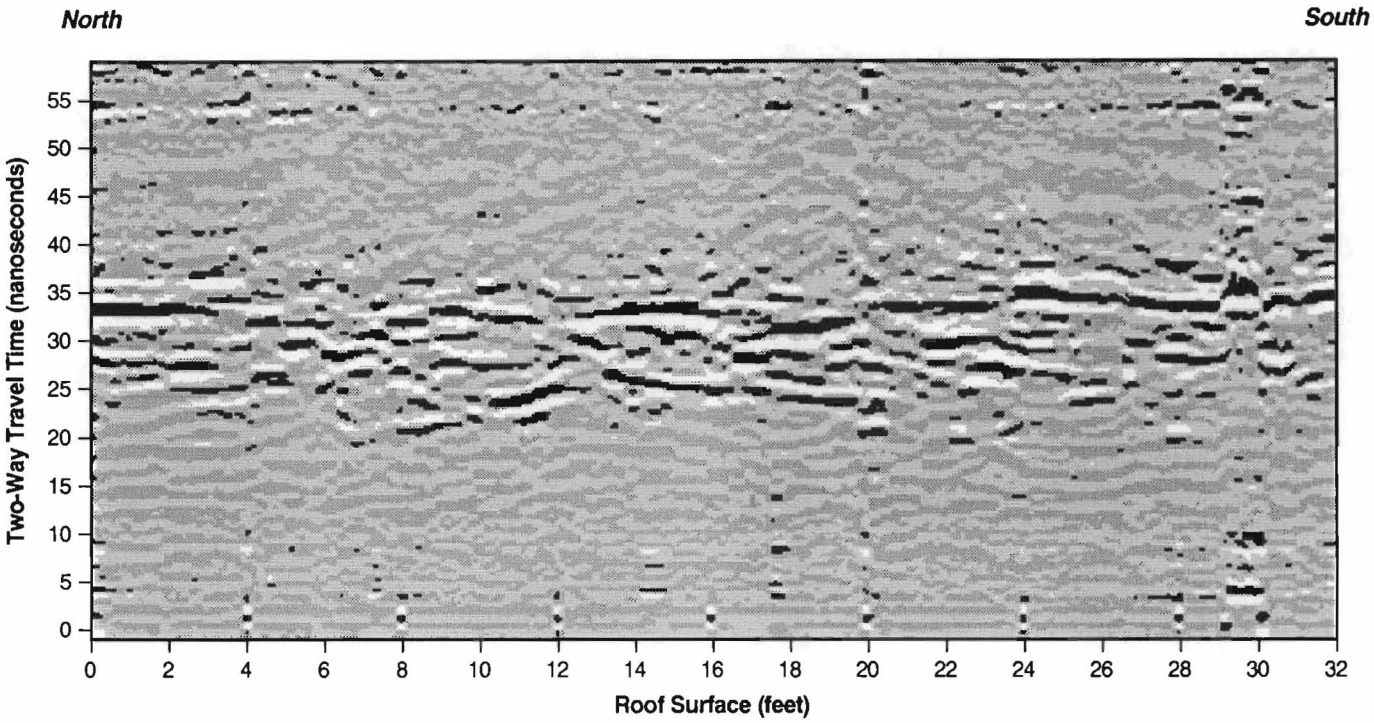

Figure D-27
E-1229 Traverse, S-1950 Drift Roof: February 1992

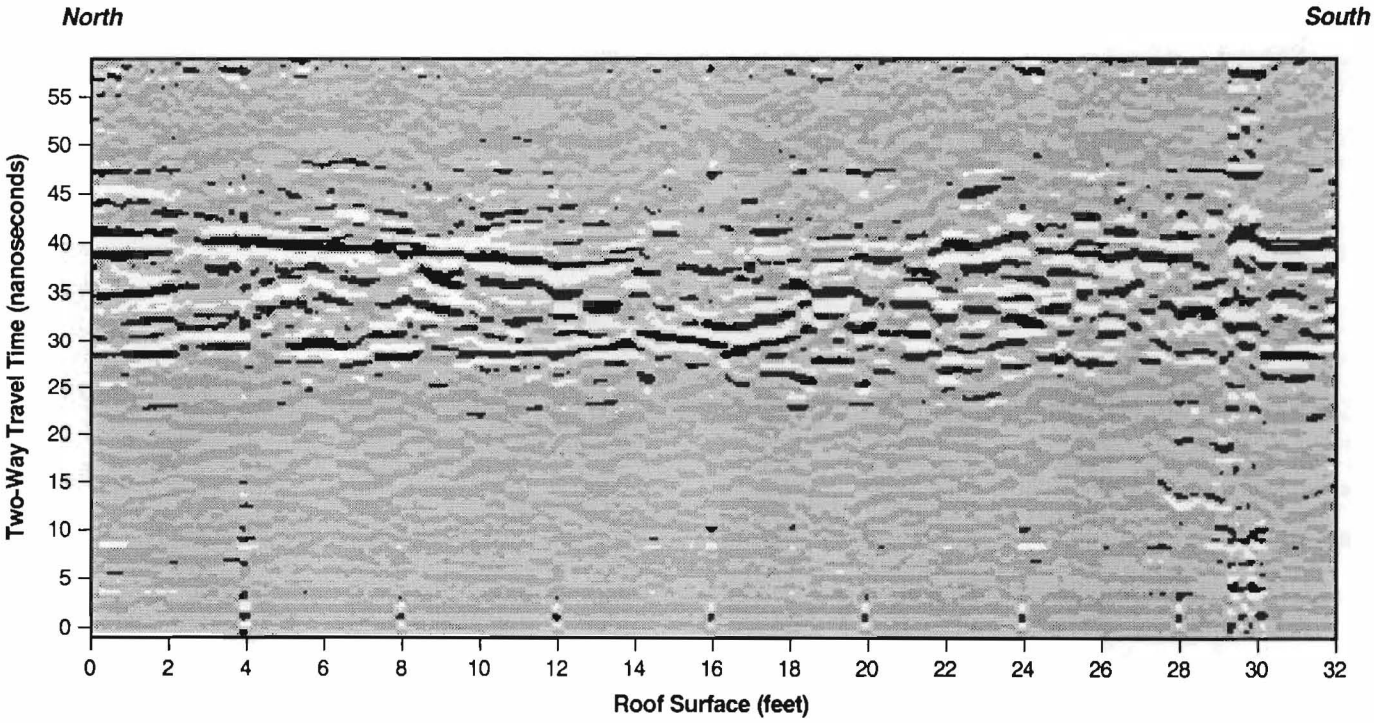

Figure D-28
E-1254 Traverse, S-1950 Drift Roof: February 1992

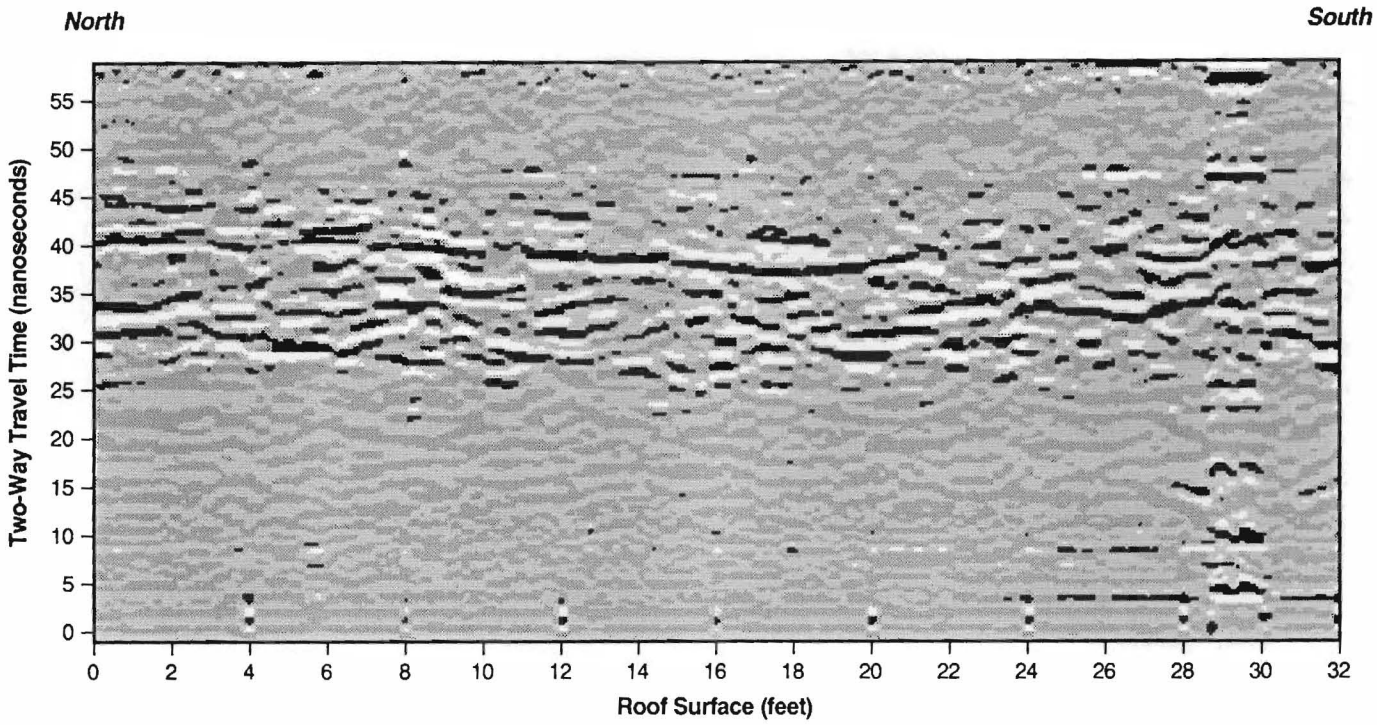

Figure D-29
E-1284 Traverse, S-1950 Drift Roof: February 1992

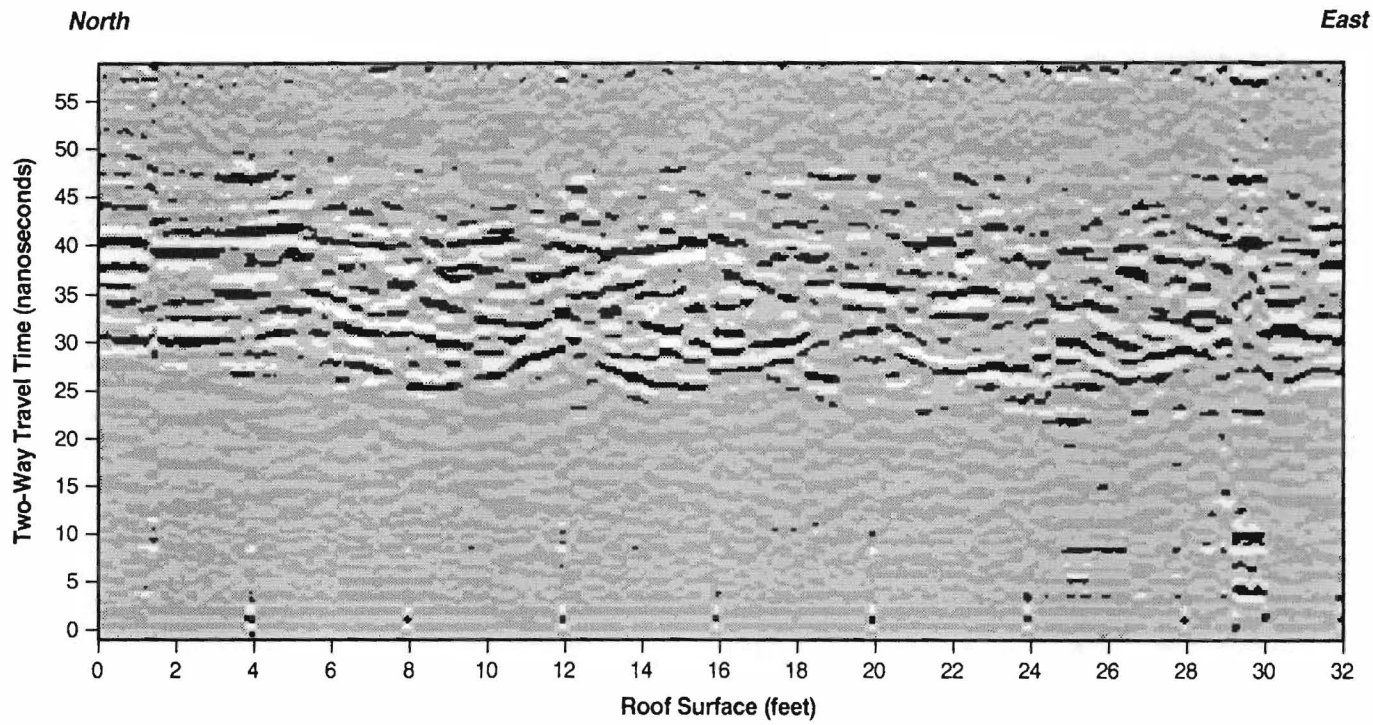

Figure D-30
E-1304 Traverse, S-1950 Drift Roof: February 1992

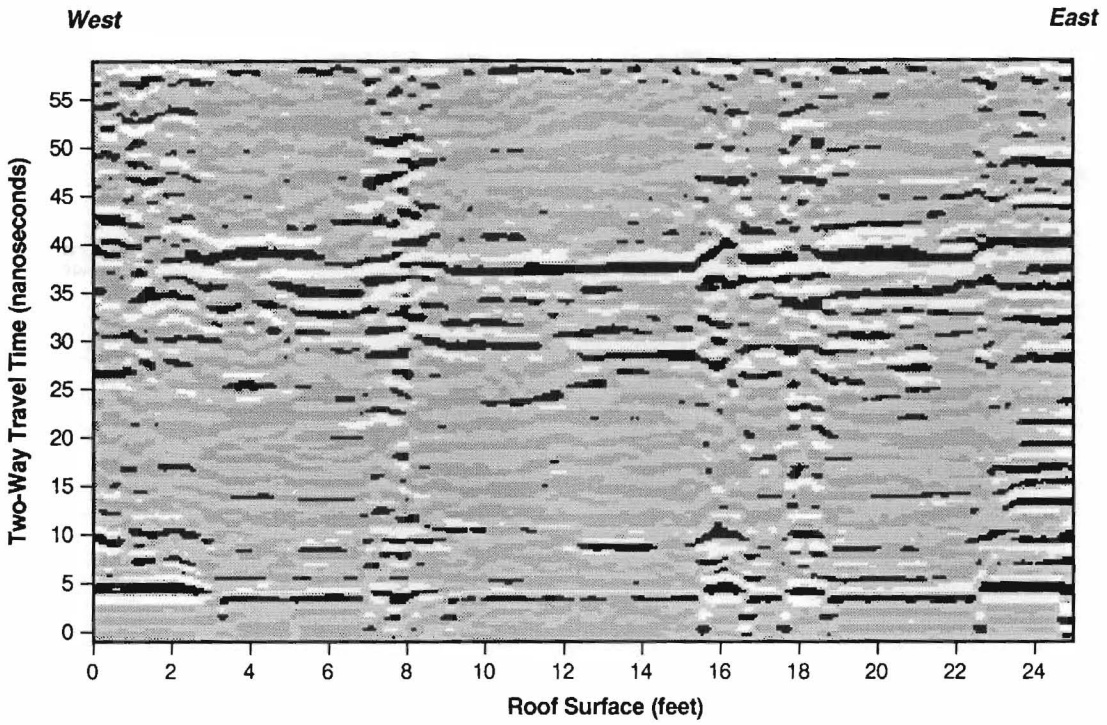

Figure D-31
Traverse A, S-1950 Drift Roof: February 1992

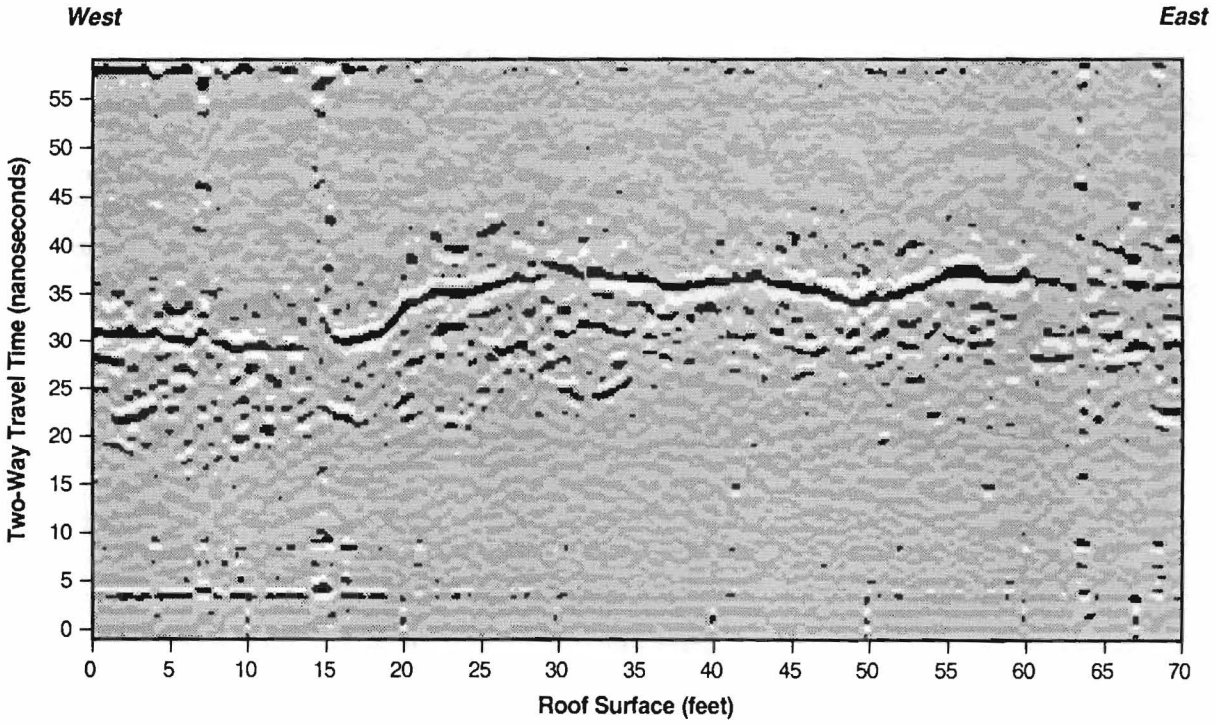

Figure D-32
Traverse B, E-0520 to E-0660 S-1950 Drift Roof: February 1992
Vertical Exaggeration 2.5x

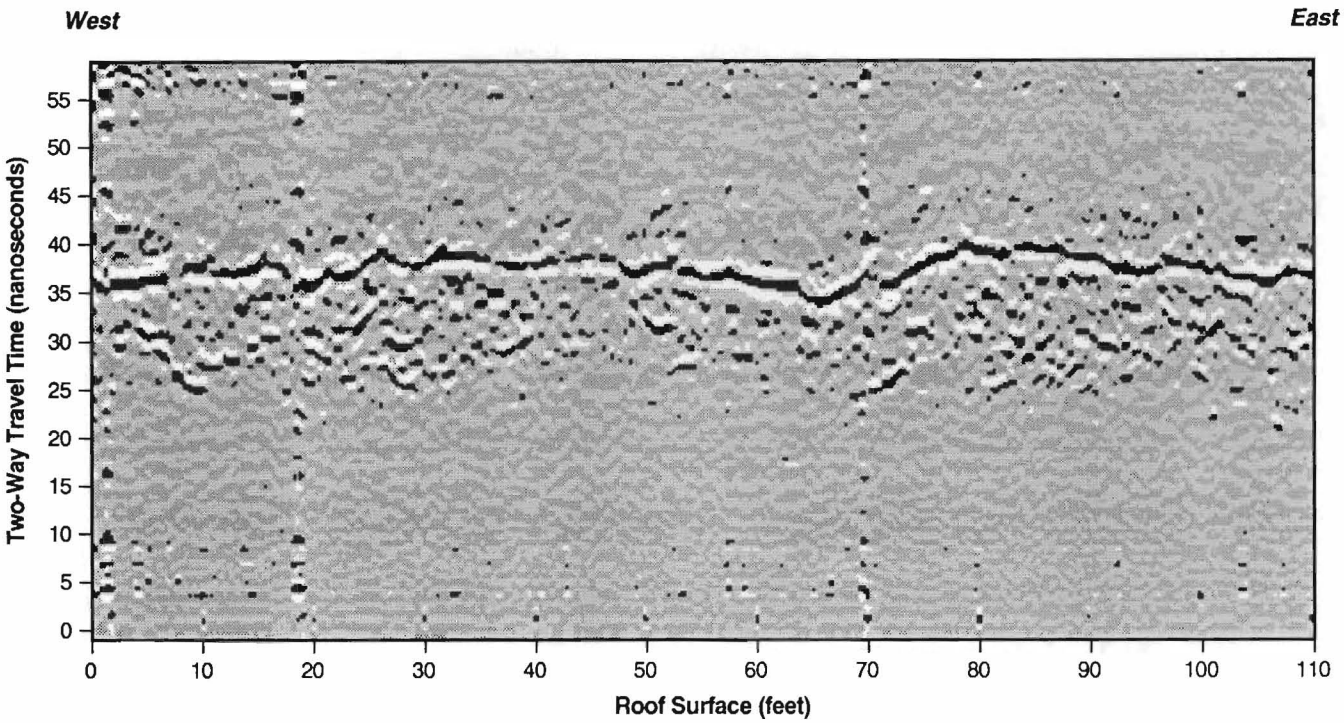

Figure D-33
Traverse C, E-0660 to E-0790, S-1950 Drift Roof: February 1992
Vertical Exaggeration 3.5x

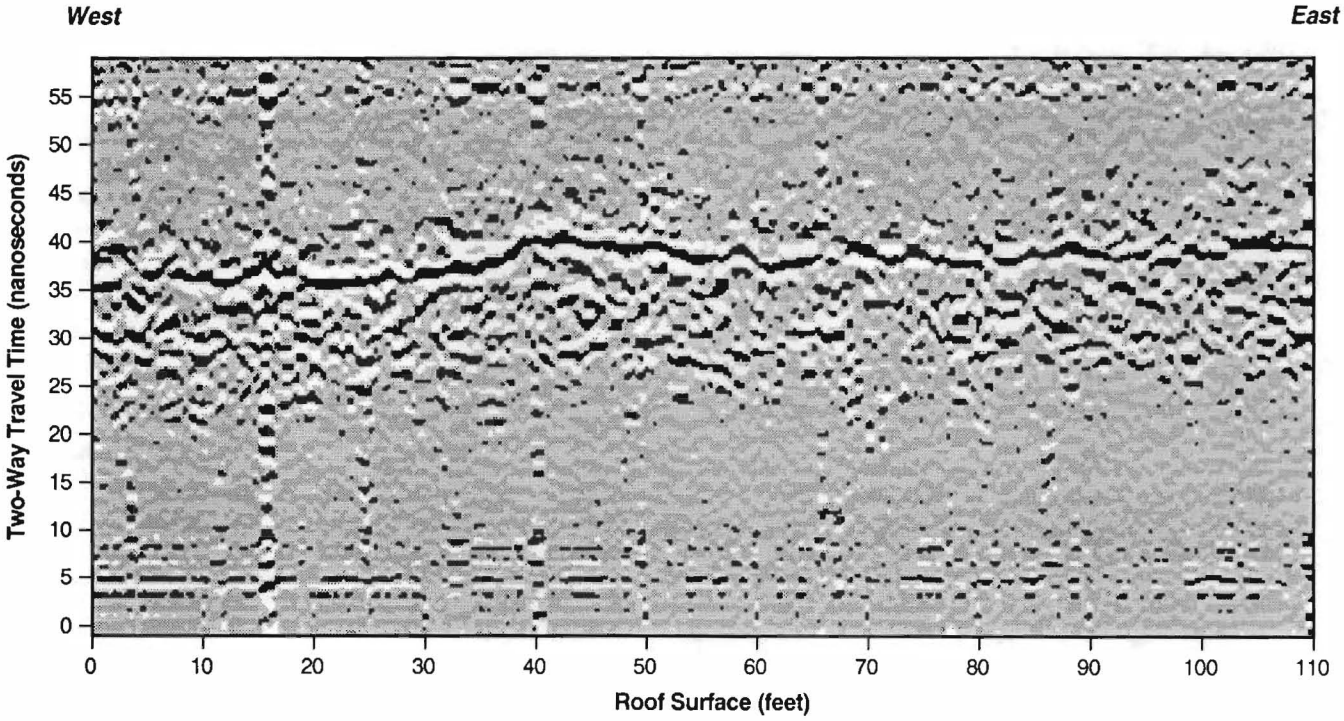

Figure D-34
Traverse D, E-0790 to E-0920, S-1950 Drift Roof: February 1992
Vertical Exaggeration 3.5x

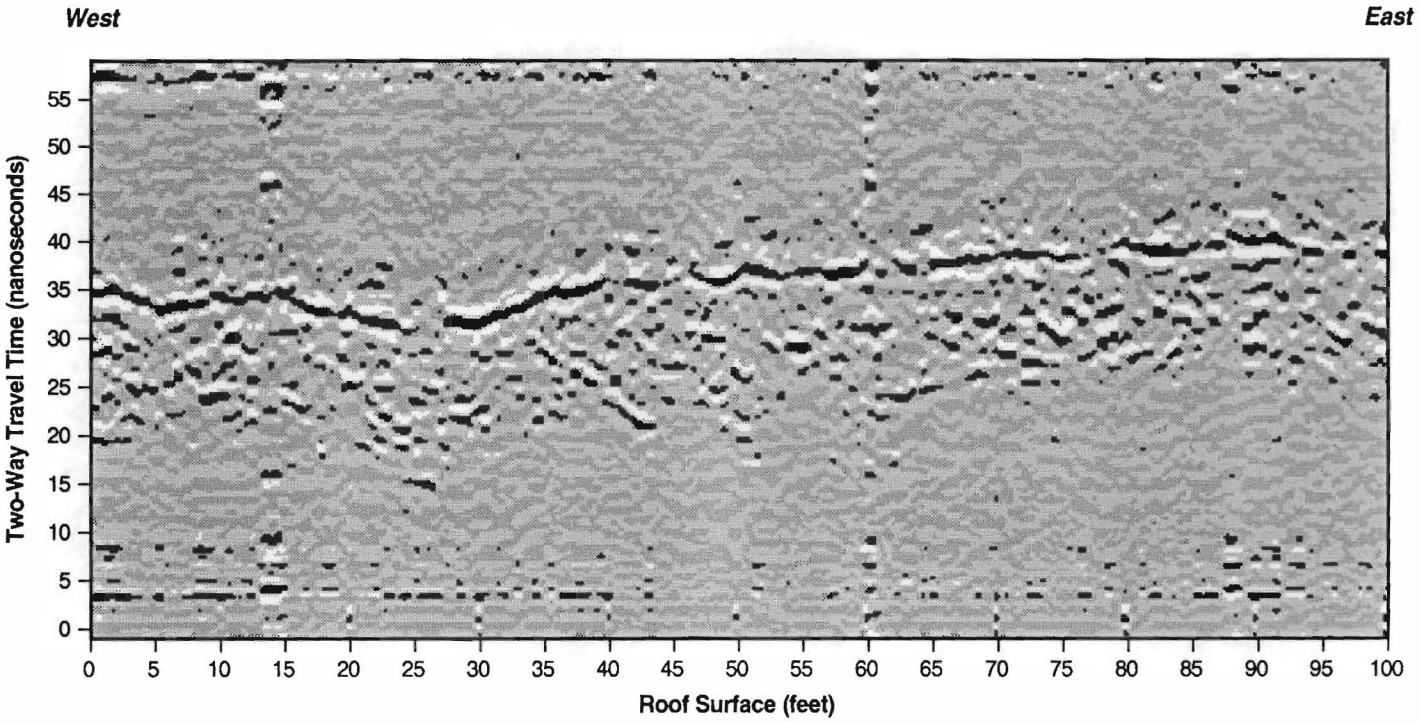

Figure D-35
Traverse F, E-1060 to E-1174, S-1950 Drift Roof: February 1992
Vertical Exaggeration 3x

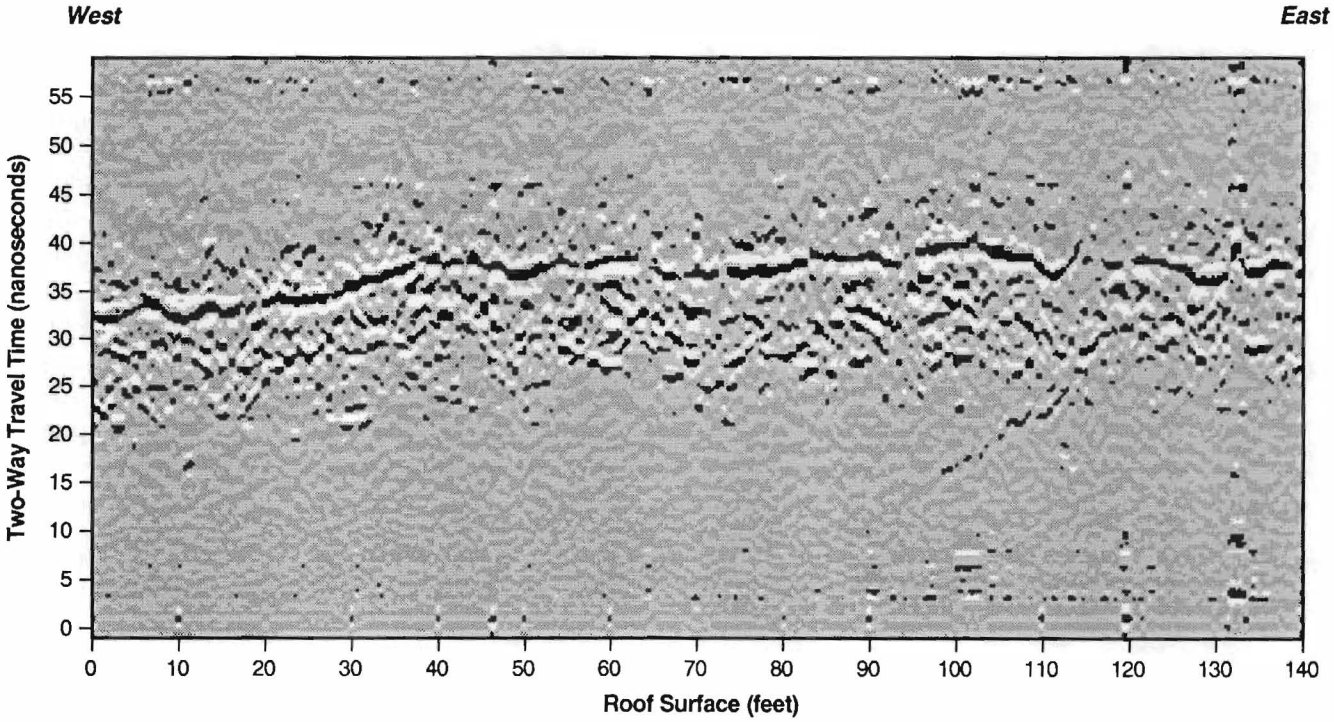

Figure D-36
Traverse G, E-1207 to E-1337, S-1950 Drift Roof: February 1992
Vertical Exaggeration 4.5x

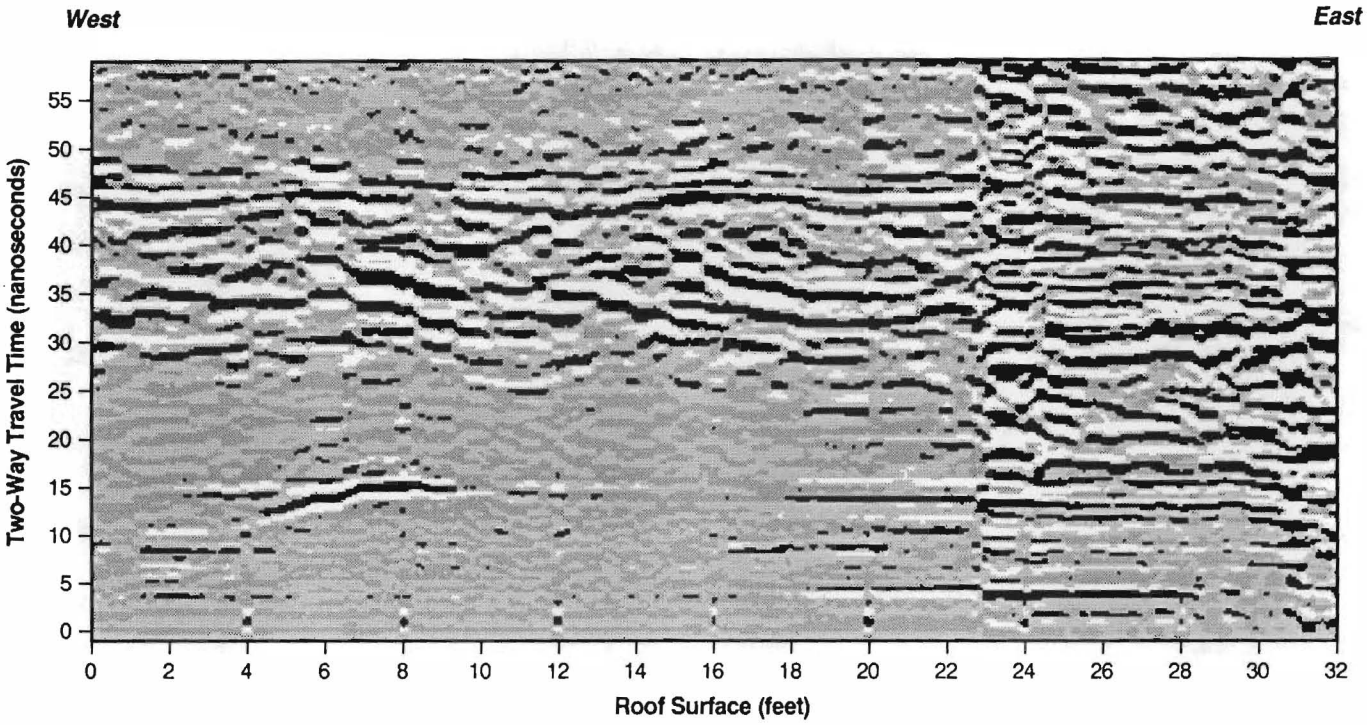

Figure D-37
Traverse H, S-1950 Drift Roof: February 1992

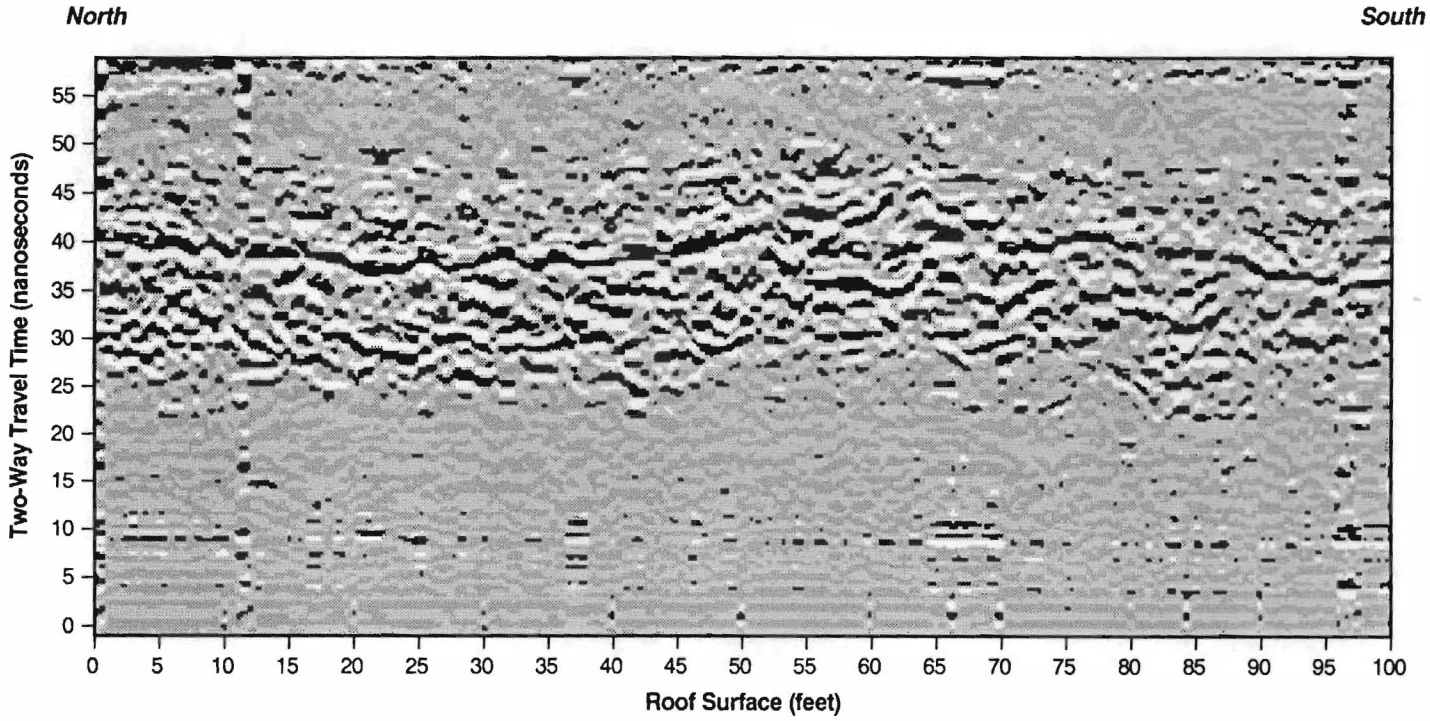

Figure D-38
Traverse I, S-1950 Drift Roof: February 1992
Vertical Exaggeration 3x

APPENDIX E

INSTRUMENTATION SETTINGS, PROCESSING SEQUENCES, AND RADAR PROFILES: N-1420 DRIFT ROOF

APPENDIX E

This appendix contains the following: (1) instrumentation settings used to conduct GPR surveys on the N-1420 Drift roof on 06/17/91, and 06/19/91; (2) processing sequences used to produce the radar profiles from the N-1420 Drift roof; and (3) radar profiles not contained in the body of this report (Figures E-1 to E-35).

E.1 Instrumentation Settings for the N-1420 Drift Roof Surveys (06/17/91, and 06/19/91)

Antenna settings:

Transmit = normal power
Receiver = normal amplification

Profiling recorder settings:

Surface gain = 4
Center gain = 3
Deep gain = 5.5
Threshold = 3
Signal position = auto
Print polarity = +/- - (negative amplitudes stippled)
Range(dial) = 600 ns
Range multiplier = 100
HP filter = 10
LP filter = 50
XMIT rate = 50 KHz
MODE = radar
Scans/sec = 16
Lines/in. = 200

E.2 *Processing Sequences for the N-1420 Drift Roof Surveys (06/17/91, and 06/19/91)*

1. LP compression, TC = 2

2. Horizontal scaling

3. Stack = 2

4. Finite impulse response filters

   Horizontal boxcar high pass = 255

5. Predictive deconvolution

   Operator length = 45
   Prediction lag = 3
   Prewhitening = 0.1%
   Gain = 2

6. Finite impulse response filters

   Vertical triangle high pass = 50
   Vertical triangle low pass = 7
   Horizontal triangle low pass = 9

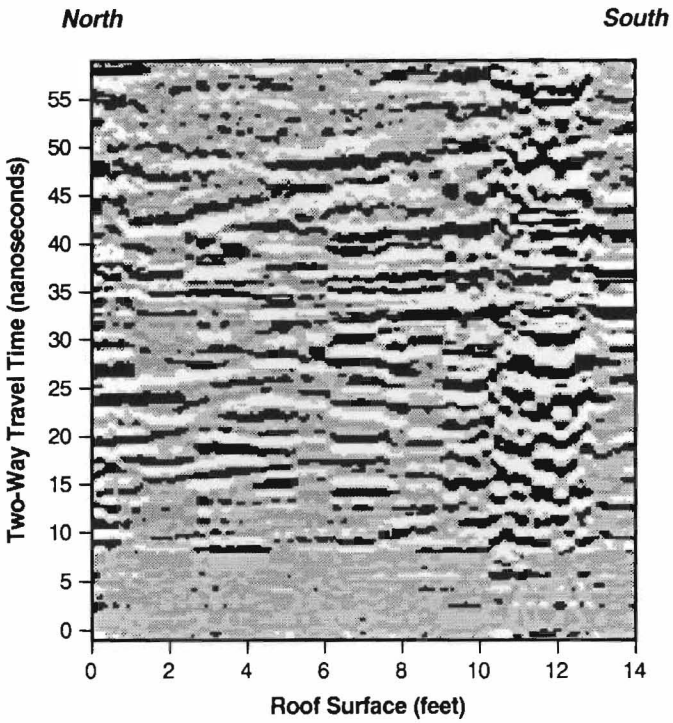

Figure E-1
E-980 Traverse, N-1420 Drift Roof: June 1991

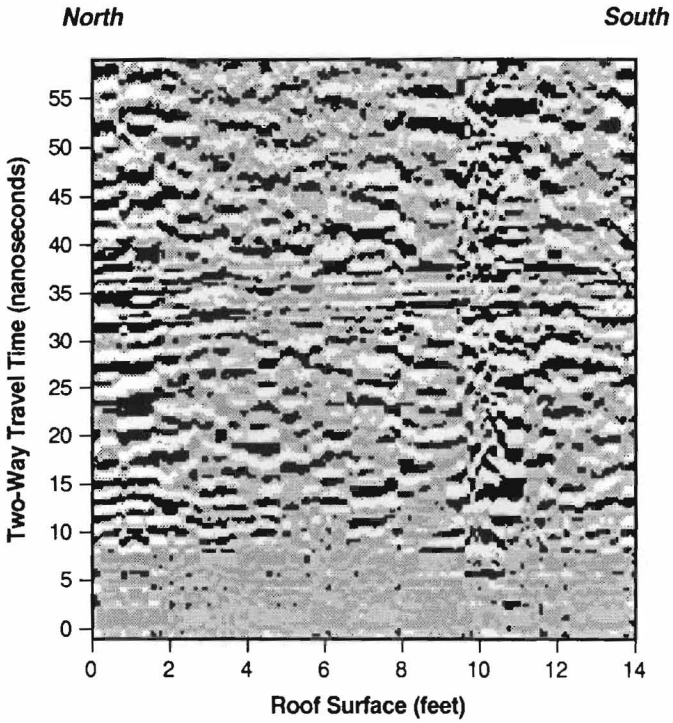

Figure E-2
E-1000 Traverse, N-1420 Drift Roof: June 1991

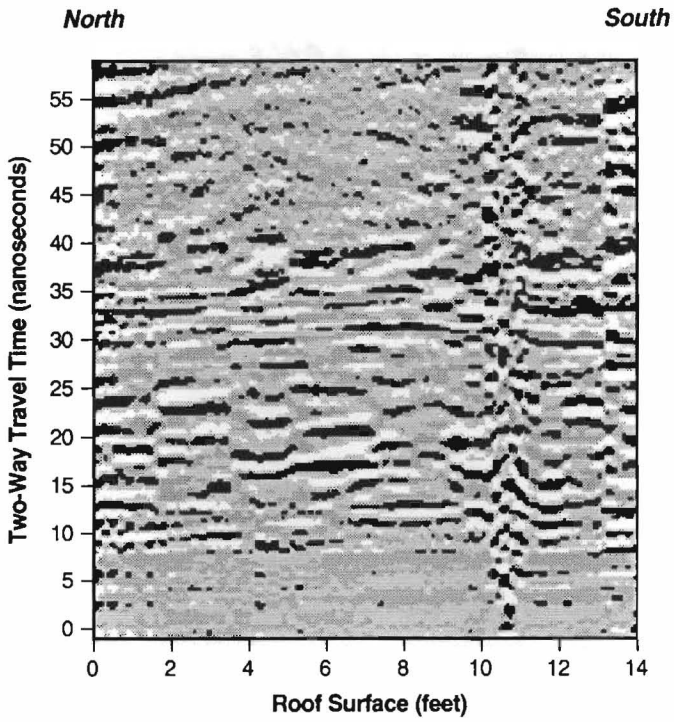

Figure E-3
E-1020 Traverse, N-1420 Drift Roof: June 1991

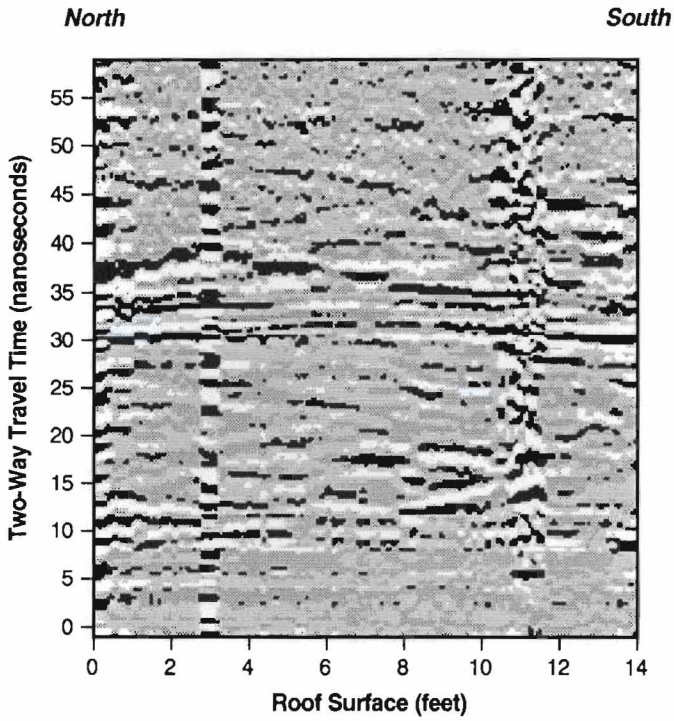

Figure E-4
E-1040 Traverse, N-1420 Drift Roof: June 1991

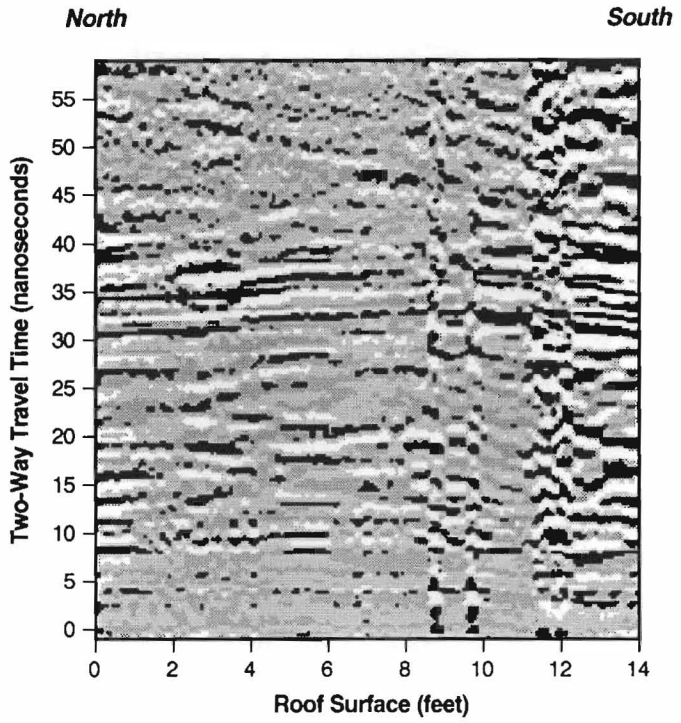

Figure E-5
E-1060 Traverse, N-1420 Drift Roof: June 1991

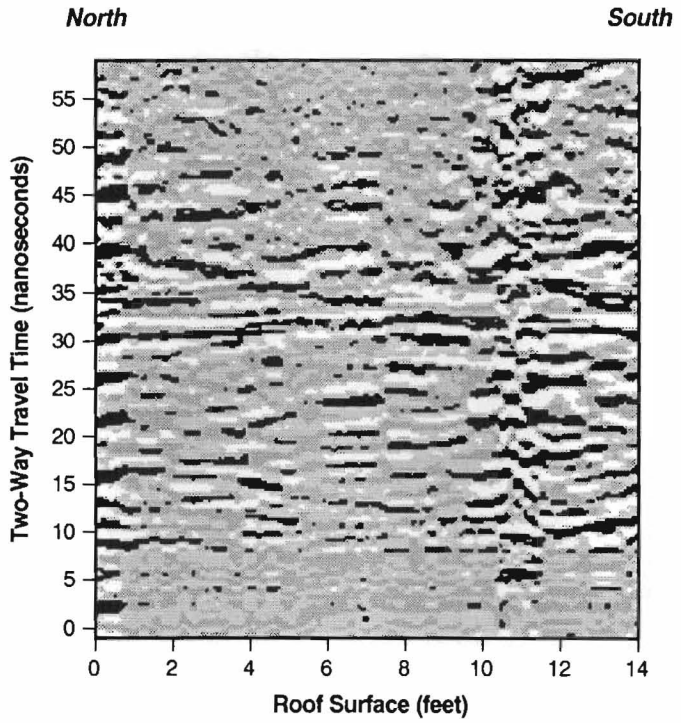

Figure E-6
E-1080 Traverse, N-1420 Drift Roof: June 1991

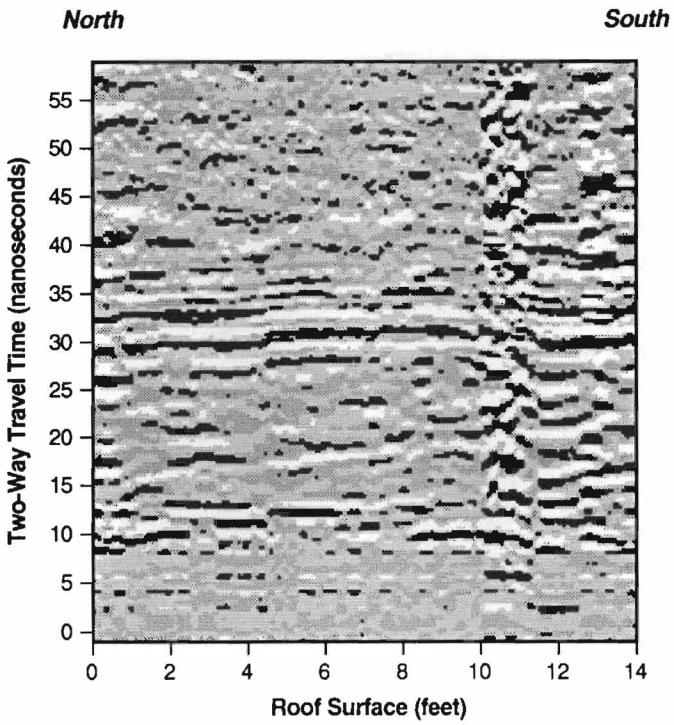

Figure E-7
E-1100 Traverse, N-1420 Drift Roof: June 1991

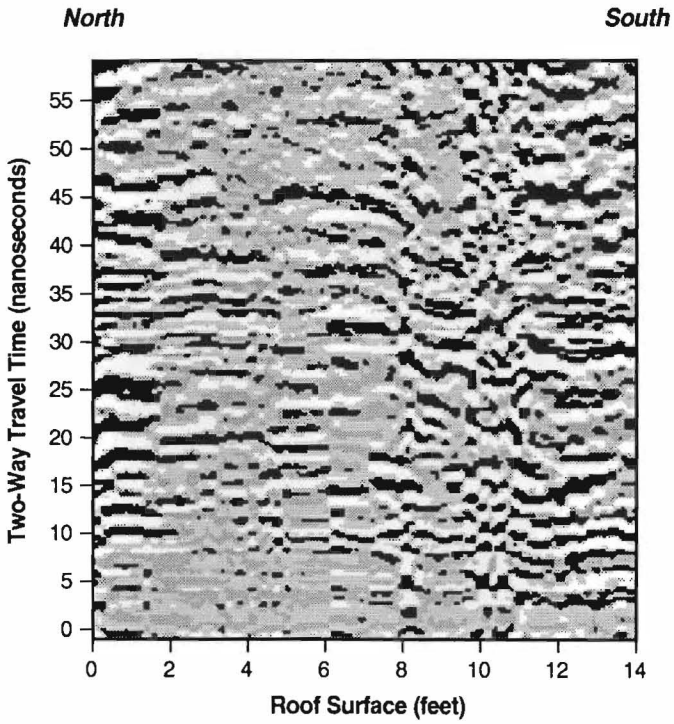

Figure E-8
E-1140 Traverse, N-1420 Drift Roof: June 1991

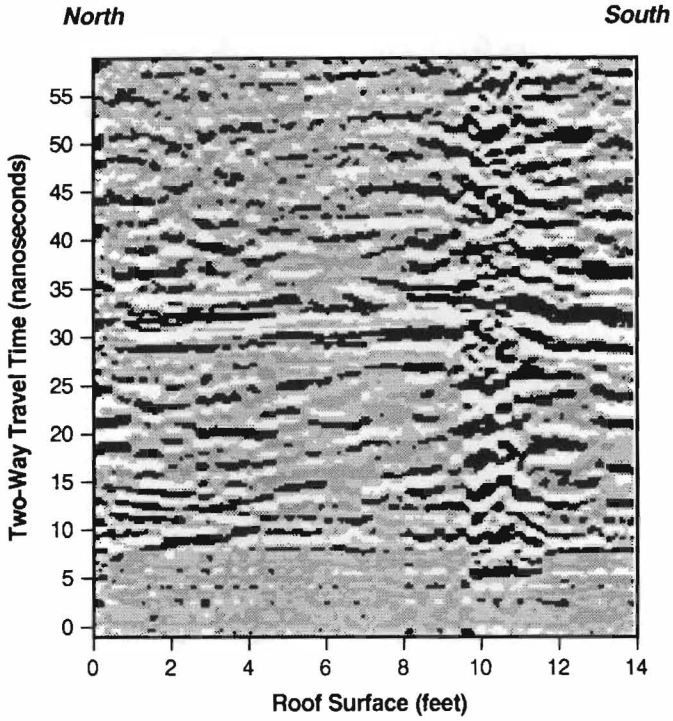

Figure E-9
E-1160 Traverse, N-1420 Drift Roof: June 1991

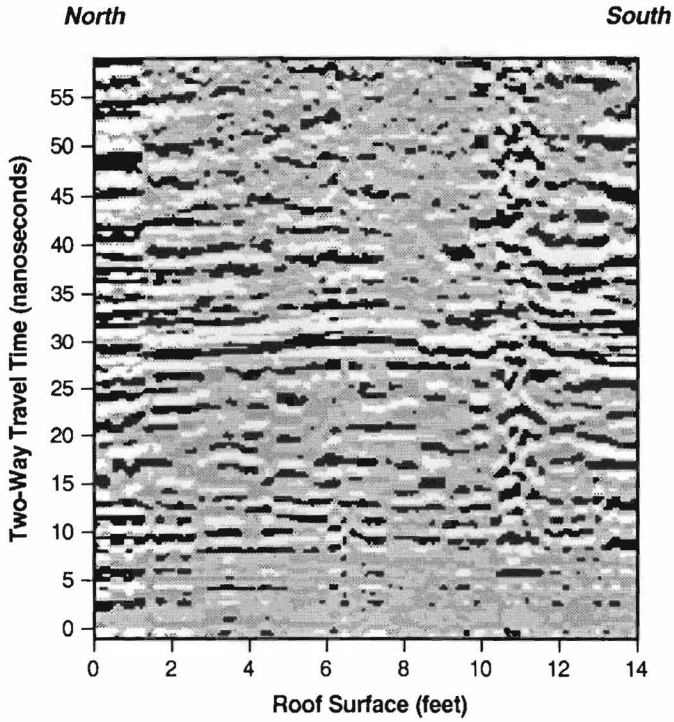

Figure E-10
E-1180 Traverse, N-1420 Drift Roof: June 1991

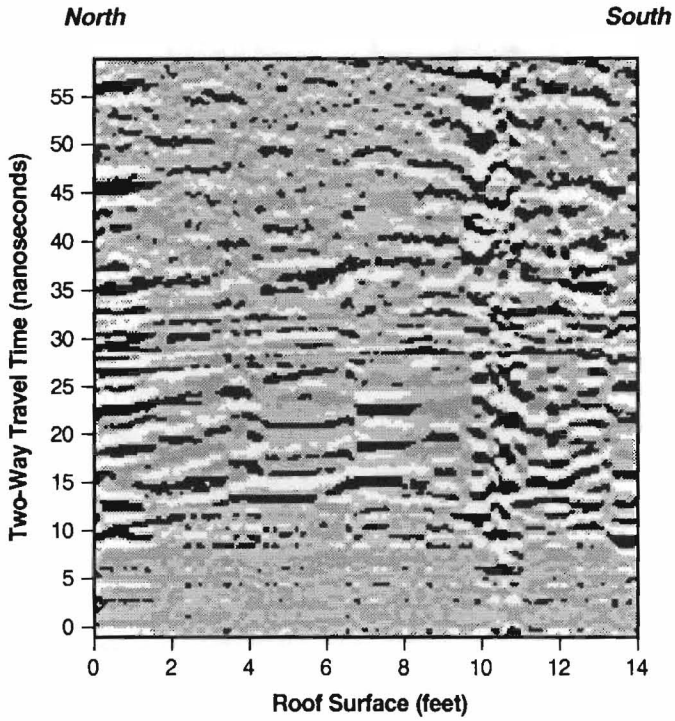

Figure E-11
E-1200 Traverse, N-1420 Drift Roof: June 1991

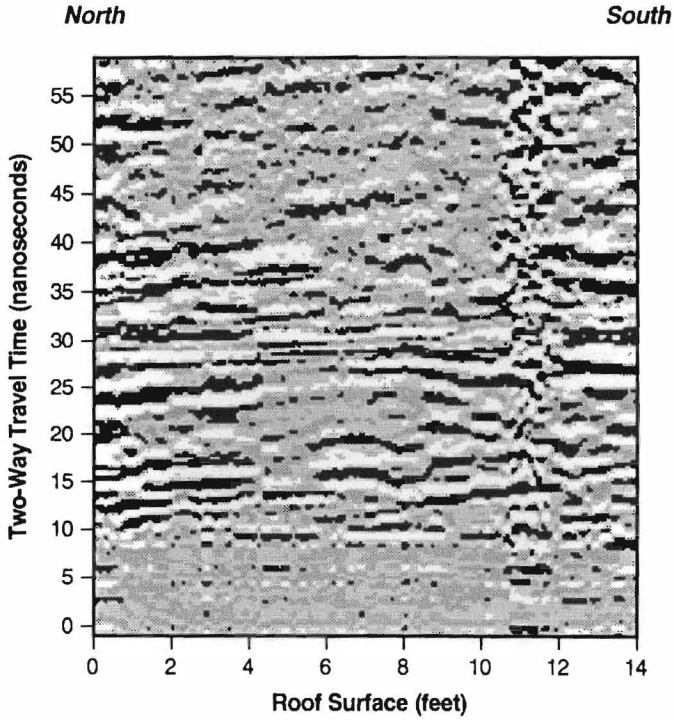

Figure E-12
E-1220 Traverse, N-1420 Drift Roof: June 1991

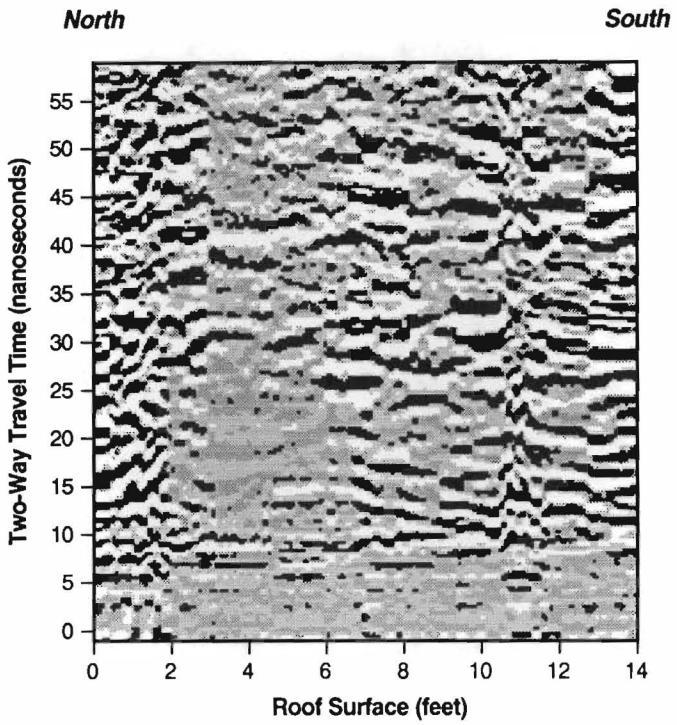

Figure E-13
E-1240 Traverse, N-1420 Drift Roof: June 1991

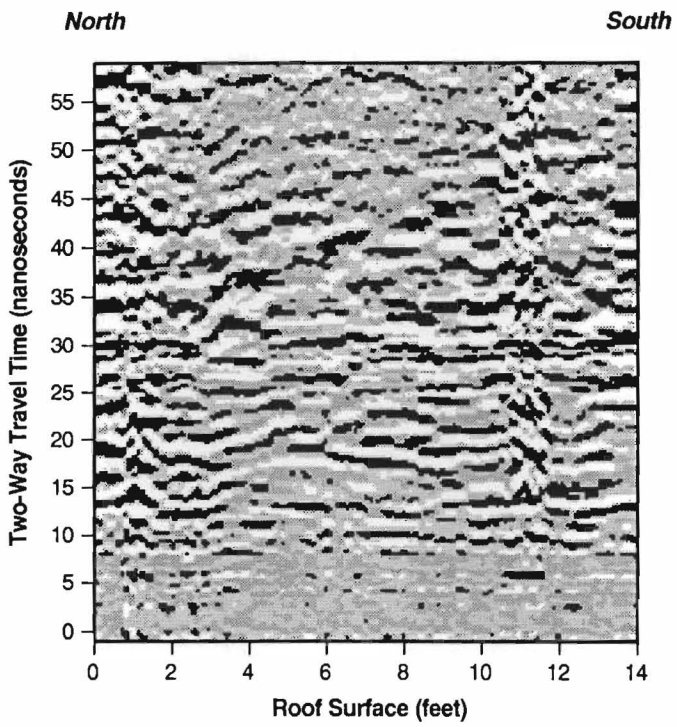

Figure E-14
E-1260 Traverse, N-1420 Drift Roof: June 1991

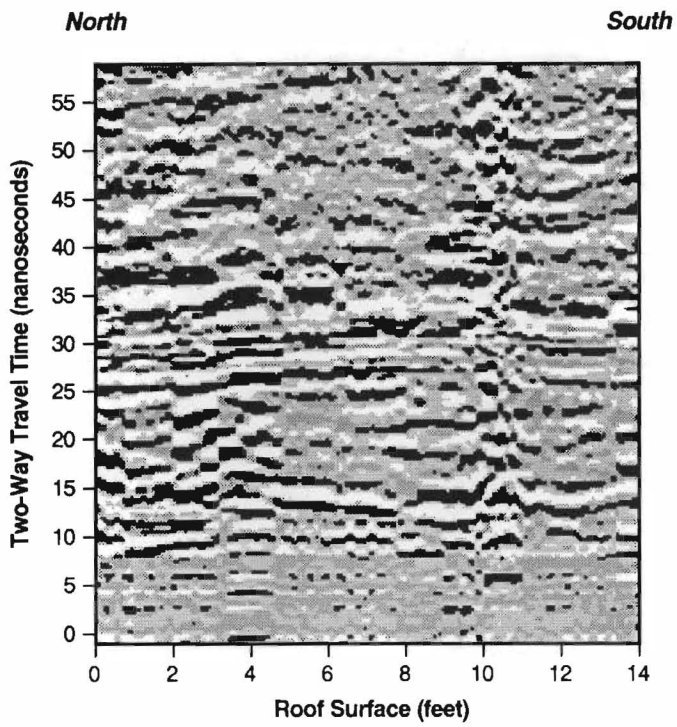

Figure E-15
E-1280 Traverse, N-1420 Drift Roof: June 1991

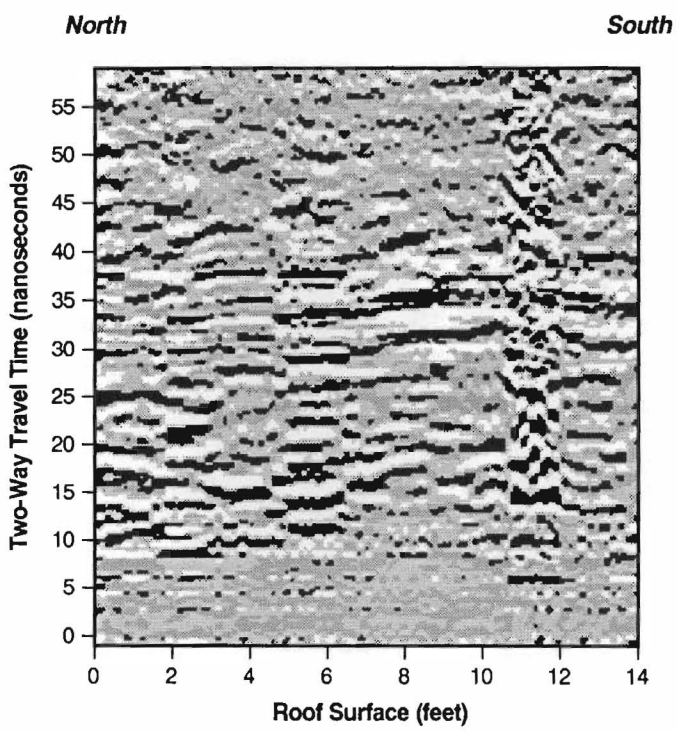

Figure E-16
E-1300 Traverse, N-1420 Drift Roof: June 1991

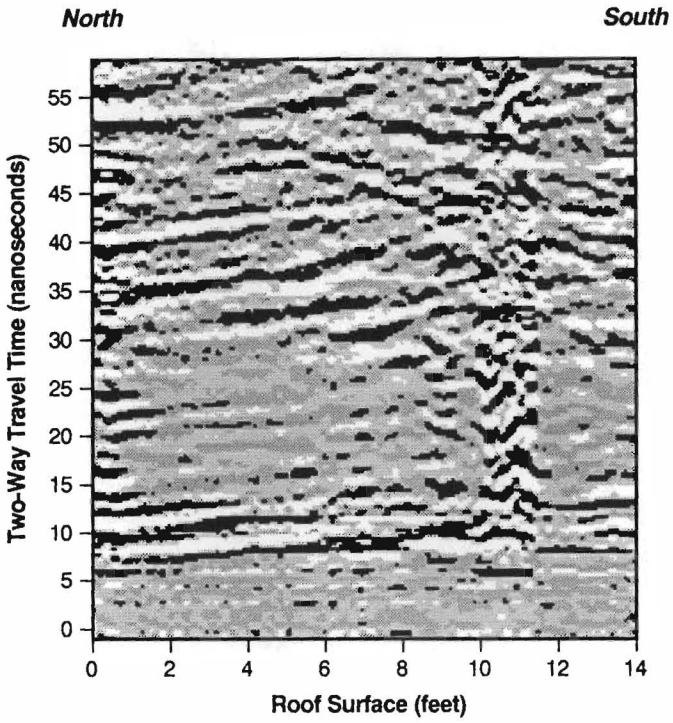

Figure E-17
E-1320 Traverse, N-1420 Drift Roof: June 1991

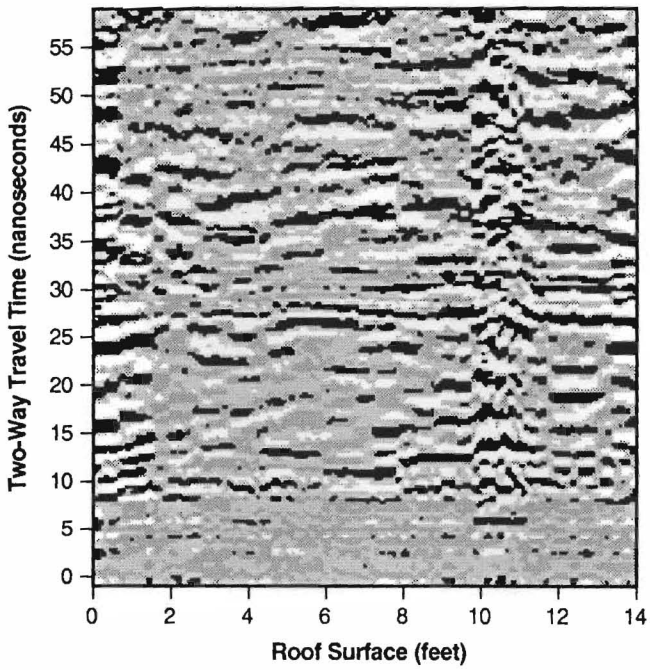

Figure E-18
E-1340 Traverse, N-1420 Drift Roof: June 1991

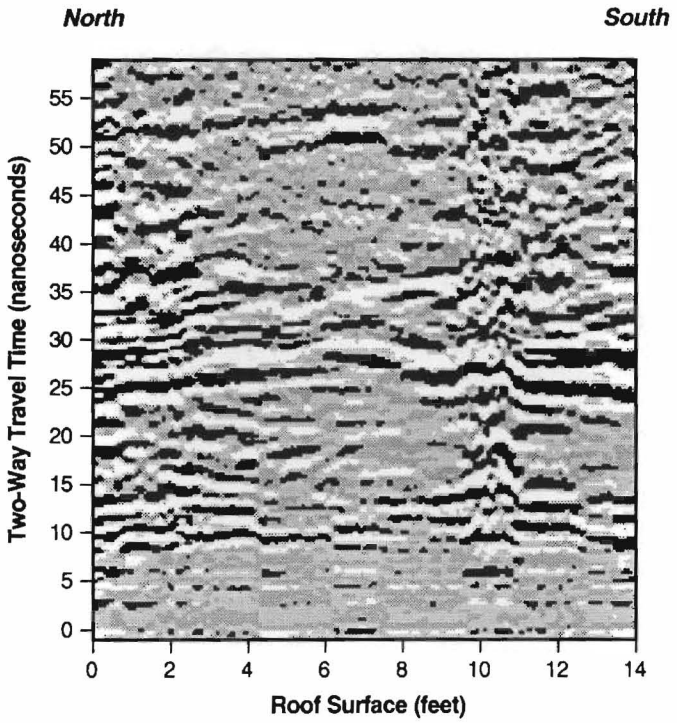

Figure E-19
E-1360 Traverse, N-1420 Drift Roof: June 1991

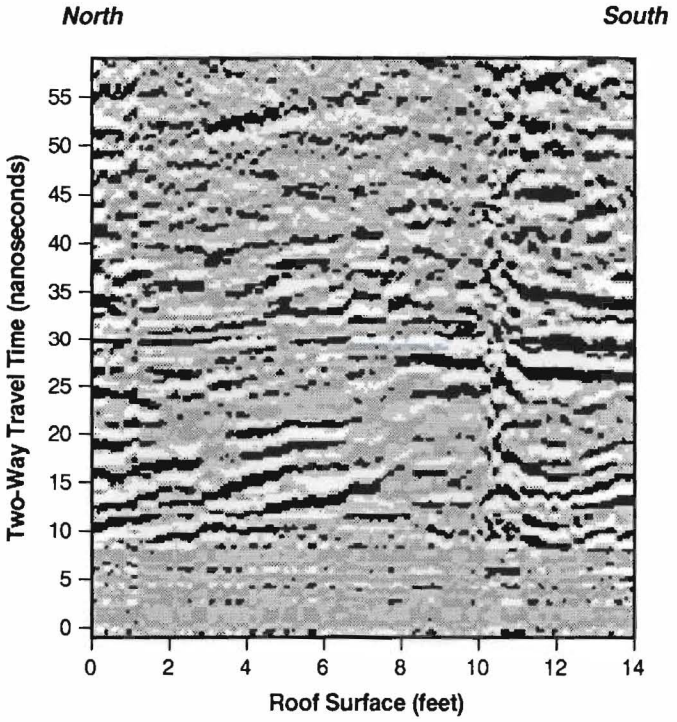

Figure E-20
E-1380 Traverse, N-1420 Drift Roof: June 1991

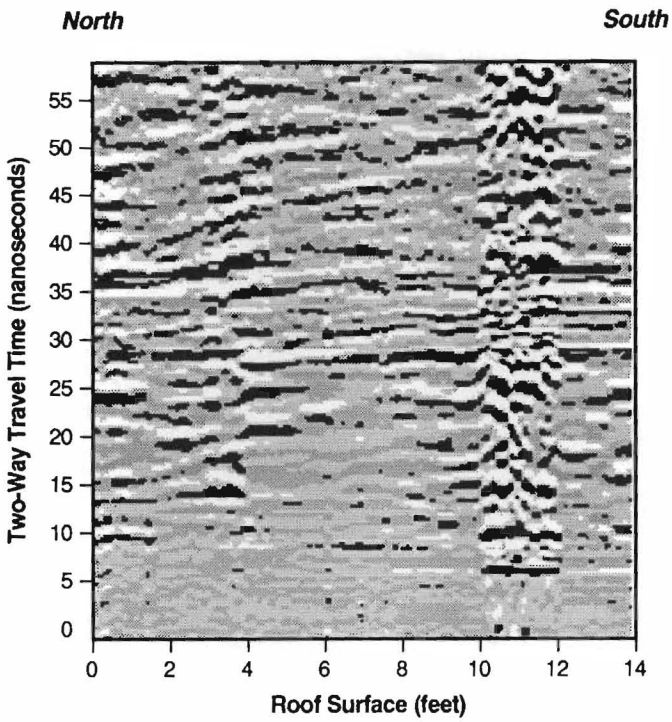

Figure E-21
E-1400 Traverse, N-1420 Drift Roof: June 1991

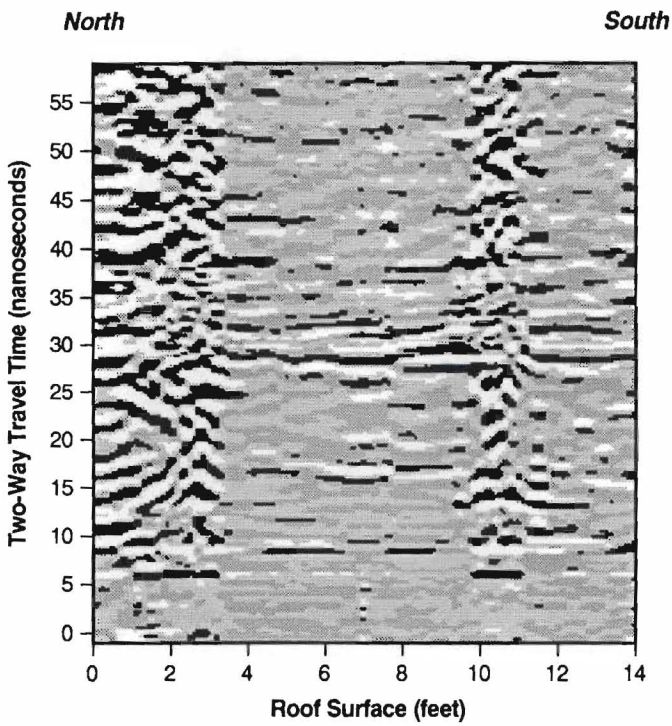

Figure E-22
E-1420 Traverse, N-1420 Drift Roof: June 1991

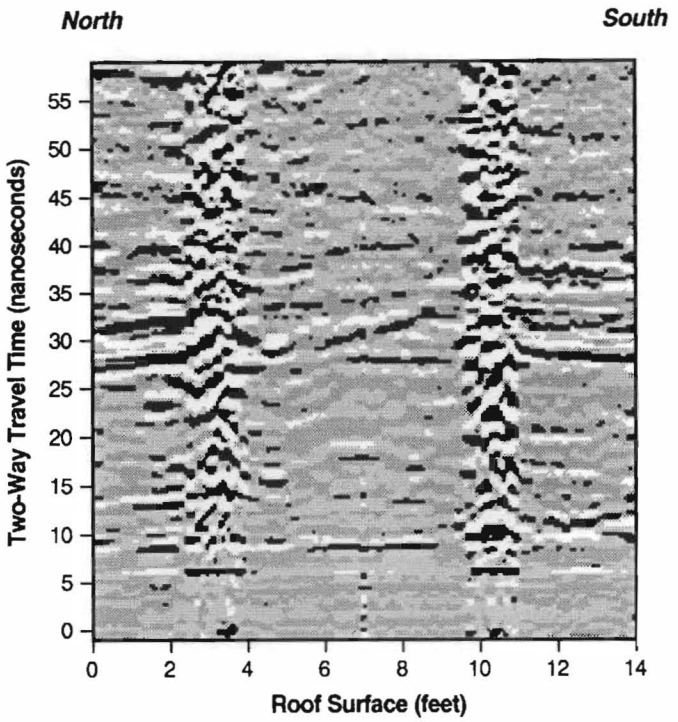

Figure E-23
E-1440 Traverse, N-1420 Drift Roof: June 1991

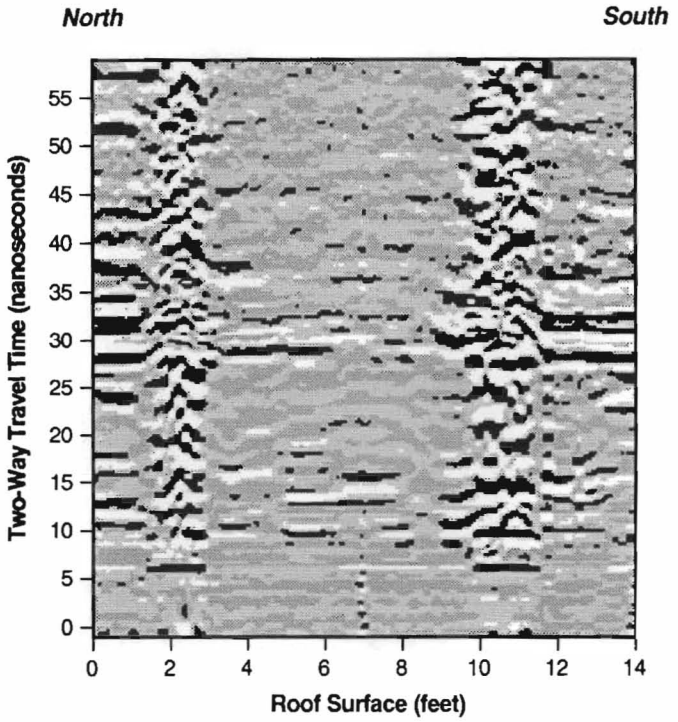

Figure E-24
E-1460 Traverse, N-1420 Drift Roof: June 1991

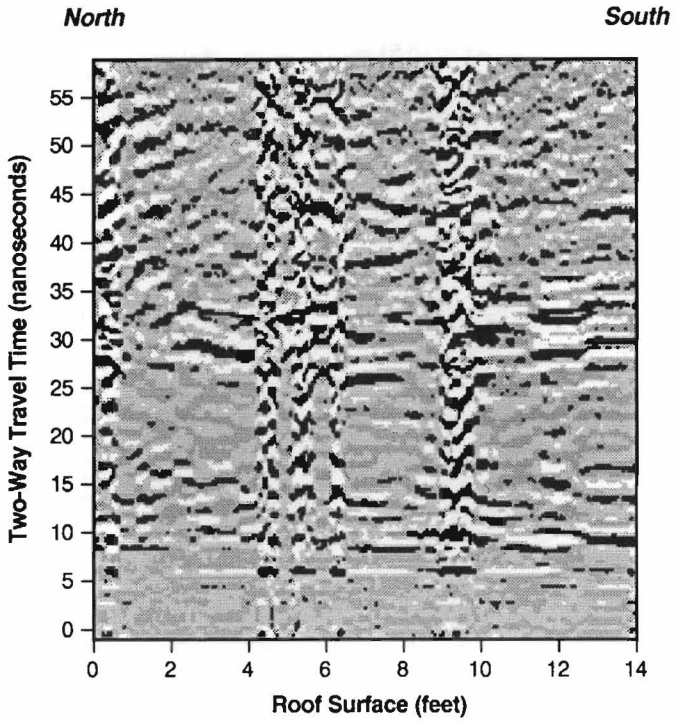

Figure E-25
E-1500 Traverse, N-1420 Drift Roof: June 1991

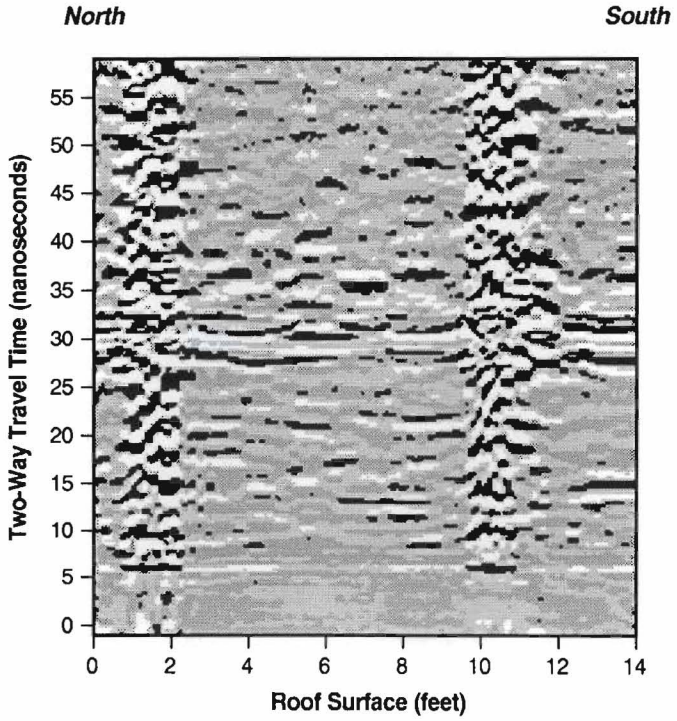

Figure E-26
E-1520 Traverse, N-1420 Drift Roof: June 1991

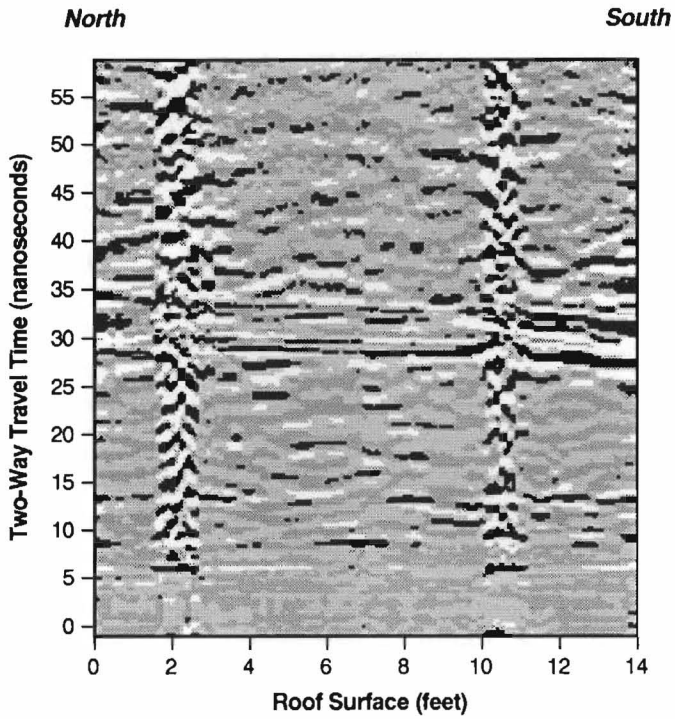

Figure E-27
E-1540 Traverse, N-1420 Drift Roof: June 1991

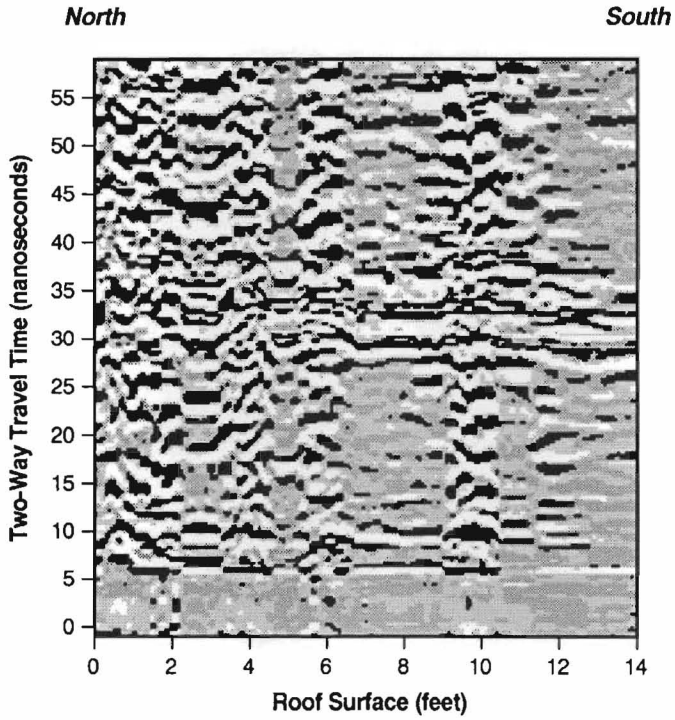

Figure E-28
E-1580 Traverse, N-1420 Drift Roof: June 1991

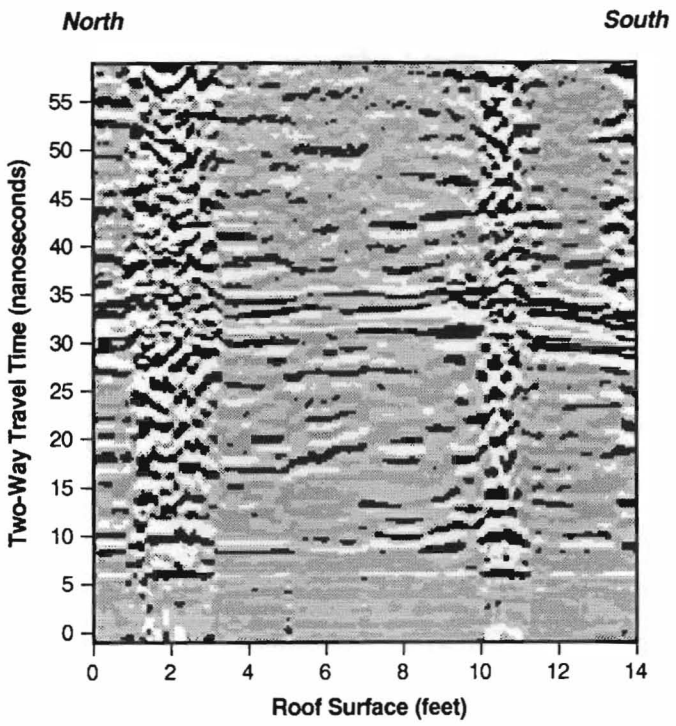

Figure E-29
E-1600 Traverse, N-1420 Drift Roof: June 1991

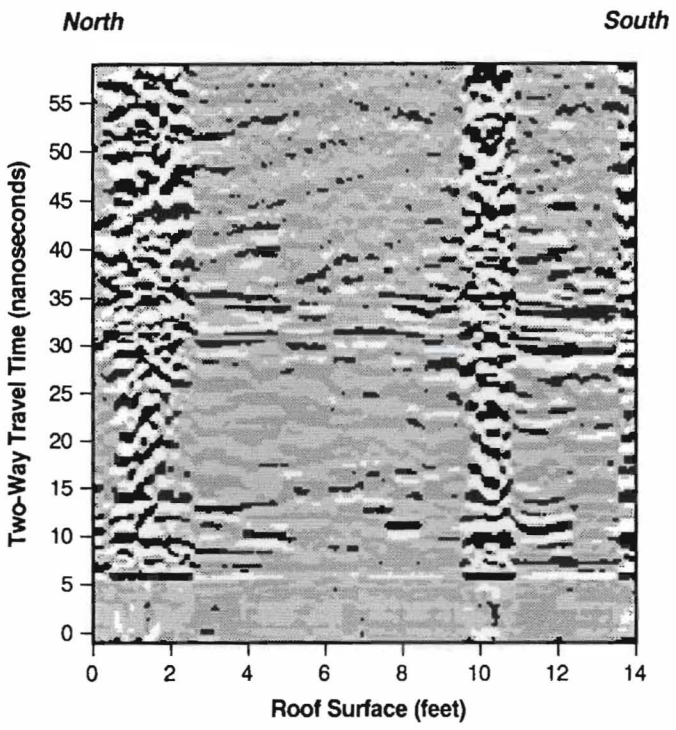

Figure E-30
E-1640 Traverse, N-1420 Drift Roof: June 1991

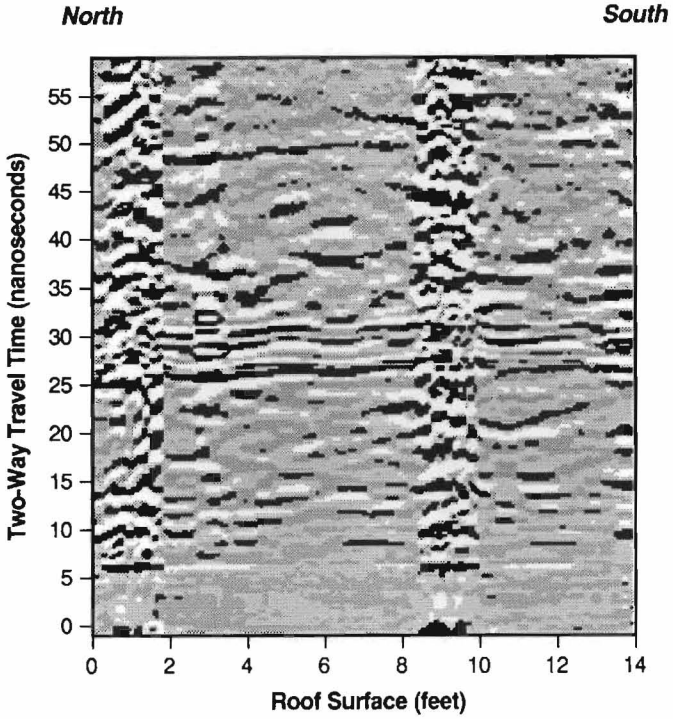

Figure E-31
E-1660 Traverse, N-1420 Drift Roof: June 1991

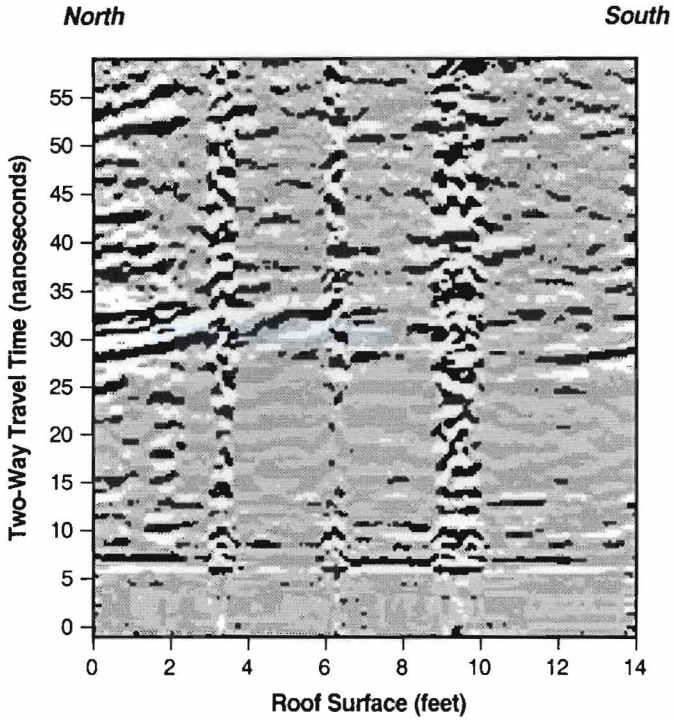

Figure E-32
E-1680 Traverse, N-1420 Drift Roof: June 1991

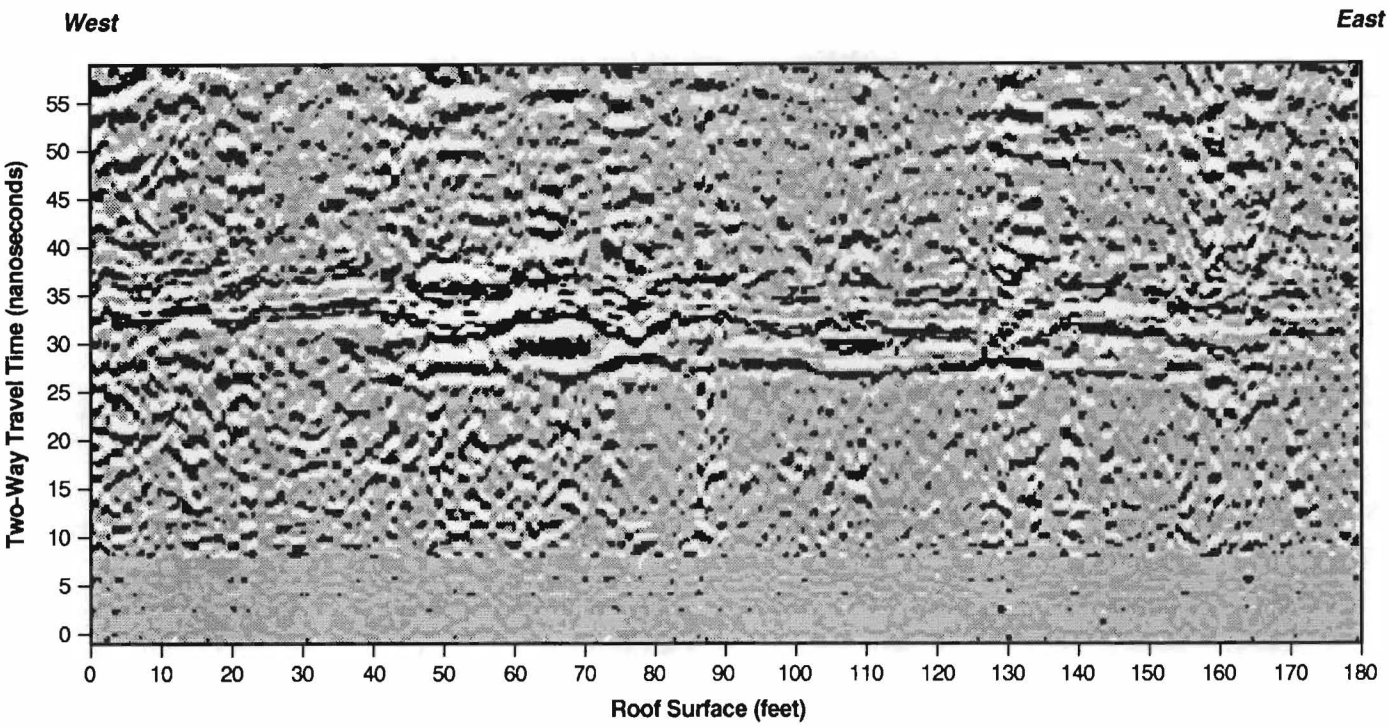

Figure E-33
Traverse A, E-980 to E-1160, N-1420 Drift Roof: June 1991
Vertical Exaggeration 5.5x

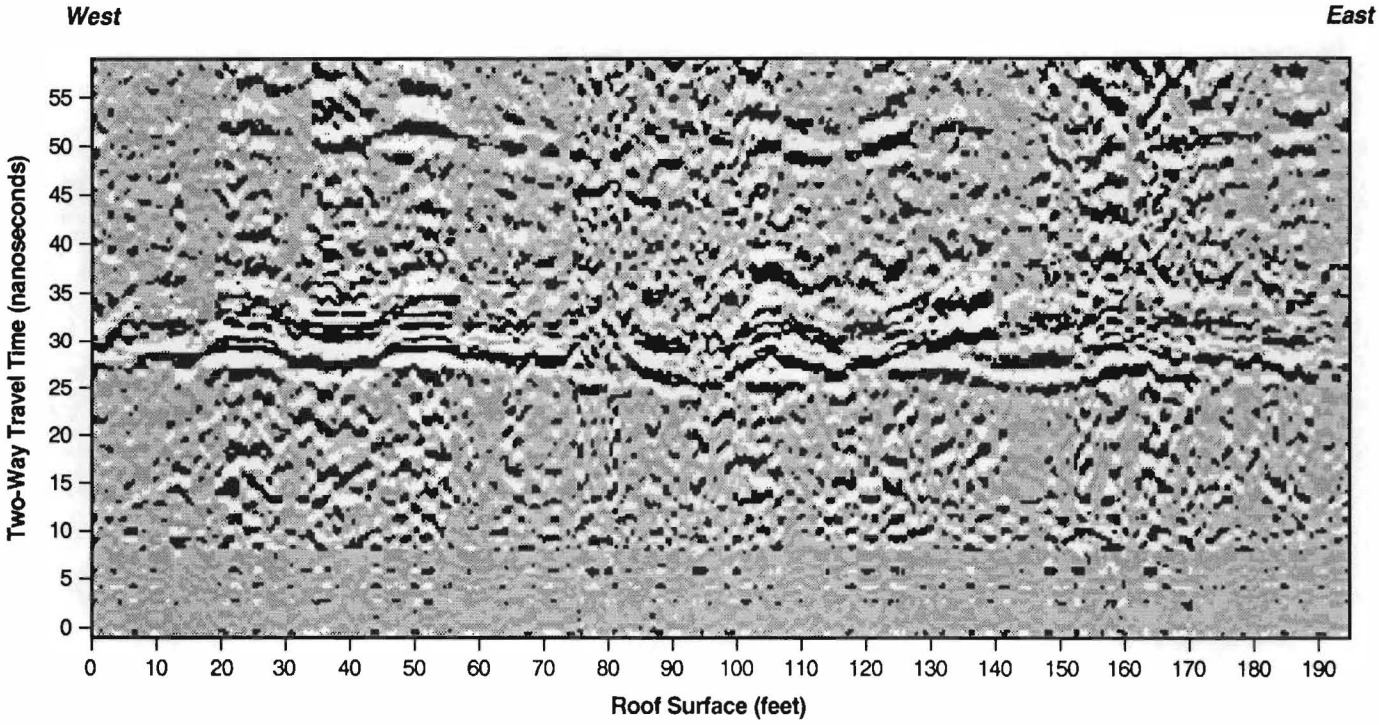

Figure E-34
Traverse B, E-1180 to 1375, N-1420 Roof: June 1991
Vertical Exaggeration 6x

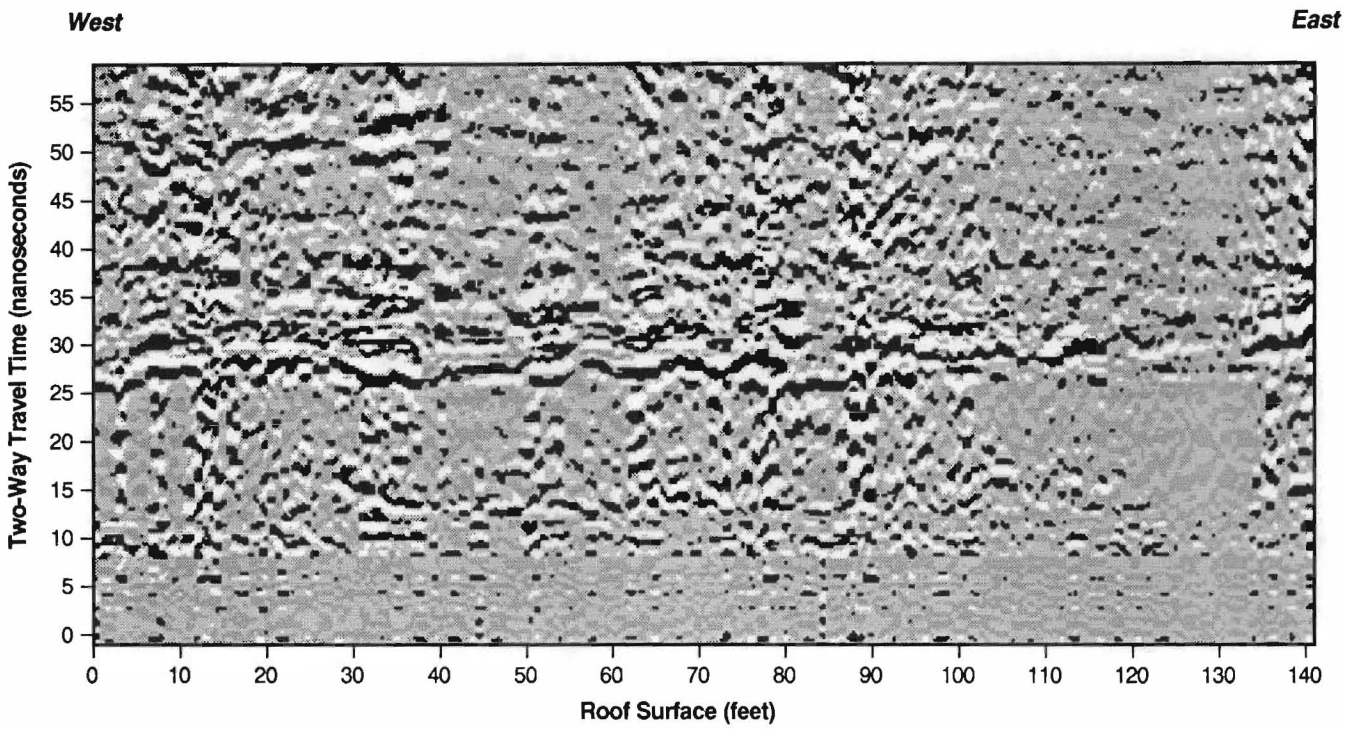

Figure E-35
Traverse C, E-1329 to E-1470, N-1420 Drift Roof: June 1991
Vertical Exaggeration 4.5x

APPENDIX F

INSTRUMENTATION SETTINGS, PROCESSING SEQUENCES, AND RADAR PROFILES: ROOM Q AND ROOM Q ACCESS DRIFT

APPENDIX F

This appendix contains the following: (1) instrumentation settings used to conduct GPR surveys in Room Q and on the floor of the Room Q Access Drift on 03/13/91; (2) processing sequences used to produce the radar profiles from Room Q and from the floor of the Room Q Access Drift; and (3) radar profiles not contained in the body of this report (Figures F-1 to F-11).

F.1.1 Instrumentation Settings for Room Q GPR Surveys (03/13/91)

Antenna settings:

Transmit = normal power
Receiver = high amplification

Profiling recorder settings:

Surface gain = 4
Center gain = 3
Deep gain = 4
Threshold = 3
Signal position = manual
Print polarity = +/-
Range(dial) = 60 ns
Range multiplier = 1000
HP filter = 10
LP filter = 50
XMIT rate = 50 KHz
MODE = radar
Scans/sec = 16
Lines/in. = 200

F.1.2 Instrumentation Settings for the Room Q Access Drift, Floor Surveys (03/13/91)

Antenna settings:

Transmit = high power
Receiver = normal amplification

Profiling recorder settings:

Surface gain = 4
Center gain = 3
Deep gain = 4
Threshold = 3
Signal position = manual
Print polarity = +/-
Range(dial) = 60 ns
Range multiplier = 1000
HP filter = 10
LP filter = 50
XMIT rate = 50 KHz
MODE = radar
Scans/sec = 16
Lines/in. = 200

F.2.1 Processing Sequences for Room Q GPR Surveys (03/13/91)

1. Horizontal scaling

2. Stack = 2

3. Predictive deconvolution

   Operator length = 35
   Prediction lag = 4
   Prewhitening = 0.1%

4. Finite impulse response filters

   Horizontal boxcar high pass = 255
   Vertical triangle low pass = 9
   Vertical triangle high pass = 35
   Horizontal triangle low pass = 7

F.2.2 Processing Sequences for the Room Q Access Drift, Floor Surveys (03/13/91)

1. Horizontal scaling

2. Stack = 2

3. Finite impulse response filters

   Horizontal boxcar high pass = 255

4. Predictive deconvolution

   Operator length = 65
   Prediction lag = 2
   Prewhitening = 0.1%
   Gain = 4

5. Finite impulse response filters

   Vertical triangle low pass = 13
   Horizontal triangle low pass = 3
   Vertical triangle high pass = 45

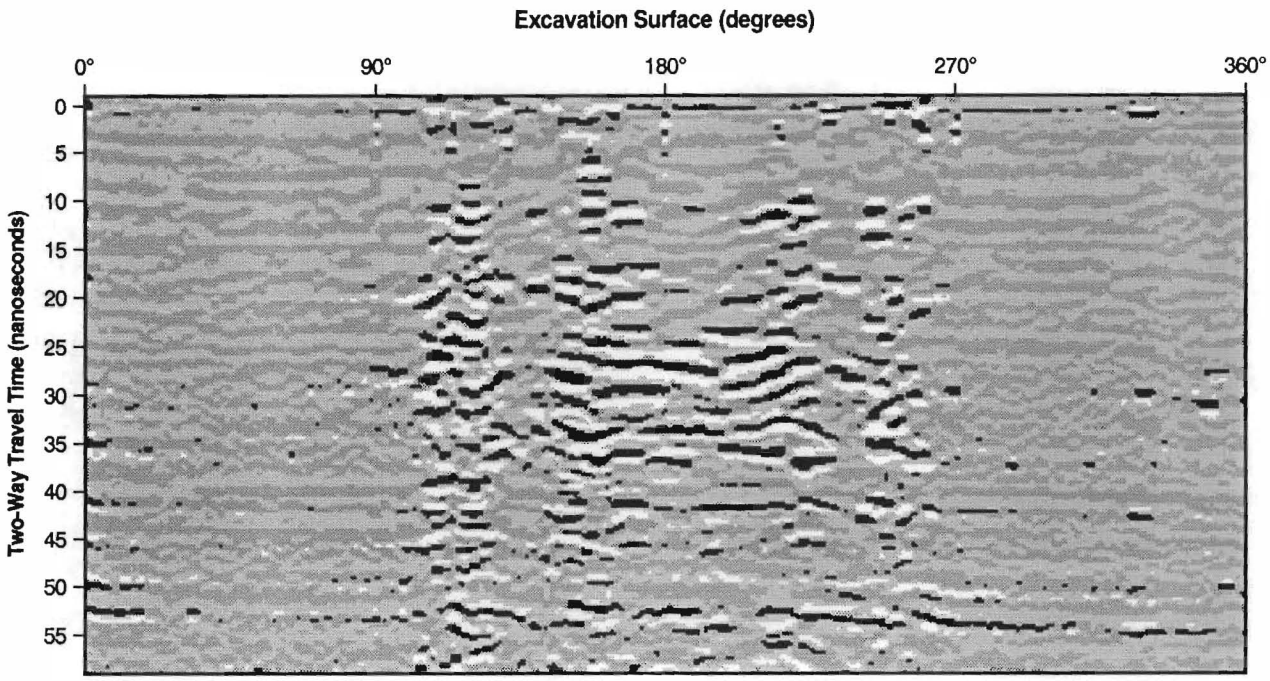

Figure F-1
Survey 1, Room Q, Circumferential Survey, 77 Feet from the Collar: March 1991

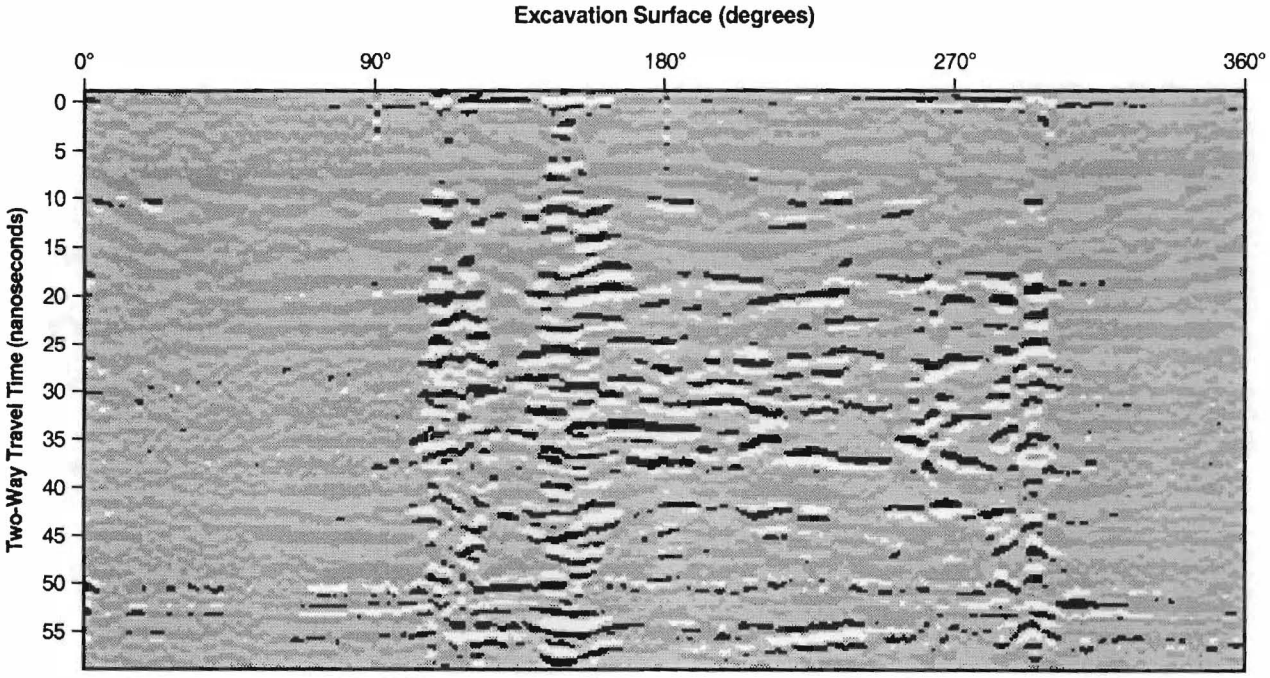

Figure F-2
Survey 2, Room Q, Circumferential Survey, 65 Feet from the Collar: March 1991

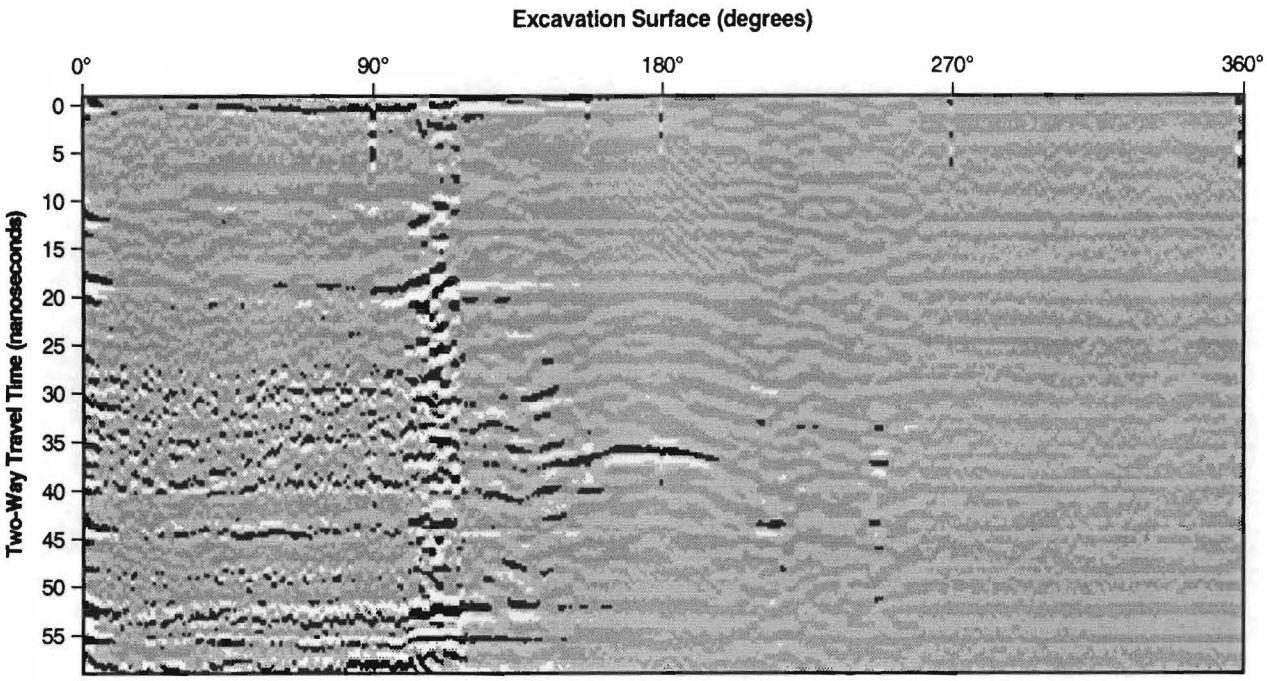

Figure F-3
Survey 3, Room Q, Circumferential Survey, 77 Feet from the Collar: March 1991

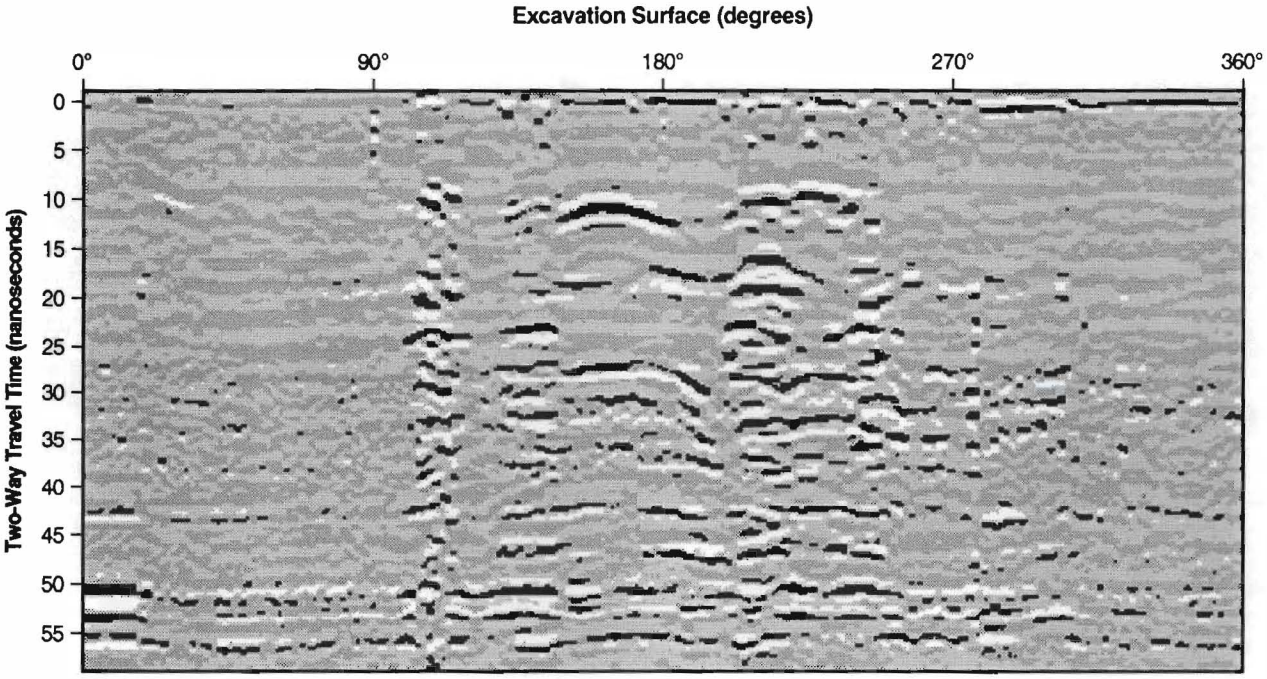

Figure F-4
Survey 5, Room Q, Circumferential Survey, 65 Feet from the Collar: March 1991

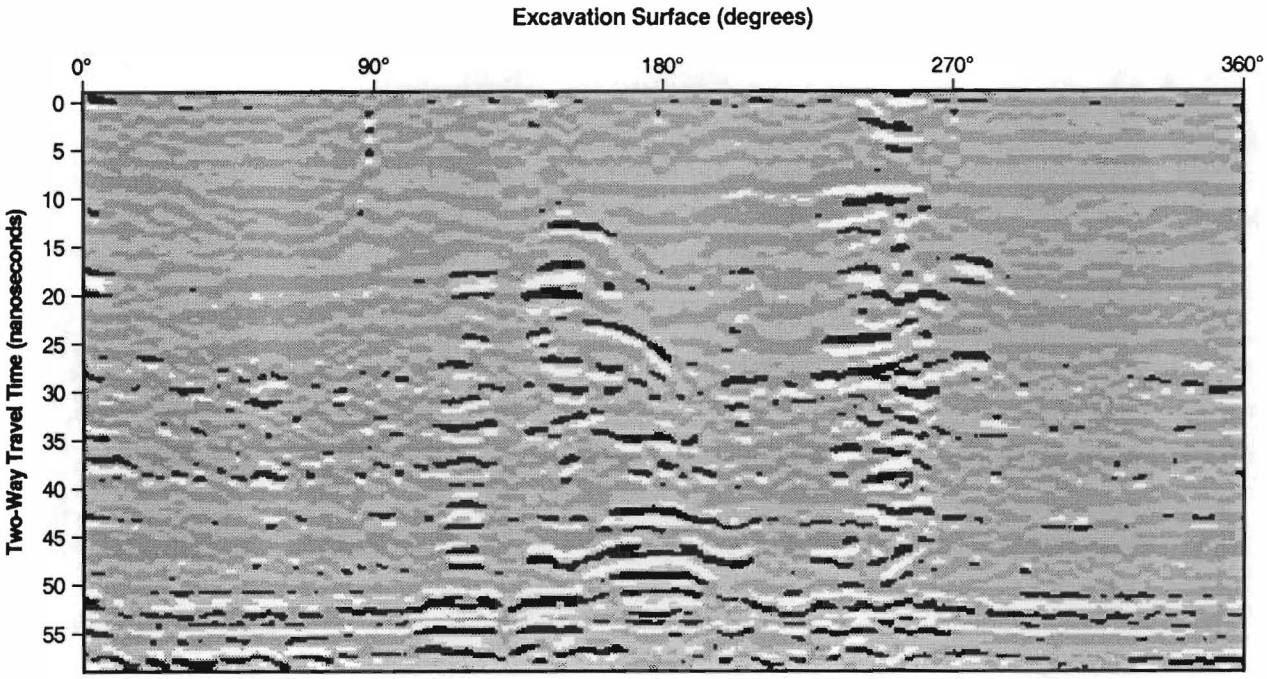

Figure F-5
Survey 7, Room Q, Circumferential Survey, 43 Feet from the Collar: March 1991

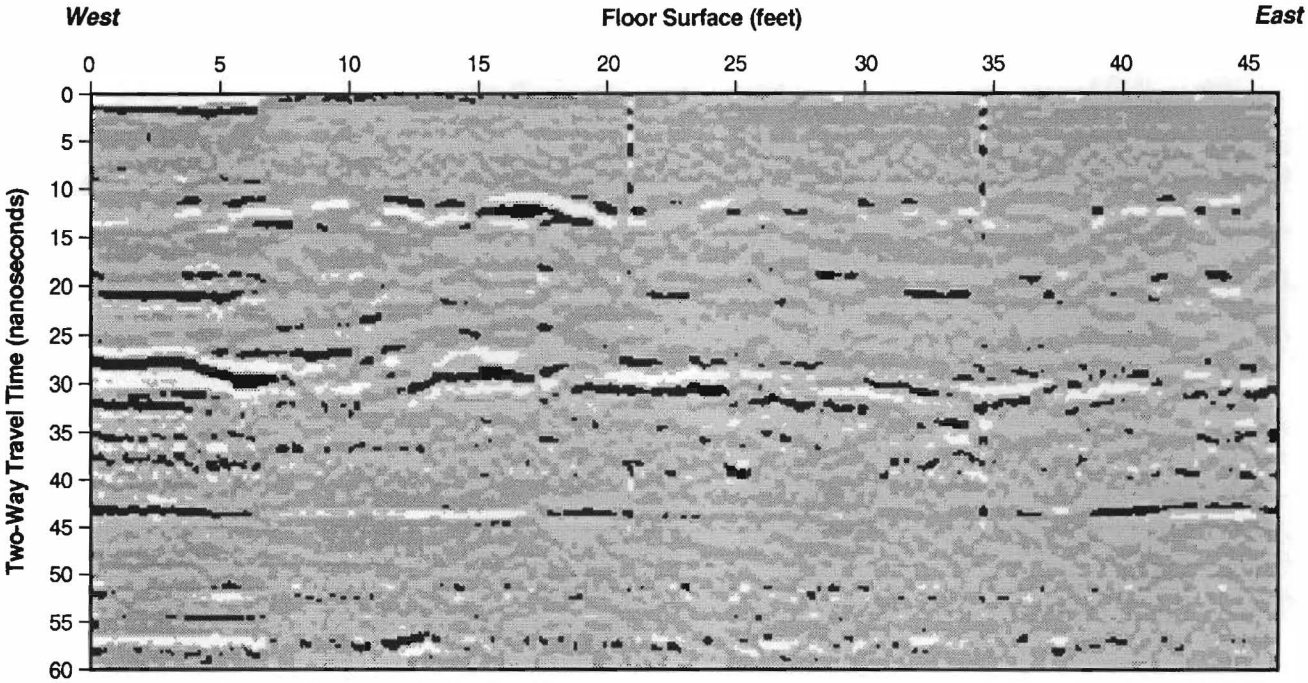

Figure F-6
Traverse 1, Room Q Access: March 1991
Vertical Exaggeration 1.5x

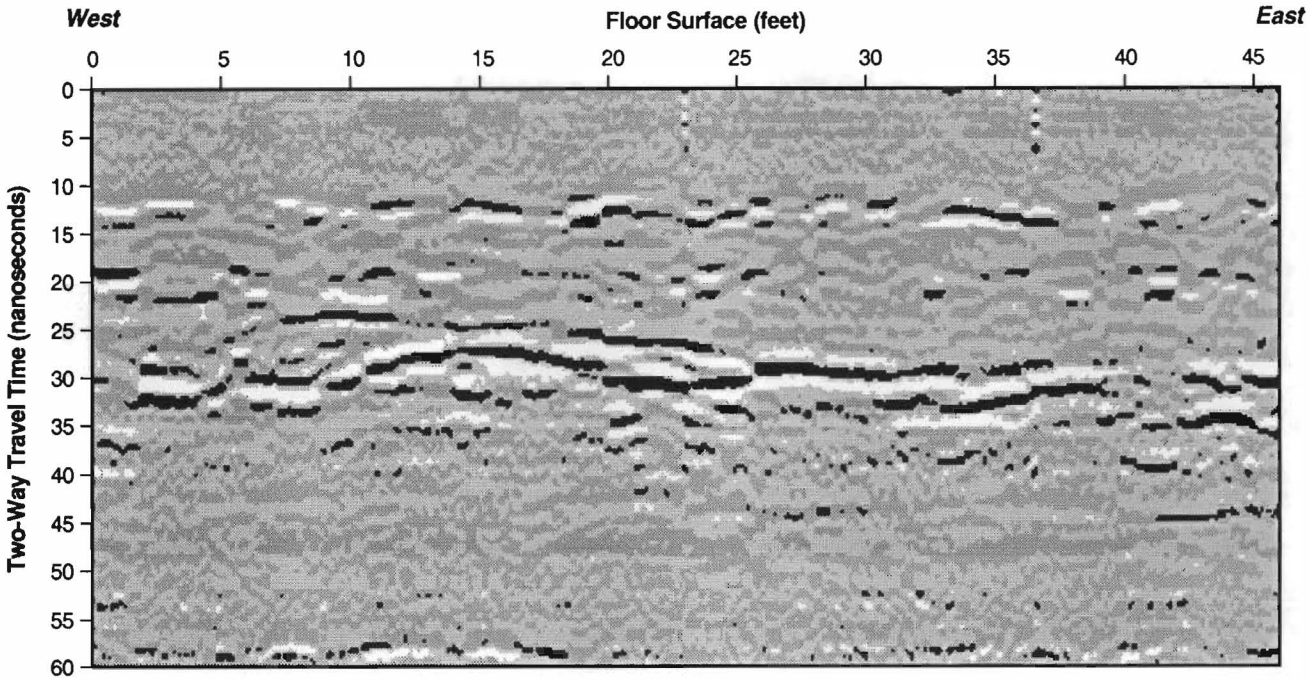

Figure F-7
Traverse 2, Room Q Access: March 1991
Vertical Exaggeration 1.5x

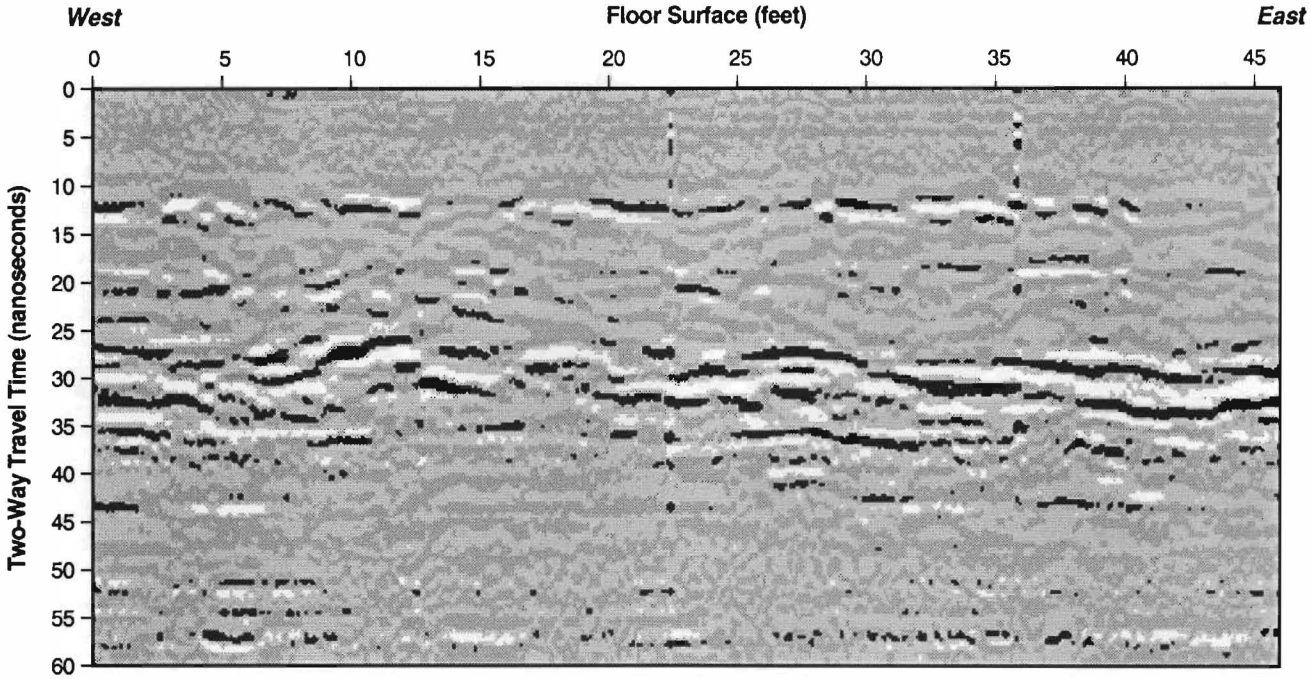

Figure F-8
Traverse 3, Room Q Access: March 1991
Vertical Exaggeration 1.5x

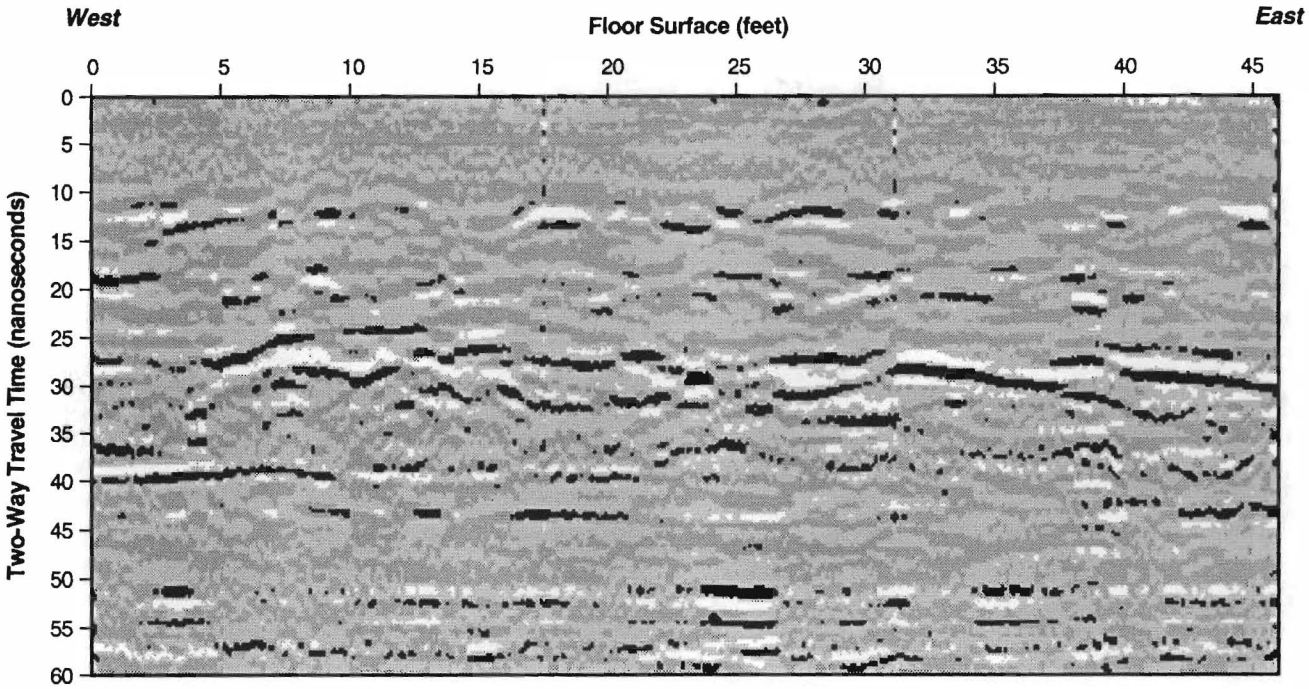

Figure F-9
Traverse 4, Room Q Access: March 1991
Vertical Exaggeration 1.5x

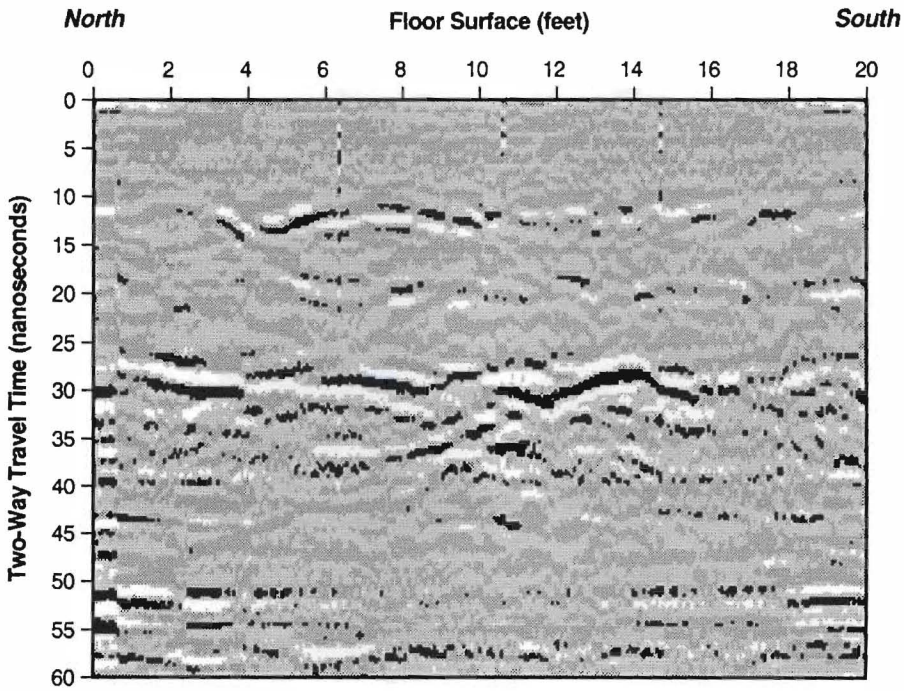

Figure F-10
Traverse 6, Room Q Access: March 1991

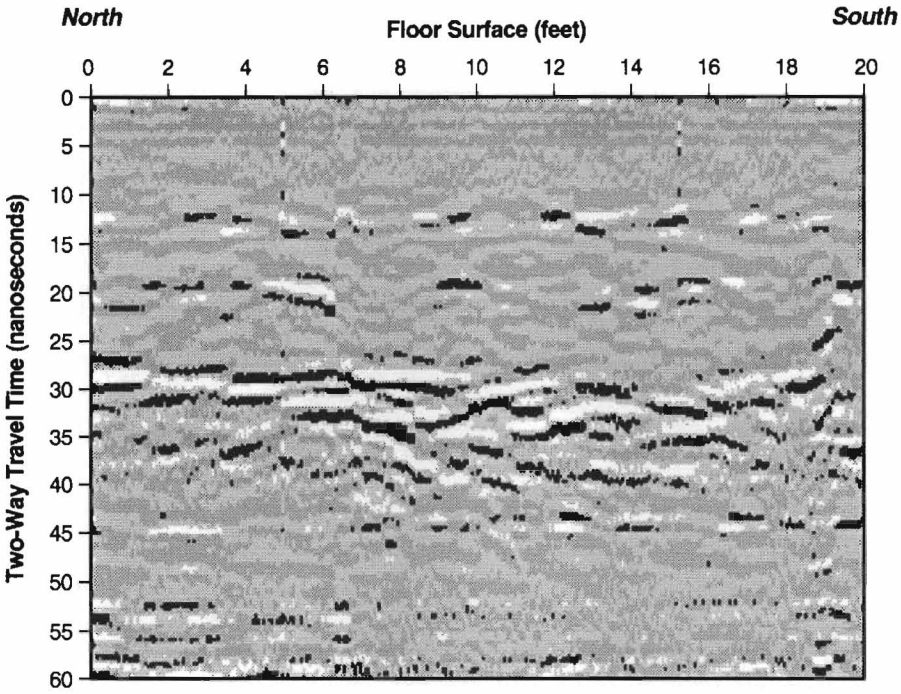

Figure F-11
Traverse 7, Room Q Access: March 1991